NASA Contractor Report 181721

Shock Tunnel Studies of Scramjet Phenomena

**R.G. Morgan, A. Paull, R.J. Stalker,
P. Jacobs, N. Morris, I. Stringer,
C. Brescianini**

UNIVERSITY of QUEENSLAND

**St. Lucia, Queensland, 4067
AUSTRALIA**

Grant NAGW-674

September 1988

National Aeronautics and
Space Administration

Langley Research Center
Hampton, Virginia 23665

SHOCK TUNNEL STUDIES OF SCRAMJET PHENOMENA

NASA GRANT NAGW 674. SUPPLEMENT 3

WORK CONDUCTED IN 1987

Commissioning of the new shock tunnel T4 at the University of Queensland implied that it was no longer necessary to focus the work of the research group about an annual test series conducted in the T3 shock tunnel in Canberra. Reflecting this, it has been possible to organize the group for work to proceed along lines such that particular personnel are associated with particular project areas.

Thus the format of this report consists of a series of reports on specific project areas, with a brief general introduction commenting on each report. The introduction is structured by project areas, with the title of the relevant report stated under the project area heading. The reports themselves follow in the order of the project area headings.

1. COMMISSIONING OF SHOCK TUNNEL T4

"The University of Queensland Free Piston Shock Tunnel T4 - Initial Operation and Preliminary Calibration"

During 1987, the free piston shock tunnel T4 was brought into operation, and a preliminary calibration was performed. This involved selection of a particular driver gas volumetric compression ratio (λ = 60), and measurement of shock speeds and pressure history at the downstream end of the shock tube after shock reflection. These measurements yielded the stagnation enthalpy and pressure in the reservoir of test gas, at the end of the shock tube, which was supplied to the hypersonic nozzle.

Preliminary test section calibration was effected through pitot rake measurements and static pressure measurement on a flat plate. Since the nozzle was a replica of one which has been used for some time with the T3 facility, the results of pitot surveys taken in that facility were used. The ratio between the static pressure and the nozzle stagnation pressure then could be used to confirm the accuracy of the chemical non-equilibrium nozzle flow code used to predict the test section conditions, with an effective nozzle area ratio obtained from the ratio of pitot pressure to nozzle stagnation pressure.

Since the static pressure is sensitive to helium contamination, the variation of static pressure with time could also be used as a check on contamination free test times. It was found that the measured times exceeded those predicted.

With this calibration, it was cosidered that the tunnel was ready for some preliminary studies of hypersonic combustion.

2. HYPERSONIC COMBUSTION STUDIES

"Hypersonic Combustion of Hydrogen in a Shock Tunnel"

Although static pressure levels were limited to approximately 20 kPa, it was found that it was possible to produce hypersonic combustion in a duct of 25 mm x 51 mm cross section, with a length of 600 mm.

As might be expected in a hypersonic flow, boundary layers appear to play a significant role. Not only do they generate high local temperatures, and thereby possibly influence ignition temperatures, but they also lead to significant pressure rises within the duct. Evidence of the first was apparent in the low ignition temperatures experienced in the experiments, and evidence of the second was apparent in measured pressure rise along the duct in the absence of combustion. Since the Reynolds' numbers of the experiments are such as to raise the possibility of the existence of turbulent, or transitional, boundary layers, it is important to learn more about transition under the conditions used in the tunnel.

It is possible that the production of hydrogen combustion in the duct at Mach numbers from 4.8 to 6.3 was due to these boundary layer effects.

When the duct was operated with the downstream part of one wall divergent, in order to produce thrust, it was found that specific impulse values up to 800 sec were produced. This value occurred at a stagnation enthalpy of approximately 11 MJ/kg, confirming that hypersonic combustion would allow higher specific impulse at high stagnation enthalpies than supersonic combustion would allow. It was found that, unlike supersonic combustion, the peak specific impulse occurred at a stagnation enthalpy well in excess of the ignition value. Noting that the flow conditions achieved by the tunnel appeared to be somewhat marginal for hypersonic combustion, it is difficult to advance reasons for the slow increase in thrust with increase in temperature, since it could be influenced by reaction kinetics, boundary layer pressure gradients and other effects. However, it seems clear that hypersonic combustion offers new phenomena which must be understood.

3. SIDEWALL FUEL INJECTION

Experiments

"Hydrogen Scramjet with Sidewall Injection. Shock Tunnel Simulations"

In previous work, it has been shown that injection of hydrogen fuel at the sidewall of a combustion duct is very effective in cooling the wall, but that observable pressure rises due to combustion did not occur until fuel equivalence ratios approached values of 2.

The present study is an examination of results of experiments performed in an effort to produce thrust with a wall injected fuel layer. For this purpose, two stage nozzle expansions were tried, anticipating that a preliminary, low angle expansion would allow combustion to develop, whilst simultaneously developing thrust, and this thrust would be added to that produced by the second stage of expansion. However, only small improvements were observed over the rather low levels of thrust produced by a single stage of expansion.

The experimental results suggested that the cool walls of the model may be lowering the temperature of the mixing gases, and thereby would inhibit combustion. A numerical study was undertaken to explore this matter further.

Numerical Study

"Numerical Modelling of Sidewall Injected Scramjet"

A numerical model, based on the CHARNAL computer code, was used to calculate the flow field for two conditions under which tests were conducted with a constant area duct, and one in which a single stage nozzle expansion was included. The code employed the k-ε turbulence model, and an 8 reaction model for the non-equilibrium process of hydrogen combustion. The validity of the model was confirmed by comparing predicted values of surface heat transfer and pressure distributions with experimental results.

The numerical simulation showed that wall quenching was not a significant factor in limiting combustion. In fact, the reason for the weak combustion effects observed in the experiments is the limited mixing which occurs between the hydrogen and the air streams. For the two cases studied (i.e. stagnation enthalpies of 4.2 MJ/kg and 8.7 MJ/kg respectively), the degree of mixing achieved 400 mm downstream of injection represented only 10% and 25% respectively of the injected hydrogen flow. The hydrogen which did mix with the air was almost completely burned.

In simulations with injection of heated hydrogen, the amount of mixing increased in the lower enthalpy case, but not for the higher enthalpy. The combustion induced pressure rise was increased in the first case, but reduced in the second case, corresponding to changes in degree of mixing.

Temperature contours in the hot hydrogen jet show that the hot regions of the

flow extend almost the entire way to the wall, indicating virtually no effect due to wall quenching. Thus the numerical simulation indicates that the temperature of the wall is not a significant factor in the experiments.

It might be noted that in the experimental studies, the substantially increased pressure rises observed when a 20:80 Silane-Hydrogen mixture was injected at a stagnation enthalpy of 4.2 MJ/kg were interpreted as evidence that it was the depression of temperatures, rather than mixing limitations, which was limiting the combustion of hydrogen alone. Given the low level of mixing evident in the numerical studies, it now seems plausible that the lower injection velocities of the higher molecular weight Silane-Hydrogen mixture could have led to an increase in mixing which was sufficient to produce the observed pressure rise.

The simulation suggests that mixing might be improved, and combustion effects increased, by using turbulence generators on the surface upstream of the injector. In fact, the moderate success achieved, in fig.9 of the experimental paper, with transverse jets in that location could be interpreted as being due to such an effect.

4. CHEMICAL KINETICS - EFFECT OF FREE STREAM ATOMIC OXYGEN

"Combustion of Hydrogen and Hydrogen/Silane Mixtures"

This study involves the use of one dimensional flow models, in which chemical reaction models are incorporated in a relatively complete form, in an attempt to explain effects observed in previous experiments in terms of chemical kinetics, and in assessing the effects of free stream atomic oxygen.

For combustion of pure hydrogen, the effect of free stream oxygen concentration on ignition delay lengths was most pronounced at low temperatures, with the presence of atomic oxygen concentration, measured as only a fractional percentage, theoretically causing considerable reaction to take place in a flow where it otherwise would not be observed. As temperatures increased above 1000 K, the differences in ignition delay lengths reduced, and at high temperatures, even the presence of 2% atomic oxygen did not significantly alter the distance required to complete combustion. Clearly, the presence of free stream atomic oxygen has negligible influence on combustion lengths only at relatively high intake temperatures.

For silane/hydrogen mixtures, previous chemical kinetics mechanisms were re-examined with respect to the role of silane in promoting ignition. Silane does this by increasing the temperature, and by increasing free radical concentrations. At temperatures below 800 K, scavenging of HO_2 also is important. The role of free radical concentrations suggests that atomic oxygen may have a less important role to play than in the case of hydrogen. Indeed, this is borne out by the computations, with the influence of free stream atomic oxygen being reduced, but nevertheless, the same trends are evident as with hydrogen, with the greatest sensitivity to atomic oxygen occurring at the lowest static temperatures.

The one dimensional models produced results which were approximatley in accord with experiments, except at intake static temperatures of approximately 500 K. There ignition distances obtained experimentally are much shorter than those predicted, whilst the pressure rise is not as large. Also, higher pressures were achieved with lower silane concentrations. These results could not be explained, although it was pointed out that the limited pressure rises experienced suggested a mechanism involving only partial burning of the fuel.

5. SCALING STUDIES

Experiments

"Pressure Scaling Effects in a Scramjet Combustion Chamber"

A re-examination was made of the results of experiments with a simple scramjet model in which the effects on net specific impulse of the pressure in the model, and the length of the combustion duct, were studied.

With a given combustion duct length, the pressure dependence effects could be classified into three regions. In the first region, temperatures were too low for combustion, whilst in the second region, vigorous combustion took place, and the level of specific impulse was strongly dependent on the pressure. The boundary between the two regions occurred at about the same temperature, for pressures in excess of one atmosphere. As pressures were reduced below that level, the ignition boundary moved to higher temperatures and, as pressures approached 25 kPa, no combustion was observed at any temperature. In the third, higher temperature, region, specific impulse was not strongly dependent on pressure level.

In varying the duct length, it was found that a short duct at a high pressure could produce the same specific impulse as a longer duct at a lower, appropriate, pressure. However, when the pressure in the longer duct was raised to the high pressure level of the shorter one, it was observed that specific impulse was the same for the two ducts over most of the range of temperatures studies. It was concluded that, at the higher pressure level, the flow was approaching complete combustion in the duct.

A numerical model give results which were reasonably consistent with the experiments in region 3, but not in region 2. However, the model was useful for indicating trends in this region.

The results were consistent with a model of combustion which allowed for a pressure sensitive region, in which the ignition and reaction lengths were a dominant chemical feature of the flow, and a region which approached chemical equilibrium. However, because Mach number and Reynolds' number also varied as pressures were varied, it was not possible to be more specific about the factors influencing the flow. This indicated a need for an experiment to be designed in which the variables likely to affect combustion could be varied independently. Also, because of the ultimate importance of geometrical sealing if laboratory experiments are to be applied to flight situations, the experiment should also include this factor as a variable.

Design of a Scaling Experiment

"Pressure Scaling in the Scramjet Model"

Since the highest thrust levels had been achieved at temperatures just above ignition values, it seemed likely that scaling effects in this range would be of most interest. Therefore, in order to bias the experiments towards this objective, it is planned to ensure that the product of pressure and a typical model dimension is held constant. Three models are to be made, of sizes such that the geometrical scaling factor varies by a factor of 10. The experiments will initially involve variation of temperature for each of the three models, aiming to obtain data for which Mach number, free stream composition and Reynolds' number are held constant between the three geometrically similar but different scale models.

In order to do this, it was necessary to use the same nozzle reservoir conditions and the same nozzle throat size for all three models. This ensured that free stream composition remained constant but, to ensure that the Mach number remained the same for the three models for differing static pressure levels, it was necessary for two of the models to expand the test flow to Mach numbers in excess of the combustion value, before compressing it through oblique shocks as it passed into the combustion duct.

The experiments can be repeated at different Reynolds' numbers by changing the shock tunnel operating pressure levels. In order to change the Mach number, it is necessary to make a new shock tunnel nozzle to operate with the smallest model, but the other two models allow adjustment of Mach number through adjustment of the angle of the oblique shock generators.

These experiments, and associated analysis, are expected to proceed over the next two or three years.

6. EXPANSION TUBE STUDIES

Experiments

"Experiments on an Expansion Tube with a Free Piston Driver"

Experiments were performed on a small expansion tube which employed a free piston driver, in order to determine if the flexibility offered by a free piston driver would allow the range of operation of an expansion tube to be extended. An existing free piston driver was used, and an expansion tube was constructed which was to be a representative ¼ scale model of the Langley expansion tube, with a free piston driver attached. Thus, both facilities exhibit a combined shock tube and acceleration tube length which is approximately 140 times the internal diameter. However, since discussions with Langley personnel indicated that there may be some advantage in using a longer shock tube than for the Langley facility, the ratio of shock tube length to acceleration tube length was 0.65 for the University of Queensland facility, compared with a value of 0.27 for the Langley one.

In the experiments, it has been shown that

(i) The pitot pressure records on the expansion tube centreline are qualitatively similar for the Langley facility and the Queensland facility, when both are operated at similar Reynolds' number. However, at the higher acceleration tube filling pressures, an irregularity occurs in the Langley results which is not evident in the University of Queensland results.

If this irregularity is ignored, then the results indicate that the University of Queensland facility is providing a reasonable simulation of the behaviour of the Langley facility.

(ii) Test times of at least 80 μsec were obtained, during which the fluctuations in pitot pressure were limited to ±5% or less. It was found that the test section velocity at which such test times could be obtained could be changed by changing the driver gas. Thus, a test section velocity of approximately 9.5 km/sec was obtained with helium driver gas, and 4.5 km/sec with argon driver gas.

(iii) The overall operating pressure levels were reduced by a factor of 2 (i.e. main diaphragm burst pressure, shock tube filling pressure, and acceleration tube filling pressure were all reduced by the same factor) whilst driver gas compression ratio was held constant and it was found that the effects on the pitot pressure tracer of varying acceleration tube pressure were qualitatively similar to those at the higher pressure levels. In particular, a useful test time was produced at the same pressure ratios. Further tests were done with the operating pressure levels reduced by another factor of 2, with the same results.

These results indicate that overall operating pressure levels can be decreased or increased by a substantial factor without changing test times.

Theory

"Expansion Tube Test Time Predictions"

Theoretical studies were made of the influence of the driver gas-test gas interface in the shock tube on the test time in the acceleration tube. Two mechanisms were considered for producing the pitot pressure fluctuations which limit the test time. The first involves the formation of low density gas inclusions ("blobs") within the test gas, due to driver gas-test gas mixing, and acceleration of these inclusions into the test region through the unsteady test gas expansion in the acceleration tube. The second involves reflection of the unsteady expansion from the turbulent interface region between the driver gas and the test gas.

An unsteady method of characteristics code was written for a McIntosh desk computer, and was used to predict the arrival of each of the two types of disturbances in the test region. For the NASA Langley expansion tube, and the University of Queensland expansion tube with argon driver gas, it was predicted that the reflected expansion disturbances would be evident on the test section pitot trace before the inclusion disturbances. In both these cases experiments showed disturbances arriving somewhat in advance of the predicted time but nevertheless, showing a trend which was compatible with predictions. For the University of Queensland expansion tube with helium driver gas, the same effects were evident for the lower shock tube filling pressures used. However, for the higher shock tube filling pressures, the theory predicted that the inclusion disturbances would arrive first at the test sections. This was supported by the experiments, which showed disturbances of larger amplitude than the reflected expansion ones, arriving at the approximate time predicted.

The encouraging results obtained with this preliminary theoretical analysis suggest that it has an important role to play in explaining the performance limitations of expansion tubes, and that it is worthwhile extending the analysis in order to test it further against experiments.

THE UNIVERSITY OF QUEENSLAND FREE PISTON SHOCK TUNNEL T4

- INITIAL OPERATION AND PRELIMINARY CALIBRATION

R.J. Stalker & R.G. Morgan

THE UNIVERSITY OF QUEENSLAND FREE PISTON SHOCK TUNNEL T4 - INITIAL OPERATION AND PRELIMINARY CALIBRATION

by *R.J. Stalker and R.G. Morgan*

1. INTRODUCTION

The University of Queensland free piston shock tunnel T-4 is the latest in a series of free piston shock tunnels, the first three of which were constructed at the Australian National University, Canberra, in the 1960's. The complete series is shown to scale in fig. 1, and is marked by an increase in size in passing from one to the next.

The increase in size in passing from T3 to T4 was associated with proposed studies in hypersonic combustion and propulsion. In order to produce static pressures in a hypersonic flow which are high enough to allow vigorous combustion of hydrogen to take place in the relatively short lengths available in a shock tunnel model, it is necessary to produce high nozzle stagnation pressures. This means that these high pressures must be produced at the downstream end of the shock tube, and sustained for long enough to establish and maintain a test flow in the nozzle for an adequate period.

A disappointing feature of T3 was the loss in pressure which occurred in the shock tube.[1] Although the cause of this loss is not understood, it has been found that it can be overcome by using a long compression tube for the free piston compressor. Hence the piston travels approximately 26 m during the driver compression stroke in T4, compared with 6 m for the T3 piston.

T4 began operation in April, 1987 and, after a settling in period, came into routine operation in September, 1987. At the time of writing, some 200 test runs of the facility have been made, and main diaphragm operating burst pressures have been raised to 28% of the design value. Experiments have shown that this is sufficient to allow combustion of hydrogen at a Mach number of 5. Although further increases in operating pressure levels are planned (in order to produce more vigorous hydrogen combustion), it seems appropriate to use the test data obtained so far for a preliminary review of the operating characteristics of the facility.

2. EXPERIMENTAL ARRANGEMENT

As noted above, the free piston driver is 26 metres long, and it is 230 mm in diameter. The piston mass is 92 kg. The shock tube is 10 m long, and 76 mm in diameter, with shock timing stations 3, 2 and 1 located 2.00 m, 4.00 m and 6.00 m respectively from the downstream end of the tube. The shock speed between station 2 and 3 was used for performance calculations, as it was considered that the gas processed in that part of the tube would be the test gas in the test section during the steady flow period.

A contoured nozzle was used, with a throat diameter of 25 mm and an area ratio of 100. This produced a test section Mach number which varied from 4.8 at a stagnation enthalpy of 35 MJ/kg to 6.3 at 3.7 MJ/kg. The change in Mach number is due to the real gas effects in the nozzle expansion.

3. SHOCK TUBE PERFORMANCE

For shock tunnel purposes, the important aspects of the shock tube performance are the stagnation enthalpy and the stagnation pressure of the test gas supplied to the nozzle, as well as the time between shock reflection and arrival of driver gas contamination at the entrance to the nozzle. The latter, of course, determines the effective shock tunnel test time.

The results reported here apply to one test condition, in which the compression tube was operated to produce a helium driver gas volumetric compression ratio of 60 (based upon the compression tube filling pressure to the main diaphragm burst pressure, and the assumption of isentropic compression), and the main diaphragm burst pressure was 57 MPa.

The nozzle stagnation pressure was obtained from two piezoelectric pressure transducers (PCb piezotronics type 118A) which were located in the shock tube wall, 65 mm upstream of the downstream end of the shock tube. The stagnation enthalpy was calculated by using the measured shock speed and the shock tube filling pressure to obtain the enthalpy and pressure immediately after shock reflection, and then assuming an isentropic expansion to the measured stagnation pressure.

Test results are presented in fig. 2, with a scale for the measured shock speed matched to the shock tube diaphragm pressure ratio at the left hand side of the figure. Noting that Earth orbital velocity corresponds to a stagnation

enthalpy of 31 MJ/kg, it can be seen that stagnation enthalpies in excess of this value have been achieved in the shock tube. This is in accord with experience in T3[2].

The nozzle stagnation pressure was measured 0.5 milliseconds after shock reflection and, after being normalized with respect to the main diaphragm rupture pressure, has been plotted at the top of fig. 2. The tendency for this pressure to increase with falling stagnation enthalpy is consistent with expectations based on coupling shock tube theory with the observation that tailored interface operation occurs at a shock speed of 6.65 km/sec., corresponding to a stagnation enthalpy of 48 MJ/kg.

The variation of the nozzle stagnation pressure with time is shown in fig. 3(a) for typical test conditions. For fig. 3(a) it can be seen that the pressure falls by approximately .. % over a period of one millisecond after shock reflection. It is thought that this is due to the use of a piston with a mass which was designed for operation at high pressures. At the pressures of tests, the piston velocity was too low at diaphragm rupture to match the flow of driver gas into the shock tube, causing the driver pressure to fall. This can be rectified by lowering the speed of sound in the driver gas, as in fig. 3(a) (ii). Here it can be seen that, when argon is used as driver gas, rather than helium, the pressure remains approximately steady for a much longer period.

Fig. 3(b) shows the limitations on test time arising from contamination of the test gas by the driver gas. This can come from two causes. One is due to drainage of the test gas through the nozzle throat, and the other is due to "jetting" of the driver gas along the walls of the shock tube from the contact surface. The "jetting" is due to the bifurcated shock pattern which forms when the strong reflected shock interacts with the shock tube boundary layer[3]. It can be see that the shock boundary layer interaction is responsible for limiting the tunnel test time. It will be noted that the test time has been expressed as an approximate length of the slug of test gas passing through the test section by multiplying the calculated test time by $\sqrt{2H_s}$. The test slug lengths which are displayed are based upon a conservative calculation and, as will be seen below, there is evidence to suggest that test times may be somewhat longer than those calculated.

4. TEST SECTION CALIBRATION

Pitot survey data are shown in fig. 4. These were obtained in shock tunnel T3, using a nozzle which was identical with the one employed in these tests. They show that the nozzle expansion is not complete for some 8 inches downstream of the expected nozzle station, yielding pitot pressures which are somewhat above the uniform flow values in a region which is downstream of the theoretical test cone boundary. This may be due to boundary layer effects in the nozzle flow, which were not taken into account in designing the nozzle. Downstream of this region, the pitot traverses indicate a uniform and parallel flow.

Static pressures were measured at a pressure orifice located 200 mm from the leading edge of a flat plate mounted in the test section with its leading edge at the nozzle exit. A static pressure record, normalized with respect to the nozzle stagnation pressure, is shown at the top of fig. 5.

Static pressure measurement provides a good indication of the static temperature at the test section, since the velocity is essentially fixed by the stagnation enthalpy, and the density therefore is fixed by mass flow considerations. The temperature in the test section is sensitive to real gas effects in the nozzle expansion, and therefore it follows that the static pressure measurement serves as a check on the validity of the numerical calculations used to predict the test section conditions. In fig. 5, static pressure measurements are seen to compare satisfactorily with prediction made using a one-dimensional non-equilibrium calculation[4]

For comparison, the static pressure predicted for a perfect gas expansion of air to the same pitot pressure level also is shown in fig. 5, and is seen to be well removed from the measured values. Expansion of helium to the same pitot pressure levels would produce an even lower pressure. In this light, the decay in static pressure after about 1 millisecond of steady pressure, which is evident in the static pressure record in fig. 5, may be seen as the onset of driver gas contamination. This would indicate that the steady test flow slug lengths indicated in fig. 3 may be conservative by as much as a factor of two. However, this should be regarded as a tentative conclusion, which is subject to confirmation when more data is obtained.

It may be noted that some points are included on fig. 5 which were taken in the intake duct of a scramjet model. The static pressure there was higher than the measured flat plate static pressure but, assuming that the proportionality

between flat plate and intake static pressures would apply at all stagnation enthalpies, the intake results were scaled to produce psuedo flat plate measurements at stagnation enthalpies where flat plate measurements were not available

The consistency between measured and calculated static pressures indicates that the numerical code may be used to calculate other test section flow properties. Results of such calculations are presented in fig. 6. The Mach number decays as stagnation enthalpy is increased because of real gas effects in the nozzle expansion. Two curves are shown for the free stream enthalpy. This is because a substantial part of the free stream enthalpy, h_∞, is invested in the sensible enthalpy associated with the temperature of the gas and, if desired, this could be converted to freestream kinetic energy by further expansion. However, the rest of the freestream enthalpy which is denoted by h_f, is associated with "freezing" of the air as it passes through the nozzle expansion, and cannot be recovered by further expansion. It can be seen that this component rises to 20% of the stagnation enthalpy at high stagnation enthalpies.

5. CONCLUSION

These results and calculations are preliminary in nature, representing an initial calibration of the tunnel at one range of operating conditions. Increases in operating pressure levels and changes in driver gas volumetric compression ratio are planned to generate new test conditions, as well as more extensive calibration measurements. However, the results reported here indicate that the shock tunnel is operating satisfactorily, at pressures and stagnation enthalpies which have been found to be high enough to allow experimentation on hypersonic combustion of hydrogen.

REFERENCES

1. Stalker, R.J. and Hornung, H.G. "Two Developments with Free Piston Drivers". Proc. Seventh International Shock Tube Symposium. University of Toronto Press 1970, PP 242-258.

2. Stalker, R.J. "Development of a Hypervelocity Wind Tunnel". Aero. J. of Roy. Aero. Soc. (1972) pp 374-384.

3. Crane, K.C. and Stalker, R.J. "Driver Gas Contamination in a High Enthalpy Reflected Shock Tunnel". AIAA Journ. V 16. pp 277-278 (1978)

4. Lordi, J.A., Mates, R.E. AND Moselle, J.R. NASA. Rep. CR-472 (1966).

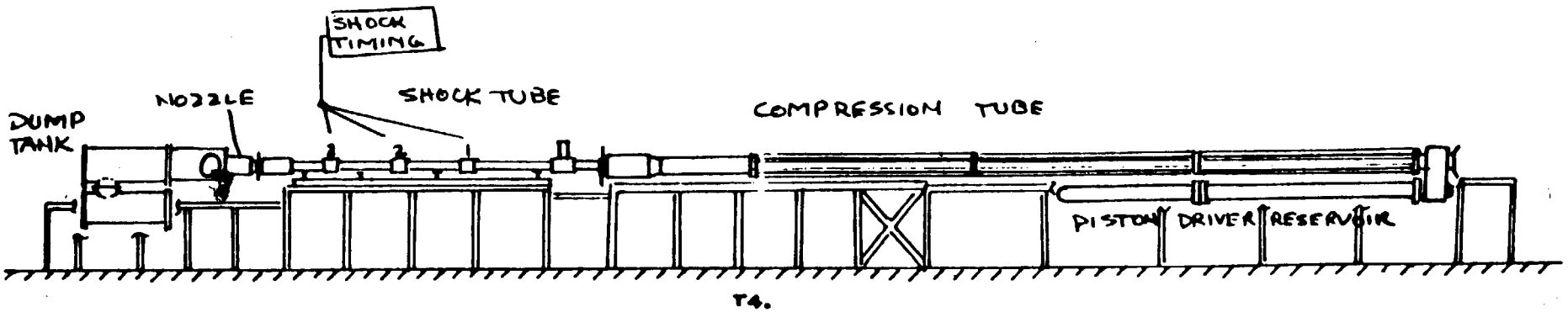

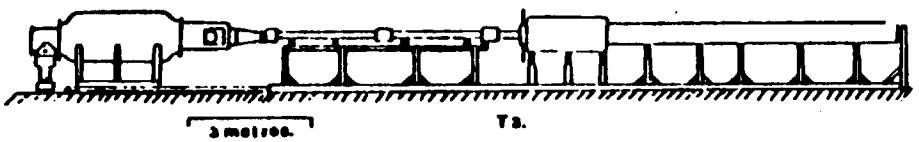

T2.

T1.

	T1.	T2.	T3.	T4.
Compression tube	150 × 5·1	300 × 7·6	600 × 30	2600 × 23
Shock tube.	135 × 1·3	300 × 3·1	600 × 7·6	1900 × 7·6
Nozzle exit dia.	5·1	11	30	30
Piston mass.	·6 kg	1·3 kg	90 kg	92 kg

Dimensions in centimeters.

FIG 1. FREE PISTON SHOCK TUNNELS

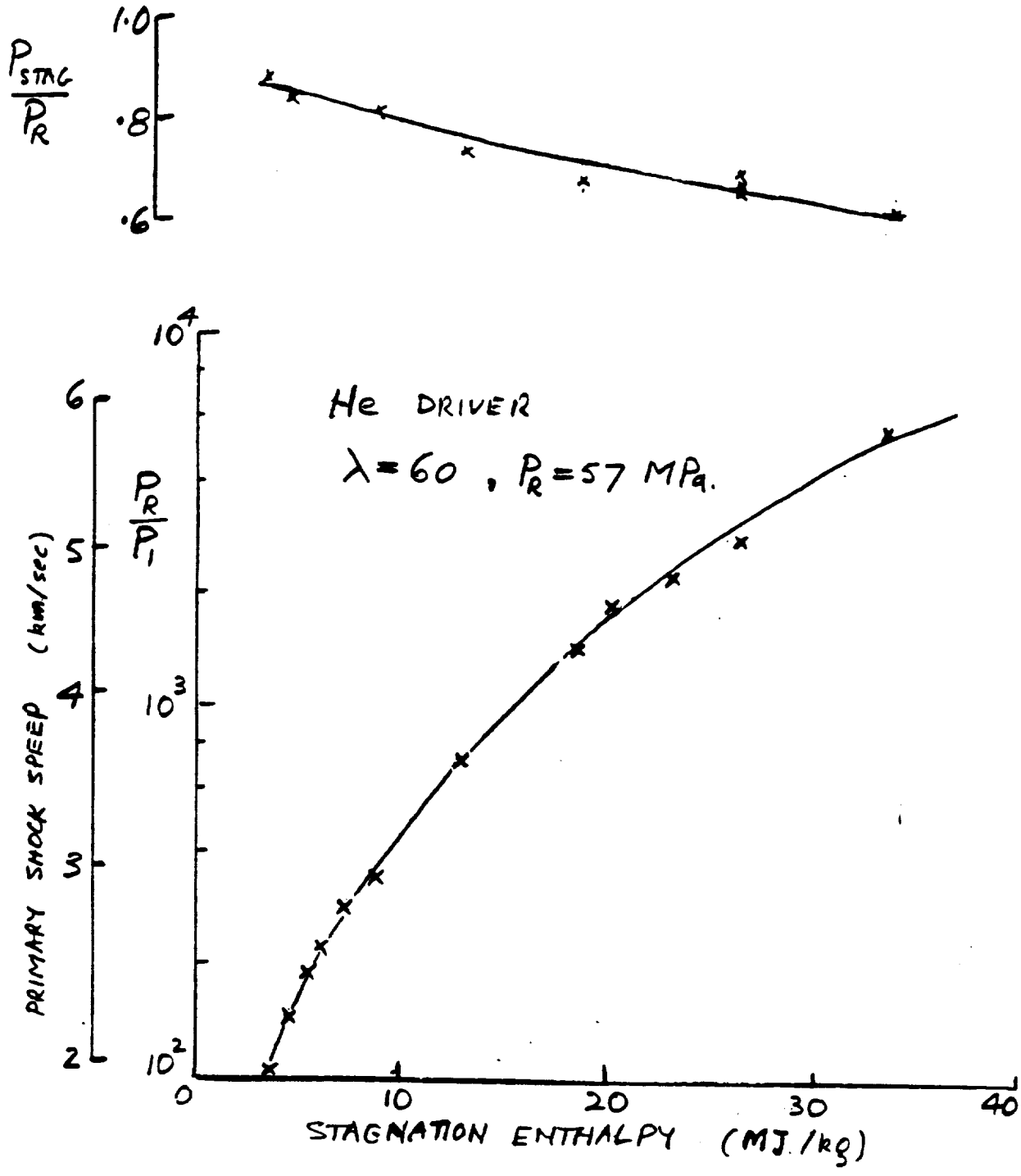

FIG. 2. SHOCK TUBE PERFORMANCE

(a) STAGNATION PRESSURE

(i) He DRIVER
H_s = 18.6 MJ./kg.

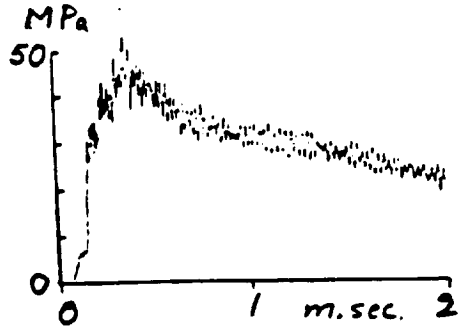

(ii) Argon DRIVER

(b) DRIVER GAS CONTAMINATION

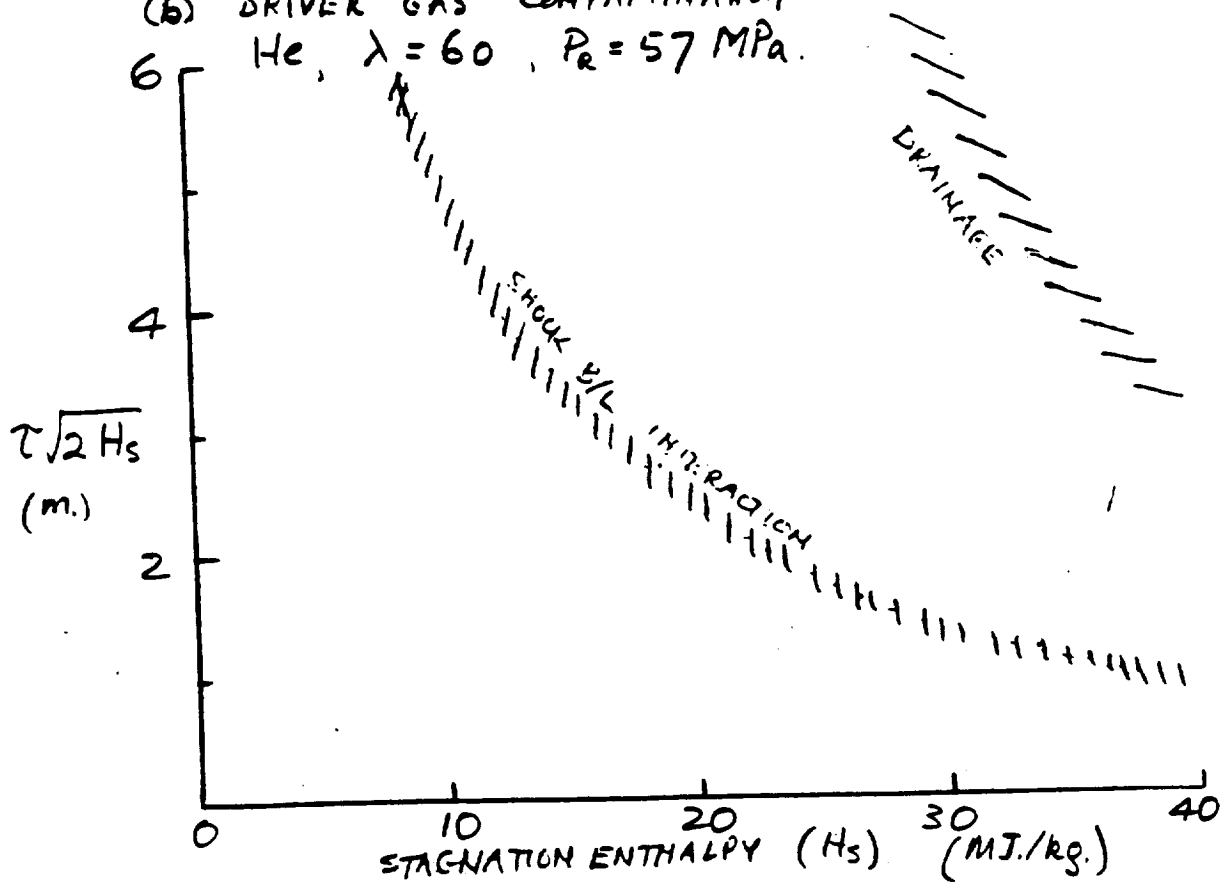

FIG 3. TEST TIMES

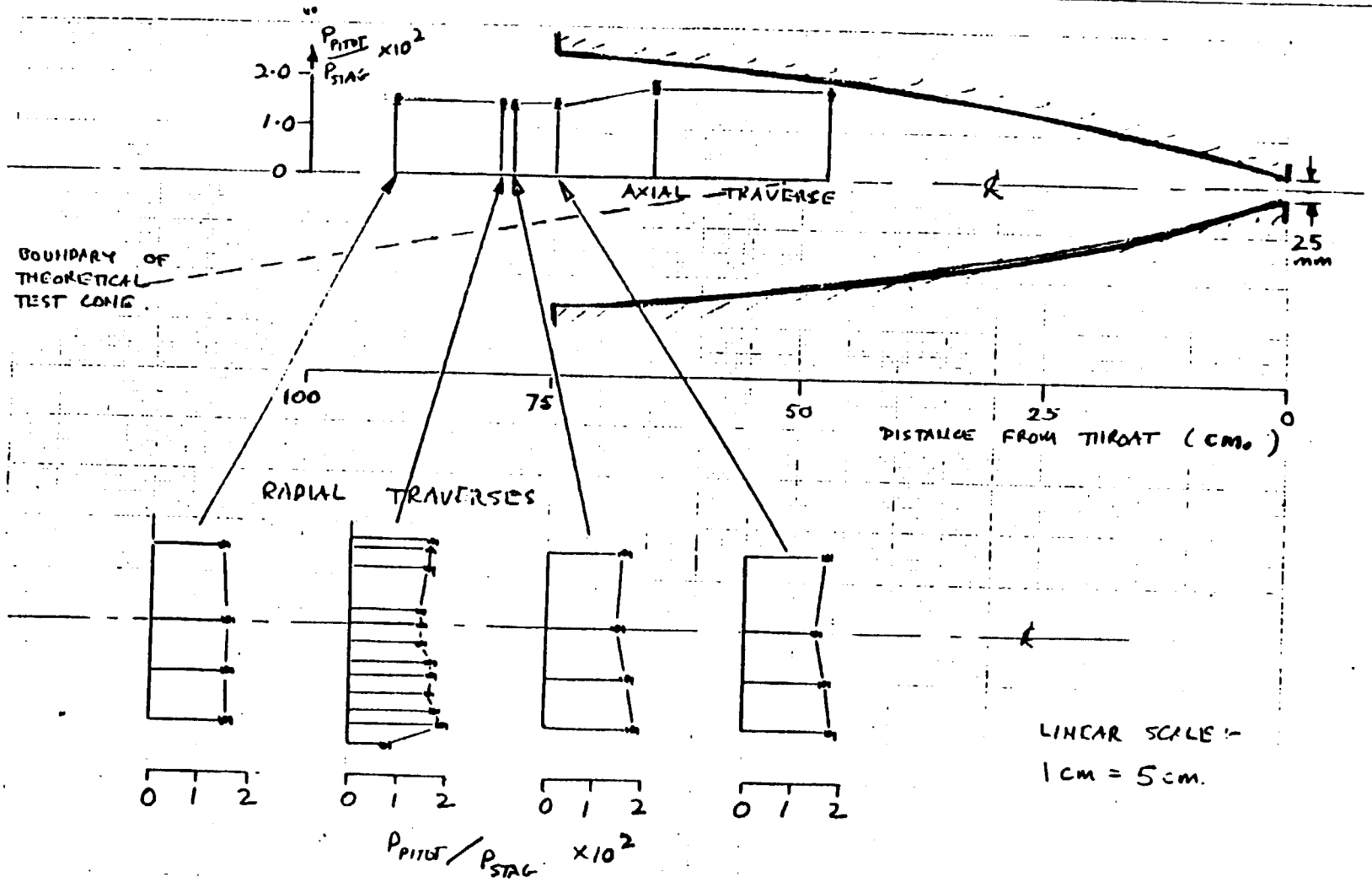

FIG 4. TEST SECTION PITOT TRAVERSE
(H_s = 15.8 MJ./kg.)

○ POINTS TAKEN FROM INTAKE OF SCRAMJET MODEL — SCALED BY FACTOR $\cdot 67/\cdot 80 = \cdot 59$ TO MATCH FLAT PLATE DATA AT 18·6 MJ/kg.

FLAT PLATE PRESSURE ORIFICE APPROX 200 mm FROM L.E.

$P_\infty U_\infty^2 / P_{STAG} = \cdot 015$

STATIC PRESSURE RECORD.

$H_s = 18{\cdot}6$ MJ./kg

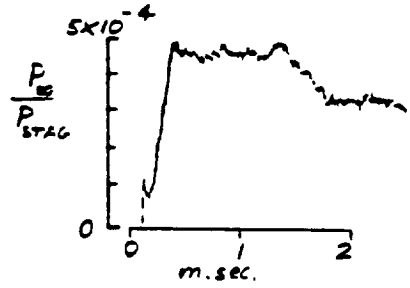

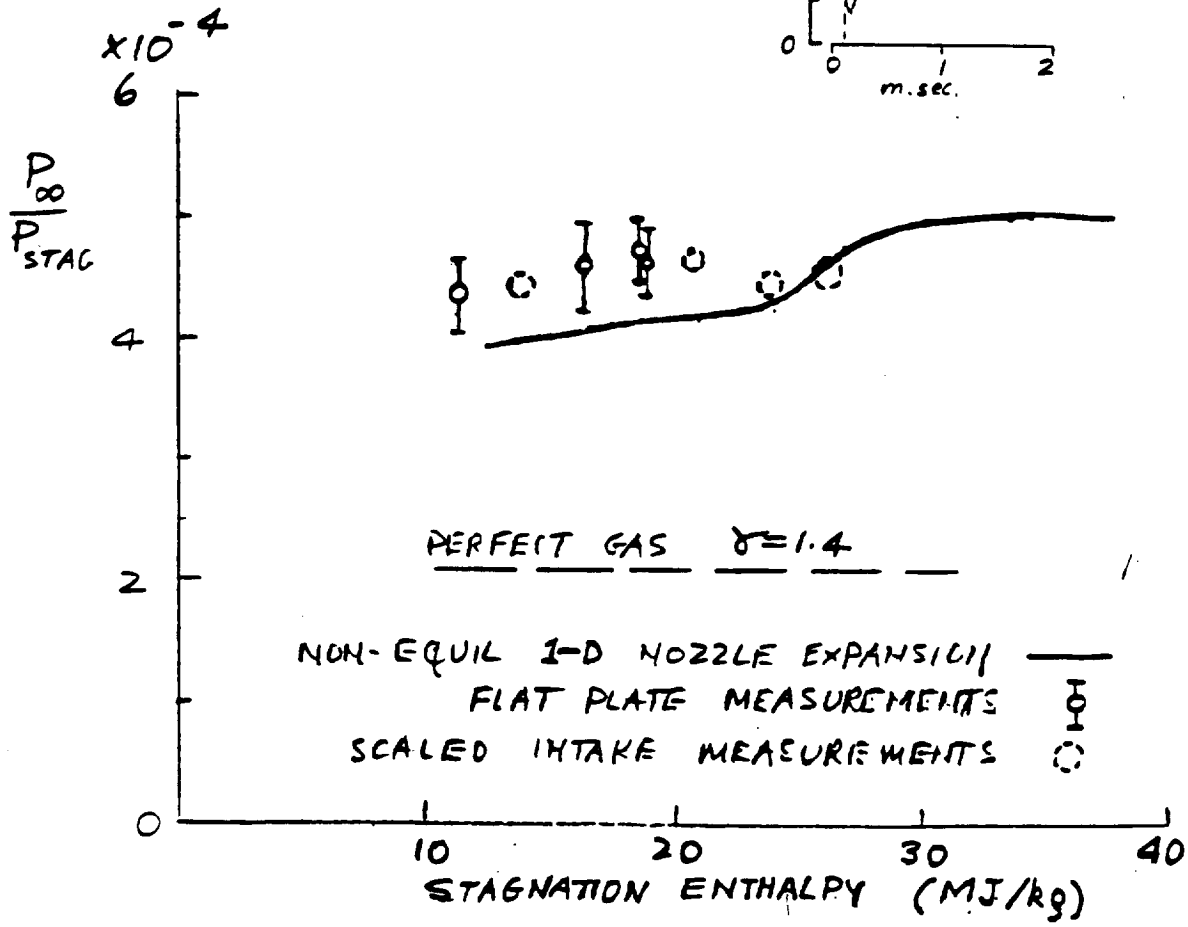

FIG. 5 THERMO CHEMICAL EFFECT ON TEST SECTION STATIC PRESSURE

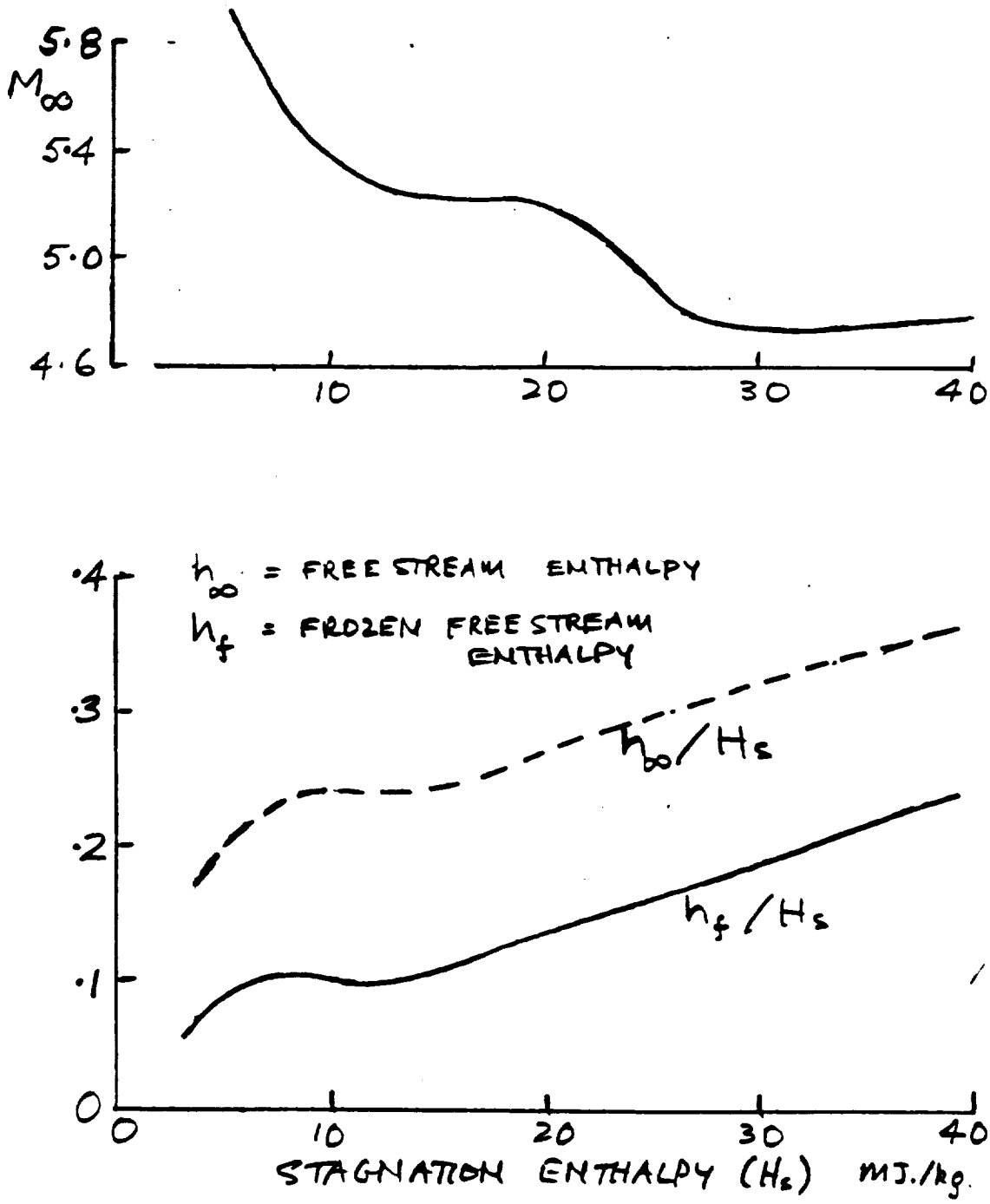

FIG 6. CALCULATED TEST SECTION FLOW PROPERTIES

HYPERSONIC COMBUSTION OF HYDROGEN IN A SHOCK TUNNEL

R.G. Morgan

Hypersonic Combustion of Hydrogen in a Shock Tunnel.

Introduction.

This paper reports the results of a preliminary series of tests in the shock tunnel, T4, on hypersonic combustion and thrust generation in a hydrogen scramjet model. The work was performed before a full calibration of the tunnel and nozzle was completed, but using a nozzle profile which had previously been tested in the shock tunnel T3. The main purpose of the experiments was to confirm the feasibility of hypersonic combustion in the flow conditions created by the new tunnel.

Previous tests with a supersonic nozzle performed in the Shock tunnel T3 at the Australian National University, Ref 1, indicate that severe performance degradation occurs at the enthalpies associated with high Mach number flight. This appears to be at least partly due to the high static temperatures created by maintaining a supersonic combustion chamber at hypersonic flight speeds. Good combustion efficiency will require low combustion chamber intake temperatures, less than 2000 K, and this can only be achieved at enthalpies higher than 13 Mj/kg, corresponding to a flight speed of approximately 5km/s, by maintaining hypersonic flow in the combustion chamber. Even at lower enthalpies it is likely that hypersonic combustion will be preferable to supersonic if it can be made to burn properly.

The methodology of the experiments was to initially perform a short series of tests in a constant area duct, to see if combustion was possible at all with the apparatus. The duct had an intake section with a height of 25 mm and a width of 51 mm . Injection was from the centreline across the full width of the duct. A thrust surface was then fitted at a suitable distance down stream of injection and specific impulse measurements were obtained for a range of conditions in the mach number range 4.8 to 6.3.

Compression wedges were then fitted to the model intake, and the flow in the combustion chamber was reduced to supersonic. With conditions adjusted to maintain the same intake pressure, a direct comparison was then obtained between supersonic and hypersonic combustion. The supersonic combustion tests were within the nominal mach number range of 4 to 4.5.

After the completion of these runs a short series of tests was performed using an enlarged constant area duct with a nominally square intake section of 51 by 49.5 mm. The purpose of this was to distance the mixing layer from the presence of the wall boundary layer in an attempt to enhance combustion.

Constant area duct, hypersonic combustion.

A schematic of the model used for these tests is shown in Fig 1. It incorporates the same injector strut as had been previously used with a supersonic nozzle, and its leading edge was extended clear of the intake so that no disturbances entered the duct. Injection was through a nozzle with a 1.6 mm throat on the centreline extending across the full duct width. Excepting disturbances from the side wall, the flow was considered to be two dimensional. Instrumentation consisted of a series of pressure transducers on the top and bottom walls, both upstream and downstream of injection.

Hydrogen was injected from a room temperature reservoir with freestream stagnation enthalpies ranging between 6.2 and 26.5 Mj/kg. Test conditions were computed using the non equilibrium nozzle expansion program of Ref 2. In table 1 the test conditions used with a hypersonic duct are given. In the constant area duct configuration only enthalpies between 26.5 Mj/kg and 6.2 Mj/kg were used. The shock tunnel does not produce perfectly steady conditions in the stagnation region, which in the normal operating mode has a continuous pressure drop with time, and this is reflected in the nozzle exit flow. Reservoir conditions are calculated by assuming an equilibrium expansion from conditions behind the reflected shock, as given by normal shock relations, to the measured stagnation pressure. The flow is considered to be 'steady' when the ratio of static pressure in the nozzle to stagnation pressure, measured in the reservoir, is constant with time. Whilst this might indicate that the nozzle is operating at a steady Mach number, the static temperature and velocity at nozzle exit reduce with time. In table 1 the results of these computation are presented. The stagnation pressure chosen corresponds to the start of the steady test time. An appropriate delay was introduced between stagnation pressure and static pressure readings when locating the duration of the steady run time. The purpose of this was to account for the time lag between pressure drops in the stagnation region effecting the exit flow. Duct static pressure divided by stagnation pressure will subsequently be referred to as 'normalised' pressures. In Fig 5 a typical normalised static pressure trace and a stagnation pressure record are shown. The spike at the start of the trace occurred due to noise when the stagnation pressure was almost zero. In Fig 7 a general idea of the overall steadiness of the flow is presented in the form of scatter bars over the time when the normalised pressure traces are steady.

Pressure rise in the duct was taken to be indicative of combustion only when significantly increased pressures were recorded when injecting hydrogen compared to injecting helium at the same nominal mass flow rate.

No signs of combustion are evident at enthalpies of between 26.5 and 18.7 Mj/kg, as may be seen from Fig 2. Fig 2 presents data only for an enthalpy of 26.5 Mj/kg, but the result is substantially the same for the other cases in this enthalpy range. In this range the duct intake mach number varies between 4.8 and 5.18 due to changes in test gas composition and reaction rates. As these conditions correspond to intake static temperatures of between 2500 and 3600 K, this may be due to the reduced combustion efficiency due to combustion product dissociation in this temperature range. Also at higher temperatures a given heat input causes a smaller temperature rise due to increased specific heat, and a given change in temperature produces a smaller pressure rise than at lower temperatures. Additionally, the intake velocity is high, in the range 4.47 to 6.09 km/s, which reduces the duct transit time and may inhibit mixing of the fuel and air jets. It is possible that combustion in this enthalpy range, which corresponds to flight speeds of between approximately 6.1 and 7.3 km/s, will require even higher combustion chamber mach numbers. Whether this may be achieved or not will depend on the static pressure levels relevant to the proposed flight altitude.

Further tests were performed in the enthalpy range of 13 to 6.2 Mj/kg, corresponding to flight speeds of between 3.5 and 5.1 km/s. Intake mach number over this range varied from 5.25 to 5.81. In Fig 3 it can be seen that pressure rise is produced when

injecting hydrogen fuel, over and above that produced by the injection of helium. In Fig 4 the fuel on traces are compared for a range of different enthalpies. The enthalpy range was not extended to identify the low temperature ignition limit, but it is noted that at the lowest enthalpy used for the constant area duct, 6.2 Mj/kg, the intake static temperature was down to 785 K. At this temperature, and at the intake pressures used, hydrogen fuel would not be expected to react within the confines of the duct without some sort of ignition enhancement.

This is possibly provided in a hypersonic duct by boundary layer heating. In Fig 8 the temperature profiles produced by equilibrium flow at mach 5 for laminar and turbulent boundary layers are shown. The flow conditions chosen correspond to the 8.39 Mj//kg stagnation enthalpy condition. In both cases the boundary layer was allowed to develop for a distance of 160 mm, which corresponds to the upstream length of the injector strut. Whilst equilibrium calculations cannot be expected to exactly represent the state of a boundary layer in non equilibrium flow, it does illustrate that temperatures of the order of twice the free stream values are to be expected. The presence of this hot layer of gas might make it possible to sustain combustion at free stream conditions where it would not otherwise be possible. Furthermore, the presence of these hot spots might lead to local dissociation of the oxygen molecules, providing a source of radicals to encourage ignition.

Another possible explanation is suggested by Fig 6, where the fuel off normalised static pressure distribution along the duct is shown, along with the predicted intake level. At an enthalpy of 8.39 Mj/kg the pressure is seen to agree well with the predicted value for a short distance after the injection strut, but further downstream the measured pressures are of the order of twice the theoretical values. This might be due to boundary layer growth in a restricted duct compressing the freestream flow. Pressure levels are uneven due to waves reflecting across the duct and from the walls, but the increased overall pressures downstream may clearly be seen. At this mach number, with the presence of waves indicated by the wall static pressure profile, it is hard to tell accurately what the local static pressure level will be in the free stream and in the mixing layer away from the wall. However the wall pressures are increased over such an extended region that it must be concluded that increased pressures also occur in the mixing zone. At mach 5, assuming any pressure increase over intake conditions occurs isentropically, a rise of approximately 20% will be produced in the static temperature when the static pressure doubles.

Also shown in Fig 6 is the fuel off pressure distribution for an enthalpy of 26.5 Mj/kg. It can be seen that the downstream pressure does not consistently rise in this instance, but fluctuates around the predicted value. Assuming the pressure rise seen at 8.39 Mj/kg is indeed induced by boundary layer growth, then this would be qualitatively consistent with the reduced displacement thickness associated with laminar boundary layers at the lower reynolds number, higher enthalpy condition. It is possible that transition is occurring at the higher Reynolds numbers. Simple calculations may be used to indicate if the pressure rises observed are consistent with laminar or turbulent boundary layer growth by considering the compressive effect of the displacement thickness in the duct.

As the boundary layer grows the free stream is displaced by means of compression waves which propagate into the flow at approximately the mach angle. As the height of the duct is reduced , the waves will reflect sooner off the far walls and pressure within the duct will rise faster and to a higher level. This may be predicted by considering the rate of boundary layer entrainment and using a characteristics approach in the freestream. However if the duct is relatively long in comparison with its' height, then the passage of multiply reflected waves across the duct enables a one dimensional approach to be made. Pressure levels may be estimated by considering the boundary layer displacement thickness to produce a corresponding reduction in duct area, and using isentropic relations for supersonic flow.

This has been done for the 8.39 Mj/kg case and the results are tabulated in Table 2. This is not being offered as a rigorous treatment, but to demonstrate that the pressure levels observed are consistent in approximate magnitude with the boundary layer mechanism suggested.

The boundary layers were assumed to behave as on a flat plate. Interactions between boundary layers on adjacent walls, and between boundary layers and waves were not considered. The boundary layer on both sides of the injector was computed for a wetted length of 160 mm, and assumed to represent constant blockage when separated in the region downstream of the injector. The wall boundary layers were developed for 400 mm, and their blockage was added to that from the injector boundary layers. No compression effects were considered due to boundary layers on vertical walls.

The turbulent boundary layer thickness was calculated using the formula 0.37*X*Re^-0.2 from Drummond et al. Ref 3. A seventh power law and similarity were then used to compute the internal boundary layer parameters.

The laminar boundary layer was calculated from incompressible profiles using the Howarth transformation and similarity.

Table 2. Effects of boundary layer growth on duct pressures.

Stagnation enthalpy 8.38 Mj/kg. Computed at 400 mm from intake with 160 mm injector strut.

	Laminar	Turbulent
Boundary layer thickness on injector (mm)	1.47	3.94
Displacement thickness on injector (mm)	0.76	1.35
Displacement thickness on sidewall at 400mm (mm)	1.2	2.82
Total effective displacement thickness(mm)	3.92	8.33
Area restriction ratio in 25 mm duct	0.843	0.667
Pressure ratio at Mach 5	1.28	1.81

On this basis it would seem that turbulent boundary layers would be necessary to cause the pressure rise shown in Fig 6 for an enthalpy of 8.39 Mj/kg. Considering also the boundary layer heating effect mentioned above, boundary layers in the combustion chamber would appear to play an important role in the ignition process. However without heat transfer or flow visualisation data it would be premature to conclude that the boundary layer is indeed turbulent, as the effects of the three dimensional nature

of the duct and the wave processes indicated by the pressure profiles are unknown. The calculations were repeated for a laminar boundary layer at the higher enthalpy of 26.5 Mj/kg. Although the lower Reynolds number produces thicker boundary layers, the displacement thickness does not increase significantly due to the higher ratio of static temperatures across the boundary layer. The physical reason for this may be seen from Fig 11 where the non dimensional density profiles across the boundary layer are shown. As both conditions share the same wall temperature of 300K, the cooled gas near the wall will have a higher non dimensionalised density in the high enthalpy flow, due to the high free stream static temperatures. This will serve to reduce the mass flow deficit of the boundary layer, and therefore the displacement thickness does not increase as would be expected in incompressible flow.

Laminar boundary layers at the higher enthalpies, with transition to turbulence occurring at the higher Reynolds numbers associated with the lower enthalpy conditions is a possibility. However, even the presence of a laminar boundary layer at the higher enthalpy conditions would be expected to produce a pressure rise of the order of 30% in the duct, and as can be seen from Fig 2 this was not observed. This might be because the approximate boundary layer model used assumes perfect gas behavior, with representative properties chosen at an appropriate mean temperature. This would lead to overpredicting the temperature, and underpredicting the density, in the boundary layer 'hot spots' where viscous heating predominates over heat loss to the wall. This in turn would lead to overestimating the displacement thickness by an amount which would be expected to increase with enthalpy.

As a summary of this section, hypersonic combustion was achieved in a constant area duct for flows with stagnation enthalpies below 13 Mj/kg. At enthalpies above 13 Mj/kg no measurable combustion effects were observed. The high temperature cut off point is somewhere between 13 and 18.7 Mj/kg. The low temperature cut off point has not yet been identified. An ignition enhancement mechanism is apparent, which is provisionally being attributed to the presence of boundary layers on the injector strut and on the side walls. Three modes are suggested whereby boundary layers might stimulate ignition. Firstly, the boundary layers on the injector contain regions of elevated temperature in close proximity to the fuel jet which might directly accelerate ignition and reaction. Secondly, the boundary layers may contain dissociated oxygen radicals which have to reach a certain concentration before the reaction 'takes off'. These two mechanisms are inherently interrelated. Finally, the growth of all boundary layers in the duct presents a restriction to the flow of the main stream and causes both pressure and temperature to rise. A preliminary look at the measured pressure profiles indicates that turbulent boundary layers may have been present for some of the conditions where combustion was observed.

Comparison of Hypersonic and supersonic combustion with a diverging duct.

A configuration with a short injector with a leading edge located downstream of the intake was chosen for the main series of tests of hypersonic combustion in the thrust producing mode. The short injector was used in the hope that the extra intake area made available by having the leading edge compression process internal would increase the duct pressure enough to improve combustion.

In Fig 12 the fuel off pressure profiles are plotted for the two geometries. Whilst the internal injector does show higher pressure in the constant area section, it is not maintained downstream of the corner. The internal strut produces uniform pressure after the expansion, as would be expected in supersonic flow. The external strut shows a smaller pressure drop round the corner, followed by a gradually falling pressure downstream. This suggests lower Mach number with the long injector and a more uneven flow field, possibly due to the extra boundary layer growth in the middle of the duct. Despite an apparent reduction in performance the totally enclosed configuration was used for the remainder of the tests as it appeared to give a more satisfactory supersonic flow.

In Fig 15 the two fuel on profiles are shown for equivalence ratios of 0.55 and 0.57 for internal and external leading edges respectively. It can be seen that the long strut of the extended injector produced more pressure rise and thrust than the short totally enclosed injector. This may again be due to the larger boundary layer entrained into the mixing layer from the trailing edge of the injector. Despite the extra mass flow induced with the internal injector, the pressure levels in the early part of the mixing layer do not reflect this due to the wave trajectory at this Mach number. This is illustrated schematically in Fig 16, where it is seen that the waves from the injector leading edge do not reflect back to the centre line until approximately 130 mm after injection.

In Figs 13 and 14 the fuel on and off pressure profiles are shown for the external and internal injector leading edges respectively. The net thrust, that is fuel off thrust subtracted from fuel on thrust, is similar for both cases. However the resultant specific impulse is less because more fuel had to be injected with the internal injector to maintain the same equivalence ratio.

In Figs 9 and 10 the results are presented for hypersonic and supersonic combustion. The supersonic test conditions were created by means of an intake scoop giving a double reflection of 7.5 degrees. The diaphragm rupture pressure was adjusted to maintain approximately the same intake pressures as for the hypersonic duct. The injector was configured with the same internal leading edge to give a direct comparison with the hypersonic results. Table 1 shows the nozzle exit conditions for the hypersonic tests, Table 3 shows the supersonic test conditions. Tables 4 and 5 contain the results of individual runs for hypersonic and supersonic ducts respectively.

Looking firstly at Fig 10, specific impulse against static intake temperature, it is seen that there is little difference between hyper and super sonic combustion. The low temperature cut off is less clearly defined in hypersonic flow, possibly due to more pronounced boundary layer heating. This effect would be hard to separate from the reduced particle residence times at the higher mach number. From a qualitative point of view it might be said that as the temperature cools down the higher mach number flow releases less heat as it has less time to mix and react within the duct. However, as it does contain a small amount of very hot gas in the boundary layer, a residual amount of fuel still gets burned even at very low temperatures, but it does not release enough heat to ignite the main body of the fuel.

The very high levels of specific impulse previously observed at Mach 3.5 just above the low temperature ignition limit were not seen here. Noting that previous tests at Mach 3.5 showed the size of this peak to be very pressure sensitive, the lack of high specific impulse is probably due to the low static pressures in the hypersonic duct. It should be noted that combustion in this regime of potentially high specific impulse, that is between 400 and 1500 K, cannot be strictly described as either a diffusion flame, where reaction times are considered insignificant, or as a premixed flame where heat release is totally reaction controlled. Overall heat release is therefore sensitive to any of the parameters effecting ignition, reaction and mixing, and is not fully understood at present. However, speculation as to the physical mechanisms dominant may be useful.

The presence of a wall alongside the combustion zone of a scramjet with a combustion mach number of 3.5 has been shown to seriously reduce the effectiveness of combustion. The reason for this is not known, but it is possible that in a hypersonic flow, with thicker boundary layers, the same wall interaction effect may propagate into the mixing layer of a central jet too. If this is the case then combustion efficiency would be significantly improved by moving the injector further away from the wall. A short series of tests has recently been performed using a square duct to test this idea. The work has not been documented yet, but the preliminary results show a complete lack of burning in the larger duct. This tends to indicate that rather than preventing combustion, the wall boundary layer may be an important ignition aid for the scramjet models used in this study. Some of the possible reasons for this are discussed in the section on the constant area duct. The reason the boundary layer was ineffective as an ignition source may be that the boundary layer compression, through the displacement thickness, produced a smaller pressure rise in the larger duct. In the small duct the gap between the injector and the wall is only 10 mm, allowing time for reflections of compression waves within the length of the injector. In the large duct this gap is increased to 22.5 mm and this would lead to a corresponding drop in pressure increase due to the boundary layer. The model was reassembled with a longer injector strut, to check if the extra boundary layer development would help with ignition. In this case also no combustion was observed.

Some apparent contradictions are evident in the supposed role the boundary layer is playing in the ignition process. In the small duct the longer injector strut was found to enhance ignition, whilst at the same time wall static pressures in the absence of injection were slightly reduced in the constant area section. This may perhaps be explained by noting that in supersonic flow strong transverse pressure gradients may exist in the flow, and that in the immediate vicinity of the injector the pressure may not have been reduced with the long strut. The high local pressure seen with the internal injector may have been due to the wave pattern from the injector leading edge, and might not apply on the centre line. Additionally the entrainment into the mixing layer of more heated gas may have enhanced ignition.

The failure of the long strut to induce ignition in the large duct is not understood at present. The small duct may have been just on the low pressure limit of combustion, and the reduced boundary layer compression in the large duct may have been just enough to quench the flame. To check this , the large duct was run with a 5 degree compression to increase the pressure and reduce the mach number slightly. Combustion was then achieved in

the large duct. It would appear that at the pressure levels currently achievable in the tunnel hypersonic combustion is only marginal. In this condition several effects, which might otherwise be of secondary importance, may be able to completely or partially prevent combustion. Further testing at higher pressures will be necessary to properly evaluate the significance of these effects. At the moment combustion chamber boundary layers appear to have a strong influence on combustion. It remains to be seen if this will still be the case when the experiments are scaled to larger dimensions and pressures.

In Fig 9 the results are presented in the form of specific impulse against stagnation enthalpy. This shows the hypersonic duct having a low temperature cut out at a higher enthalpy than the supersonic, as is to be expected from the lower static temperatures associated with higher mach numbers. It also shows that above an enthalpy of about 7 Mj/kg hypersonic combustion produces more thrust than supersonic. This is because hypersonic flow allows the combustion chamber static temperature to be kept in the region of peak specific impulse. The performance at the higher enthalpies is well below theoretical maxima, based on equilibrium combustion, but it is does demonstrate that at hypersonic combustion can under some circumstances be better than supersonic.

Conclusions.

Tests with a constant area duct show that hypersonic combustion is possible with central injection at static intake pressures of about 20 kpa. At stagnation enthalpies above 13 Mj/kg, corresponding to static intake temperatures of about 1900 K, no measurable combustion effects could be observed in comparison to the injection of helium at the same mass flow rate. At lower enthalpies significant heat release occurs, as evidenced by the static pressure rise in the duct. At the higher enthalpies the duct static pressure levels agreed well with non equilibrium nozzle flow calculations. At the lower enthalpies pressure levels agreed with calculations in the upstream sections of the duct, but increased further downstream, in some cases doubling the theoretical values. This rise is shown to be compatible with the presence of turbulent boundary layers in the duct, but should not be taken as confirmation of such a condition.

In the thrust producing mode values of specific impulse above 800 sec were measured. Combustion was observed in a diverging duct for conditions with static intake temperatures as low as 400 K, which would require some means of ignition enhancement. Viscous heating in the hypersonic boundary layer is proposed as a possible mechanism.

A comparison was made between supersonic (intake mach number 4 to 4.54) and hypersonic (intake mach number 4.8 to 6.3) combustion by means of an intake attachment made of symmetrical inclined wedges. Intake static pressure was maintained at the same approximate value of 20 kpa. Hypersonic combustion was shown to give improved performance at enthalpies above 7 Mj/kg. The specific impulse achieved correlated approximately to the intake static temperature rather than to mach number. The exception to this is in the low temperature cut off region where the hypersonic combustion shows a gradual reduction in thrust, compared to the sudden extinction shown in the supersonic case. Increased boundary layer heating in the hypersonic flow is suggested as a possible cause of this effect.

The flow conditions currently achieved by the tunnel appear to be marginal for hypersonic combustion. Small changes in model geometry can cause substantial reduction in the amount of heat release in the duct. In this regime the state of the combustion chamber boundary layers appears to have a strong influence on combustion, but it is not clear yet if this will still apply at higher pressures.

References

1. R.J.Stalker,R.G.Morgan.
"Supersonic Combustion with a Short Thrust Nozzle".
Journal of Combustion and Flame,Vol. 57, No. 1.
July 1984, pp 55-70.

2. J.A.Lordi, R.E.Mates, J.R.Moselle.
"Computer program for the numerical solution of non-equilibrium expansion of reacting gas mixtures".
NASA rep. NASA CR-472. 1966.

3. J.P.Drummond et al.
"Numerical study of scramjet engine flowfields".
AIAA Vol 20 No 9, pp 1182-1187.

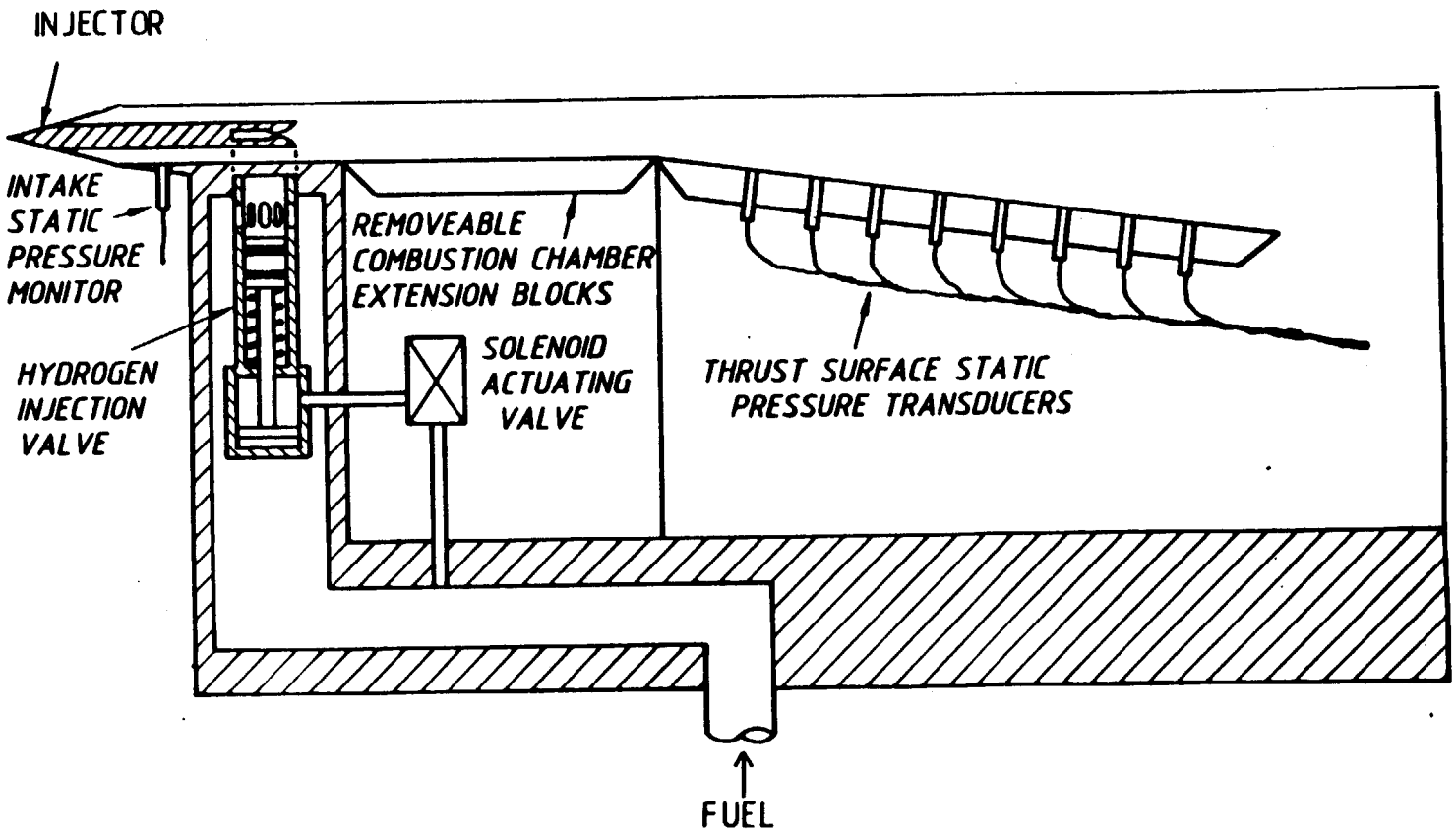

FIG 1 SCHEMATIC OF SCRAMJET MODEL

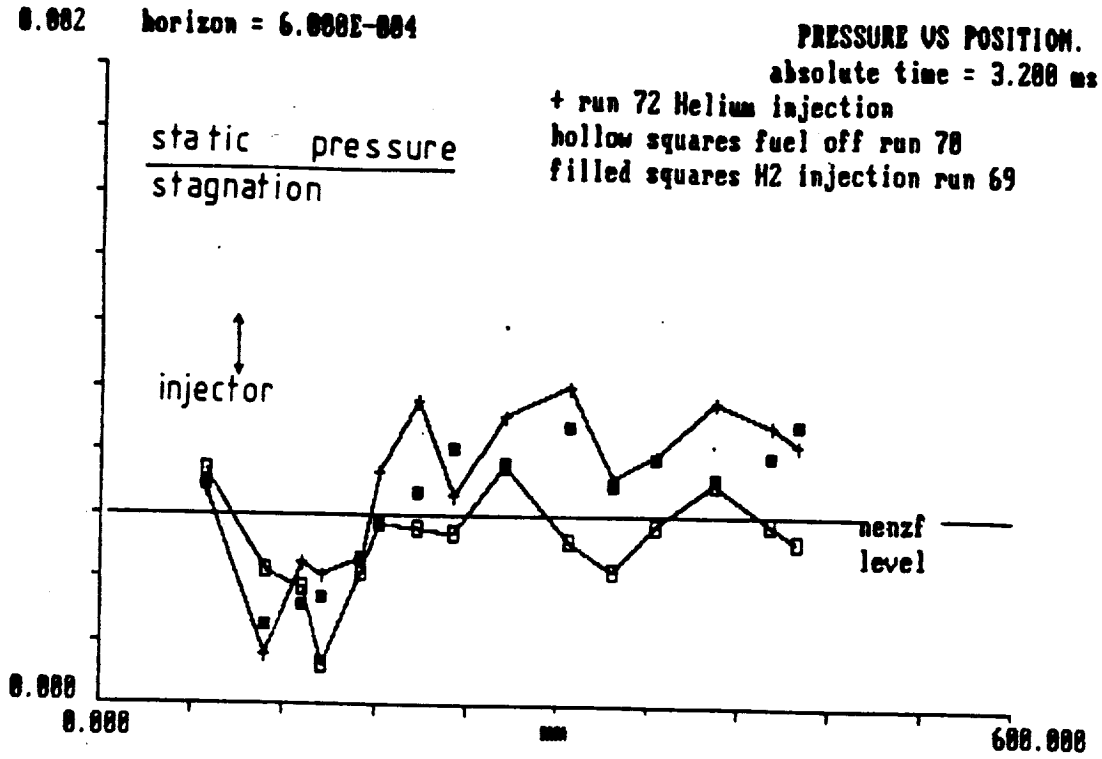

Fig 2 Constant area duct, helium and hydrogen injection stagnation enthalpy 26·5 Mj/kg

DATA FILE. s81
TEXT FILE. t81
NORM MOD/CHNL NUMBER.. 16/1

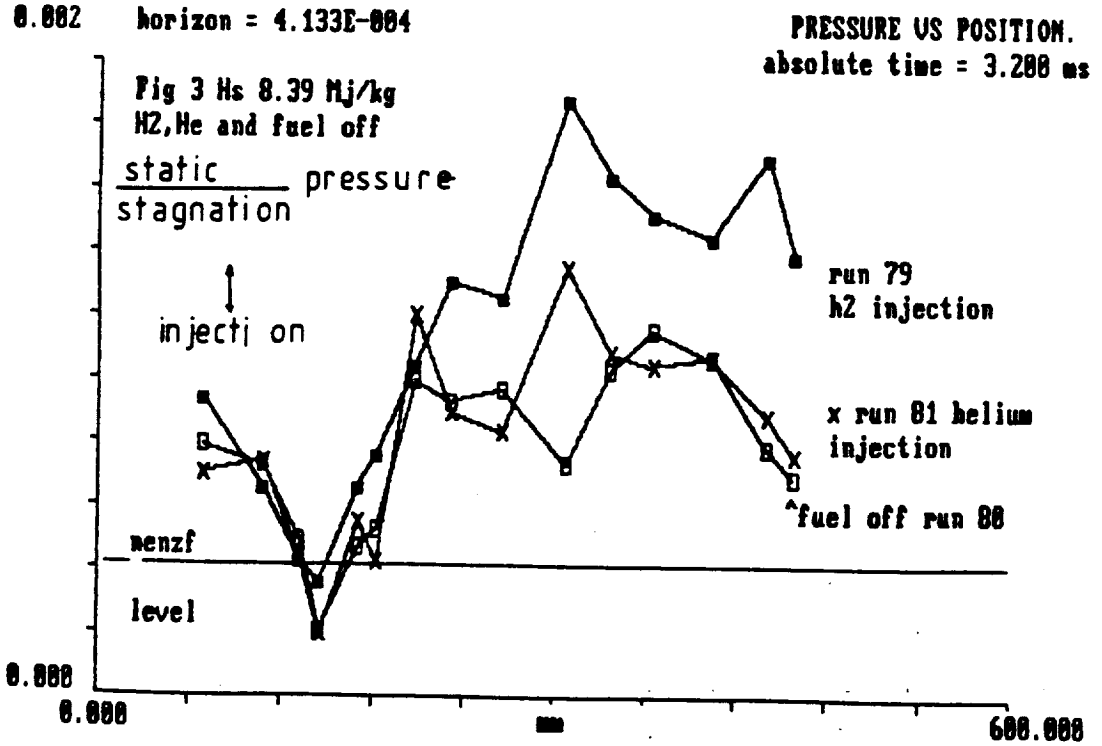

Fig 3 Constant area duct, helium and hydrogen injection stagnation enthalpy 8.39 Mj/kg

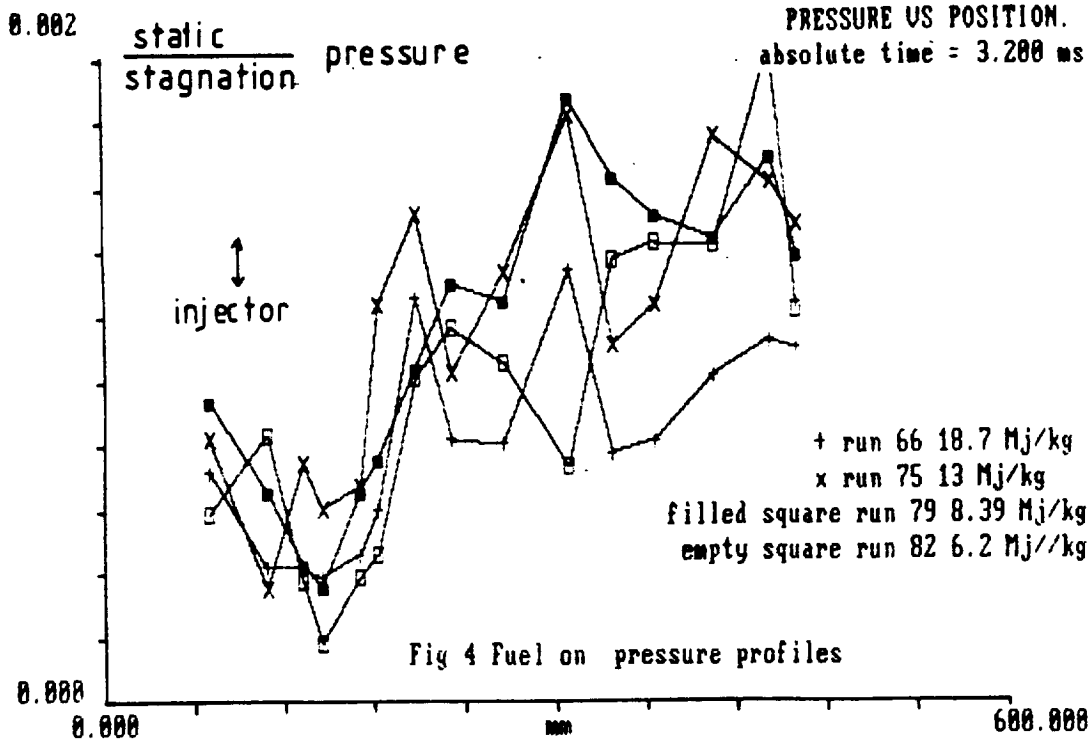

Fig 4 Normalised pressure profiles, constant area duct

DATA FILE. s75
TEXT FILE. t75
MODULE/CHANNEL NUMBER. 16/1

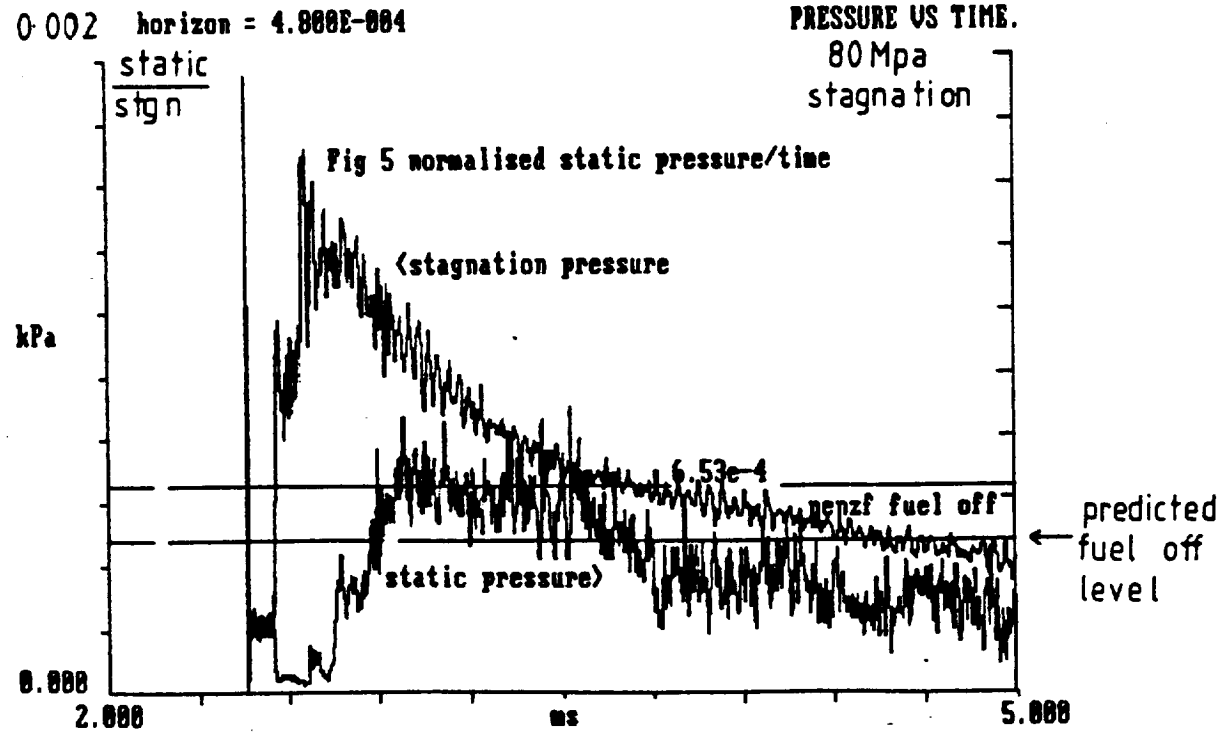

Fig 5 Typical normal ised pressure-time record

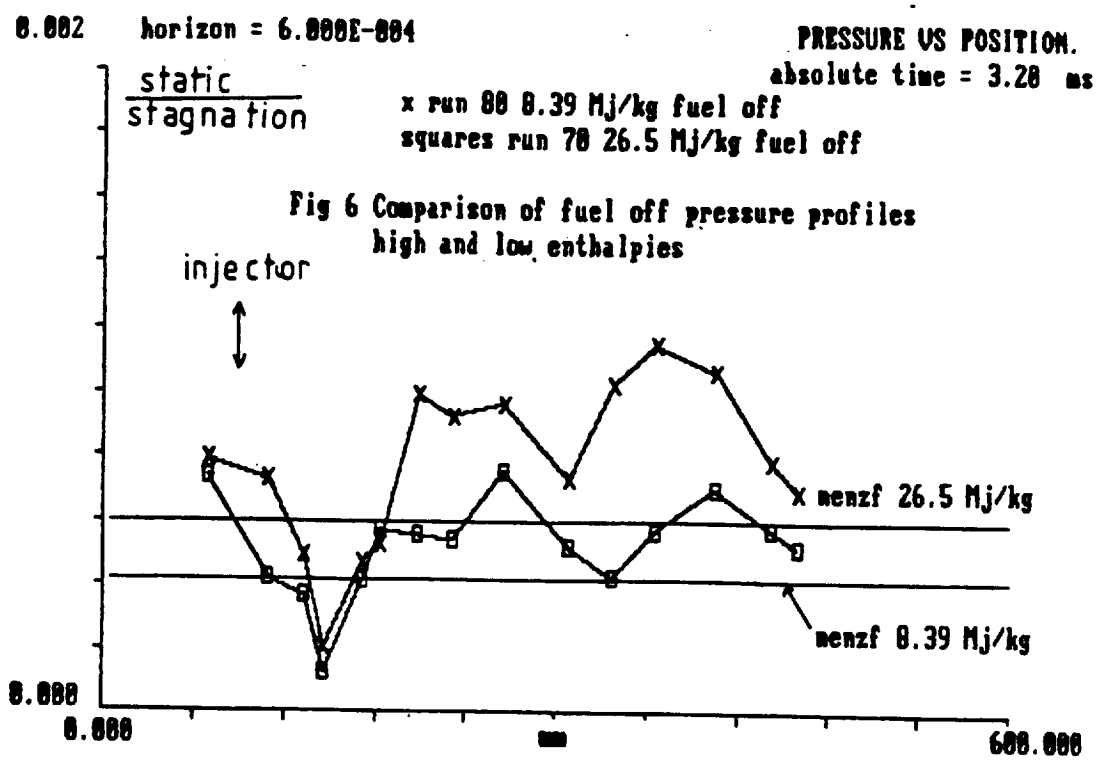

Fig 6 Effect of enthalpy on fuel off pressure constant area duct

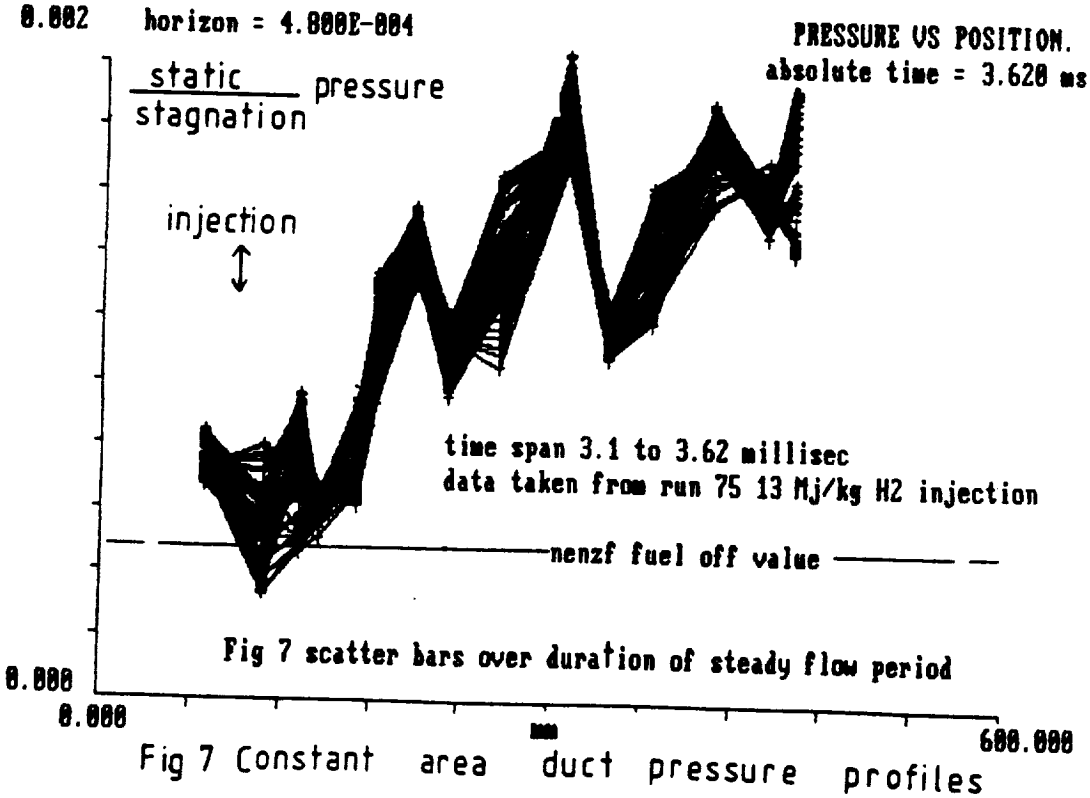

Fig 7 Constant area duct pressure profiles

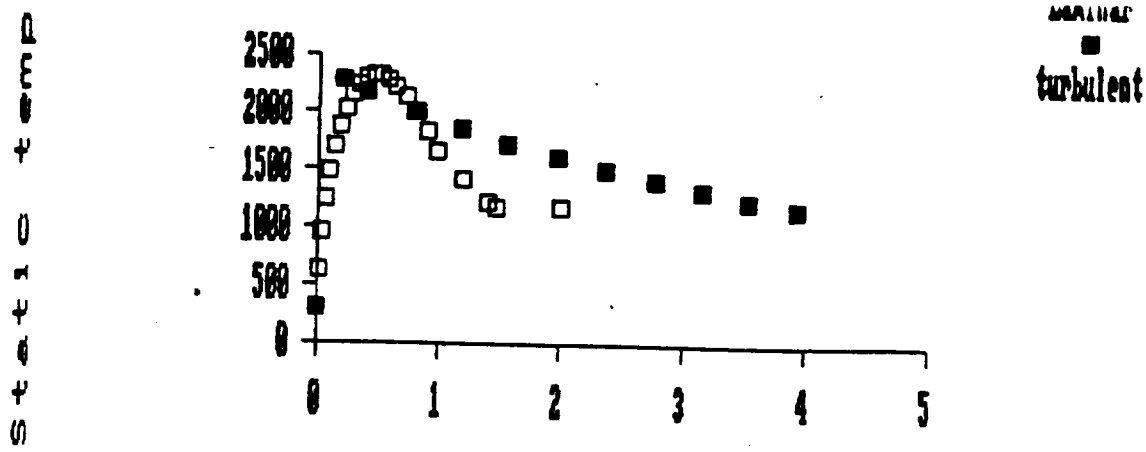

Fig 8 Computed boundary layers

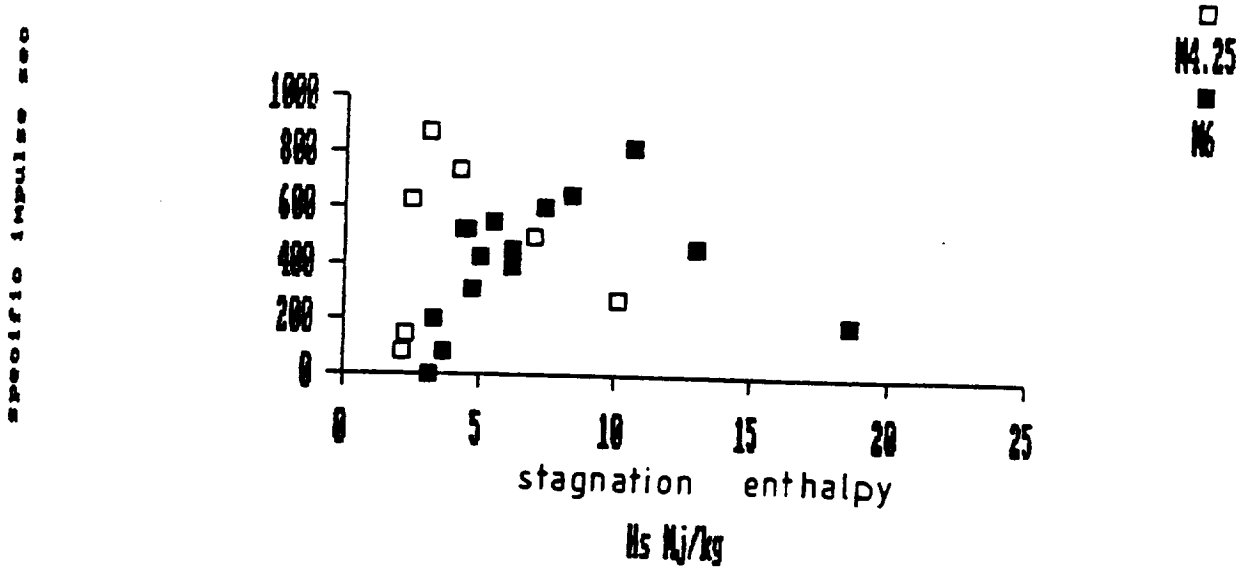

Fig 9 Super/hyper sonic combustion

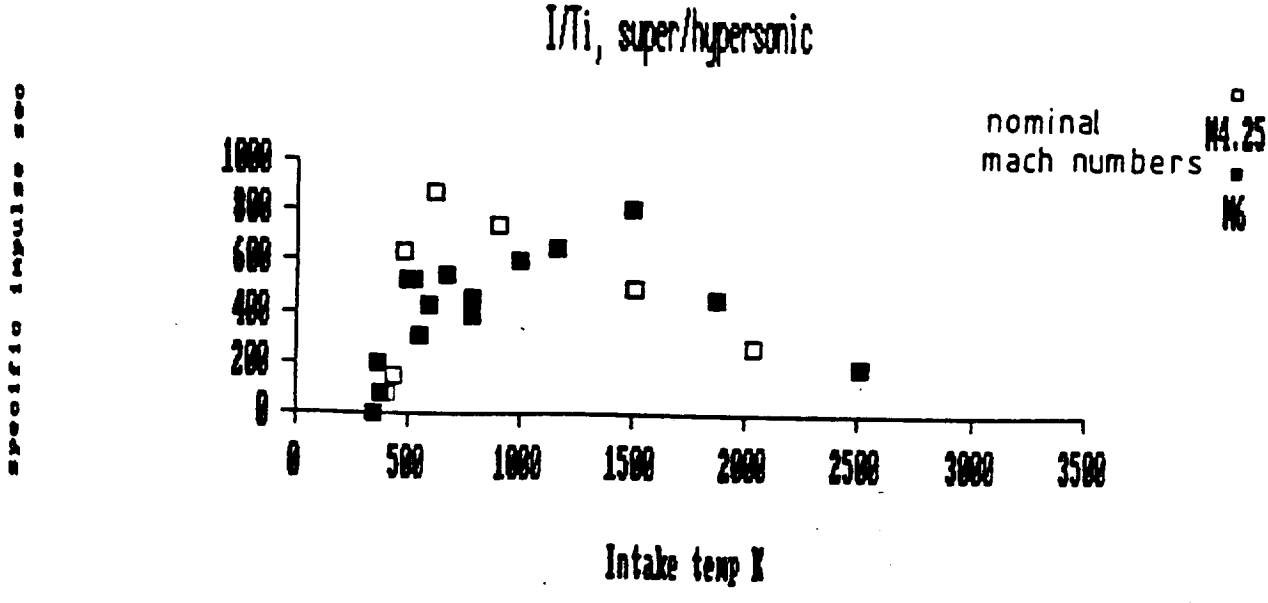

Fig 10 Comparison of super/hyper sonic combustion

Fig 11 density profiles

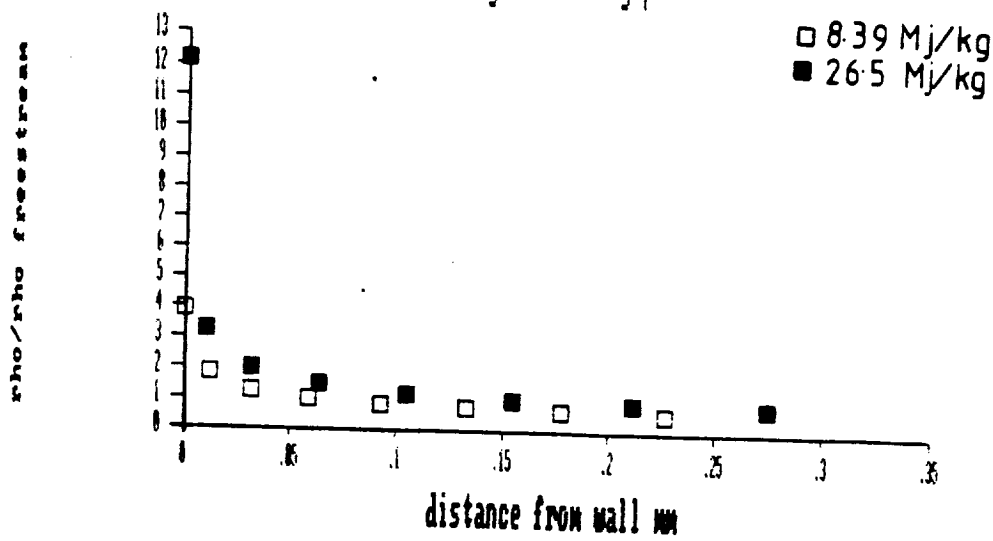

Fig 11 Computed laminar boundary layers

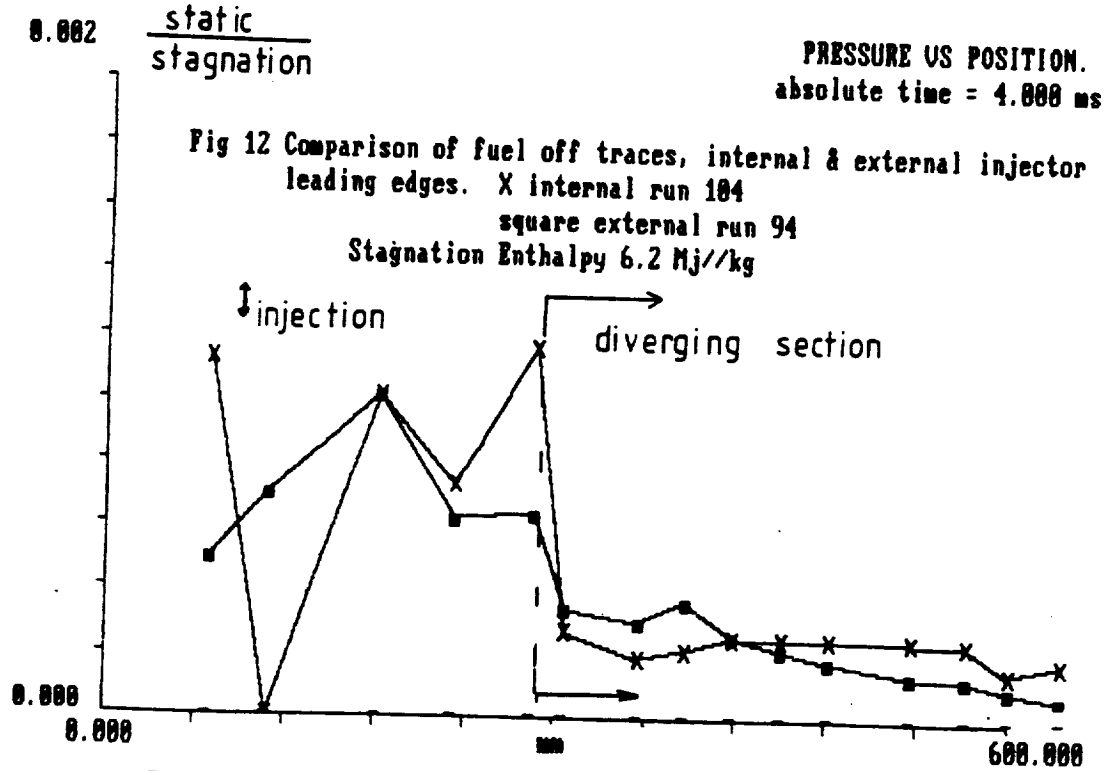

Fig 12 Effect of long and short injectors

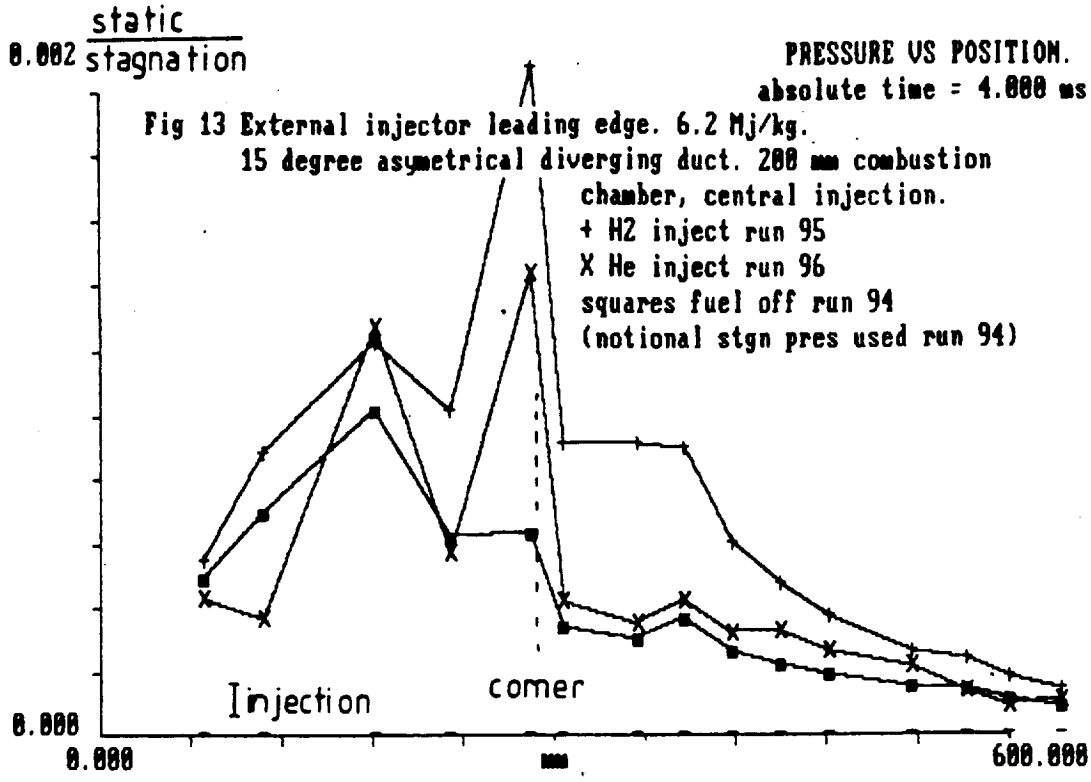
static
stagnation
0.002
PRESSURE VS POSITION.
absolute time = 4.000 ms
Fig 13 External injector leading edge. 6.2 Mj/kg.
15 degree asymetrical diverging duct. 200 mm combustion
chamber, central injection.
+ H2 inject run 95
X He inject run 96
squares fuel off run 94
(notional stgn pres used run 94)
Injection
comer
0.000
0.000
mm
600.000

Fig 13

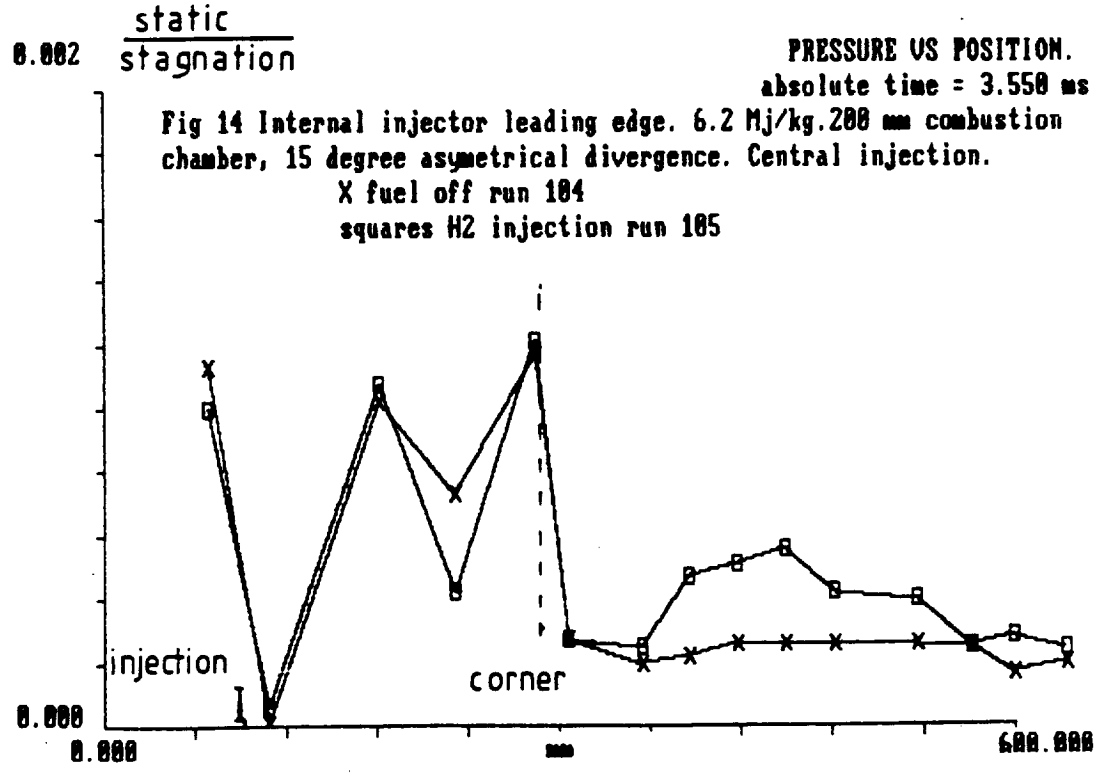
static
stagnation
0.002
PRESSURE VS POSITION.
absolute time = 3.550 ms
Fig 14 Internal injector leading edge. 6.2 Mj/kg.200 mm combustion
chamber, 15 degree asymetrical divergence. Central injection.
X fuel off run 104
squares H2 injection run 105
injection
corner
0.000
0.000
mm
600.000

Fig 14

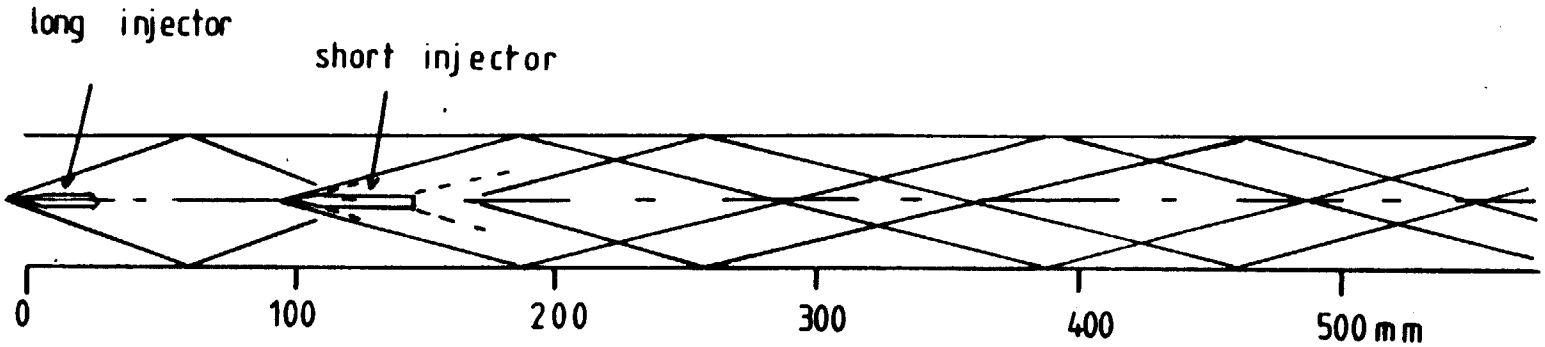

A. Square duct. Intake section 51 x 49·5 mm

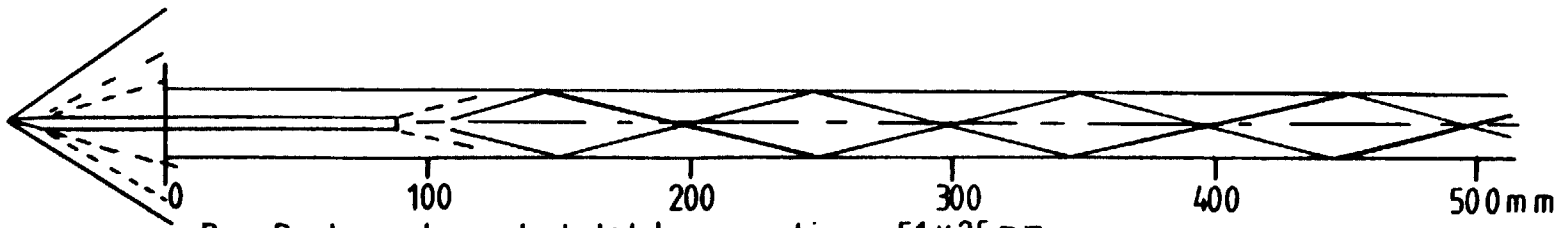

B. Rectangular duct. Intake section 51 x 25 mm
long injector fitted

Fig 16 Approximate path of compression waves

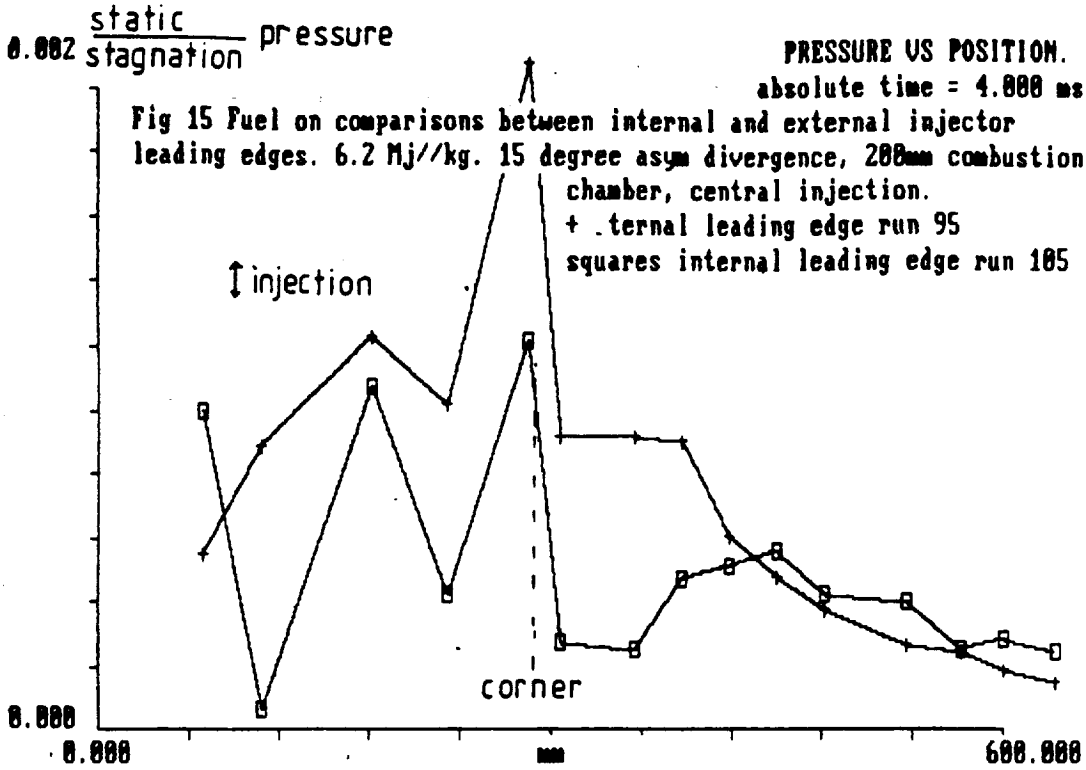

Fig 15

DATA FILE. s294
TEXT FILE. t294
NORM MOD/CHNL NUMBER.. 16/1

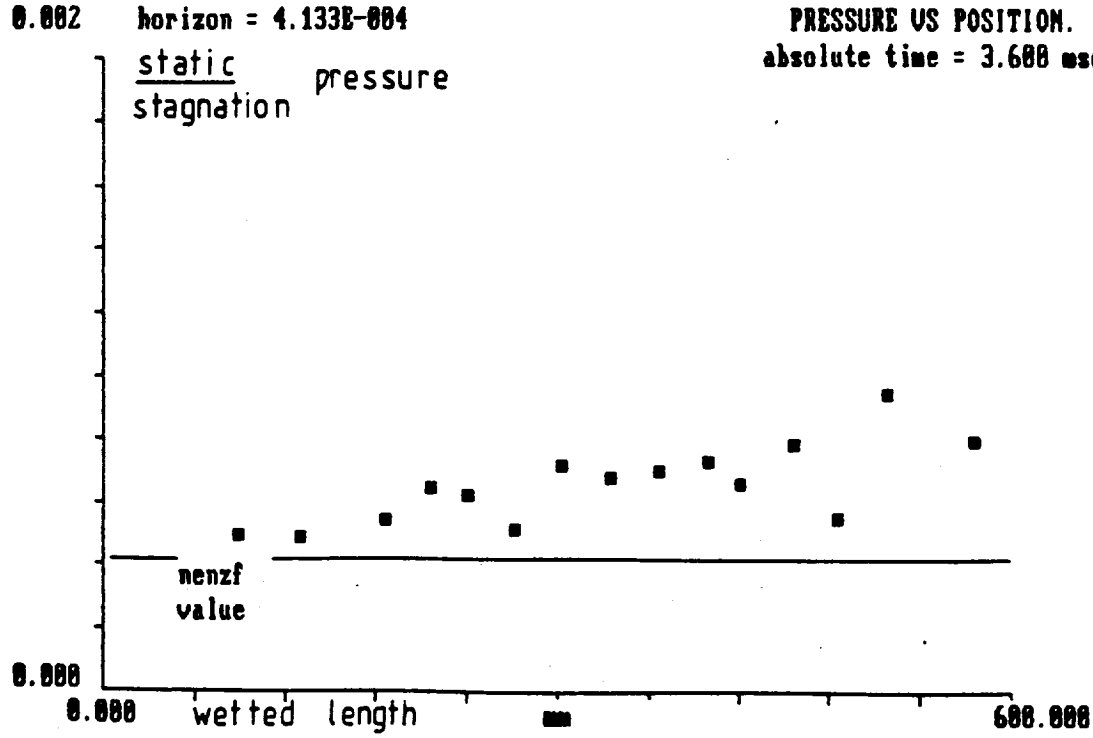

Fig 17 Square duct. Injector removed

1 Table 1,M5 nozzle,4mm diaphragm;nozzle exit conditions without scoops,56.6 Mpa rupture (S)/p

Hs Mj/kg	shock tube fill kpa	shock speed km/sec	Prupt /Pshock	stagnatio pressure Mpa	Mach number	static pressure kpa	static temp K	rho kg/m**3	velocity km/sec	Reynolds no (1e6/m)	H2 inj phi=1	computed by program
26.54	20	5.17	2830	37	4.80	22.29	3642	1.77E-2	6.09	1.26	118	estc/nenzf
23.16	25	4.83	2264	39	5.07	20.71	2975	2.07E-2	5.76	1.55	131	estc/nenzf
20.74	30	4.58	1886.67	40	5.19	20.20	2650	2.32E-2	5.49	1.77	140	estc/nenzf
18.67	40	4.33	1415	48	5.18	24.31	2516	3.03E-2	5.24	2.31	174	estc/nenzf
12.98	80	3.71	707.50	48	5.25	23.20	1874	4.12E-2	4.47	3.09	202	estc/nenzf
10.60	120	3.30	471.70	49	5.40	22	1500	5.20E-2	4.05	4	220	interpolated
8.39	163.50	3.03	346.18	50	5.54	20.50	1164	6.09E-2	3.70	4.96	248	estc/nenzf noneq
7.40	200	2.85	283	50	5.65	20	995	6.97E-2	3.49	5.88	267	estc/nenzf noneq
6.20	256	2.62	221.09	50	5.81	18.40	785	8.11E-2	3.22	7.29	287	estc/nenzf noneq
5.49	300	2.46	186.67	52	5.92	18.10	668	9.38E-2	3.04	8.82	313	estc/nenzf noneq
5	350	2.36	161.71	52	6	17.40	592	1.02E-1	2.91	9.93	326	estc/nenzf noneq
4.73	375	2.28	150.93	54	6.04	17.70	551	1.11E-1	2.83	11	345	estc/nenzf noneq
4.57	400	2.25	141.50	54	6.09	17.40	526	1.15E-1	2.79	11.60	352	estc/nenzf noneq
4.36	450	2.18	125.78	60	6.12	19	496	1.33E-1	2.73	13.70	399	estc/nenzf noneq
3.68	550	1.99	102.91	60	6.30	17.30	379	1.58E-1	2.46	17.70	427	estc/nenzf noneq
3.31	600	1.91	94.33	60	6.30	18	365	1.65E-1	2.43	18.70	440	shock
3.17	650	1.86	87.08	63	6.30	18.20	347	1.80E-1	2.38	20.80	471	shock

2 Table 3,M5 nozzle exit conditions,7.5 scoops 1 mm diaphragm;rupture pressure 14.5 Mpa (S)/p

Hs Mj/kg	shock tube fill kpa	shock speed km/sec	P rupt /P shock	stagnatio pressure Mpa	Mach number	static pressure kpa	static temp K	rho kg/m**3	velocity km/sec	H2 inj phi=1 kpa	computed by program
10.10	20	3.33	725	7.80	4.01	18.50	2040	2.96E-2	3.75	122	nenzf/oblique
7	40	2.77	362.50	9.50	4.08	21.90	1510	4.96E-2	3.21	175	nenzf/oblique
4.32	80	2.17	176	10.50	4.30	21.90	863	8.79E-3	2.54	245	nenzf/oblique
3.05	120	1.84	118	10.50	4.44	21.50	613	1.21E-1	2.21	294	shock/oblique
2.45	160	1.64	88	10.50	4.49	20.90	477	1.52E-1	1.97	328	shock/oblique
2.27	180	1.58	78	10.50	4.52	20.60	435	1.64E-1	1.90	341	shock/oblique
2.16	200	1.55	70	10.50	4.54	20.20	407	1.72E-1	1.84	347	shock/oblique

1 Table 4,4 mm diaphragm;test results for no scoop,internal injector,56.6 Mpa rupture 1.6 mm central,injector (S)/p

200mm combustion chamber, 15° divergence

Run number	Hs Mj/kg	shock tube fillpressure kpa	stagnatiotemp Mpa	intake K	intake pressure kpa	H2 injection kpa	phi	thrust/ stagn n/kpa	Max thrust N	net thrust N	specific impulse sec	comments
191	18.67	40	48	2516	24.30	207	1.19	1.75E-6	64.90	12	185	
193	18.67	40	48	2516	24.30	0	0		46.10			
190	12.98	80	48	1874	23.20	237	1.17	2.32E-6	90.10	35	457	
194	12.98	80	48	1874	23.20	0	0					
192	10.60	120	49	1500	22	234	1.06		114	62	819	
196	10.60	120	49	1500	22	0	0		52.10			
121	8.39	163.50	50	1164	20.50	240	.97	2.57E-6	103.20	50.70	653	
123	8.39	163.50	50	1164	20.50	0	0	1.32E-6	52.50			
122	7.40	200	50	995	20	243	.91	2.41E-6	99.80	47.30	602	
103	6.20	256	50	785	18.40	237	.83	2.97E-6	111.80	65.50	845	unsteady
104	6.20	256	50	785	18.40	0	0	1.21E-6	46.30			
105	6.20	256	50	785	18.40	157	.55	1.72E-6	69.30	23	453	
107	6.20	256	50	785	18.40	300	1.05	1.93E-6	84.10	37.80	390	
108	6.20	256	50	785	18.40	328	1.14					very unsteady
109	5.49	300	52	668	18.10	241	.77	1.99E-6	88.90	42.60	547	
111	5	350	52	592	17.40	231	.71	2.04E-6	78.20	31.90	427	
112	4.73	375	54	551	17.70	227	.66	1.72E-6	68.70	22.40	305	a little unstead
110	4.57	400	54	526	17.40	232	.66					very unsteady
114	4.57	400	54	526	17.40	240	.68	2.08E-6	86.80	40.50	522	
115	4.36	450	60	496	19	235	.59	2.13E-6	86.10	39.80	524	
117	4.36	450	60	496	19	0	0	1.31E-6	47.90			
118	3.68	550	60	379	17.30	237	.56	1.71E-6	53.70	5.80	76	
119	3.31	600	60	365	18	228	.52	1.73E-6	62.90	15	196	
120	3.17	650	63	347	18.20	183	.39	1.76E-6	44.10	0	0	

4 Table 5,7.5 scoop,1 mm diaphragm rupture 14.5Mpa,15 deg asym;experimental results (S)/p

200 mm combustion chamber,15° divergence

Run number	Hs Mj/kg	shock tube fillpressure kpa	stagnatiotemp Mpa	intake K	intake pressure kpa	H2 injection kpa	phi	thrust/ stagn n/kpa	Max thrust N	net thrust N	specific impulse sec	comments
182	10.10	20	7.80	2040	18.50	171	1.40		61.90	14.70	266	
183	10.10	20	7.80	2040	18.50	0	0		42.50	0		
181	7	40	9.50	1510	21.90	181	1.03		78	29.20	499	
180	7	40	9.50	1510	21.90	0	0		47.20	0		
165	4.19	80	10.50	899	22.60	0	0	6.40E-3	44.10			
166	4.19	80	10.50	899	22.60	200	.82	1.17E-2	92	47.90	740	
167	3.05	120	10.50	613	21.50	219	.75	1.27E-2	106	62	875	
169	2.45	160	10.50	477	20.90	200	.61		120	76	1200	unsteady
173	2.45	160	10.50	477	20.90	0	0		44.70			
176	2.45	160	10.50	477	20.90	0	0		48.90			
177	2.45	160	10.50	477	20.90	239	.73		93.60	46.90	633	
172	2.27	180	10.50	435	20.60	207	.61		53.60	9.50	142	
170	2.16	200	10.50	407	20.20	205	.59		49.20	5.10	77	

HYDROGEN SCRAMJET WITH SIDEWALL INJECTION

SHOCK TUNNEL SIMULATIONS

R.G. Morgan, A. Paull, N. Morris, R.J. Stalker

HYDROGEN SCRAMJET WITH SIDEWALL INJECTION.

SHOCK TUNNEL SIMULATIONS.

R.G.Morgan*.A.Paull.N.Morris.R.J.Stalker.
Department of Mechanical Engineering.
University of Queensland.
St Lucia. Queensland. 4067.

ABSTRACT.

This paper presents the results of experiments on a scramjet combustion chamber with sidewall injection performed in the free piston shock tunnel, T3, at the Australian National University. A two dimensional model was used with provision for parallel and transverse injection. The results indicated that combustion was strongly influenced by a region of fuel whose temperature was held below its ignition temperature by wall cooling effects. This leads to a large amount of unburned fuel, and produces a significant drop in specific impulse. This is a feature of shock tunnel experiments with cold walls which would not necessarily apply to a flight situation, where aerodynamic heating would keep the walls above the hydrogen ignition temperature. Maximum specific impulse was produced by using a combination of parallel and transverse injection in a long combustion chamber followed by a dual stage expansion. The presence of a layer of fuel attached to the wall was seen to significantly reduce the surface heat transfer rates, indicating the potential for weight savings because of reduced thermal insulation requirements. However, this effect may be dependent on the wall quenching layer and might not apply to a flight situation.

INTRODUCTION.

Scramjets potentially represent the most attractive form of propulsion for high altitude and Mach number flight in the upper atmosphere, down to the point where subsonic combustion becomes more efficient at about Mach 4, Ref (1). Due to the high flight speeds involved, considerable aerodynamic heating of the exposed surfaces occurs. Active cooling of these surfaces will be required in the ducted sections of the engine where radiative cooling cannot be used. Liquid hydrogen is carried on the craft as a fuel, and is therefore the most suitable coolant.

Studies have shown , Ref. (2), that the hydrogen required for propulsion is adequate to meet the cooling requirements up to flight speeds of Mach 10. Above this speed additional hydrogen, or some other coolant, must be carried in order to maintain a heat balance at reasonable surface temperatures. This weight penalty would reduce the useful payload of the craft, and therefore engine design must aim to reduce heating loads wherever possible.

A particular heat transfer and materials problem is presented by the construction of the fuel injection system itself. From a combustion point of view, an injector strut projecting into the flow is desirable, as this maximises mixing and fuel heating rates by providing two fuel air interfaces. However the total heat input to the strut is high because it is heated from two surfaces. The strut would be made as thin as possible to minimise drag, and this would compound the problem of removing the heat by means of a coolant.

Cooling requirements are considerably alleviated for the wall injector because there is only one heating surface, and there is not the same space restriction for the coolant passages. At Mach numbers above 10 hydrogen in excess of propulsion needs must be carried, and this will be ejected unburned from the craft. If wall injectors are used then the excess hydrogen will form an unburned layer attached to the wall, and this will provide further thermal protection.

The reduced cooling requirements of wall injection will be of little use if it does not perform well in the thrust producing mode. There is now considerable experimental data available for injection struts, and a basic understanding has been obtained about the associated thrust producing mechanisms. Ref. (3) has studied large scale models up to flight speeds of 2.2 km/s in blow down tunnels, and Ref. (4) has done shock tunnel studies up to 5.5 km/s.

A program of experimental research into wall injection was started in 1985 under contract to the NASA Langley Research Center. The preliminary results of this work were presented in Ref. (5), using a simple geometry with the thrust surface formed behind a single Prandtl Meyer expansion fan. Two effects were noticed which lead to reduced performance compared to central, strut mounted injectors.

Firstly, with the mixing and combustion zone being attached to the wall, net thrust due to expanding the combustion products

* Senior Lecturer, Mechanical Engineering, Member AIAA.
● Senior Research Assistant, Mechanical Engineering.
– Research Assistant, Mechanical Engineering.
■ Professor, Mechanical Engineering, Member AIAA.

was only developed over a small section of the thrust surface for the short combustion chamber studied.

Secondly, reduced combustion was observed, and the existence of a quenched layer of fuel attached to the wall was postulated as an explanation for this effect. No combustion at all could be achieved below an equivalence ratio of about 1.5. When more hydrogen was injected it would burn well, but the heat release obtained indicated that the hydrogen in the immediate vicinity of the wall was still unburned. This lead to low values of specific impulse.

In the light of these results a further series of tests were performed, designed to optimise specific impulse within the limitations of models with cold walls and partially quenched mixing layers, and to gain an understanding of thrust production mechanisms in this configuration.

By means of two stage expansions in the exhaust nozzle, extended combustion chambers and a combination of parallel and transverse injection it was possible to increase the thrust and specific impulse developed. However the quenching effect of having the combustion zone attached to the wall was still found to be predominant, and only small improvements were observed. Wall injection of silane, which is able to burn spontaneously at room temperature, was used to confirm that the lack of combustion with pure hydrogen was indeed due to thermal effects.

The thermally quenched mixing layer is not expected to be a problem in a flight situation with aerodynamically heated walls, and several means of making shock tunnel testing more representative are available. These include the addition of a small amount of silane to the fuel, preheated fuel, and preheated walls.

EXPERIMENTAL APPARATUS.

The experiments were performed in a two dimensional model chosen to follow as closely as possible the dimensions of a previous model with a central injector strut. A schematic of the model is shown in fig 1. Injection was from behind a 5 mm step in the wall. The height of the step was identical to the thickness of the central injector strut in order to give realistic comparisons between the two geometries. The construction of the injector is shown in Fig 2. Equivalence ratio was controlled by means of interchangable throat blocks, and injection Mach number was set by the hydrogen reservoir pressure. Throat blocks were available to produce a parallel jet, and jets inclined at 7.5 and 15 degrees to the intake flow. In a slight departure from two dimensional flow, there was provision for a combination of transverse and parallel injection by means of a series of holes drilled at 45 degrees to the flow and pointing downstream.

The injector was followed by a parallel section, the length of which could be varied between 25 and 150 mm. The exhaust nozzle of the combustor consisted of flat thrust surfaces, with provision for staged expansions and variable divergence angles.

Thrust and heat transfer were measured by means of transducers mounted on the intake and on the thrust surfaces. The shock tunnel was operated in the reflected shock mode, with a mach 3.5 contoured nozzle creating conditions appropriate to the intake of a scramjet combustion chamber. The experimental apparatus and procedure is described more fully in Ref (4).

MECHANISMS OF THRUST PRODUCTION.

Combustion produces heat release in the flow field, which can in turn produce increased thrust in the expansion nozzle. There are two mechanisms by which thrust is transmitted from the burning jet to the walls of the model. Compression waves from the two mechanisms are shown schematically in fig 3.

Firstly, the heat release causes the burned gases to expand, and this sends compression waves through the rest of the flow. The waves reflect off the model walls, causing increased local static pressures and a corresponding increase in thrust.

Secondly, the fuel jet creates a region of lower Mach number, due to the increased speed of sound after combustion, and when this low Mach number zone is subsequently expanded in the nozzle it will experience a smaller pressure drop than the high mach number freestream or the fuel off flow. The pressure mismatch creates compression waves in the freestream and expansion waves in the fuel jet. When the compression waves reach the wall they create a region of increased surface pressure, and hence a thrust increment. This mechanism of thrust production is subsequently referred to as the expansion interaction effect. If the jet Mach number drops below 1.41 then the

effects are reversed. with expansion waves in the freestream and compressions in the jet.

For central injection the low mach number region is in the middle of the duct. and the thrust generated by the expansion interaction mechanism is realised at some distance downstream of the corner. For wall injection the low mach number flow is attached to the wall. and thrust is generated in the region immediately downstream of the corner. until the point where the pressure differential between the burnt gases and the freestream is eliminated. The thickness of the fuel/air jet determines the distance over which thrust is developed by the interaction mechanism. Wall injection is limited in comparison to central injection because the mixing layer has only one fuel air interface. and consequently would not be expected to develop so rapidly. Also the distance required for the expansion to propagate from the corner to the jet permits extra mixing with central injection.

RESULTS.

Extra length in the combustion chamber before expanding the flow may be expected to allow the mixing layer to spread further from the wall across the duct, producing more thrust upon expansion of the jet. A weight penalty would be associated with the longer combustion chamber, and it is advantageous to start expanding the flow as soon as possible after injection. However, expansion of the jet before complete combustion is achieved can have a quenching effect on the flame, and it also slows down the spread of the jet across duct. The optimum configuration of combustion chamber and expansion nozzle is likely to be a compromise between these two effects.

It was noted in previous experiments that the thrust produced by wall injection was not very sensitive to the thrust surface divergence angle when the expansion / jet interaction is absent. This applies to short combustion chambers which do not allow for significant propagation of the mixing layer from the wall. It was therefore decided to construct a combustion chamber with a 2 stage divergence.

The first stage includes a thrust surface inclined at 4 degrees to the intake flow. This geometry was shown in Ref 5 to produce significant thrust due solely to compressions from the burning fuel jet. Because only a small pressure drop is associated with a 4 degree expansion . it was hoped that the jet would continue to mix and react and spread across the duct in the first thrust producing stage. When the jet is subsequently expanded by the second stage its thickness should be such that substantial thrust could be produced by the expansion interaction method.

The advantage over a single expansion of 15 degrees is twofold.
Firstly , if the full 15 degrees expansion is introduced too early, no further combustion will take place. By limiting the initial expansion to 4 degrees, thrust may be developed in a region that is still supporting combustion.

Secondly, the final expansion takes place at a point where the jet has had time to spread away from the wall, and this gives potential for increased thrust from the expansion interaction effect.

Short combustion chamber.
Two stage divergence.
The initial series of tests was done with the model configured as shown in Fig 3 with a 25 mm length of constant area duct after injection before the start of the 4 degree diverging section.

In Fig 4 the results of the dual stage divergence are compared to previous data for a single thrust surface with 15 degrees divergence. It is seen that at an enthalpy of 8.7 MJ/kg no improvement in performance was produced.

In Fig 5 the pressure against distance profiles are shown. It is seen that despite significant heat release in the 4 degree section, as shown by the pressure rise above fuel off levels, very little net thrust is developed on the downstream thrust surface.

At an enthalpy of 4.2 MJ/kg no improvement in specific impulse was produced, as can be seen from Fig 4 b. However it can be seen from Fig 5 b that the effects of the reduced divergence are just beginning to be felt in the form of combustion induced pressure rises towards the downstream end of the first thrust surface. This would suggest that somewhat more distance for combustion was required before the start of the 15 degree section. Consequently the two stage thrust surface was then used with an extended combustion chamber, although this does to a certain extent defeat the purpose of the two stage expansion, which is to obtain thrust in all sections where the fuel is burning.

Long combustion chamber, 4/15 degrees divergence.

At an enthalpy of 8.7 MJ/kg no improvement was produced by the extra mixing length, as may be seen by comparing Figs 6a and 4a for specific impulse, and Figs 7a and 5a for P/X dependence.

At 4.2 MJ/kg a noticeable improvement in performance was gained by adding the combustion chamber extension. This is shown both by the increased value of specific impulse , Fig 6b , and also by the development of net thrust on the second thrust surface, Fig 7b.

It would appear that at the higher enthalpy condition ,8.7 MJ/kg , the temperature after the initial expansion of 4 degrees is sufficiently high to produce rapid combustion , and the heat release is only limited by the quenched zone attached to the wall. The addition of extra combustion chamber length does not change this, and no increase in the difference between fuel on and fuel off was observed, as may be seen by comparing Figs 5a and 7a.

However at the lower enthalpy condition , 4.2 MJ/kg , it is seen in Fig 5b that without the combustion chamber extension significant heat release only occurs towards the end of the 4 degree section , and not much net thrust is produced on either surface. This is thought to be due to the longer ignition delay at the lower temperature. In this case ,when a longer combustion chamber was used, ignition occurred upstream of the first expansion , and increased thrust was developed on both surfaces, as seen in Fig 7b.

A similar effect has previously been observed with central injection. Ref 9 , where increasing combustion chamber length is only beneficial at the lower enthalpies. This may also be true for wall injection.

Transverse and parallel injection.

In an attempt to improve the performance of the wall injected scramjet , a modified injector was constructed with transverse holes as well as the parallel injection throat. It was hoped that the transverse momentum of the jets would carry some of the fuel through the boundary layer and away from the quenching effect of the wall, and would also increase the mixing rates.

A schematic of the injector is shown in Fig 8. It consists of a series of holes drilled at 45 degrees to the flow and pointing downstream. The percentage of transversely injected hydrogen was controlled by changing the throat of the parallel injector, and setting the hydrogen reservoir pressure to give the required total equivalence ratio. Transverse hydrogen mass flow rates equal to 27% and 79% of that passing through the parallel injectors were produced for the 0.9 mm and the 0.1 mm throats respectively. No other combinations were used.

Reduction of the size of the quenched zone would be evident in the form of increased values of specific impulse, and also combustion would be possible at lower values of equivalence ratio.

Combustion in a scramjet using fuel from a room temperature reservoir requires heating of the fuel to its' ignition temperature by transfer of heat from the free stream. In the wall injection case this flow of heat is partially offset by the flow of heat to the wall, and is also limited by only having one fuel air interface, as opposed to two for central injectors. In the two dimensional configuration the area for heat transfer from the flow to the jet is equal to the area for transfer from the jet to the wall, and this limits the temperature which may be achieved in the jet. However a circular jet propagating transversely across a duct will have a much larger area exposed to the flow , and may be expected to get hotter.

Transverse injection, long combustion chamber.

In Fig 9 the results of transverse injection with an extended combustion chamber are shown.

Transverse injection at the 8.7 MJ/kg enthalpy condition again gives no improvement over any of the other results, except at low values of equivalence ratio. Combustion with transverse injection occurred at lower equivalence ratios than was possible with parallel injection alone. This is indicated by the two points on Fig 9a at equivalence ratios of 0.83 and 1.11. This would suggest that above a certain fuel injection pressure the transverse jets are to some extent penetrating the boundary layer, and burning at lower equivalence ratios than is possible for wall injection. However, the heat release from this combustion is not reducing the size of the quenched zone in the parallel injected component, and so no increase in specific impulse is observed at higher equivalence ratios.

Also shown on Fig 9a is a data point obtained by injecting Helium instead of hydrogen. This was done for selected

conditions, together with the injection of hydrogen into nitrogen test gas, to separate the effects of combustion from the physical presence of a jet of foreign gas in the flow. In this case a genuine combustion effect appears to be present as the hydrogen is producing significantly more specific impulse than the helium gas.

At 4.2 MJ/kg combustion at low equivalence ratios is again observed. In addition there also appears to be significant improvement in performance in the equivalence ratio range of 1 to 2.5 , as may be seen from Fig 9b. Also shown on this figure are the results of 4.2 MJ/kg tests with a transverse component equal to 79% of the parallel injection, the only condition for which this was done. This shows no improvement over the 27% case. It had been hoped that a larger proportion of transversely injected fuel would lead to more combustion, and higher specific impulse. This effect would seem to indicate that the transverse jets are not penetrating very far into the flow, and are still restricted by wall quenching.

Further evidence of this is given in Fig 10, which compares the wall pressure and temperature profiles for a single 15 degree expansion at an enthalpy of 6.1 MJ/kg for parallel and 27% transverse injection. No difference is apparent between the pressure traces , and only a slight increase in heat transfer with transverse injection was observed. Both tests were taken at an equivalence ratio of about 2, where no thrust increment was observed with transverse injection. A more significant result would be at equivalence ratios of order one where the transverse injection appears to be effective, but no heat transfer data was taken at those conditions.

It is possible that the transverse jets also require a layer of fuel as a thermal buffer to insulate them from the wall, and if this is not supplied by the parallel jet then more of the transverse component will be quenched. Another factor which may be significant is the effect of the expansion from the trailing edge of the injector. The strength of this expansion is dependent on the amount of fuel injected through the parallel throat. Less fuel from the parallel throat would lead to a stronger expansion and a region of cooler fuel downstream of the injector.

WALL INJECTION OF SILANE.

The presence of the cold model walls represents a sink of heat to the flow, because in the short duration of the tests the wall temperature does not rise significantly above ambient. The cooling effect of the wall penetrates a significant distance into the flow. With central injection this does not have a critical effect on the development of combustion.

However, when the fuel is injected from the wall in shock tunnel testing, there is always a region whose temperature will be held below the ignition temperature, regardless of how much combustion may take place further away from the wall. The hydrogen contained in this low temperature region appears to correspond to an equivalence ratio of approximately 1.5, because no ignition at all is possible at lower equivalence ratios. This represents a serious defect in the ability of shock tunnel tests to accurately model a real flight situation with aerodynamically heated walls.

The fuel in the quenched region may be mixed with oxygen, with only the low temperature inhibiting combustion. To confirm that this is indeed the case, and that the lack of combustion is not the result of some other cause, a test was done with the injection of a 20% silane hydrogen mixture.

The fuel was injected at an equivalence ratio of 0.5 into a flow of enthalpy 4.2 Mj/kg. With hydrogen injection alone no combustion would be expected at this condition. The results of this test are shown in Fig 11, and it can be seen by the pressure rise above the fuel off levels that it burnt well.

This result is significant in that it demonstrates that oxygen is diffusing to the fuel layer close to the wall, and that it is thermal effects which are preventing it from burning. This gives encouragement to efforts which are currently being made to design a model which can use heated fuel, and possibly even heated walls. It also suggests that in the absence of the above, silane might be used to investigate other aspects of combustion which are difficult to study properly in the presence of an extensive layer of quenched fuel.

CONCLUSIONS.

Significant combustion was achieved in a scramjet with wall injection, but the presence of cold walls lead to the quenching of a significant fraction of the fuel, and this produced reduced values of

specific impulse. This effect was partially offset by the use of transverse injection and staged expansions. The successful combustion of a silane hydrogen mixture at an equivalence ratio of 0.5 was taken as confirmation that the reduced combustion was due to thermal effects, and was not the result of some other limitations of the facility.

To make shock tunnel testing with wall injection more representative of flight conditions where hot walls would not be expected to quench the fuel, the use of preheated fuel, preheated walls or the injection of small amounts of silane are being investigated.

ACKNOWLEDGMENTS.

This work was performed under a grant from the NASA Langley Research Center, Hypersonics Propulsion Branch.

The experimental work was performed in the shock tunnel of the Physics department of the Australian National University, and the assistance of many members of the staff for all the back up support required for the operation of a major test facility is greatly appreciated.

REFERENCES.

1. Robert A. Jones, Paul W.Huber. "Towards Scramjet Aircraft".
Technology Report. AIAA Journal of Astronautics and Aeronautics.
Feb. 1978.

2. Griffin Y. Anderson. "An Examination of Injector/Combustor
Design effects on Scramjet Performance".
Presented at the 2nd International Symposium on Air Breathing Engines.
Sheffield, England, March 1974.

3. Robert W. Guy, Earnest A. Mackley.
"Initial Wind Tunnel Tests at
Mach 4 and 7 of a Hydrogen Burning-Airframe integrated Scramjet".
Presented at the 4th international Symposium on Air Breathing Engines.
Lake Buena Vista, Florida, April 1-6, 1979.

4. R.J.Stalker,R.G.Morgan.
"Supersonic Combustion with a Short Thrust Nozzle".
Journal of Combustion and Flame.Vol. 57, No. 1.
July 1984. pp 55-70.

5. R.G.Morgan,A.Paull,
N.A.Morris,R.J.Stalker.
"Hydrogen Scramjet With Sidewall Injection".
Paper presented to the 2nd I.E.Aust. National Symposium on Space Engineering.Sydney May 1986.

TABLE OF TEST CONDITIONS

H	M	T	P
MJ/kg		K	kPa
8.70	3.50	2500	160
4.20	3.50	1100	160

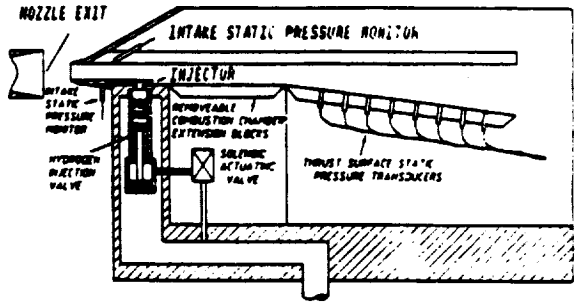

Fig 1. Schematic of experimental apparatus.

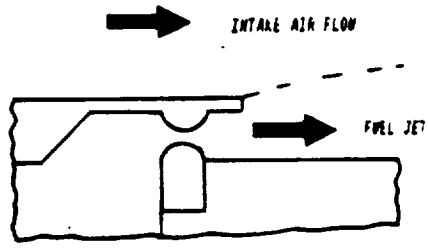

Fig 2. Schematic of wall injection.

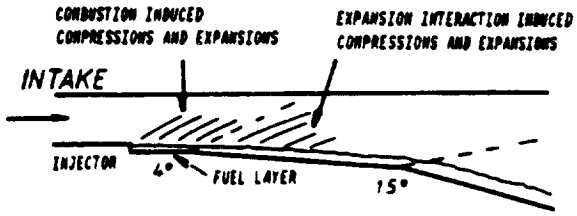

Fig 3A. Dual staged expansion

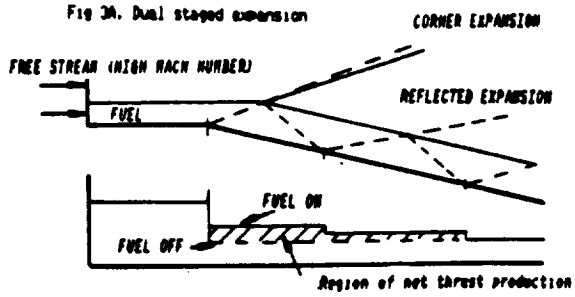

Fig 3B. Corner expansion/wall jet interaction.

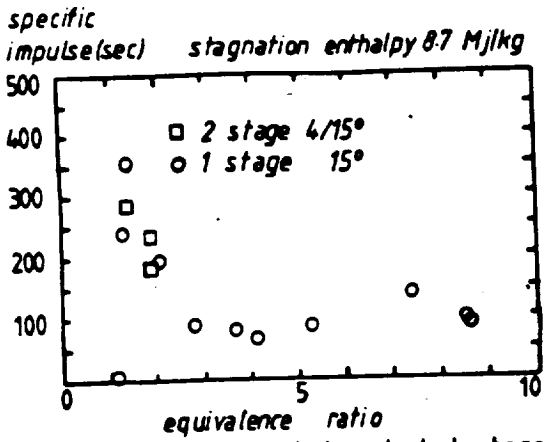

Fig 4A. Comparison of single and dual stage expansions. Parallel wall injection, short combustion chamber.

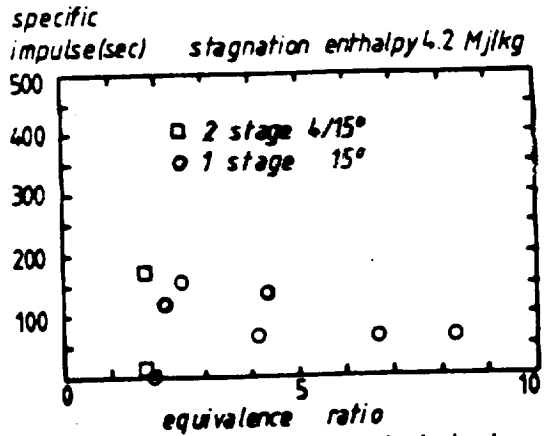

Fig 4B. Comparison of single and dual stage expansions. Parallel wall injection, short combustion chamber.

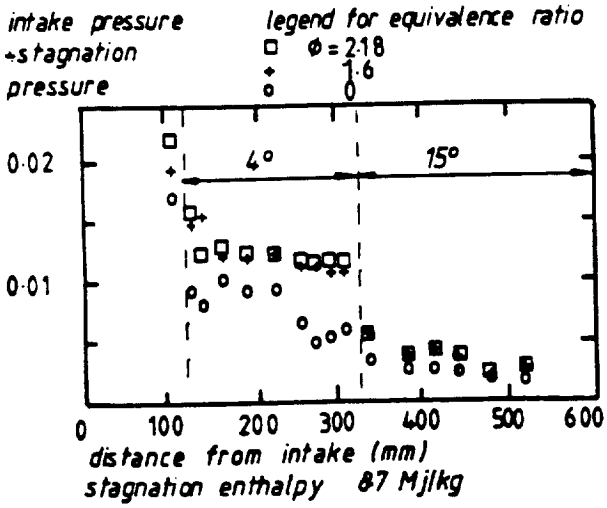

Fig 5A. Dual stage expansion, short duct, Parallel wall injection.

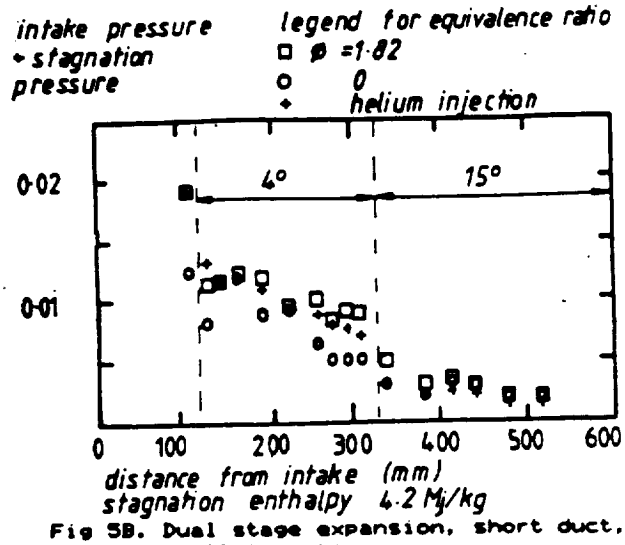

Fig 5B. Dual stage expansion, short duct, Parallel wall injection.

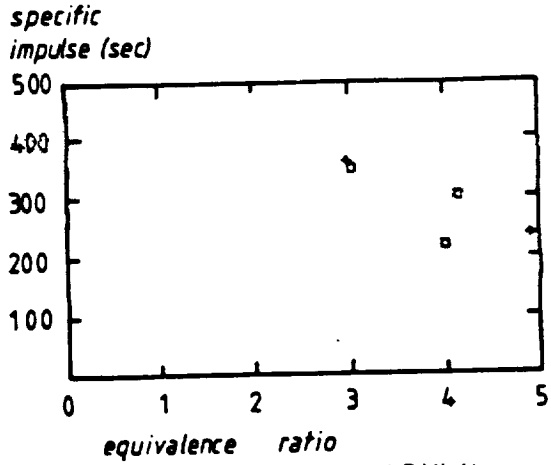

Fig 6 A. Stagnation enthalpy 8·7 Mj/kg
legend + long duct
□ short duct

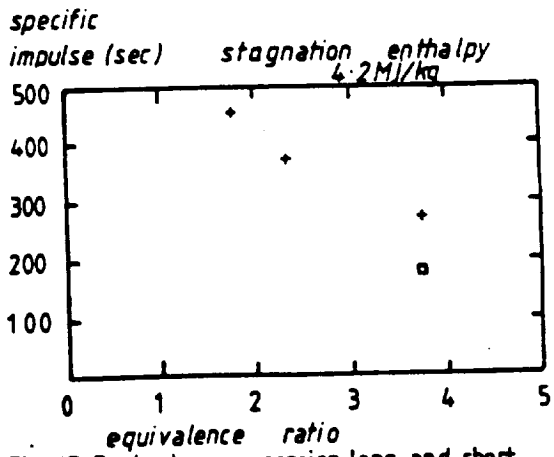

Fig 6B. Dual stage expansion, long and short combustion chambers. Parallel injection.

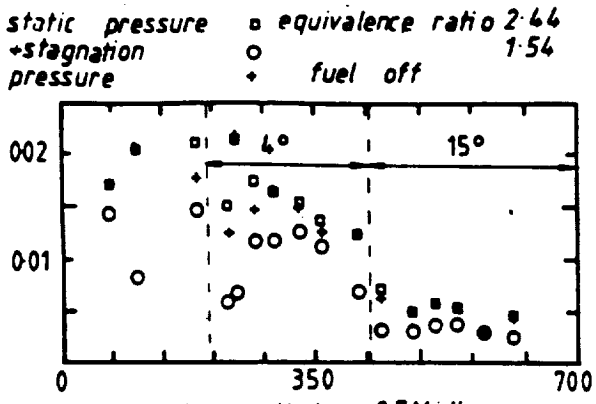

Fig 7B. stagnation enthalpy 8·7 Mj/kg

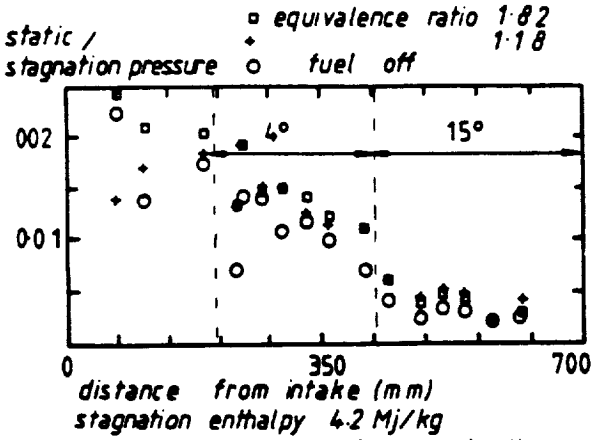

stagnation enthalpy 4·2 Mj/kg

Fig 7A. Dual stage expansion, long combustion chamber, parallel wall injection.

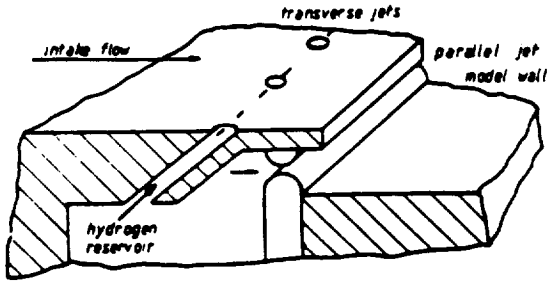

Fig 8 Mixed parallel and transverse wall injection.

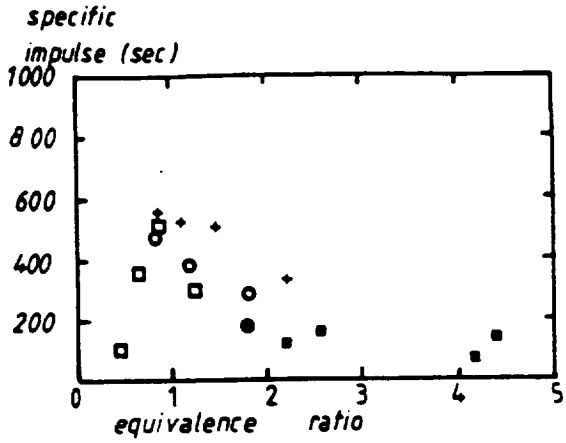

B. stagnation enthalpy 4·2 Mj/kg

- □ 2 stage expansion. long duct, 7½% transverse injection.
- + 2 stage expansion. short duct, 27% transverse injection.
- ○ 2 stage expansion. long duct. parallel injection.
- ● 2 stage expansion. short duct. parallel injection.
- ■ 1 stage expansion. short duct. parallel injection.
- ✕ 1 stage expansion. short duct. 27% transverse. helium injection.

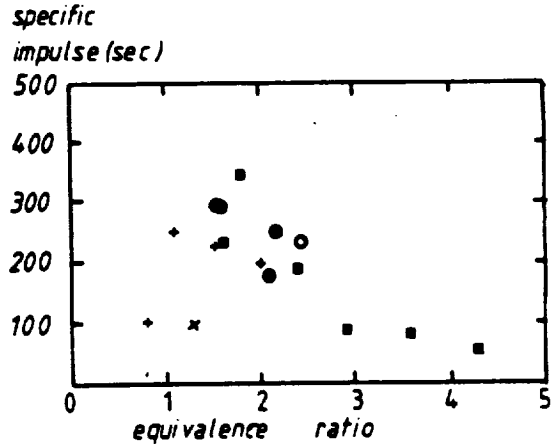

A. stagnation enthalpy 8·7 Mj/kg

Fig 9 Various configurations of wall injection.

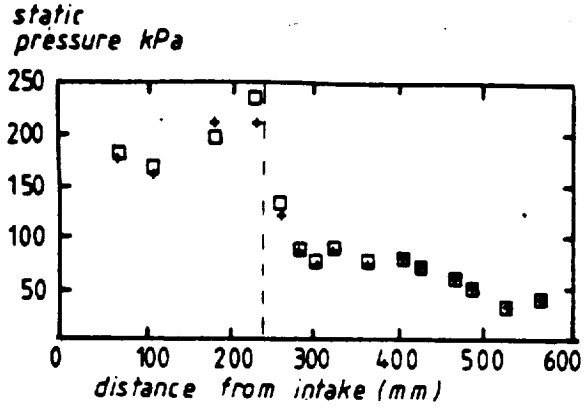

A. Pressure profiles

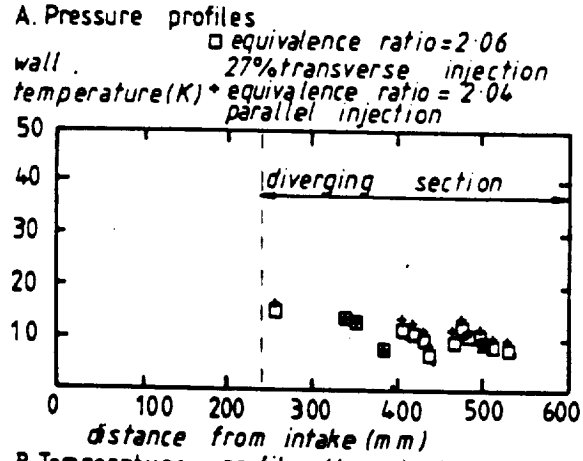

B. Temperature profiles *(transient)*

Fig 10. Comparison of parallel and transverse wall injection, long duct, 15° expansion.

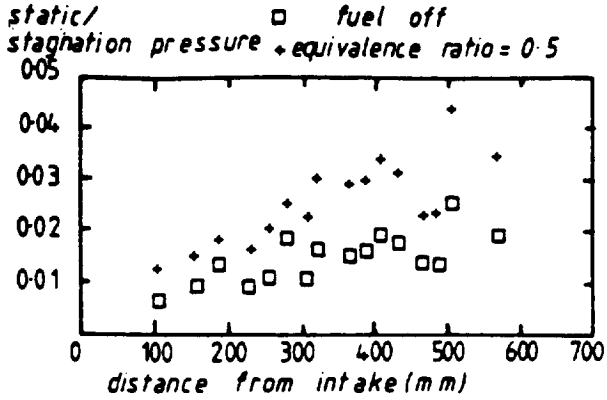

Fig 11. Wall injection of silane/hydrogen mixture. Constant area duct

NUMERICAL MODELLING OF SIDEWALL INJECTED SCRAMJETS

C. Brescianini & R.G. Morgan

NUMERICAL MODELLING OF SIDEWALL INJECTED SCRAMJET

Side wall injection is an attractive alternative to central injection in a scramjet engine, since the hydrogen layer can shield the walls of the scramjet engine from the high temperatures found in the free stream. Previous experiments using a model scramjet in the high enthalpy flow created by shock tunnels, however, have indicated that the performance of the wall injected scramjet is significantly reduced when compared with the performance of the central injected scramjet (Ref. 1). A numerical study of the scramjet's flowfield was undertaken to see if the experimental results could be reproduced; and if they could, to see what other details of the flow might be learned from the numerical results.

All scramjet experiments in the shock tunnel, to date, have been performed using fuel with a total temperature equal to the local room temperature. In future experiments it has been proposed to heat the hydrogen fuel so that the temperatures will better simulate those which occur in a real flight vehicle. The numerical program was also used here as a predictive tool, so that the likely changes in performance due to fuel heating may be ascertained.

DESCRIPTION OF COMPUTER PROGRAM

A two-dimensional, parabolic computer program was used to compute the flow field inside the scramjet model. The computer program (known as CHARMS at the University of Queensland) is based on the CHARNAL computer program which is described in Ref. 2. The program is specifically designed to calculate the turbulent mixing and chemical reactions which occur when hydrogen is injected parallel to a main stream of air. The program solves the time-averaged parabolic partial differential equations for the transport of momentum, energy, and species. The solution to the differential equations is accomplished by the finite difference method of Patanker and Spalding (3).

A finite rate chemistry scheme is used in the program to calculate the chemical reaction rates. This scheme is described in more detail in Ref. 4. This reference describes the use of two available reaction systems. The first involves the use of 7 species and 8 reactions (treating N_2 as inert), and the second involves 12 species and 25 reactions. In addition the chemical reaction rates may be reduced to allow for the effects of "unmixedness" often found in turbulent reacting flows. For the cases studied in Ref. 4 it was found that the 25 reaction system was superior in

predicting ignition, however once ignition had occurred the 8 reaction system was as good as the 25 reaction system. For all the cases studied in this report the 8 reaction system has been used, and the effects of unmixedness have not been included.

The turbulent viscosity in the program is calculated by the well known k-ε model of turbulence (Ref. 5). In its most common form (known as the kε1 model) the viscosity is found from the formula:

$$\mu_t = C_\mu \rho \frac{k^2}{\varepsilon} \tag{1}$$

where the quantities k and ε are found by solving a pair of transport equations simultaneously with the equations governing the mean flow, and C_μ is a constant.

The kε2 model is an extended version of the k-ε model which contains a weak shear flow correction (Ref. 5) in the form of

$$C_\mu = g(\overline{P/\varepsilon}) \tag{2}$$

Here, $\overline{P/\varepsilon}$ represents the average value of P/ε across the layer. This correction greatly improves the k-ε models's ability to predict flows where the production P and dissipation ε of the turbulence are not in balance.

The k-ε turbulence model was developed for incompressible flows, and its application to compressible shear layers has shown that it tends to overestimate the mixing rate in high Mach number flows. To help overcome this problem an empirical compressibility correction has been developed (Ref. 6) which is applied to the turbulent viscosity calculated from the k-ε model. This correction factor is applied whenever the Mach number is above one. The correction factor is evaluated as follows:

$$K(M_\tau) = 0.25 + 0.75 \,/\, (\, 1.0 + \exp(\, 24.73(\, M_\tau - 0.2\,))) \tag{3}$$

where M_τ is $k^{1/2}$ divided by the local speed of sound.

The compressibility corrected version of the kε2 model has been used to obtain all the results presented in this report. The turbulence constants used in the calculations are as follows:

$$C_\mu = 0.09\ g(\overline{P/\varepsilon}) \quad , C_{\varepsilon 1} = 1.44 \quad , C_{\varepsilon 2} = 1.92 \quad , \varkappa = 0.435$$

$$\sigma_{t,k} = 1.00 \quad , \sigma_{t,\varepsilon} = 1.30 \quad , \text{other } \sigma_{t,\phi} = 0.9 \quad , \sigma_{l,\phi} = 0.7$$

CHARNAL makes use of wall functions to relate the fluxes through the walls with the values of the dependant variables at the near-wall nodes. The use of wall functions is required because the k-ε model employed is not valid in the low Reynolds number region near the walls. The wall functions used in this report assume uniform shear stress prevails in the region near the walls, an assumption which is not entirely valid if large pressure gradients exist. Wall functions which do consider the effects of pressure gradient are available in CHARNAL, however they have not been used to obtain the results presented here due to instability problems.

Pressure gradients in the lateral direction are calculated in the program by using the SIMPLE (Semi-Implicit Method for Pressure-Linked Equations) algorithm. The application of this procedure for use in the CHARNAL program is described in Ref. 7.

TEST CONDITIONS

Free Stream

Two nominal , free stream stagnation enthalpy conditions were used, namely 4.2 MJ/kg and 8.7 MJ/kg, and one Mach number, M = 3.5 . The values of velocity, temperature, and dissociation at the exit of the shock tunnel nozzle (and thus at the entrance to the scramjet) were estimated by using NENZF (Ref. 8) , which takes into consideration the non-equilibrium effects occurring as the flow in the nozzle expands. It should be noted that only nominal free stream conditions were used in making the calculations. The results are shown in Table 1.

TABLE 1 FREE STREAM CONDITIONS AT SCRAMJET INLET

H_∞ (MJ/kg)	T (K)	PIN (kPa)	U (m/s)	α (%)	M
8.7	2520	160	3250	10.3	3.34
4.2	1160	158	2380	0.18	3.59

Hydrogen

Hydrogen reservoir (injection) pressures were taken directly from the experimentally recorded reservoir pressures where available (room temperature fuel). When the experimental hydrogen reservoir pressures were not available (heated fuel runs), the same reservoir pressures as the equivalent room temperature run was used.

INITIAL CONDITIONS FOR COMPUTER PROGRAM

Hydrogen static pressures at the exit of the injector were generally not matched with the free stream static pressures during experiments. In reality this would result in a strong wave/shock structure immediately downstream of the injector. Current attempts to model this structure with CHARNAL have shown stability problems which are yet to be overcome. As a result a much more approximate treatment of the flow characteristics near the injector have been taken in this report. First the hydrogen and air mass flow rates, total temperature, and stagnation pressures are calculated. The two gases are then allowed to expand in a 1-D isentropic fashion, keeping the static pressures the same in both streams, until the combined thickness of the two streams match the height of the duct after the injector. The velocities, and temperatures of the two streams, and the common static pressure, are then used as the initial conditions for the program. A step change in the velocity and temperature is assumed at the mixing layer. If any recirculating regions are present near the injector, their effects have been ignored in the calculations. This is necessary since CHARNAL, being a parabolic program, cannot predict regions with recirculation.

A fuel preheating rig is nearing completion at the Mechanical Engineering Department. This rig will quickly heat the hydrogen fuel by burning some of the hydrogen fuel with oxygen before injection. Initial estimates show that the total temperature of the fuel after this heating may be as high as 1800 K, with static temperatures of the order 1000 K. For this reason hydrogen total temperatures of 1800 K have been used in the heated fuel computations. The experimental rig will also result in some water vapour being injected along with the hydrogen. CHARNAL currently cannot handle the initial presence of water with the injected hydrogen. As a result the effects of the initial water vapour have also been neglected in this report.

Initial values of turbulent kinetic energy and dissipation length

scale are also required before computations can begin. Since these values are not measured an estimate is required. The values used in this report are:

Hydrogen $\frac{k}{U^2} = 0.005$

Air $\frac{k}{U^2} = 0.001$

$\frac{\ell_\varepsilon}{DJ} = 0.03$

A constant temperature is used as the boundary condition for the energy equation along the top and lower walls. The temperature of the lower wall was fixed at 291 K for the calculations.

RESULTS

(A) CONSTANT AREA DUCT RESULTS

H_s= 4.2 MJ/kg . ϕ = 1.43 .

Room Temperature Fuel

Shock tunnel experiments in Ref. 1 ,using the scramjet model with wall injection, had shown that very little pressure rise occurred in the scramjet duct when the equivalence ratios were below approximately 1.5 . In an attempt to explain this phenomena it was proposed that a region of hydrogen fuel, which was injected along the lower wall of the model, was being quenched by the cold walls, and thus preventing combustion from occurring. Since the particular test case under study here was also at a low equivalence ratio, it presented a good case to test this theory against the results from numerical computations.

Fig. 1 displays a plot of the computed pressure (normalized against initial pressure) versus distance from the injector. Also plotted on the same figure are two sets of experimental data taken from Ref. 9. The first set are the results when a cylindrical nozzle was used in the injector, and the second are the results when a source-flow nozzle was used. (The shape of these nozzles is explained in more detail in Ref. 9). Both sets of experimental data have been normalized against the experimentally recorded pressure in the inlet to the scramjet (upstream of the injector).

Fig. 1 displays a reasonable amount of agreement between theory and experiment when the inaccuracies of the experimental pressures, and the large assumptions required to obtain the initial conditions for the computations are considered. The normalized pressure does not rise above 1.25 until approximately 27 cm downstream of the injector.

Fig. 2 shows the experimentally recorded heat transfer results along the lower wall of the model (these results have been taken from Ref. 9 and have been amended by a factor of 2), along with the numerically computed results. Again, considering the large scatter in the experiments, the agreement is very good.

Since there is a reasonable amount of agreement between the computations and all the experimental results currently available at this particular test condition, it is now interesting to turn to the computations to see what other information may be obtained.

Fig. 3 displays the mass fraction of water versus distance from the lower wall at 3 different distances downstream of the injector. It can be seen that very little reaction has occurred at a distance of 10 cm.

Temperature contours are shown in Fig. 4 ,with distances downstream of the injector along the lower side, and the 2.5 cm duct height along the vertical side. Very little temperature rise is seen until approximately 12 cm downstream. It would appear that the ignition is quite slow at this lower enthalpy, delayed by both the low temperatures and low oxygen dissociation levels. A 25 reaction chemistry system, if it had been used, may have produced a more accurate estimate of the ignition delay length than the 8 reaction system used here.

The temperature contours in Fig. 4 also indicate quite a large cold region of hydrogen near the lower wall which could possibly prevent combustion. However, it is also important to consider the local mixture equivalence ratios. Self ignition may be expected to occur in region where the mixture equivalence ratio is approximately 0.2 ,and the temperatures are above 800 K (Ref. 10). Fig. 5 displays local equivalence ratio (ignoring O_2 and H_2 in the form of water) contours at levels of 0.2, 1.0 and 1.8 .These contours give some indication of where the flame front is likely to occur. The ϕ = 0.2 contour can be seen to be very close to the T = 750 K contour for some distance downstream of the injector, helping to explain the long ignition delay. However, after ignition, the flame front

continues to penetrate into the hot main free stream air. The cold hydrogen, located near the walls, is quite a distance from the flame front and its effects on the combustion seem small. The combustion efficiency of the mixed hydrogen (η_{RR}) after 40 cm was 71% ,while only 7% of the total hydrogen (η_{TF}) had burnt. It would appear that the amount of combustion which occurs after ignition is mainly limited by the rate at which the hydrogen is penetrating into the free stream.

Hot Fuel

The simulation at 4.2 MJ/kg was repeated using hot hydrogen fuel. Since the total amount of fuel injected was identical, but the density was lower, the initial thickness of the hydrogen jet was thicker than for the room temperature case, and the initial static pressures where slightly higher.

Normalized pressures versus distance is shown in Fig. 6 ,and indeed indicates a larger pressure rise in the duct than was calculated for the room temperature hydrogen results. Fig. 7 shows that, unlike the room temperature fuel case, ignition has already occurred well before x = 10 cm. Water mass fraction contours ,in Fig. 8 ,show some water forming almost immediately after injection. Temperature contours, in Fig. 9 ,show that the hot regions of the flow extend almost the entire way to the lower wall, indicating virtually no effect due to wall quenching. Fig. 10 shows that the flame front has penetrated very little into the main stream flow. Combustion efficiencies (Fig. 11) show that the combustion efficiency of the mixed hydrogen (η_{RR}) is 92%, while only 15% of the total amount of hydrogen available for combustion (η_{STOICH}) has been converted to water. Again the total amount of hydrogen which has combusted seems to be limited mainly by the mixing rate.

8.7 MJ/kg . ϕ = 2.64

Room Temperature Fuel

Since the equivalence ratio is well above 1.5 this is a condition where a reasonably large pressure rise would be expected. Fig. 12 displays the normalized pressure versus distance from the injector. The experimental values have again been taken from Ref. 9. The computed pressures seem to rise periodically under the influence of some pressure wave travelling down the duct. The overall pressure rise predicted is in reasonable agreement with experiment, but the location of the pressure rises is in some

question. Again, this is not surprising considering the initial condition assumptions, and the scatter in the experimental results. The source of the pressure wave is evident from the pressure contour diagram shown in Fig. 13. Here a strong pressure wave is seen to emanate from the initial mixing region between the hydrogen and the free stream air. This pressure wave is due mainly to combustion. This was shown by running the program again with identical conditions ,but without chemical reactions. The pressures along the lower wall when reactions where not used is also shown on Fig. 12.

Water mass fraction contours, shown in Fig. 14, show that with chemical reactions, ignition has been almost immediate. No advantage would probably have been gained here if the 25 reaction system had been used.

Fig. 15 displays the predicted heat transfer results, along with experiments. The experimental results show a lower heat transfer rate (and thus better insulation for the wall) than predicted by the computer results. This may suggest that a lower dissipation length scale should have been used in the computations. The heat transfer rates were also found to be quite sensitive to the initial conditions chosen. For example, reducing the velocity of the free stream air in a small region near the injector, to the same velocity as used for the hydrogen (while keeping the total temperatures the same), resulted in the heat transfer results shown in Fig. 16. Results here are in much closer agreement with experiment.

Temperature contours shown in Fig. 17 show a large cold region near the wall, but this appears to be mainly due to the large amount of cold hydrogen which has been injected rather than due to the quenching effects of the walls. From Figures 17 and 18 the combustion region can be seen to easily extend into regions where the temperatures are well above those required for combustion. The combustion region, however, only extends to approximately halfway across the scramjet duct. Fig. 19 shows that 90% of the mixed hydrogen available for reaction has reacted (η_{RR}), however, only 23% of the total hydrogen available for reaction has been converted to water (η_{STOICH}).

Hot Fuel

Figure 20 shows normalized pressure versus distance when heated hydrogen is used. Again the initial pressures and jet thickness are larger here than those used in the room temperature case. The total pressure rise recorded is 1.36, compared with 1.68 for the room temperature hydrogen. The

pressure wave emanating from the initial mixing region seems to be of a much lower strength, than was seen in the room temperature result.

Temperature contours can be seen in Fig. 21. Figure 22 shows that the flame front is spreading into the oxygen rich region, but that the spreading rate is quite slow. Combustion efficiencies in Figure 23 show that 87% of the mixed hydrogen available for reaction has burnt (η_{RR}), while 18% of the total hydrogen available for reaction has been completely converted to water (η_{STOICH}).

(B) 15° DIVERGENCE

H_S=4.2 MJ/kg . ϕ = 1.43

The conditions at 4.2 MJ/kg were repeated except that a 15° diverging thrust surface was located on the lower wall, 20 cm downstream from the injector. The thrust surface was extended for 20 cm in the axial direction. Both room temperature and hot hydrogen runs were performed. The results for room temperature fuel are displayed in Fig. 24, while those for heated fuel are shown in Fig. 25. Also shown on these diagrams are the results obtained when no chemical reactions where used, and the result when no fuel at all was injected. The pressures have been normalized against the nominal pressure in the inlet to the scramjet, before the injector. This inlet pressure is common to all the computational results presented at this stagnation enthalpy.

By comparing the results with and without reactions for the room temperature hydrogen it can easily be seen that ignition is delayed to some 8 cm downstream of the injector. Pressures then begin to slowly rise above the no-reaction case. Approximately 2 cm downstream of the expansion corner a slight hump can be seen in the pressure on the thrust surface. This may be due to the compression waves produced when an expansion fan from the corner interacts with the Mach number gradient in the flow (Ref. 11).

In comparison the hot hydrogen fuel results (Fig. 25) show almost almost immediately ignition. The pressures obtained when reactions are included quickly rise above those obtained without reactions. Again a slight hump in pressure is seen in the thrust surface just downstream of the expansion corner.

A summary of the thrusts obtained are shown in Table 2, the specific impulses in Table 3, and the combustion and mixing efficiencies in Table 4.

From Table 3 it can be seen that the specific impulse for the hot hydrogen case is significantly larger than those obtained with the room temperature. However, note that the gain in specific impulse due to chemical reaction is of the same approximate size in both cases. It would appear that the main gain in specific impulse is due to the larger initial static pressure.

Table 4 indicates that only 54% of the mixed hydrogen available for reaction had reacted by the end of the duct when room temperature hydrogen was used, while 93% of the hydrogen had reacted when heated fuel was used. It seems that although significantly more hydrogen had reacted when heated fuel was used, the gain in pressure was not proportional.

TABLE 2 COMPUTED THRUST

H_s = 4.2 MJ/kg. ϕ = 1.43. 15° DIVERGENCE x = 40 cm

THRUST (N)	ROOM TEMP	HOT
WITH REACTIONS	2451	3816
NO REACTIONS	1849	3141
NO FUEL	1463	1463

TABLE 3 COMPUTED SPECIFIC IMPULSE

H_s = 4.2 MJ/kg ϕ = 1.43 15° DIVERGENCE x = 40 cm

I (sec)	ROOM TEMP	HOT
WITH REACTIONS	257	400
NO REACTIONS	194	330

TABLE 4 COMPUTED EFFICIENCIES

H_s = 4.2 MJ/kg ϕ = 1.43 15° DIVERGENCE x = 40 cm

η (%)	ROOM TEMP	HOT
η_{RR}	54	93
η_{TF}	4	7
η_{STOICH}	6	11
η_{MIX}	11	12

DISCUSSION

Numerical results for the test conditions here seem to indicate that the finite rate reactions are fast, and that combustion is mainly limited by the mixing rate. It is, however, significant to note that at least one set of experiments reported in References 1 and 9 would seem to indicate that this is not the case. Namely, when the sidewall injected model scramjet was configured as a constant area duct, with free stream test conditions H_e = 4.2 MJ/kg, M = 3.5, and ϕ < 1.3 ,very little pressure rise was observed in the duct. However, when the same model and test conditions were used, but a 20% silane(SiH_4)/hydrogen mixture (based on mole fractions) was injected at ϕ = 0.69, a significant pressure rise was recorded. The fact that the silane/hydrogen mixture produces such a large pressure rise would seem to indicate that there was significant mixing and combustion with the free stream. This large pressure rise may, in fact, be due to the smaller ignition times, or some other gas dynamic effect which has not yet been considered. Experiments to check for gas dynamic effects in the central injection configuration have been performed by injecting argon gas to simulate the molecular weight of silane, but avoiding the chemical reactions. These argon experiments did not produce the large pressure rise that was seen when silane was used. This demonstrated that, at least in the central injection configuration, the pressure rises were a genuine combustion effect. Computer simulations of the silane experiments to date have only been one-dimensional, so no simulations which include mixing rates have yet been performed. If these were available it would provide a useful comparison for the computer simulations presented here.

It is also worthwhile mentioning certain points about the hydrogen/air simulations performed in this report which have not yet been considered.

Firstly, the effects of unmixedness on the reaction rates have not been determined. If unmixedness was taken into consideration it may indicate that there are certain slow reactions which are significant in delaying the combustion rate. Secondly, a single value of C_μ in the turbulence model was taken across the flow (although C_μ varied with axial distance). It may well be that a high turbulence production rate in the boundary layers was adversely affecting the calculation of a suitable value of C_μ for use in the mixing layer. If C_μ was allowed to vary across the flow this may result in a faster mixing rate in the free stream, and a slower diffusion rate in the boundary layers. Thirdly, it is obvious that the method of calculating the heat transfer rate to the walls must be reasonably accurate in this work if the hypothesis of a wall quenched hydrogen layer is to tested. A low Reynolds number version of the $k-\varepsilon$ model, which does away with the need for wall functions, should be able to predict the heat transfer rates with greater accuracy. However, such turbulence models are computationally more expensive and would require significant alterations to CHARNAL. In any case the predicted heat transfer rates here are in reasonable agreement with experiment, at least at the 4.2 MJ/kg condition. Fourth, only nominal free stream conditions have been used in this report. It would be preferable if NENZF, along with the experimentally recorded pressures at the inlet to the scramjet, were used to calculate the free stream conditions for each individual experimental test case. Finally, the assumption of equal static pressures in the hydrogen and air jets at the initial station is obviously incorrect. If the current instability problems can be overcome, these simulations should be repeated including the effects of the unmatched free stream and hydrogen pressures at the injector, so that the significance of the wave/shock interactions can be determined.

CONCLUSIONS

The numerical results for pressure and heat transfer in a constant area duct, using room temperature fuel, indicate a fair agreement with experiment. The numerical results show that at the low enthalpy (4.2 MJ/kg) and low equivalence ratio (ϕ = 1.43) case there is a significant ignition delay. In comparison the 8.7 MJ/kg and high equivalence ratio (ϕ = 2.64) case showed almost immediate ignition. For both enthalpy conditions the flame front spread outwards into the hot, oxygen rich, free stream. The cool layer of hydrogen near the walls was due to the large amount of hydrogen which had not reacted, or mixed with the free stream, rather than due to cold model walls. The total amount of mixed hydrogen which had combusted to form water was found to be quite high, while the percentage of the total amount of injected hydrogen which had reacted was small. This

indicated that the main limiting factor, after ignition, seemed to be the rate at which the hydrogen mixed with the free stream, rather than the finite rate chemistry.

Heated hydrogen fuel seemed to have its greatest benefit at the lower enthalpies where ignition lengths were greatly reduced, and the total amount of reacted hydrogen was significantly increased. However, the pressure rise and thrust due to combustion effects were not significantly different. The predicted total thrust and specific impulse of the heated fuel scramjet was much improved over the room temperature fuel case. The major part of this improvement seems to be due to the larger static pressures immediately after the injector, which are due to a gas dynamic effect, rather than due to combustion.

It is well recognized that the k-ε turbulence model does have certain limitations, however the CHARNAL computer code has performed reasonably well considering no adjustment of the turbulence constants were required to produce any of the results presented here. Work is currently underway in the Department to carry out flow visualizations in the scramjet model, and to measure species profiles. This information will greatly assist in providing initial conditions for the CHARNAL program, and should enable a fine tuning the turbulence constants, and a more accurate selection of the dissipation length scale.

REFERENCES

1. Morgan,R.G.,Paull,A.,Morris,N.,and Stalker,R.J.,"Scramjet Sidewall Burning -Preliminary Shock Tunnel Results", University of Queensland, Department of Mechanical Engineering Research Report No.12/85.

2. Spalding,D.B.,Launder,B.E.,Morse,A.P.,and Maples,G.,"Combustion of Hydrogen-Air Jets in Local Chemical Equilibrium (a Guide to the CHARNAL computer program)", NASA CR-2407, June 1974

3. Patanker,S.V.,and Spalding,D.B.,"Heat and Mass Transfer in Boundary Layers', 2nd. Edition, Int. Textbook Co, Ltd. (London), 1970

4. Evans,J.S.,and Schexnayder,C.J.,Jr.,"Influence of Chemical Kinetics and Unmixedness on Burning in Supersonic Hydrogen Flames", AIAA Journal, Vol.18, No.2, Feb. 1980, pp 188-193

5. Launder,B.E.,Morse,A.,Spalding,D.B.,and Rodi,W.,"Prediction of Free Shear Flows -A Comparison of the Performance of Six Turbulence Models", Proceedings of Free Shear Flows Conference, NASA SP 321, 1972

6. Dash,S.,Weilerstein,G.,and Vaglio-Laurin,R.,"Compressibility Effects in Free Turbulent Shear Flows", AFOSR-TR-76-1436, Aug. 1975

7. Elghobashi,S.and Spalding,D.B.,"Equilibrium Chemical Reaction of Supersonic Hydrogen-Air Jets (The ALMA Computer Program)", NASA CR-2725, Jan. 1977

8. Lordi,J.A.,Mates,R.E.,and Moselle,J.R.,"Computer Program for the Numerical Solution of Non-Equilibrium Expansions of Reacting Gas Mixtures", NASA CR-472, 1966

9. Morgan,R.G.,Paull,A.,Morris,N.A.,and Stalker,R.J.,"Further Shock Tunnel Studies of Scramjet Phenomena", University of Queensland, Dept. of Mechanical Engineering Research Report No.10/86.

10. Huber,P.W.,Schexnayder,C.J.,Jr.,and McClinton,C.R.,"Criteria for Self-Ignition of Supersonic Hydrogen-Air Mixtures", NASA TP-1457, 1979

11. Stalker,R.J.,Morgan,R.G.,and Netterfield,M.P.,"Wave Processes in Scramjet Thrust Generation ",Combustion and Flame, Vol.71, No.1, Jan. 1988

SYMBOLS

C_μ, $C_{\varepsilon 1}$, $C_{\varepsilon 2}$	Constant coefficients appearing in turbulence model
DJ	Injector step height
H_S	Stagnation Enthalpy
I	Specific Impulse
k	Kinetic energy of turbulence
ℓ_ε	Dissipation Length Scale $C_\mu k^{3/2}/\varepsilon$
M	Mach number
M_τ	Mach number of turbulence
P	Production rate of turbulence energy
PHI	Equivalence Ratio (ϕ)
PIN	Nominal static pressure in inlet to scramjet
PO	Computations: Initial static pressure used in computations Experiments: Experimentally recorded pressure in inlet to Scramjet

q	Heat transfer rate
T	Static Temperature
T_t	Hydrogen Total Temperature
TH	Thrust
U	Velocity
x	Axial distance downstream of injector
y	Distance normal to lower wall

GREEK SYMBOLS

α	Percentage mass of oxygen that has dissociated
ε	Turbulence energy dissipation rate
η	Efficiency
η_{MIX}	Mixing Efficiency. Defined as the amount of reacted H_2 (H_2 in the form of water) if all mixed hydrogen and oxygen reacted completely, divided by the same quantity if mixing had been complete
η_{RR}	Reaction Rate Combustion Efficiency. Defined as reacted H_2 ,divided by the amount of reacted H_2 if the hydrogen and oxygen which are mixed reacted completely
η_{STOICH}	Stoichiometric Combustion Efficiency. Defined as reacted H_2 ,divided by amount of reacted H_2 if mixing was complete and the hydrogen and oxygen reacted completely
η_{TF}	Total Fuel Combustion Efficiency. Defined as reacted H_2 ,divided by the total amount of H_2
θ_D	Thrust surface (lower wall) divergence angle
κ	von Karman's constant
μ_t	Turbulent viscosity
ρ	Density
σ_t	Turbulent Prandtl/Schmidt No.
σ_l	Laminar Prandtl/Schmidt No.
ϕ	Equivalence Ratio

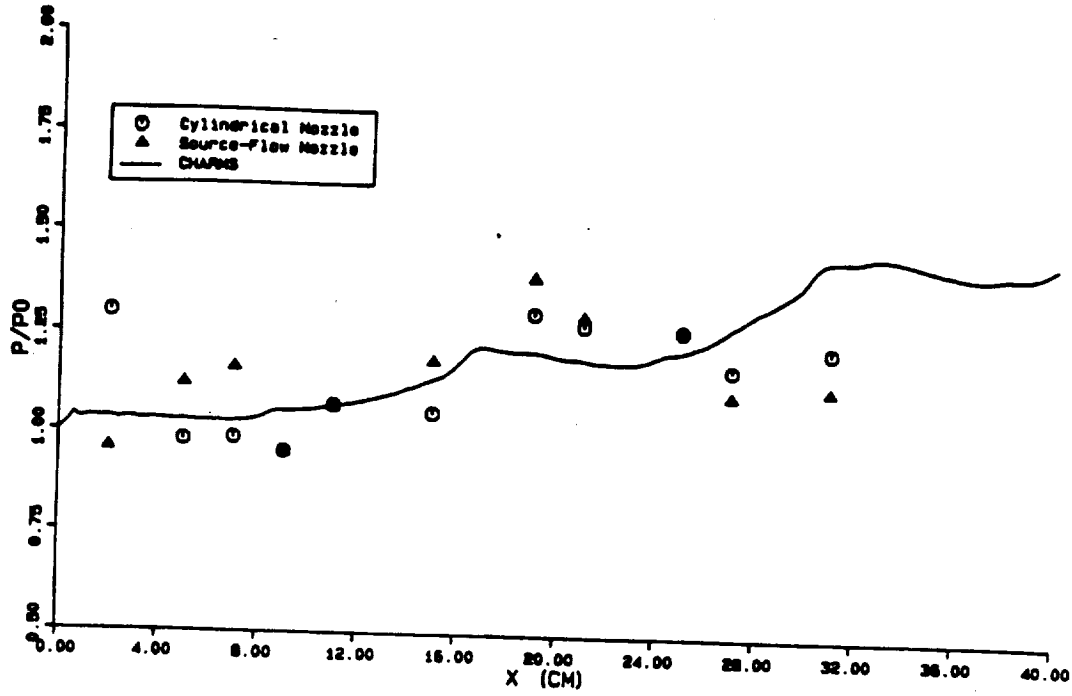

Fig. 1 Axial variation of pressure in a constant area duct.
ϕ = 1.43 , H_s = 4.2 MJ/kg , M = 3.5 , T_t = 300 K

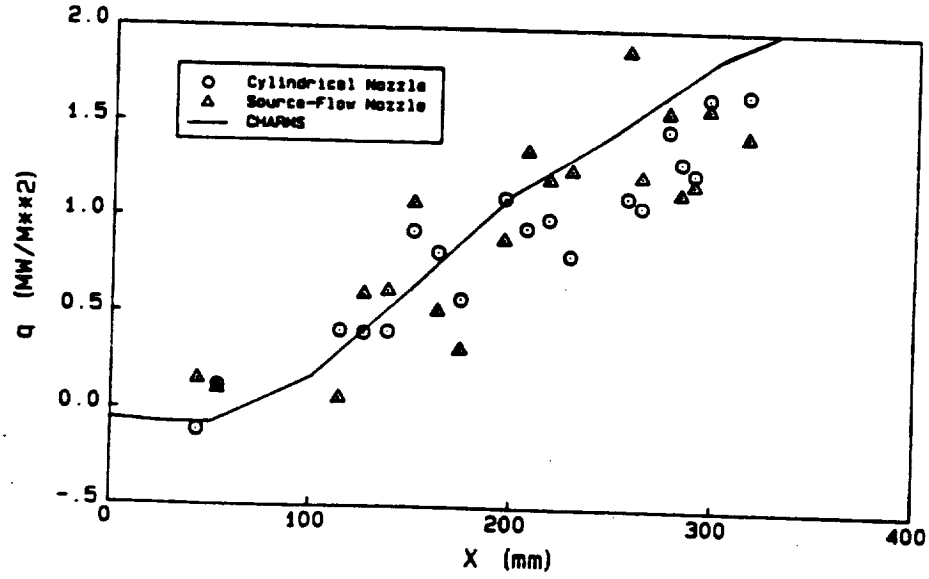

Fig. 2 Axial variation of heat transfer rate in a constant area duct
ϕ = 1.43 , H_s = 4.2 MJ/kg , M = 3.5 , T_t = 300 K

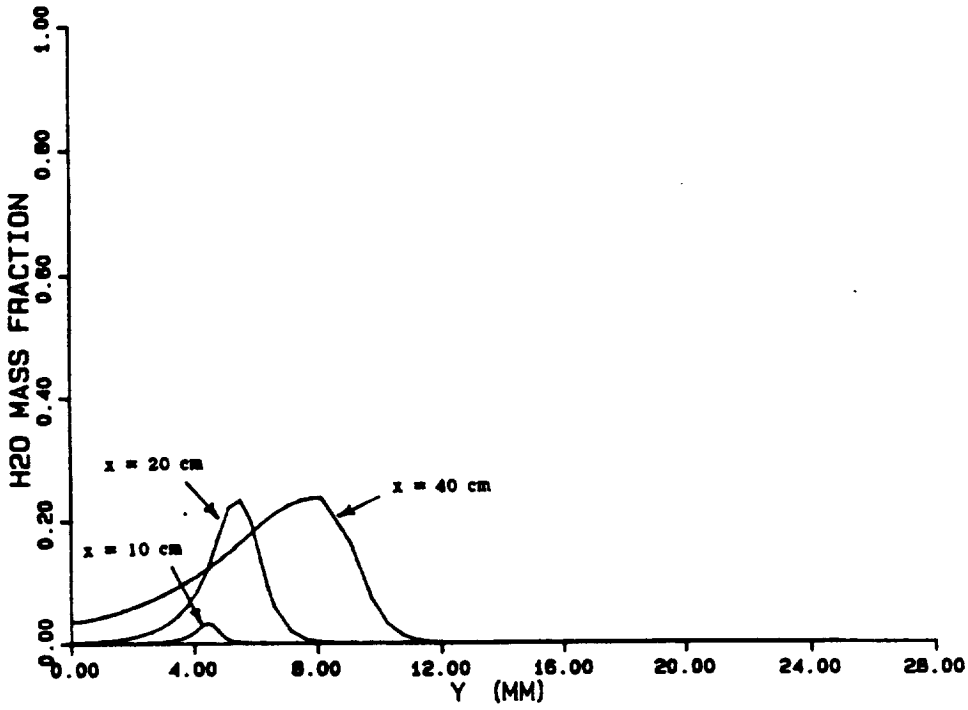

Fig. 3 Profiles of water mass fractions at 3 axial locations in a constant area duct

ϕ = 1.43 , H_s = 4.2 MJ/kg , M = 3.5 , T_t = 300 K

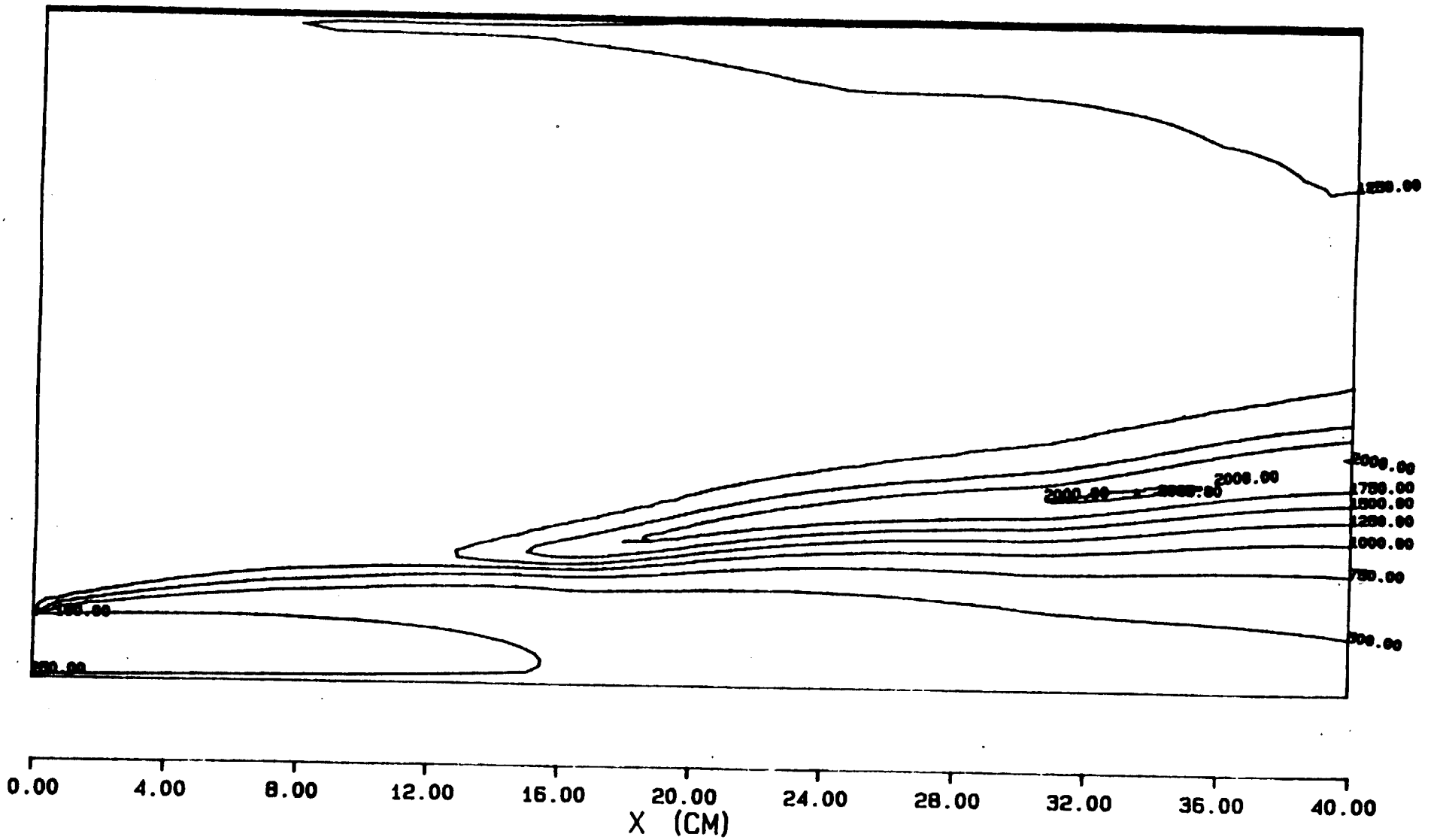

Fig. 4 Temperature contours (K) in a constant area duct

ϕ = 1.43, H_s = 4.2 MJ/kg , M = 3.6 , T_t = 300 K

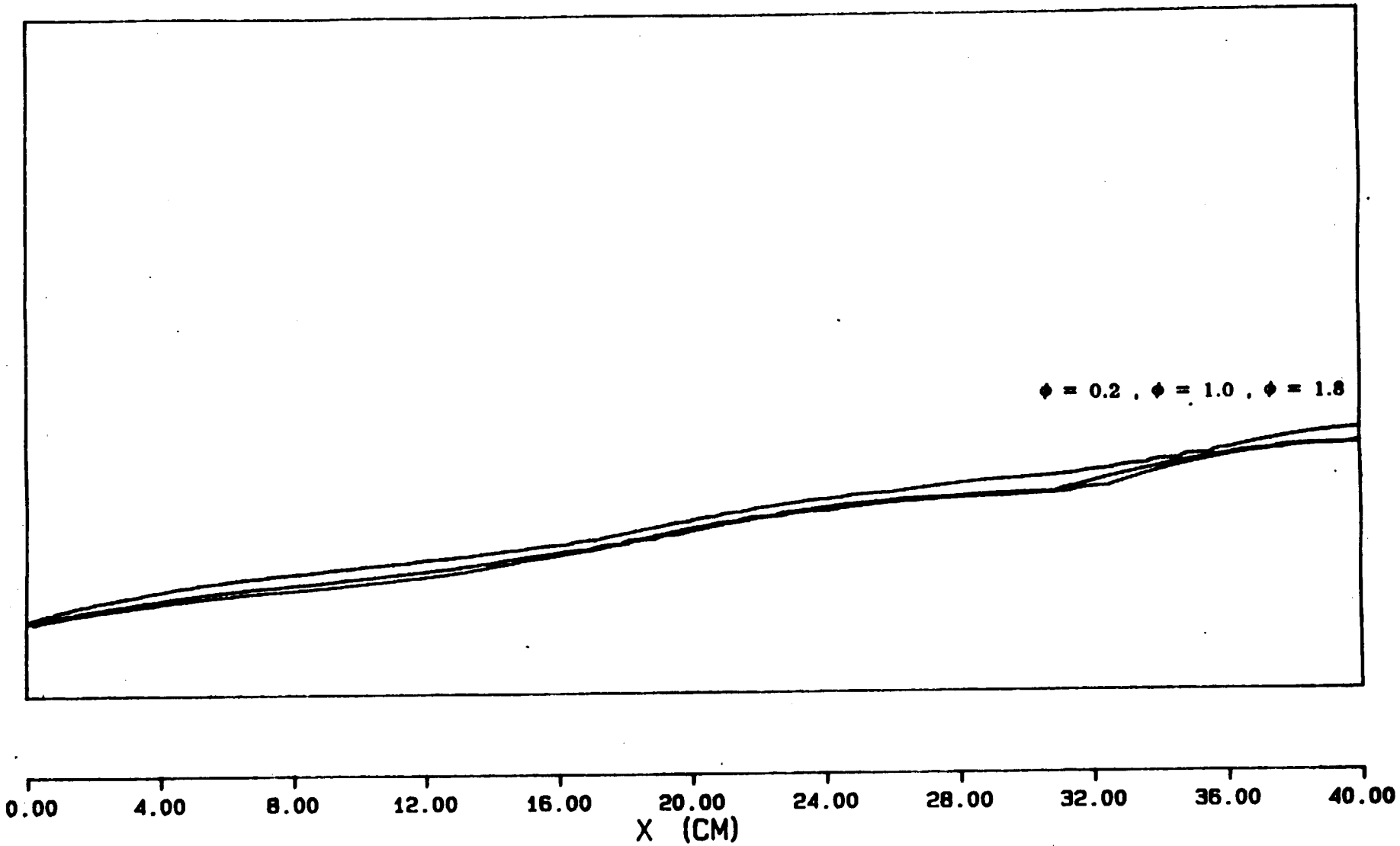

Fig. 5 Local equivalence ratio contours in a constant area duct

ϕ = 1.43, H_s = 4.2 MJ/kg , M = 3.6 , T_t = 300 K

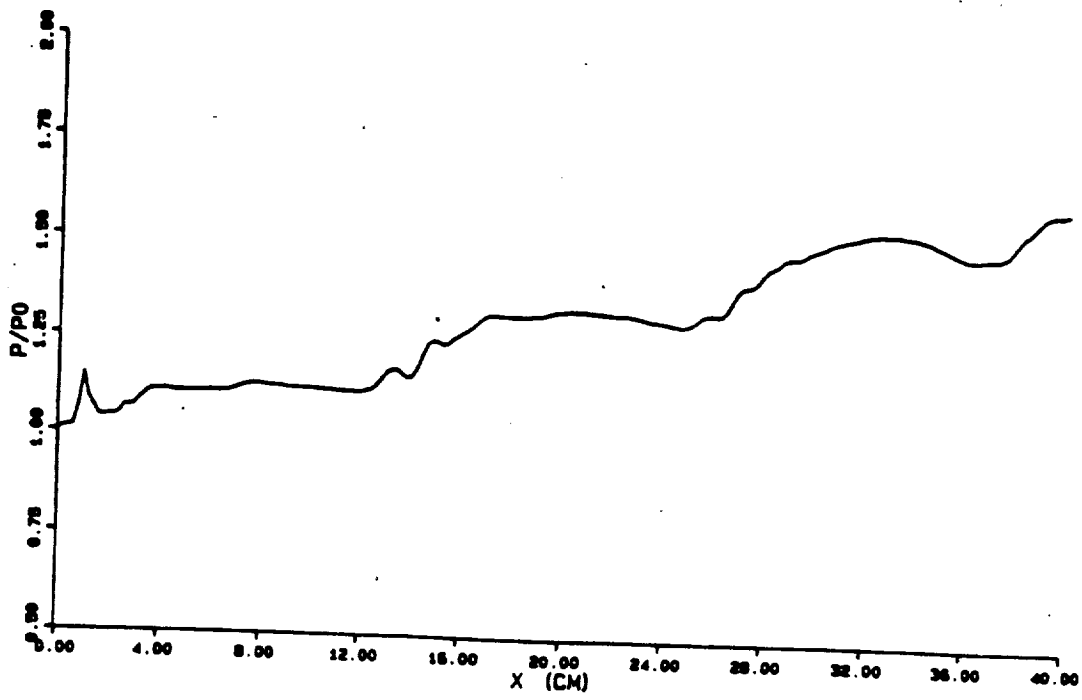

Fig. 6 Axial variation of pressure in a constant area duct
ϕ = 1.43, H_s = 4.2 MJ/kg , M = 3.5 , T_t = 1800 K

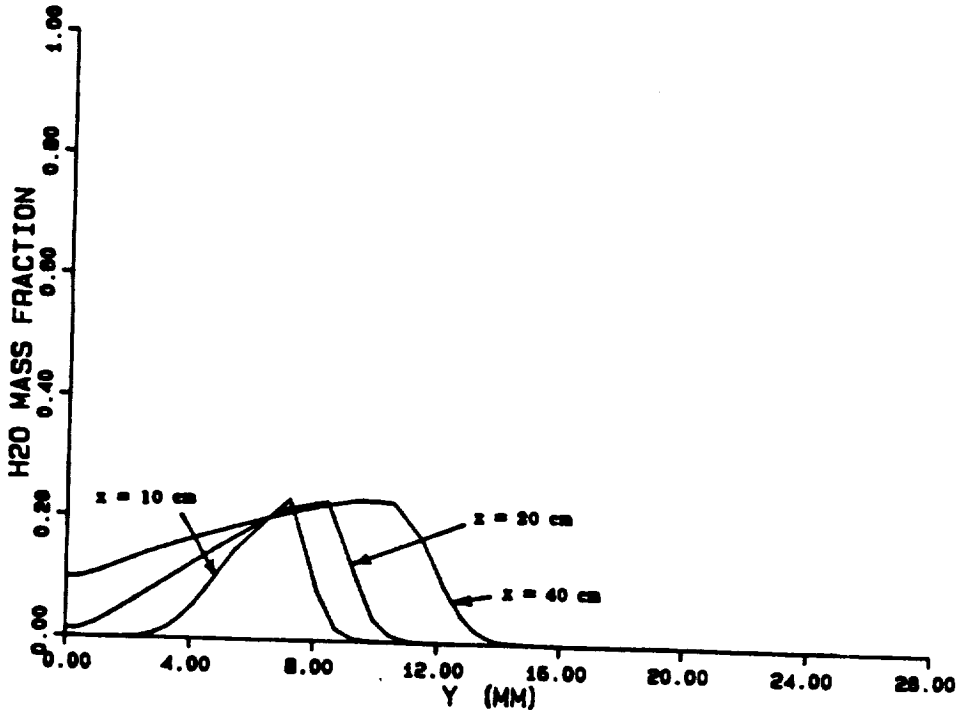

Fig. 7 Profiles of water mass fractions at 3 axial locations in a constant area duct
ϕ = 1.43 , H_s = 4.2 MJ/kg , M = 3.5 , T_t = 1800 K

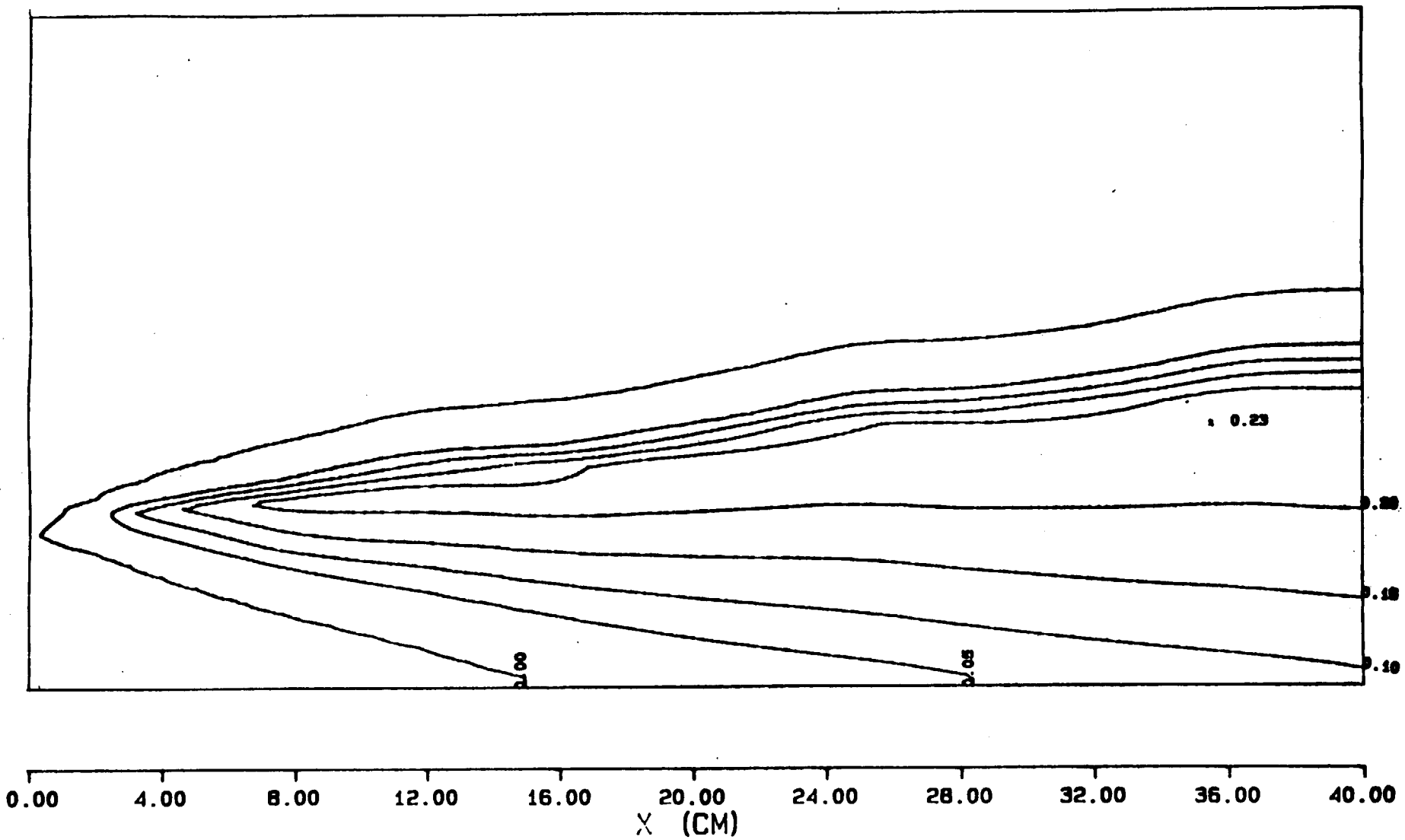

Fig. 8 Water mass fraction contours in a constant area duct

ϕ = 1.43, H_S = 4.2 MJ/kg , M = 3.5 , T_t = 1800 K

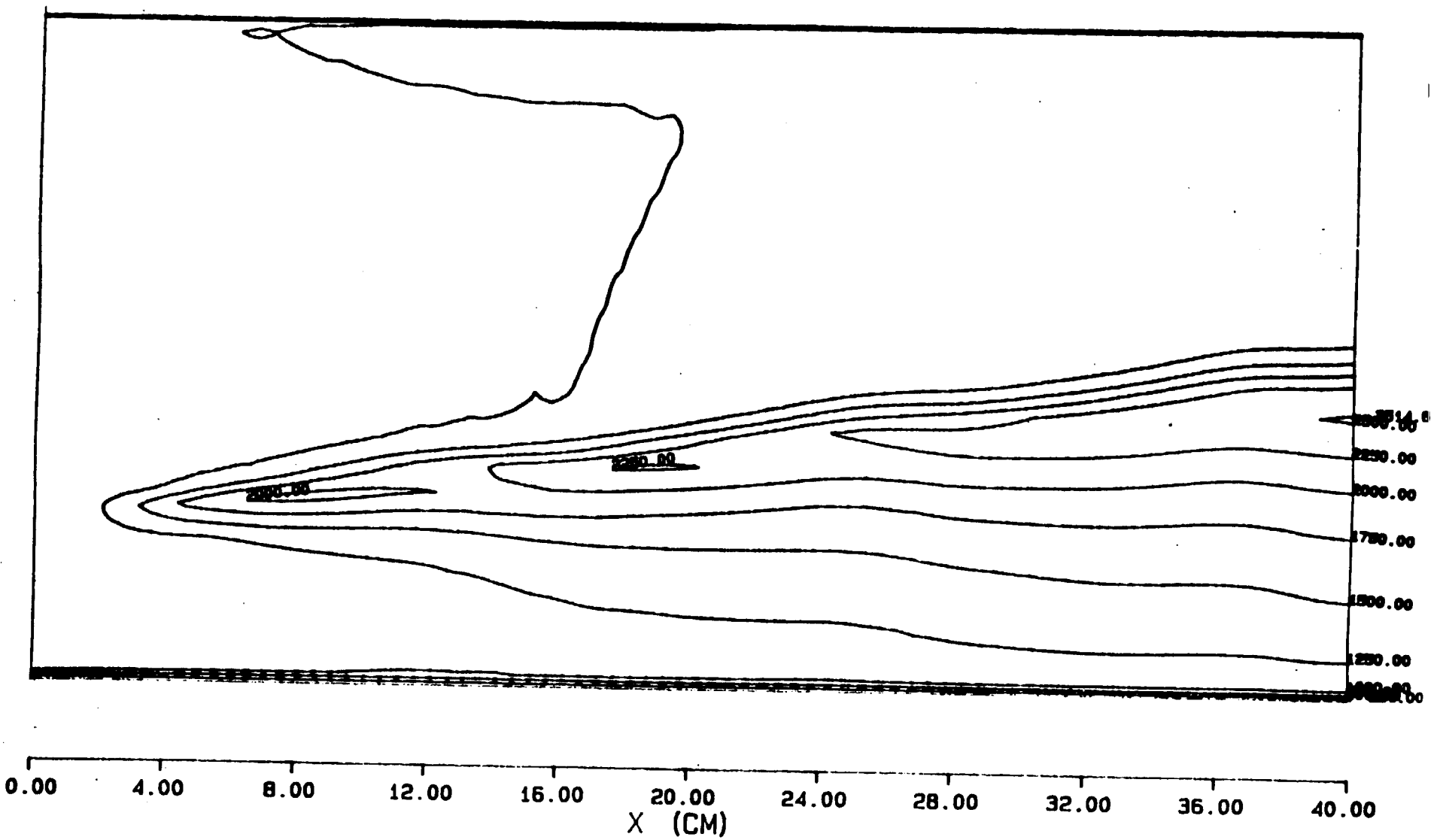

Fig. 9 Temperature contours (K) in a constant area duct
ϕ = 1.43, H_s = 4.2 MJ/kg , M = 3.6 , T_t = 1800 K

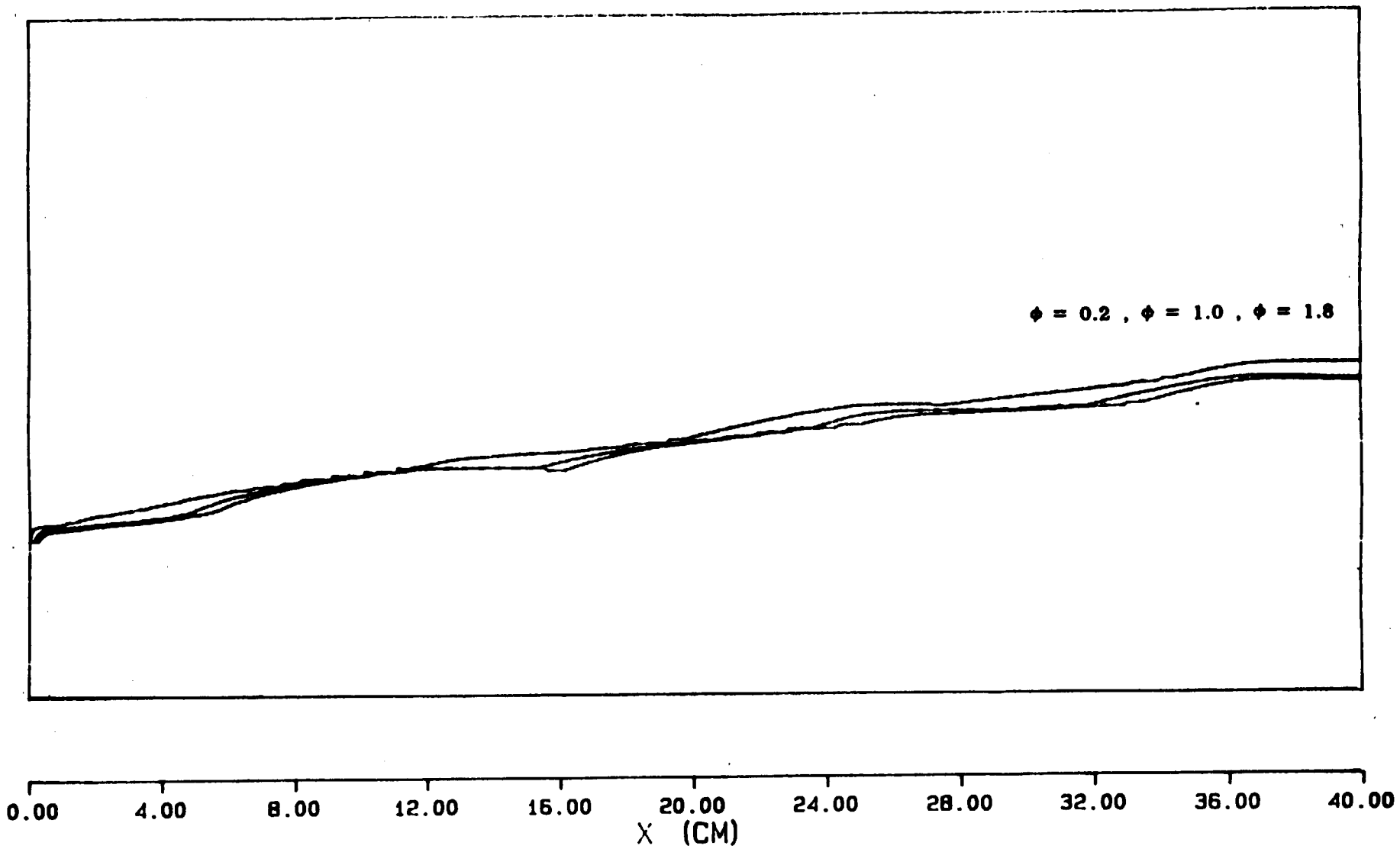

Fig. 10 Local equivalence ratio contours in a constant area duct
ϕ = 1.43, H_s = 4.2 MJ/kg , M = 3.5 , T_t = 1800 K

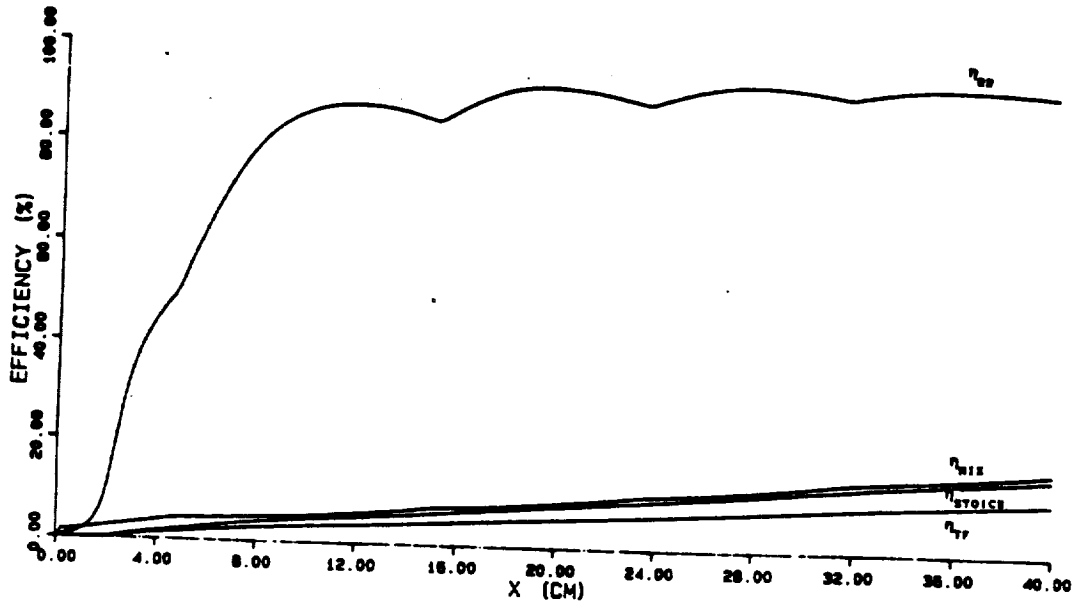

Fig. 11 Axial variation of combustion and mixing efficiencies

ϕ = 1.43, H_S = 4.2 MJ/kg , M = 3.5 , T_t = 1800 K

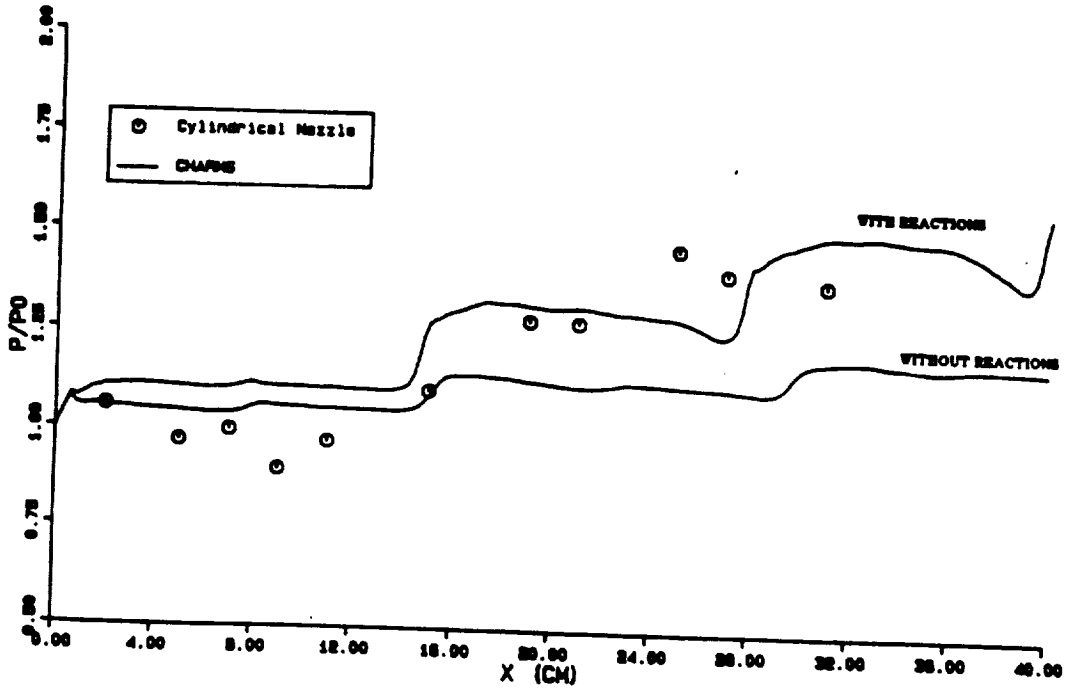

Fig. 12 Axial variation of pressure in a constant area duct

ϕ = 2.64 , H_S = 8.7 MJ/kg , M = 3.5 , T_t = 300 K

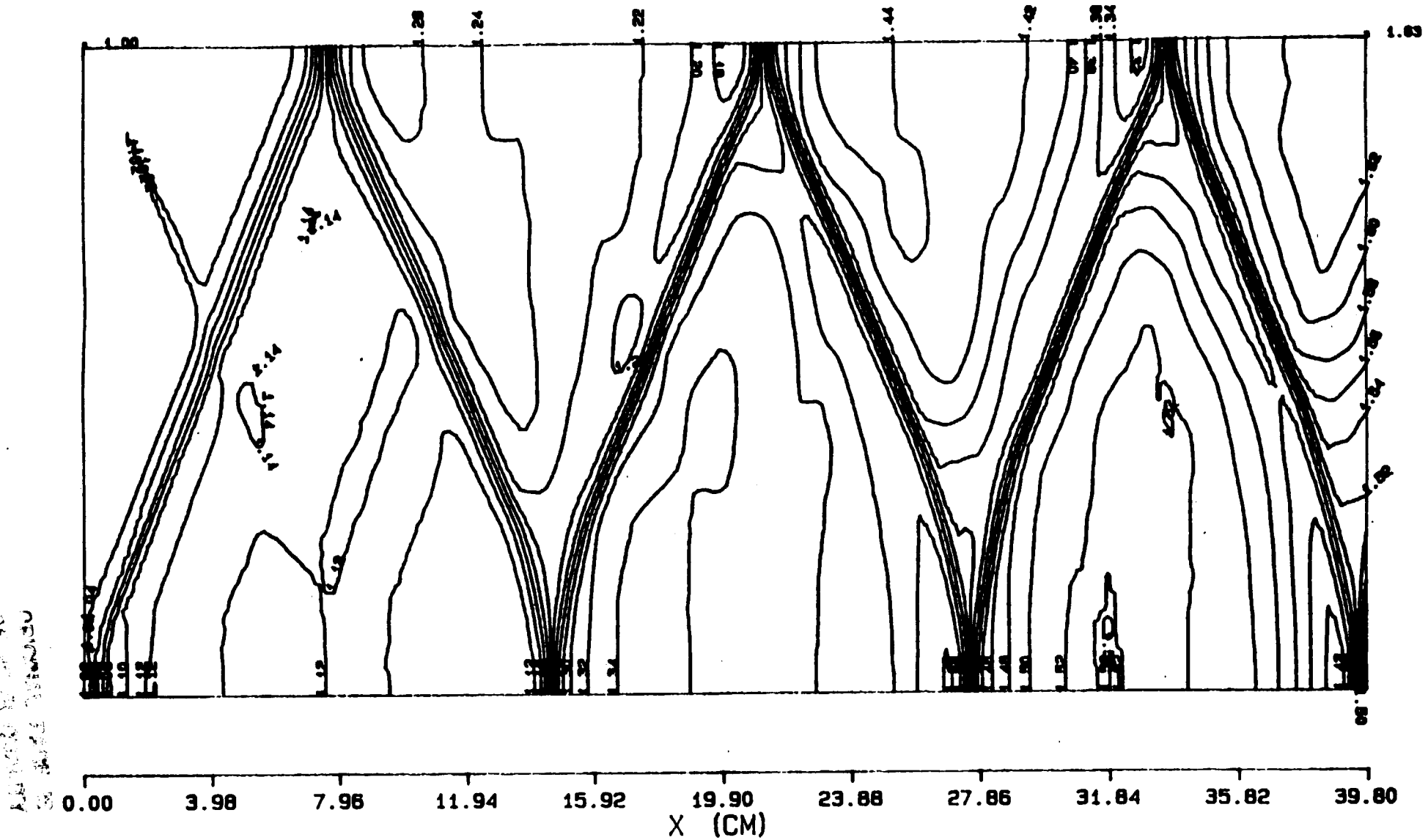

Fig. 13 Pressure contours (normalized against initial pressure) in a constant area duct

ϕ = 2.64, H_s = 8.7 MJ/kg , M = 3.5 , T_t = 300 K

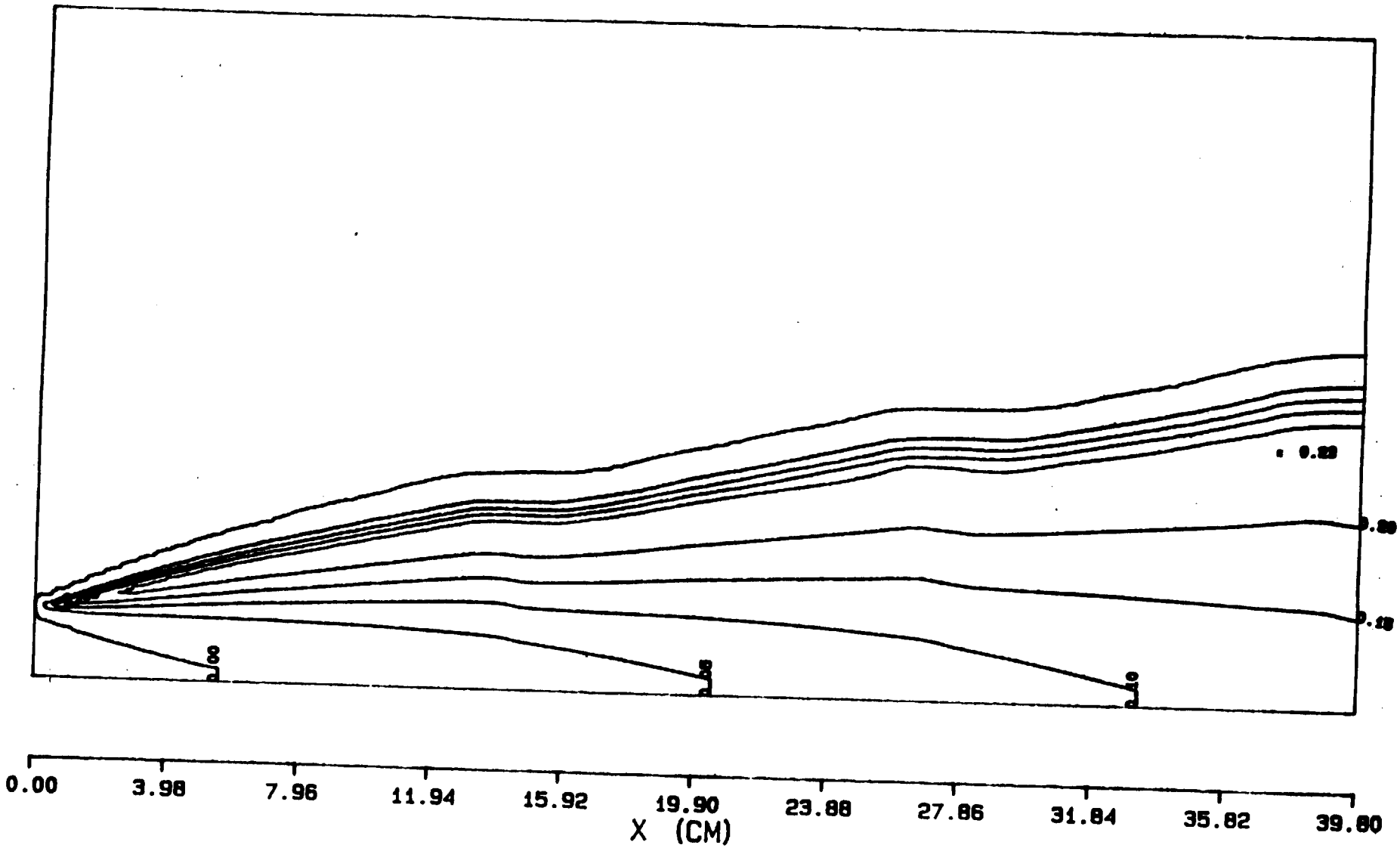

Fig. 14 Water mass fraction contours in a constant area duct
ϕ = 2.64, H_S = 8.7 MJ/kg , M = 3.5 , T_t = 300 K

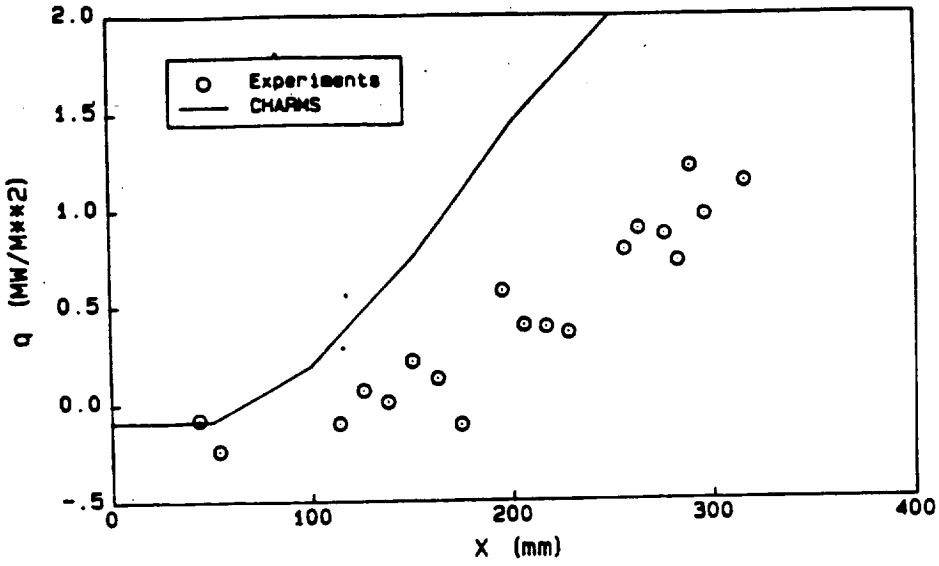

Fig. 15 Axial variation of heat transfer rate in a constant area duct

ϕ = 2.64 , H_s = 8.7 MJ/kg , M = 3.5 , T_t = 300 K

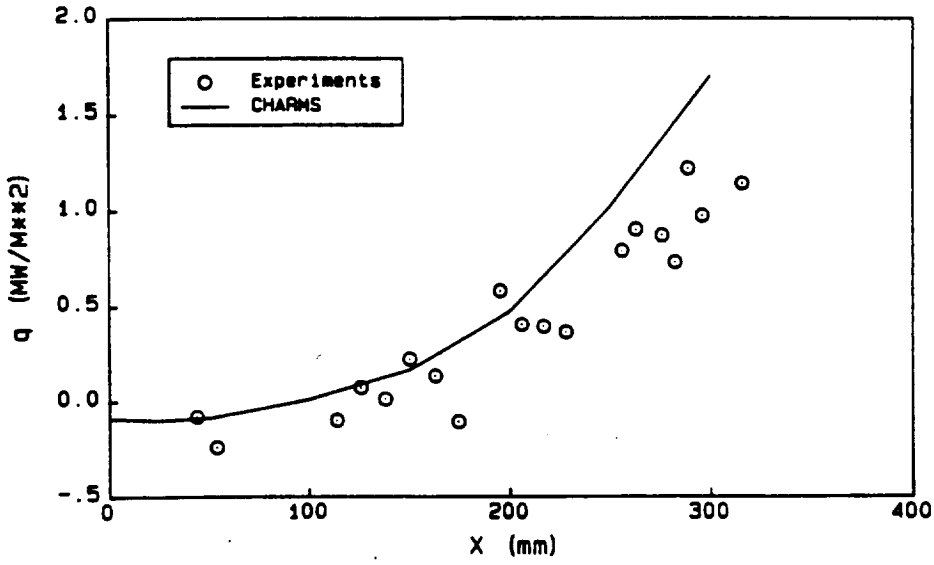

Fig. 16 Axial variation of heat transfer rate in a constant area duct. Low velocity region in free stream near injector

ϕ = 2.64 , H_s = 8.7 MJ/kg , M = 3.5 , T_t = 300 K

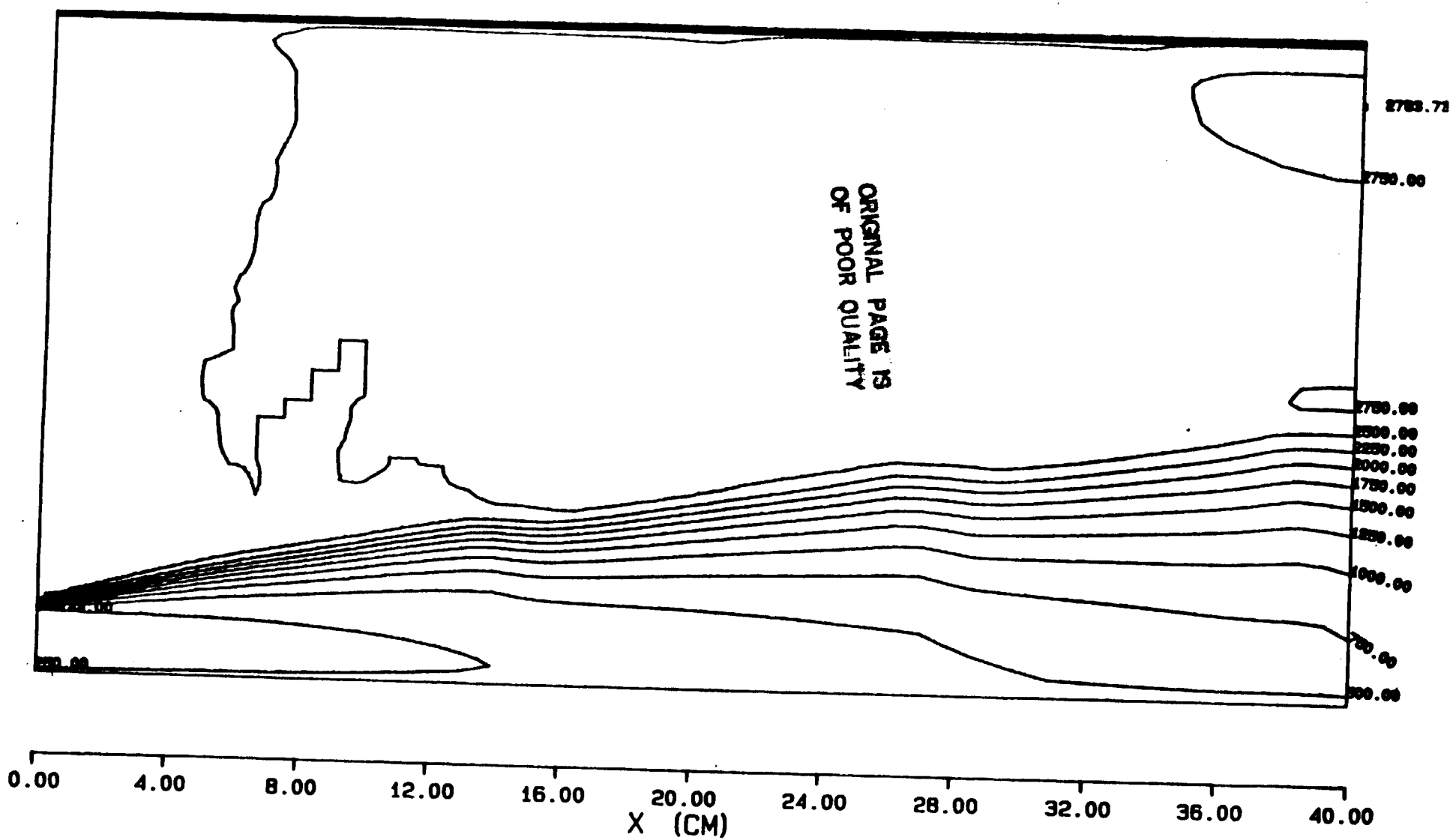

Fig. 17 Temperature contours (K) in a constant area duct
ϕ = 2.64, H_S = 8.7 MJ/kg , M = 3.5 , T_t = 300 K

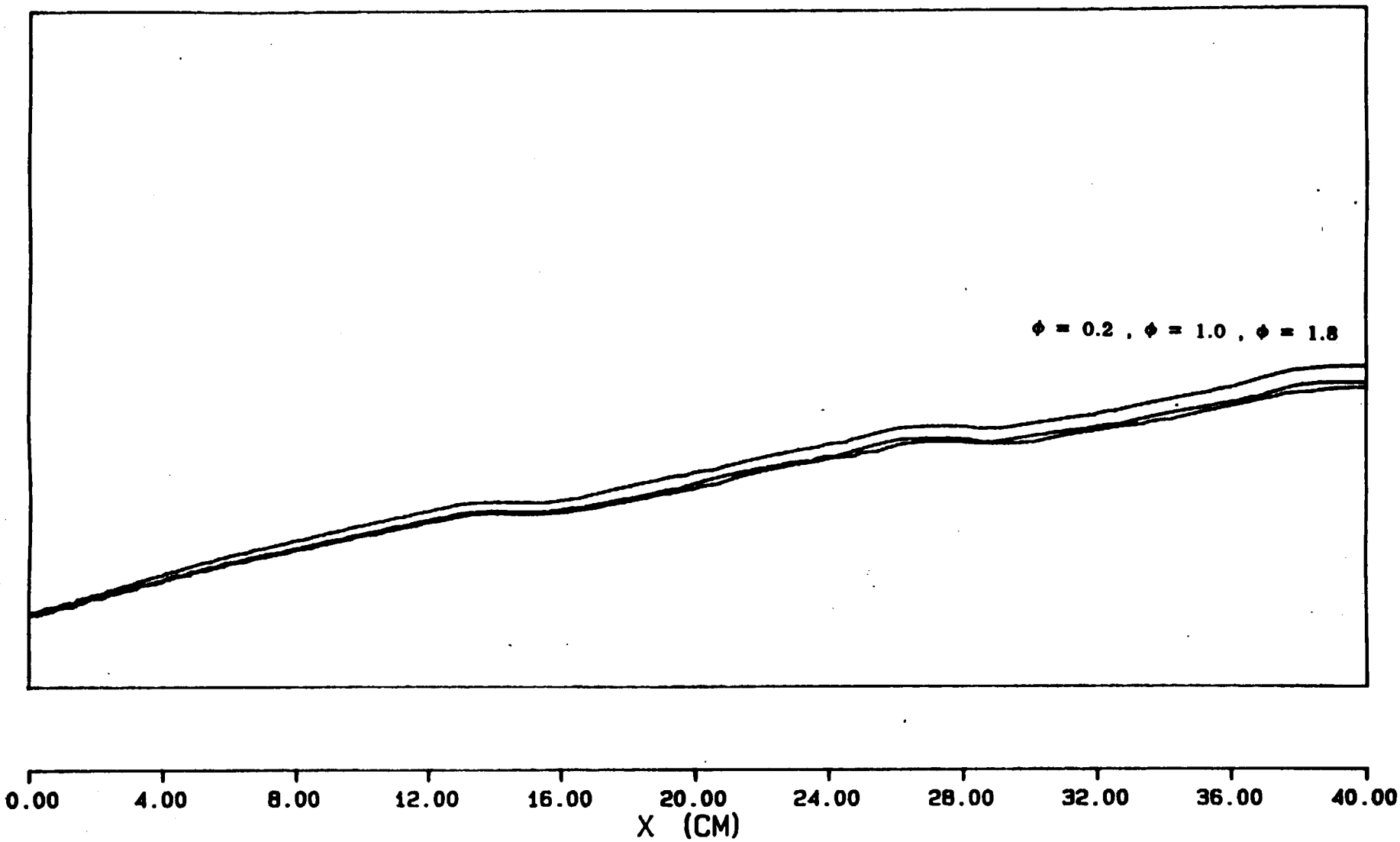

Fig. 18 Local equivalence ratio contours in a constant area duct

ϕ = 2.64, H_S = 8.7 MJ/kg , M = 3.5 , T_t = 300 K

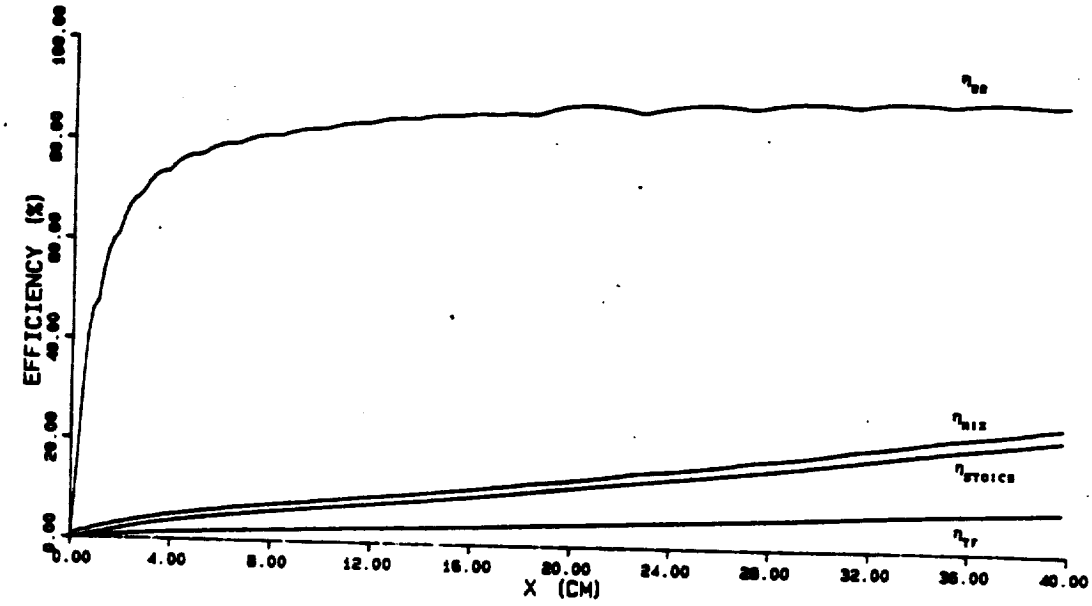

Fig. 19 Axial variation of combustion and mixing efficiencies

ϕ = 2.64 , H_S= 8.7 MJ/kg , M = 3.5 , T_t= 300 K

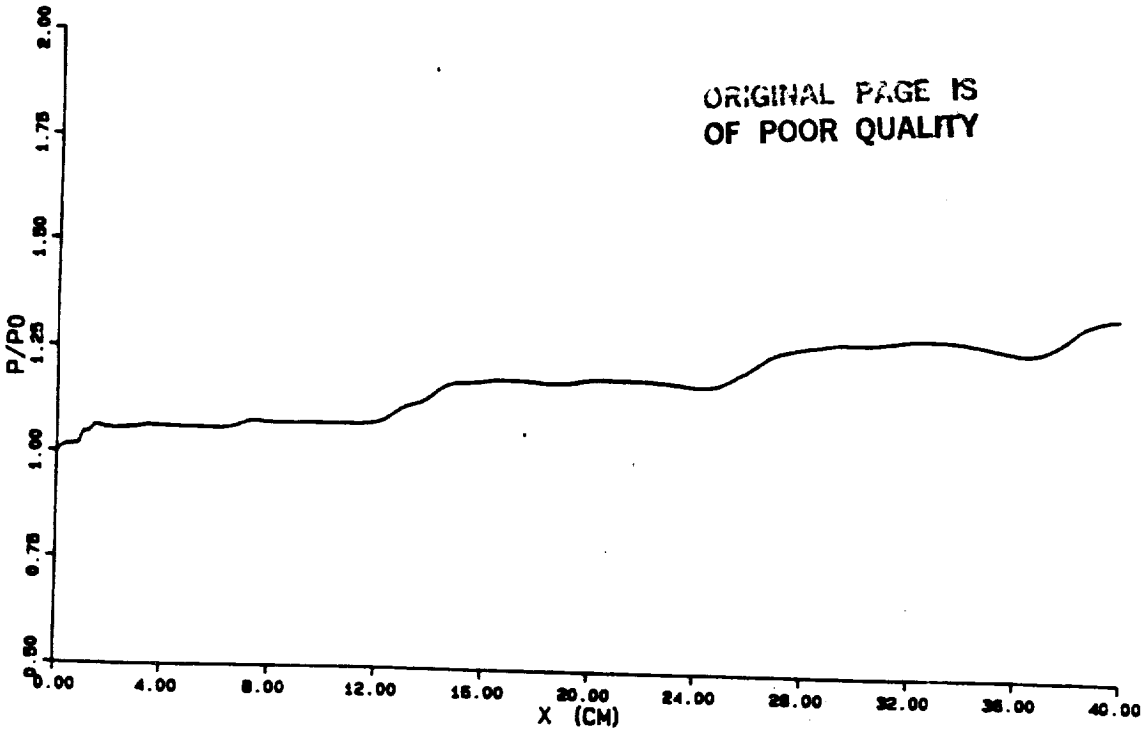

Fig. 20 Axial variation of pressure in a constant area duct

ϕ = 2.64 , H_S= 8.7 MJ/kg , M = 3.5 , T_t= 1800 K

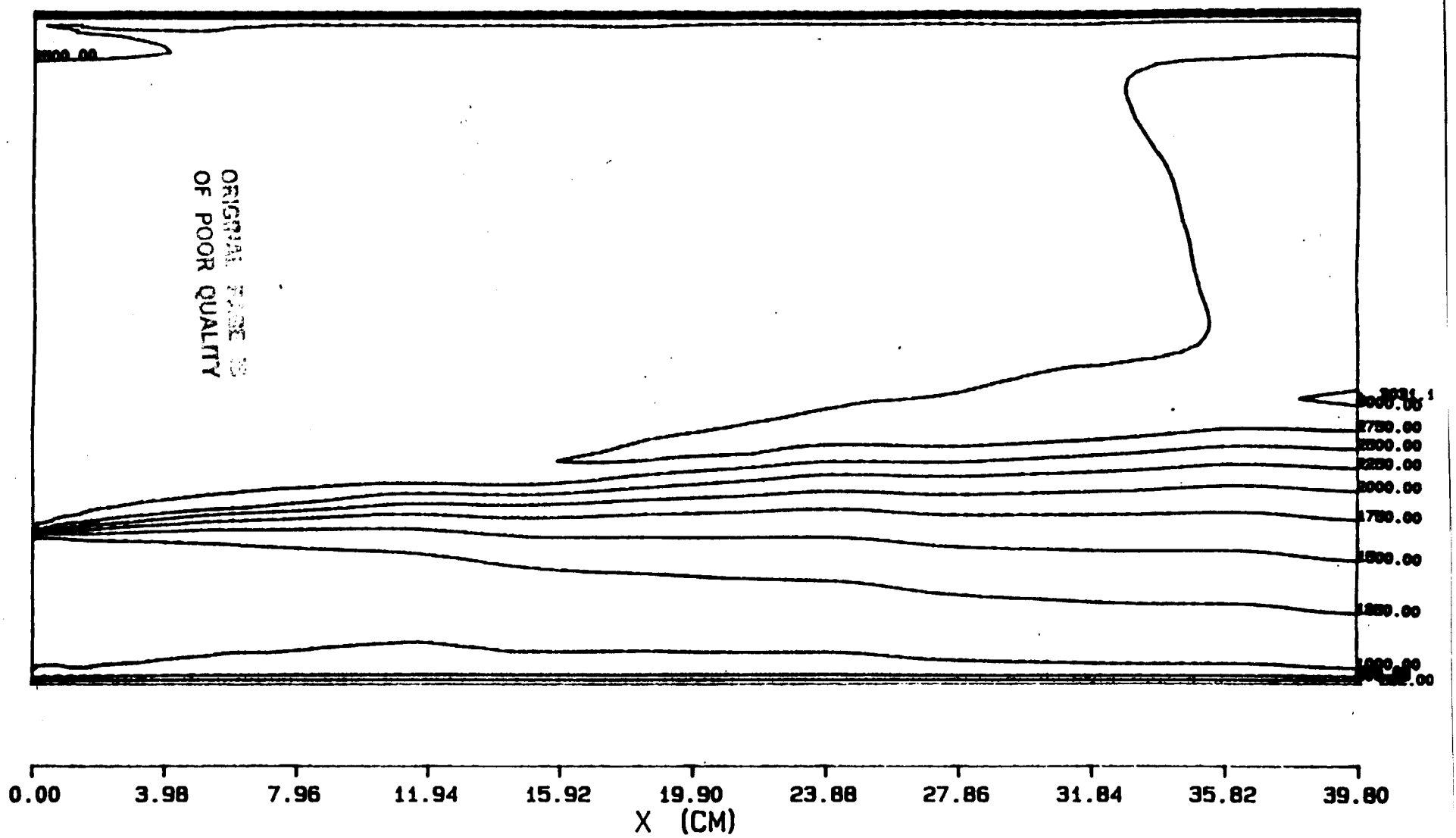

Fig. 21 Temperature contours in a constant area duct

Φ = 2.64, H_s= 8.7 MJ/kg , M = 3.5 , T_t= 1800 K

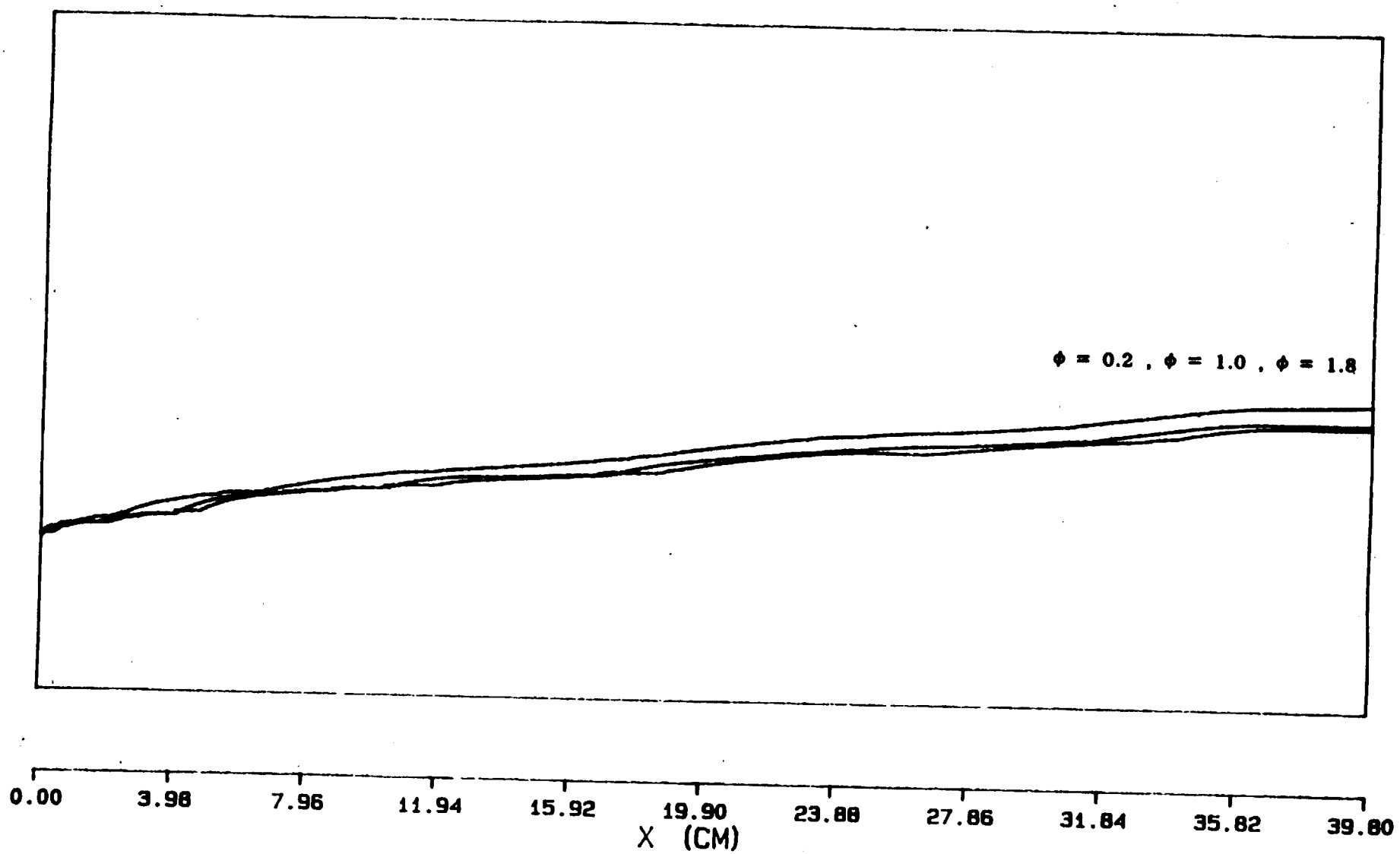

Fig. 22 Local equivalence ratio contours in a constant area duct
ϕ = 2.64 , H_S = 8.7 MJ/kg , M = 3.5 , T_t = 1800 K

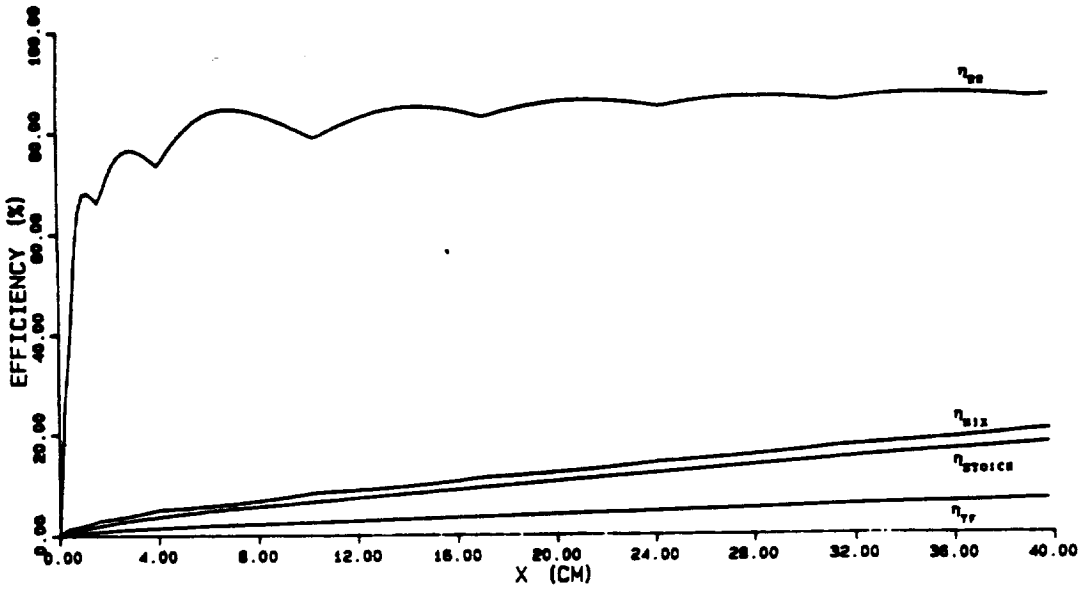

Fig. 23 Axial variation of combustion and mixing efficiencies

ϕ = 2.64 , H_s = 8.7 MJ/kg , M = 3.5 , T_t = 1800 K

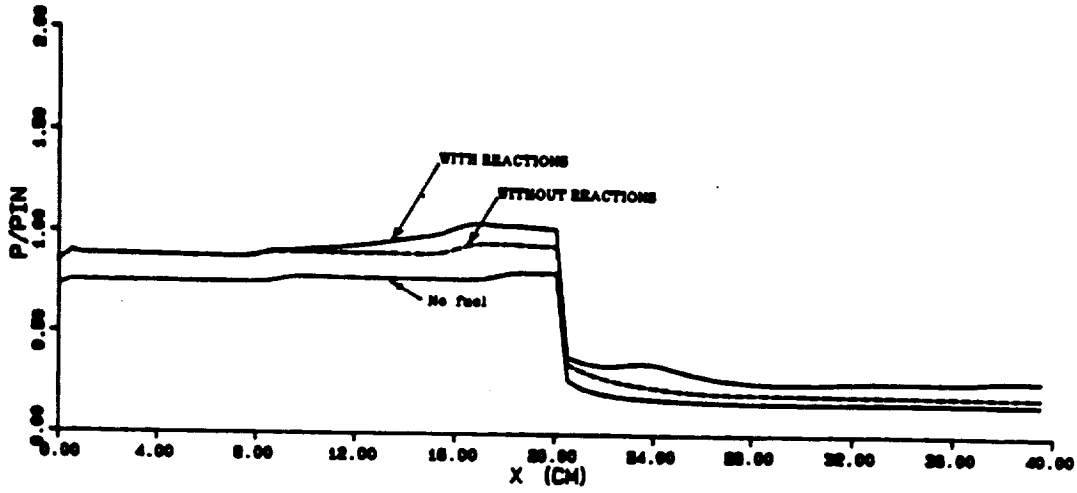

Fig. 24 Axial variation of pressure $\theta_D = 15°$

ϕ = 1.43 , H_S = 4.2 MJ/kg , M = 3.5 , T_t = 300 K

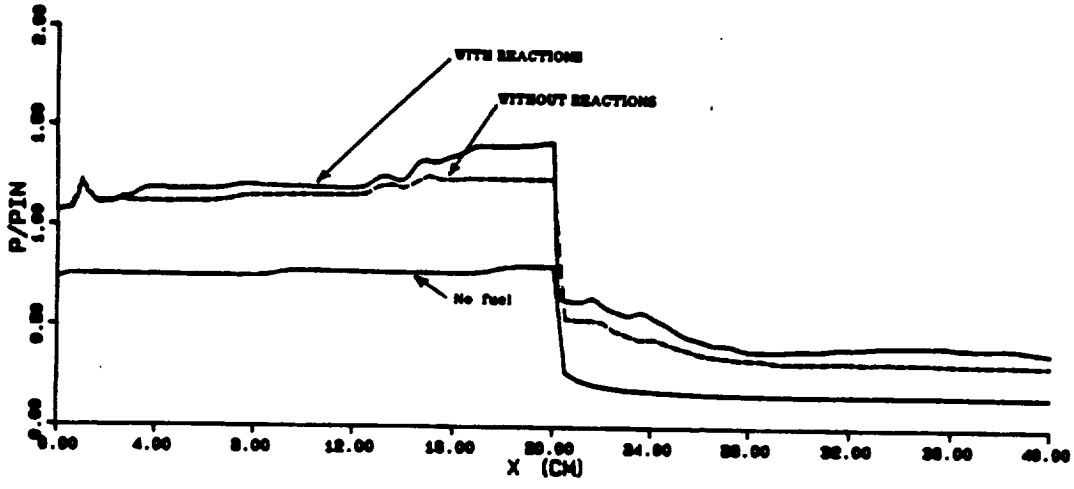

Fig. 25 Axial variation of pressure $\theta_D = 15°$

ϕ = 1.43, H_S = 4.2 MJ/kg , M = 3.5 , T_t = 1800 K

COMBUSTION OF HYDROGEN AND HYDROGEN/SILANE MIXTURES

N. Morris

SECTION 1

COMBUSTION OF HYDROGEN/AIR MIXTURES

This section examines hydrogen/air reactions in supersonic and hypersonic flows. Ignition limits have been found by experiment for a few cases (1) and these can be compared with computer simulations using a 1-D premixed finite rate chemical kinetics program (2) presented in this section. The number of reactions used in the simulation of hydrogen combustion is reduced from 60 to 17 reactions by eliminating groups of reactions that do not appear to have a great effect on the combustion process at the experimental conditions. This is done in order to reduce computation time.

1.1 Reactions of Hydrogen in Air

Analysis of reactions of hydrogen in air can be initially investigated by considering only the oxidation of hydrogen gas into water. Using mass, momentum, and energy conservation equations, together with heats of reaction, final state properties can be easily calculated. These can be used for a quantitative comparison with experimental results of supersonic reacting hydrogen/air mixtures. This approach does not take into account viscous effects, heat transfer to the walls, or mixing but is a useful tool in understanding the combustion process as well as giving a reasonable approximation to final state conditions.

A more rigorous approach, however, is needed when investigating the ignition-combustion limits of such a mixture. Ignition delay times become significant in very high speed flows where reaction speeds are critical to a scramjet's performance. Therefore, a chemical kinetics approach is needed to simulate the burning process. The combustion process is controlled by the chemical kinetics of a series of reactions whose rates can usually be found in the literature. For hydrogen based reactions, these rates are usually well documented. The difficulty lies in the choice of reactions which sufficiently model the actual combustion process.

At temperatures above 1000 K, the hydrogen/air system can be closely represented by the reactions:

$$H + O_2 \rightleftarrows OH + O$$

$$O + H_2 \rightleftarrows OH + H$$

$$OH + H_2 \rightleftarrows H_2O + H$$

$$H_2 + M \rightleftarrows H + H + M$$

$$H_2O + M \rightleftarrows H + OH + M$$

$$O_2 + M \rightleftarrows O + O + M$$

$$OH + M \rightleftarrows O + H + M$$

However, if most of the major chemical species which comprise air are considered, then there are at least sixty chemical reactions which can be used in the simulation of hydrogen/air combustion. These include the reactions that involve the gases N_2 and CO_2 in conjunction with O_2

By increasing the number of known reactions in the analysis, the simulation would be expected to approximate more closely the combustion process. However, some groups of reactions involving a single chemical specie play only a very small part in the ignition process and so could be ignored to save computer time.

In continuation of work carried out by Morgan (3) an optimal reaction scheme was found for the combustion of hydrogen/air mixtures using a 1-D chemical kinetics analysis at high temperatures. Groups of equations were combined differently until the least number of reactions were able to produce results that were comparable with the sixty reaction scheme.

In all, the optimal combination comprises 17 reactions which include the seven reactions stated above together with the HO_2, NO, and HNO groups of reactions. It is noted that carbon species play only a very small role in hydrogen/air combustion because of the low concentration of carbon dioxide in air. The 17 reactions together with reaction rate coefficients are found in Appendix A together with the remaining reactions that make up the 60 reaction scheme.

1.2 Effect of Free Radicals on Combustion

Previous work on the effect of free radicals has been done by Carson (4). Using a finite rate chemical kinetics program, Carson was able to demonstrate that small amounts of atomic oxygen, atomic hydrogen, and hydroxyl radicals reduced induction time , defined as the time to 5% of the temperature rise from the initial mixture temperature to the calculated equilibrium temperature. It was also shown that hydroperoxyl (HO_2) plays a significant role in the early part of the ignition process - the inflection in its rate of formation could be used to define induction time. The reaction time, defined as the time between 5% and 95% of the temperature was not affected by the initial amount of free radicals. All of the radicals were more effective in reducing induction time at low initial temperatures. For all mixtures and states, atomic oxygen was most effective in reducing induction time at low initial temperatures. In order to optimize the combustion chamber length or permit operation in a pressure or temperature limited regime, it was implied that additives that yield free radicals could be used.

For work presented in this section, simulations were run at an initial nominal Mach number of 3.5 and static pressure of 160 kPa to coincide with experimental conditions discussed in (1). Using a One-Dimensional Non-Equilibrium Nozzle Flow (NENZF) program (5), the percentage dissociation of molecular oxygen, α, was calculated for the conditions found at the exit of the shock tunnel nozzle. Because experimental results are presented as pressure/distance profiles, simulations are presented in the same way for comparison of relative ignition distances and relative pressure rises. Because mixture velocities stay roughly constant up until the point of ignition, ignition distances are directly related to ignition delay times for runs with identical initial conditions.

Figure 1.1 shows a pressure-distance profile for reacting flow over 30 cm for a premixed stoichiometric hydrogen air mixture initially at Mach 3.5 (nominal), a temperature of 1100 K, and pressure of 160 kPa. These conditions correspond to an airflow stagnation enthalpy of 4.2 MJ/kg or a flight speed of 2.9 km/s. For this case, there was no assumed initial dissociation of oxygen. It can be seen that a ten reaction scheme has the longest ignition delay time. The 17, 22, and 28 reaction schemes' pressure profiles lay on top of each other at this condition and the

60 reaction scheme produces the fastest ignition.

At these conditions, NENZF calculates an oxygen dissociation of 0.18% when the shock tunnel T3 is run. Figure 1.2 illustrates the effect this fraction of dissociated oxygen has on the simulation. The 7 and 10 reaction schemes show a marginally longer ignition delay time over the 17,22,28 and 60 reaction schemes. All reaction schemes show a significantly reduced induction time over the cases when there is no initial free radical oxygen present.

When the temperature is reduced to 900 K (corresponding to an airflow stagnation enthalpy of 3.43 MJ/kg),a run over 30 cm produces no combustion when there is no initial free radical oxygen present (Fig. 1.3). When an initial concentration of 0.13% atomic oxygen is included, the same that would be present in a shock tunnel run at those conditions, combustion occurs within the first 10 cm as shown in Figure 1.4. Again the 7 and 10 reaction schemes fall upon one another and the 17,22,28 and 60 reaction schemes yield essentially the same result at a shorter distance.

When the temperature is further reduced to 700K, no combustion is observed in the simulations for both cases when there is no atomic oxygen included in the analysis and with an α of 0.06% as predicted by NENZF for a shock tunnel run at these conditions. This confirms experimental observations of no combustion at this condition, which is discussed in (1).

The increase in ignition distance for the lower temperature case of 900K over the 1100K case when a small amount of free radical oxygen is added confirms the observations by Carson (4). The simulations also demonstrate that the 17 reaction scheme is the lowest number of reactions that most follows the 60 reaction scheme, particularly when there is some free radical oxygen present. Because shock tunnels produce high speed air flows with traces of free radicals, simulations of H_2 combustion suggest that early ignition at lower temperatures in the shock tunnel is probably due to the presence of free radical oxygen.

However, at higher enthalpy (hence higher temperature) conditions, the presence of larger amounts of free radical oxygen does not appear to have an appreciable effect on the ignition distance. This is illustrated in pressure-distance profiles plotted for simulations run at conditions corresponding to a stagnation enthalpy of 6.1 MJ/kg with initial pressure of 160 kPa and

temperature of 1700 K. Figure 1.5 shows the results for no initial atomic oxygen included in the analysis. The 60 reaction scheme gives marginally faster ignition over the 28,22 and 17 reaction schemes with the 10 and 7 reaction schemes giving the largest ignition distance. At this enthalpy condition, NENZF calculates an oxygen dissociation of around 2.0% . When this is included in the combustion simulation (Fig. 1.6), the ignition is only marginally faster than when no atomic oxygen is included in the analysis. This suggests that if the reaction scheme is valid, then freestream radical oxygen production by the shock tunnel at high enthalpies does not have a significant effect on the ignition distance at this pressure.

A numerical simulation of hydrogen combustion was carried out at the conditions corresponding with the use of the hypersonic nozzle at stagnation enthalpies of 4.2, 6.1, and 8.7 MJ/kg and this is shown as plots of pressure against distance in Fig. 1.7.

At 4.2 MJ/kg (T_I =650 K), no hydrogen combustion is observed and this is in agreement with experiment shown in (1).

At 6.1 MJ/kg (T_I = 1000 K), the simulation predicts that ignition occurs between 30 and 40 cm downstream from the point of injection, but hydrogen does not appear to burn at all in the experiment. At this condition, the ignition distance appears to be nearing the length of the experimental model. Experiments using a longer model would be useful to check that the ignition was merely delayed rather than completely quenched for this case.

At 8.7 MJ/kg (T_I = 1500 K), the simulation predicts almost immediate combustion with pressure increases of between 5 and 10 kPa (0.05 and 0.1 atm.). This agrees reasonably well with experiment shown in (1) with small pressure rises of around 5 kPa above fuel-off levels.

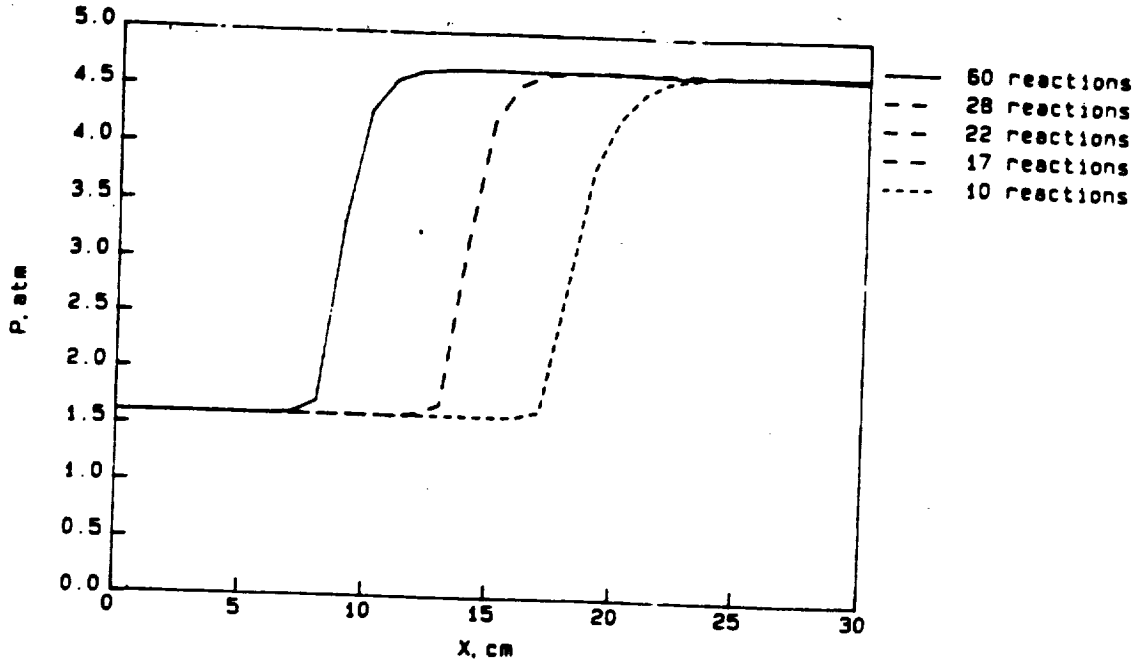

Fig. 1.1 Hydrogen Combustion Simulation.
Effect of Varying Reactions, Mach 3.5 nominal.
H_S = 4.2 MJ/kg, P_I = 160 kPa, T_I = 1100 K, ϕ =1.0, α = 0.00 %

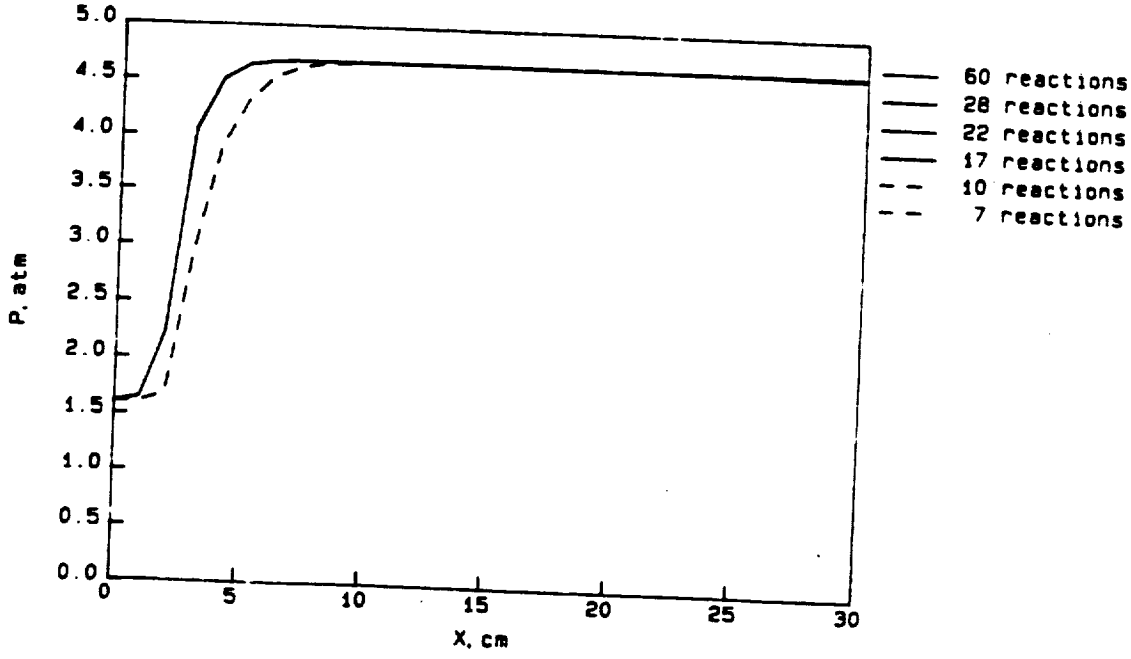

Fig. 1.2 Hydrogen Combustion Simulation.
Effect of Varying Reactions, Mach 3.5 nominal.
H_S = 4.2 MJ/kg, P_I = 160 kPa, T_I = 1100 K, ϕ =1.0, α = 0.18 %

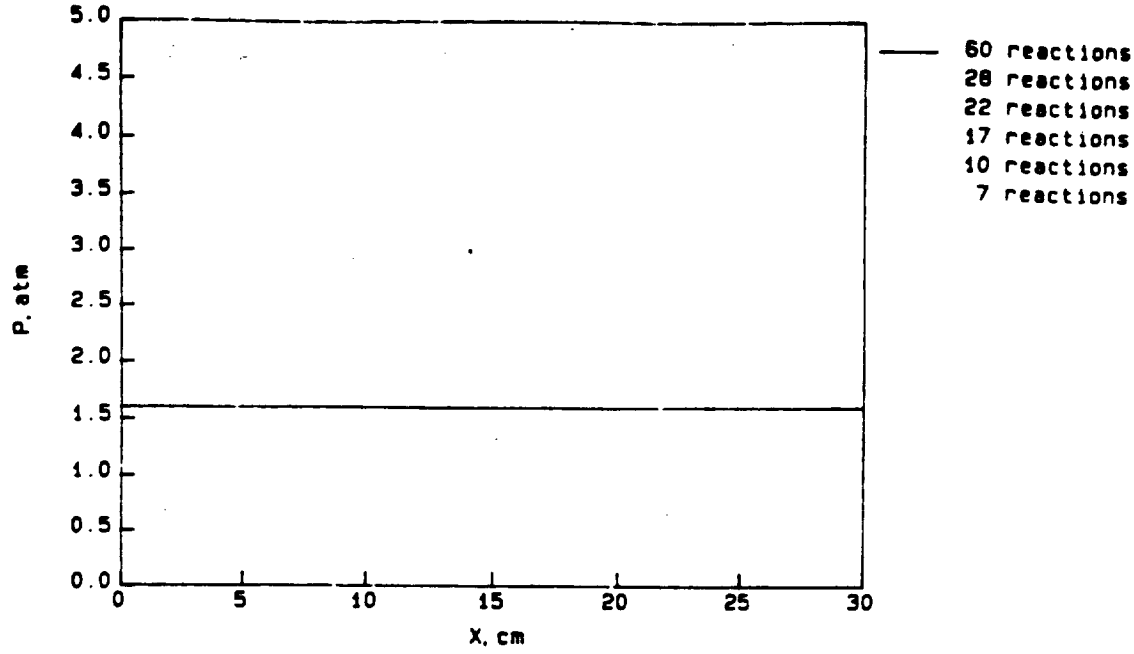

Fig. 1.3 Hydrogen Combustion Simulation.
Effect of Varying Reactions, Mach 3.5 nominal.
H_S = 3.43 MJ/kg, P_I = 160 kPa, T_I = 900 K, ϕ =1.0, α = 0.00 %

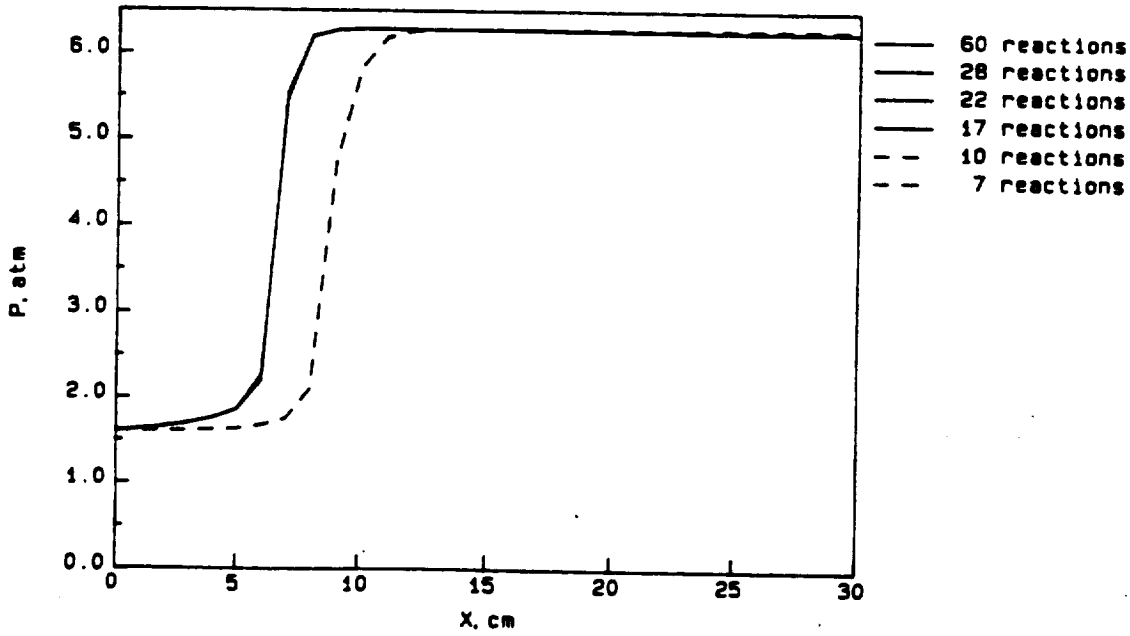

Fig. 1.4 Hydrogen Combustion Simulation.
Effect of Varying Reactions, Mach 3.5 nominal.
H_S = 4.2 MJ/kg, P_I = 160 kPa, T_I = 900 K, ϕ =1.0, α = 0.13 %

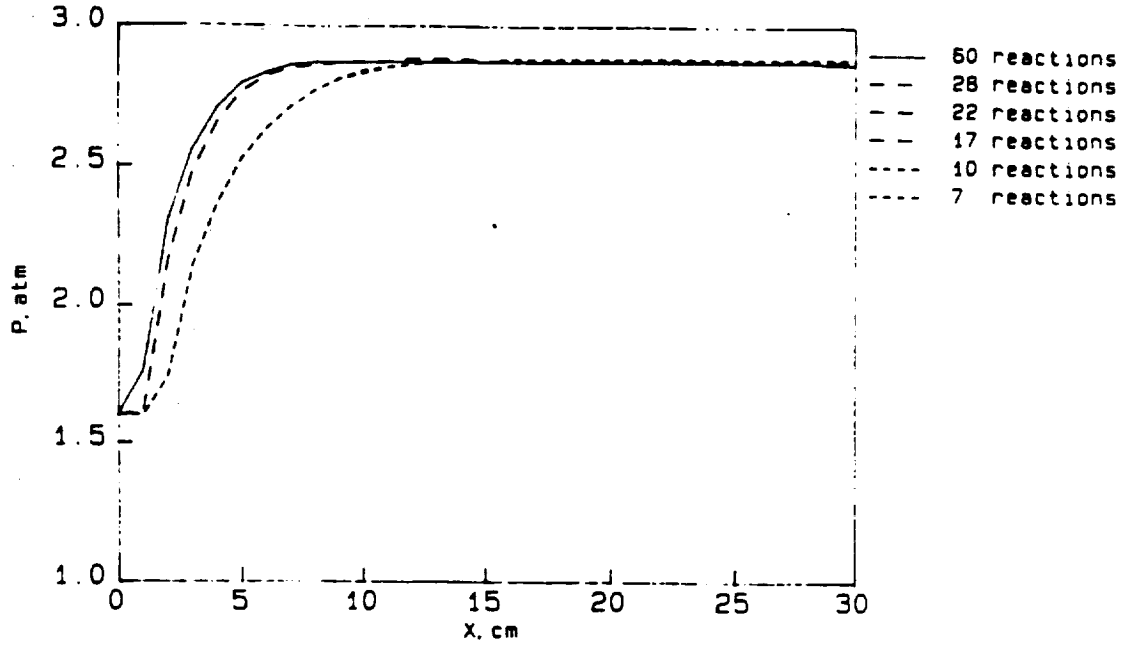

Fig. 1.5 Hydrogen Combustion Simulation.
Effect of Varying Reactions, Mach 3.5 nominal.
H_S = 6.1 MJ/kg, P_I = 160 kPa, T_I = 1700 K, ϕ =1.0, α = 0.00 %

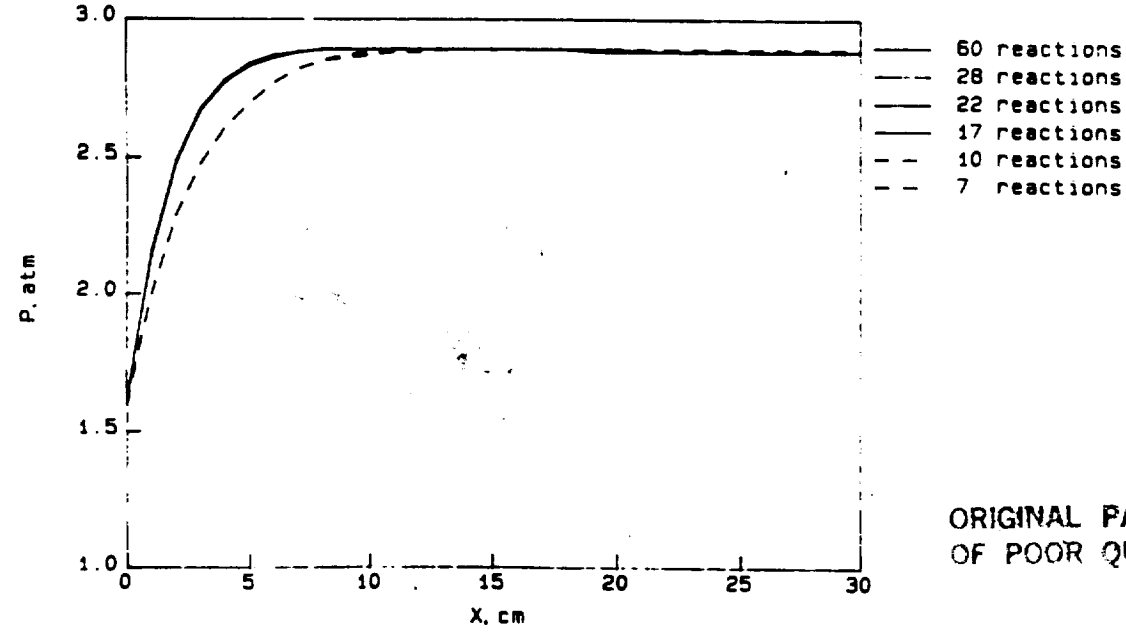

ORIGINAL PAGE IS
OF POOR QUALITY

Fig. 1.6 Hydrogen Combustion Simulation.
Effect of Varying Reactions, Mach 3.5 nominal.
H_S = 6.1 MJ/kg, P_I = 160 kPa, T_I = 1700 K, ϕ =1.0, α = 2.0 %

C-2

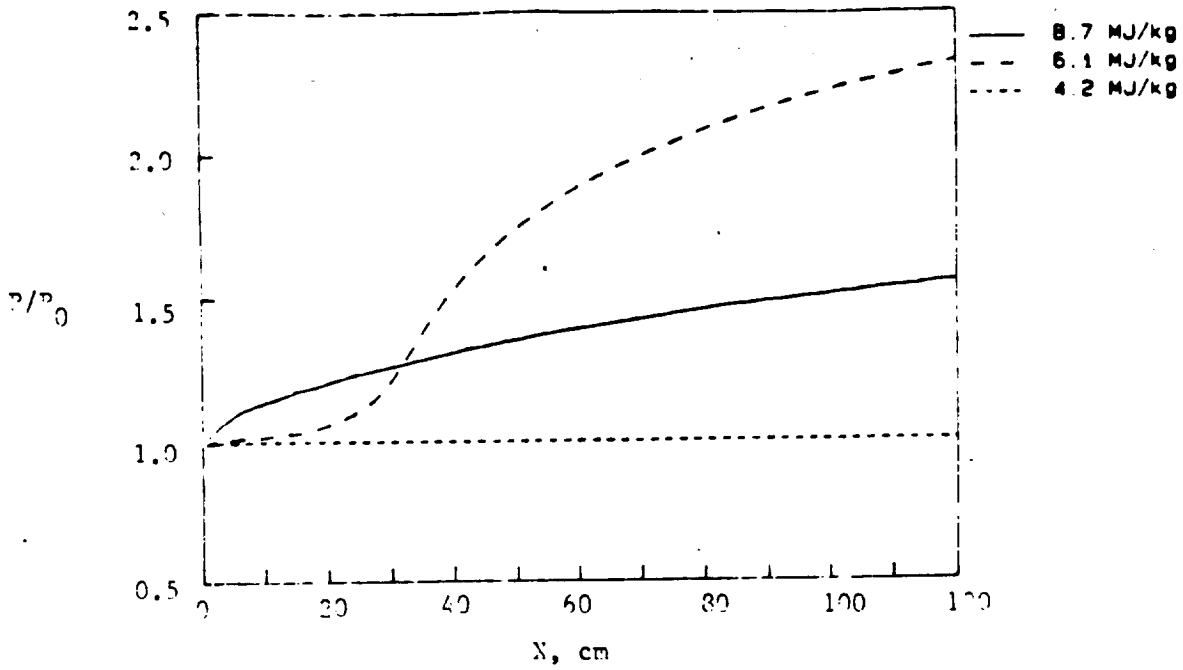

Fig. 1.7 Hydrogen Combustion Simulation.
Effect of Varying Enthalpies, Mach 5 nominal.
$P_1 = 20$ kPa, $\phi = 1.0$

APPENDIX A

17 REACTIONS

				A	N	E
M	1 O2	1 O	1 O	7.2E18	-1.	11790R.
M	1 H2	1 H	1 H	5.5E18	-1.	103298.
M	1 H2O	1 H	1 OH	5.2E21	-1.5	118000.
1 H	1 O2	1 HO2	M	2.3E15	0.0	-800.
1 O	1 H	1 OH	M	7.1E18	-1.0	0.
1 H2	1 OH	1 H2O	1 H	2.0E13	0.0	5166.
1 O2	1 H	1 OH	1 O	2.2E14	0.0	16800.
1 H2	1 O	1 OH	1 H	7.5E13	0.0	11099.
1 H	1 HO2	1 H2	1 O2	2.4E13	0.0	695.
1 H	1 HO2	1 OH	1 OH	2.4E14	0.0	1887.
1 H2O	1 O	1 H	1 HO2	5.8E11	0.5	57000.
1 O	1 HO2	1 OH	1 O2	5.0E13	0.0	1000.
1 OH	1 HO2	1 O2	1 H2O	3.0E13	0.0	0.
1 H2	1 HO2	1 H2O	1 OH	2.0E13	0.0	25000.
1 O	1 N2	1 NO	1 N	5.0E13	0.0	75386.
1 H	1 NO	1 OH	1 N	1.7E14	0.0	48491.
1 O	1 NO	1 O2	1 N	1.5E09	1.0	38746.

APPENDIX A

ORIGINAL PAGE IS
OF POOR QUALITY

REACTION SCHEME FOR HYDROGEN COMBUSTION — 40 REACTIONS

				A	N	E
M	1 O2	1 O	1 O	7.2E18	-1.	117908.
M	1 H2	1 H	1 H	5.5E18	-1.	103298.
M	1 H2O	1 H	1 OH	5.2E21	-1.5	118000.
1 H	1 O2	1 HO2	M	2.3E15	0.0	-800.
M	1 NO2	1 NO	1 O	1.1E16	0.0	64995.
M	1 NO	1 N	1 O	4.1E18	-1.	149680.
1 O	1 CO	1 CO2	M	3.0E14	0.0	3000.
1 H	1 NO	1 HNO	M	5.4E15	0.0	-596.
M	1 H2O2	1 OH	1 OH	1.2E17	0.0	45500.
1 OH	1 NO	1 HNO2	M	8.0E15	0.0	-1987.
1 OH	1 NO2	1 HNO3	M	1.3E16	0.0	-2200.
M	1 O3	1 O2	1 O	1.3E21	-2.0	25433.
M	1 HCO	1 CO	1 H	2.0E12	0.5	27400.
1 O	1 H	1 OH	M	7.1E18	-1.0	0.
1 H2O	1 O	1 OH	1 OH	5.8E13	0.0	15000.
1 H2	1 OH	1 H2O	1 H	2.0E13	0.0	5166.
1 O2	1 H	1 OH	1 O	2.2E14	0.0	16800.
1 H2	1 O	1 OH	1 H	7.5E13	0.0	11099.
1 H2	1 O2	1 OH	1 OH	1.0E13	0.0	43000.
1 H	1 HO2	1 H2	1 O2	2.4E13	0.0	695.
1 H2	1 O2	1 H2O	1 O	4.1E13	0.0	50470.
1 H	1 HO2	1 OH	1 OH	2.4E14	0.0	1887.
1 H2O	1 O	1 H	1 HO2	5.8E11	0.5	57000.
1 O	1 HO2	1 OH	1 O2	5.0E13	0.0	1000.
1 OH	1 HO2	1 O2	1 H2O	3.0E13	0.0	0.
1 H2	1 HO2	1 H2O	1 OH	2.0E13	0.0	25000.
1 HO2	1 H2	1 H	1 H2O2	7.3E11	0.0	18677.
1 H2O2	1 H	1 OH	1 H2O	3.2E14	0.0	8950.
1 HO2	1 OH	1 O	1 H2O2	5.2E10	0.5	21062.
1 HO2	1 H2O	1 OH	1 H2O2	2.8E13	0.0	32785.
1 HO2	1 HO2	1 H2O2	1 O2	2.0E12	0.0	0.
1 O	1 O3	1 O2	1 O2	1.0E13	0.0	4790.
1 O3	1 NO	1 NO2	1 O2	5.4E11	0.0	2384.
1 O3	1 H	1 OH	1 O2	7.0E13	0.0	1113.
1 O3	1 OH	1 O2	1 HO2	9.0E11	0.0	1987.
1 O	1 N2	1 NO	1 N	5.0E13	0.0	75386.
1 H	1 NO	1 OH	1 N	1.7E14	0.0	48681.
1 O	1 NO	1 O2	1 N	1.5E09	1.0	38746.
1 NO2	1 H	1 NO	1 OH	3.5E14	0.0	1470.
1 NO2	1 O	1 NO	1 O2	1.0E13	0.0	600.
1 NO2	1 H2	1 HNO2	1 H	2.4E13	0.0	29000.
1 HO2	1 NO	1 NO2	1 OH	3.0E12	0.5	2400.
1 NO2	1 H2O	1 HNO2	1 OH	3.2E12	0.0	43714.
1 NO2	1 OH	1 HNO2	1 O	2.1E12	0.0	24996.
1 CO	1 OH	1 CO2	1 H	7.0E11	0.0	1987.
1 CO2	1 O	1 O2	1 CO	2.5E12	0.5	55040.
1 H2O	1 CO	1 HCO	1 OH	6.5E13	0.3	103026.
1 OH	1 CO	1 HCO	1 O	5.8E12	0.32	86295.
1 H2	1 CO	1 HCO	1 H	1.2E13	0.29	88242.
1 HO2	1 CO	1 CO2	1 OH	1.5E14	0.0	23645.
1 HNO	1 H	1 H2	1 NO	4.8E12	0.0	0.
1 HNO	1 OH	1 H2O	1 NO	3.6E13	0.0	0.
1 NO	1 CO	1 CO2	1 N	4.6E08	0.5	23983.
1 NO2	1 CO	1 NO	1 CO2	1.0E12	0.0	27600.
1 NO	1 HO2	1 HNO	1 O2	7.2E11	0.5	10928.
1 HNO	1 O	1 NO	1 OH	5.0E11	0.5	0.
1 HNO3	1 O	1 HO2	1 NO2	1.0E11	0.0	0.
1 HO2	1 NO2	1 HNO2	1 O2	2.0E11	0.0	0.
1 HCO	1 O2	1 CO	1 HO2	1.0E11	0.5	5400.
1 O3	1 HO2	2 O2	1 OH	1.0E11	0.0	2800.

SECTION 2

MODELLING THE SILANE IGNITION PROCESS

This section describes the reaction scheme used for modelling the silane/hydrogen ignition process together with underlying assumptions. Computer simulations use a 1-D chemical kinetics program (2). Methods for determining the thermochemical properties of chemical species produced during the silane oxidation process as well as chemical rate coefficients are also discussed.

2.1 An Analogy to Methane Oxidation - The Jachimowski Model.

A chemical reaction mechanism was assembled by Beach (6) using a direct analogy with the methane oxidation reaction mechanism. The mechanism was tested by comparing the calculated consumption of silane with experimental results from a low temperature (500-700K) isothermal flow reactor. Jachimowski (7) refined this mechanism by comparing the observed behaviour determined in shock tube studies with that predicted by the mechanism. It is this work by Jachimowski on which the modelling of the combustion process in this section is based.

Basic features of the high temperature oxidation of silane were taken from the methane oxidation mechanism since little chemical kinetic information is known about the silane oxidation process. The methane oxidation process has been studied for many years and the essential reaction paths, intermediates, and products are relatively well known.

The silane molecule has a structure similar to that of the methane molecule, and the silane oxidation products (SiO, SiO_2) are similar to the methane oxidation products (CO, CO_2). Jachimowski argued that it therefore seemed reasonable to assume that similar reactions and reaction intermediates would occur. It was recognised that silicon and carbon bonds were not identical therefore the actual reactivity and nature of the intermediate species may be different

from the methane scheme. However, it was the objective to develop a silane mechanism which contained enough detail to describe the essential features of the oxidation process rather than exactly model the process.

The silane reaction mechanism used is shown in Fig. 2.1. This together with the 17 reaction hydrogen scheme outlined in section 2 as being optimum were used for any subsequent modelling work in this section. Rate coefficients are well documented for the current hydrogen schemes. However, little is known about the silane oxidation reactions. Rate coefficients estimated by Jachimowski using the carbon based analogy are therefore used for the work presented in this section.

Reaction	Rate coefficient
$SiH_4 \rightarrow SiH_2 + H_2$	6.0×10^{13} exp(-54960/RT)
$SiH_4 + O_2 \rightarrow SiH_3 + HO_2$	2.0×10^{11} exp(-44000/RT)
$SiH_4 + HO_2 \rightarrow SiH_3 + H_2O_2$	3.0×10^{12} exp(-5600/RT)
$H + SiH_4 \rightarrow H_2 + SiH_3$	1.5×10^{13} exp(-2500/RT)
$O + SiH_4 \rightarrow OH + SiH_3$	4.2×10^{12} exp(-1600/RT)
$OH + SiH_4 \rightarrow H_2O + SiH_3$	8.4×10^{12} exp(-100/RT)
$H + SiH_3 \rightarrow SiH_2 + H_2$	1.5×10^{13} exp(-2500/RT)
$O + SiH_3 \rightarrow SiH_2O + H$	1.3×10^{14} exp(-2000/RT)
$OH + SiH_3 \rightarrow SiH_2O + H_2$	5.0×10^{12}
$SiH_3 + O_2 \rightarrow SiH_2O + OH$	†8.6×10^{14} exp(-11400/RT)
$SiH_2 + O_2 \rightarrow HSiO + OH$	1.0×10^{14} exp(-3700/RT)
$H + SiH_2O \rightarrow H_2 + HSiO$	3.3×10^{14} exp(-10500/RT)
$O + SiH_2O \rightarrow OH + HSiO$	1.8×10^{13} exp(-3080/RT)
$OH + SiH_2O \rightarrow H_2O + HSiO$	7.5×10^{12} exp(-170/RT)
$H + HSiO \rightarrow H_2 + SiO$	2.0×10^{14}
$O + HSiO \rightarrow OH + SiO$	1.0×10^{14}
$OH + HSiO \rightarrow H_2O + SiO$	1.0×10^{14}
$HSiO + M \rightarrow H + SiO + M$	5.0×10^{14} exp(-29000/RT)
$HSiO + O_2 \rightarrow SiO + HO_2$	3.0×10^{12}
$SiH_2O + HO_2 \rightarrow HSiO + H_2O_2$	1.0×10^{12} exp(-8000/RT)
$SiO + O + M \rightarrow SiO_2 + M$	2.5×10^{15} exp(-4370/RT)
$SiO + OH \rightarrow SiO_2 + H$	4.0×10^{12} exp(-5700/RT)
$SiO + O_2 \rightarrow SiO_2 + O$	1.0×10^{13} exp(-6500/RT)

Fig. 2.1. Silane Reaction Mechanism

2.2 Thermochemical Properties of Intermediate Species

As indicated in (2), thermochemical properties for the program are of the form of a polynomial with seven constants describing the properties specific heat, enthalpy and entropy. The first five constants $A_1 \cdots A_5$ describe the specific heats while A_6 and A_7 describe standard

enthalpies and entropies respectively (divided by the universal gas constant). In simple terms, A_6 and A_7 take the form:

$$A_6 = \frac{\Delta H_{298f}{}^0}{R} - \left(A_1 T + \frac{A_2}{2} T^2 + \frac{A_3 T^3}{3} + \frac{A_4 T^4}{4} + \frac{A_5 T^5}{5} \right)_{T=298K} \quad (1)$$

where

$$\Delta H^0_{298\,f}(AB) = \Delta H^0_{298\,f}(A) + \Delta H^0_{298\,f}(B) - D_{A-B} \quad (2)$$

D_{A-B} refers to bond energy and heats of formation are found from assigned reference elements. An example of equation 3 would be

$$\Delta H^0_{298\,f}(SiH_2O) = \Delta H^0_{298\,f}(HSiO) + \Delta H^0_{298\,f}(H) - D_{H-HSiO}$$

For the constant relating to standard entropy

$$A_7 = \frac{S^0_{298}}{R} - \left(A_1 \ln T + A_2 T + \frac{A_3}{2} T^2 + \frac{A_4}{3} T^3 + \frac{A_5}{4} T^4 \right) \quad (3)$$

and

$$S^0_{298}(AB) = S^0_{298}(A) + S^0_{298}(B) - \Delta S \quad (4)$$

where ΔS is the standard entropy change for the reaction

$$AB \rightarrow A + B$$

In the Jachimowski model, four species SiH_4, SiH, SiO and SiO_2 have documented thermochemical properties (8). The thermochemical properties for the other silicon containing species were estimated because they were not available. Heat capacities of the species SiH_3, SiH_2, SiH_2O, and SiO were assumed to be equal to those of their analogous carbon containing species. Standard enthalpies for SiH_3 and SiH_2 were calculated using known values of enthalpies of formation and known bond energies while standard enthalpies for SiH_2O and SiO were calculated using known values of enthalpies of formation and bond energies in analogous carbon containing species. Standard entropies for SiH_3, SiH_2, SiH_2O, and SiO were calculated using known standard entropies and entropy changes for analogous carbon containing species.

2.3 Estimation of Rate Coefficients

The rate coefficient comprises two characteristic values for each reaction, a pre-exponential factor A, and an activation energy E. In the Jachimowski model, 5 reactions are documented and referenced with both values. The rest of the equations use the methane analogy, drawing on either one or both of the pre-exponential factor and activation energy making up the rate equation. In five cases, activation energies are calculated from bond energies or changes in enthalpy while the rest are set equal to values found in the analogous methane reactions.

Plots shown in Fig. 2.2 reproduced from reference (7) show the results of computer simulations compared with experimental shock tube results. Calculations using original estimated rate coefficients by Beach (6) give a much longer ignition delay time than that which was observed in experiment. The model was refined by Jachimowski (7) by carrying out a sensitivity analysis to determine which reactions had the largest effect on the ignition delay times. Rate coefficients were varied between 0.1 and 10 times their original value shown in Fig. 2.1.

Three reactions appeared to have the greatest effect on the ignition delay time when their rate coefficients were adjusted. These were

$$SiH_4 \rightarrow SiH_2 + H_2 \tag{5}$$

$$SiH_3 + O_2 \rightarrow SiH_2O + OH \tag{6}$$

$$SiO + OH \rightarrow SiO_2 + H \tag{7}$$

Each rate coefficient of each of these reactions was adjusted separately until calculated results agreed with experimental results. Two of the reactions yielded rate coefficients with unreasonably large values. Consequently it was decided that the rate coefficient should be adjusted for the equation which had the largest influence on calculated ignition delay times. This was for the reaction

$$SiH_3 + O_2 \rightarrow SiH_2O + OH$$

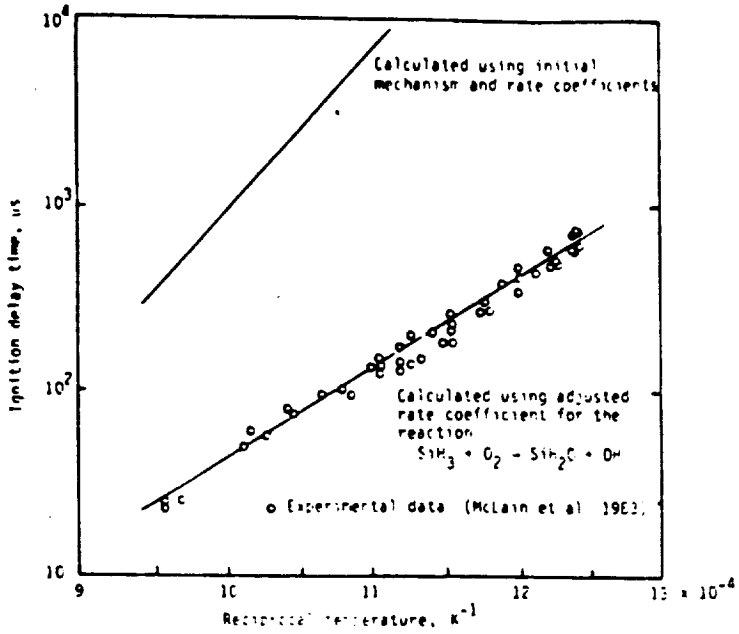

(a) 2 percent SiH_4, 8 percent H_2, 4 percent O_2, and 86 percent N_2 mixture; Pressure = 1.25 atm.

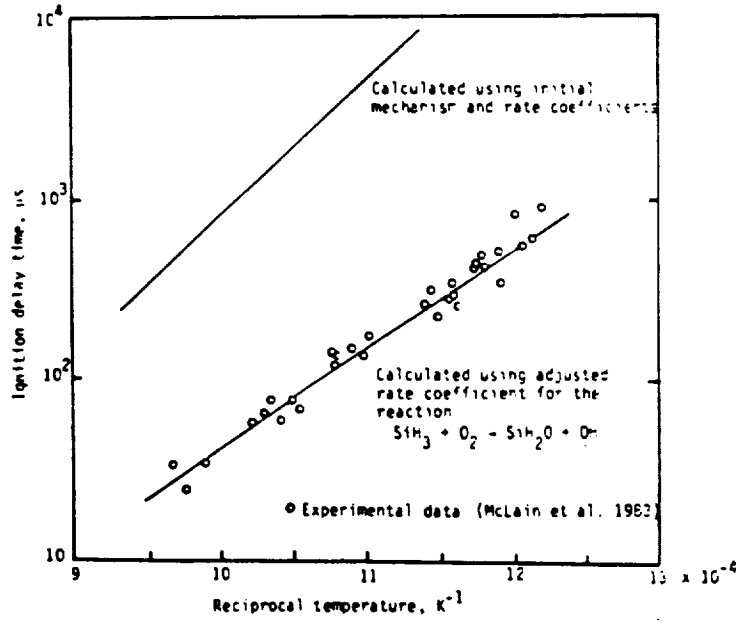

(b) 1.68 percent SiH_4, 6.72 percent H_2, 6.74 percent O_2, 84.86 percent N_2 mixture; Pressure = 1.35 atm.

Fig. 2.2. Comparison between Calculated and Experimental Ignition Delay Times.

The rate coefficient which gave the best agreement with experimental values was

$$k = 8.6\times10^{14}\, e^{\frac{-11400}{RT}}\ \ cm^3mole^{-1}s^{-1}$$

2.4 Kinetic Mechanisms

By examination of the output from the 1-D program, conclusions can be drawn about the chemical mechanisms involved in the ignition process. Comparison with experiment can then be used to discuss the correctness of these conclusions.

Figs. 2.3a and 2.3b show plots of ignition delay time vs reciprocal temperature reproduced from reference (7). The ignition delay time was defined as the time to achieve ignition as signified by the sudden increase in temperature. The equivalence ratios (ϕ) considered were 1.0 and 0.5. The silane/hydrogen mechanism with the modified rate coefficient was used.

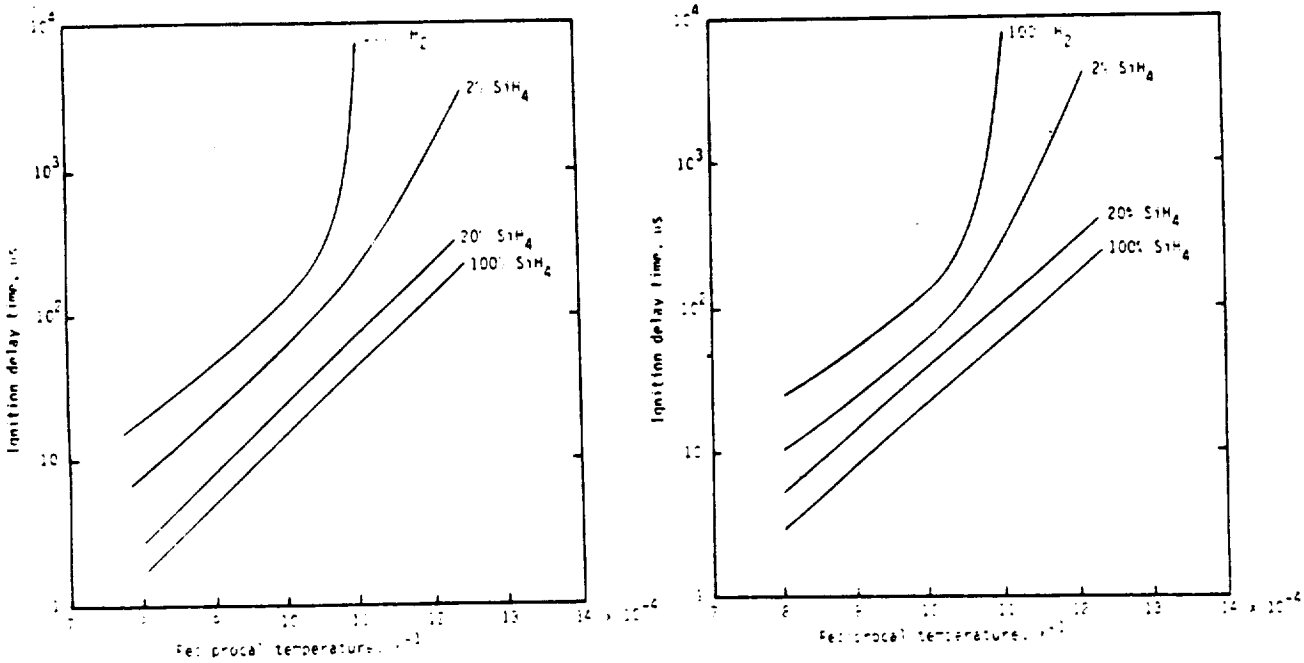

(a) ϕ = 1. (b) ϕ = 0.5.

Fig. 2.3 Ignition Delay time as a Function of Temperature for Various Silane/Hydrogen Mixtures at 1 Atm.

It is noted that the results from experiments performed at intake temperatures less than 1000 K with central injection (9) gave ignition delay times considerably less than those calculated using the 1-D premixed simulation presented in Fig. 2.3. For example, at a reciprocal

temperature of 15×10^4 ($T_1 = 650$ K), the ignition delay time as calculated approximately from the distance to ignition for a stoichiometric 20% silane/hydrogen mixture, is around 70 μs. This is much less than is predicted by an extrapolated version of Fig. 2.3 (a). This suggests that during experiments, additional factors other than initial temperature and pressure of the freestream air come into play. These could be boundary layer heating on the central injection strut and/or free radical oxygen production in the shock tunnel which would both have an accelerating effect on the ignition process. These phenomena are discussed in section 3.

It is noted from Figs. 2.3a and 2.3b that increasing concentration of the silane in hydrogen has a greater effect (i.e. a greater sensitization) in the stoichiometric mixtures than in the mixture of lower equivalence ratio. Also, ignition delay times decrease rapidly from the pure hydrogen value as the amount of silane is increased. Jachimowski noted that whereas the Beach mechanism (6) predicts that the same ignition delay times are obtained for temperatures above 900K and for all percentages of added silane, the modified mechanism predicts that ignition delay times decrease as the silane concentration increased over the range of temperature examined. This is supported by experimental results using the hypersonic nozzle at 6.1 MJ/kg (approx 1000K intake temperature) indicated in Fig. 2.4 where there is indeed a decrease in ignition delay time with an increase in silane concentration.

A calculated time history reproduced from (7) of silane, molecular hydrogen, and hydroxyl radical concentrations and mixture temperature for the stoichiometric 2% and 20% silane/hydrogen mixtures at an initial temperature of 800 K and constant pressure of 1 atm is shown in Fig. 2.5. Jachimowski notes that for the 2% mixture that the silane is consumed before any significant amount of hydrogen begins to react. The hydrogen is then aided by the large amounts of free radicals H, O, and OH which are produced by the ignition of silane. As silane concentration is increased, temperature increase due to the ignition of silane also contributes to the enhanced oxidation of the hydrogen. This thermal effect becomes more important for silane concentrations greater than 10%. At 20% concentration the combined free radical and thermal effect is evident. After most of the silane has been consumed, and prior to significant oxidation of the hydrogen, the temperature has increased almost 200 K. The increase in tem-

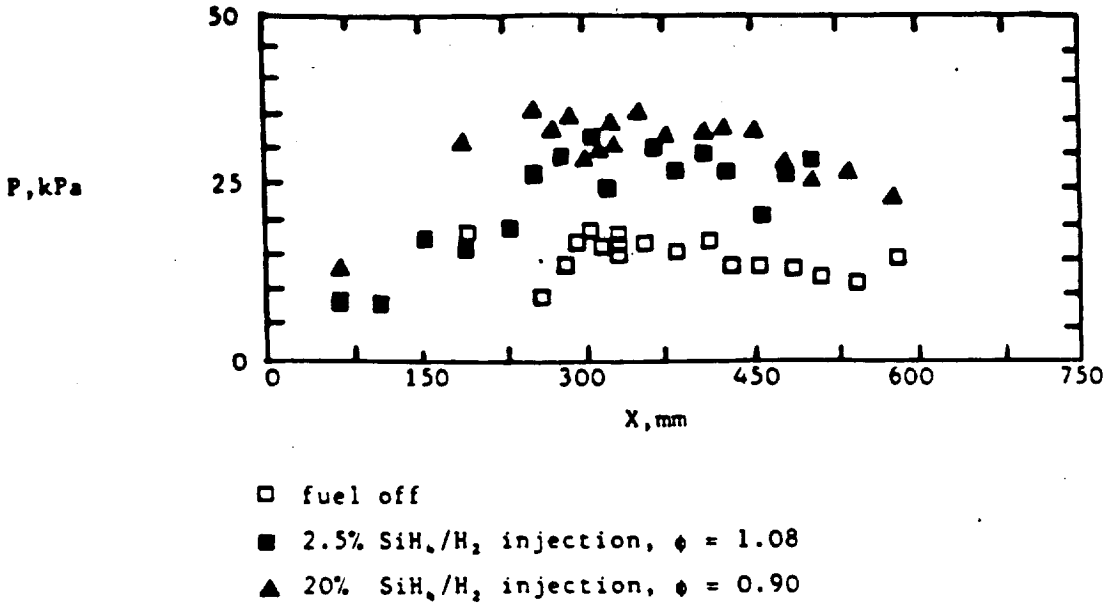

Fig. 2.4 Silane Combustion - Effect of Concentration.
Mach 5 nominal.
H_S = 6.1 MJ/kg, P_I = 20 kPa, T_I = 1000 K, ϕ =1.0

perature and presence of free radicals both contribute to the increased rate of hydrogen oxidation.

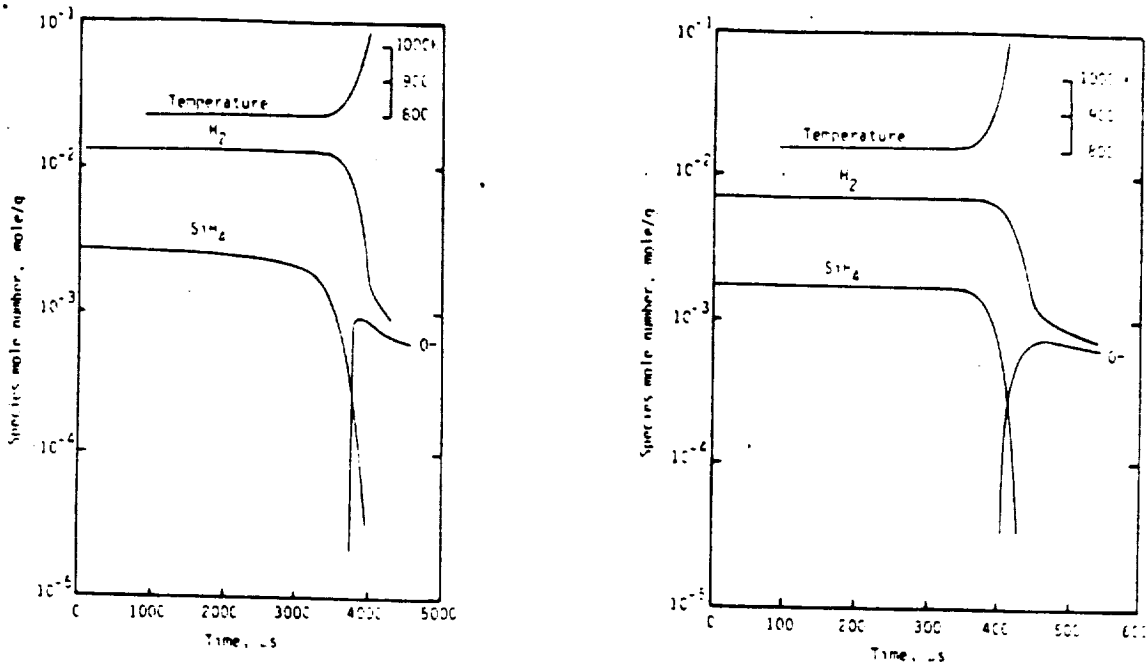

(a) 2 percent SiH_4/98 percent H_2.

(b) 20 percent SiH_4/80 percent H_2.

Fig. 2.5. Time Histories of Selected Species and Temperature During Ignition at 1 Atm and Initially at 800 K.

As well as enhancement of the ignition process through generation of free radicals, silane also aids ignition to some extent by scavenging the HO_2 radicals through the reaction sequence:

$$SiH_4 + HO_2 \rightarrow H_2O_2 + SiH_3 \qquad (8)$$

$$H_2O_2 + M \rightarrow OH + OH + M \qquad (9)$$

At temperatures above 800 K, free radical generation and the thermal effect are the dominant enhancement mechanisms while below 800 K, the scavenging is probably more important (7).

Kinetic reaction mechanisms have a hierarchical structure with mechanisms for complex fuels built up on sub-mechanisms for simple fuel molecules (10). The base for all hydrocarbon oxidation is the submechanism for the oxidation of hydrogen and carbon dioxide. The most important of these reactions are those that consume H_2 and CO using OH (11). A reasonable assumption that could be made for silane oxidation based on the methane analogy is that the important reactions would be those that consume H_2 and SiO using OH. These would be :

$$H_2 + OH \rightarrow H_2O + H \quad (10)$$

$$SiO + OH \rightarrow SiO_2 + H \quad (11)$$

together with the dominant chain branching reaction

$$H + O_2 \rightarrow O + OH \quad (12)$$

and its primary competitor for H atoms

$$H + O_2 + M \rightarrow HO_2 + M \quad (13)$$

Reactions competing with H_2 and SiO for OH should inhibit or retard oxidation of these species as well as the heat release associated with the production of water and silicon dioxide, and reactions competing with reaction 12 for H atoms (reaction 13) should reduce the rate of chain branching and overall rate of combustion. Alternatively, reactions which produce additional H atoms which can then react with molecular oxygen by reaction 12 should accelerate the overall rate of combustion.

It will be seen, however, in section 3.5 that according to a numerical chemical kinetics analysis, reaction equations 10 and 11 do not play any significant part in the ignition process for particular initial conditions. In fact, hydroxyl radicals are important in producing intermediate silicon containing species but not silicon dioxide. Heat release is achieved by a series of reactions culminating in the direct attack of silicon monoxide on molecular oxygen and then by the ignition of hydrogen. At lower temperatures, hydrogen stays essentially "inert" and does take part to any significant degree in the ignition process. Direct modelling on a hydrocarbon analogy, therefore, has its drawbacks. Conclusions which can be drawn from modelling work concerning methane, for example, cannot be always applied directly to silane combustion even though the silane reaction scheme is based on an equivalent methane reaction scheme.

The oxidation of silane takes place through the gradual dismantling of the fuel molecule into progressively smaller fragments. The first major step is the abstraction of H atoms from the parent fuel molecule. Once a viable radical pool has been established, most of the H atom abstraction is accomplished by reactions between small radical and atomic species and the fuel molecules. The most important radical species are H, O, OH, HO_2, and SiH_3. From previous

hydrocarbon modelling work, H atom abstractions by H and OH are dominant for fuel rich and near stoichiometric mixtures while reactions with OH and to a much lesser extent, O atoms are most important for fuel lean mixtures (11). Work in section 3.5 tends to support the trend of H and especially OH radicals being responsible for most hydrogen abstraction from the parent silane molecule when there is a stoichiometric fuel/air mixture. In this particular manner, silane tends to behave like its hydrocarbon counterpart.

2.5 An Alternative Method for Approximating Thermochemical Properties

The Jachimowski model approximates for 4 of the silicon species involved in the silane oxidation process (SiH_3, SiH_2, SiH_2O, HSiO) that the heat capacities are the same as those for the analogous carbon containing species. An indication of the possible difference between assumed values and actual values can be demonstrated by comparing specific heats of say SiH_4 and CH_4. For example, at 1000 K, the specific heat of SiH_4 is 20.2 cal/mole K while that of CH_4 is 17.4 cal/mole K which represents an error of 14% if the analogous carbon containing specie was used in this case. It was thought that an independent method of determining heat capacities could be investigated to check the effects on simulations.

Using the method of Bennewitz, Rossner and Dobratz (12), molecular specific heats can be determined approximately by considering contributions due to translational and rotational energies together with vibrational energies expressed as functions of temperature. Using the principle of equipartition, translational and rotational contributions to C_p are 3R. Vibrational contributions depend on bond frequencies in stretching or bending. Average stretching or bending frequencies are expressed as wave numbers (frequency divided by the speed of light), where ω_ν is the wave number for stretching and ω_δ is the wave number for bending. Vibrational contributions to heat capacities are related to these wave numbers independent of the bond type and take the form of functions dependent on temperature. These contributions are then multiplied for multiple bonds.

The average stretching vibration wave number for the C–H bond is $\omega_\nu = 2920\ cm^{-1}$ (12). For Si–H, $\omega_\nu = 2190\ cm^{-1}$ (8). This represents a difference of $730\ cm^{-1}$ in wave number between analogous species. For the sulphur bond S–H, $\omega_\nu = 2570\ cm^{-1}$ (12) which represents a

smaller difference of 380 cm^{-1}. It would be expected therefore that using S–H bonds instead of C–H bonds would give a better approximation to the specific heat of the silicon containing specie. This is indeed the case and at 1000 K, C_p calculated for SiH_4 using this "sulphur analogy" is 19.5 cal/mole K compared with the documented value of 20.2 cal/mole K, an error of 3%.

The model is even more accurate for the documented specie Si=O. For Si=O bonds, $\omega_v = 1295\ cm^{-1}$ (8), while for S=O bonds $\omega_v = 1250\ cm^{-1}$ (12), representing a difference in wave number of only 45 cm^{-1}. Calculated specific heat using the "sulphur analogy" for SiO at 1000 K is 8.56 cal/ mole K compared with the documented value of 8.54 cal/mole K, an error of only 0.2%. This compares with an error of 7% when using the analogous carbon containing specie CO.

It was on this basis that specific heats were calculated for the undocumented silicon species using a sulphur bond analogy. Standard heats of formation were calculated using the method of Franklin, Verma and Doraiswamy (12), and absolute entropies using the same method as Jachimowski except that entropy changes for reactions were approximated by sums of known entropy changes involved in the breaking of single bonds rather than using the carbon reaction analogy.

The modified thermochemical properties were used for numerical simulations in conjunction with reaction rate coefficients suggested by Jachimowski. The modified properties gave similar results for the Jachimowski model for several cases, with slightly longer ignition delay times but similar final pressures. Computation time was increased greatly and reasons for this are not known. Overall, it could be concluded that small errors in calculating thermochemical properties have a far less effect on simulation results than choice of reaction rate constants.

SECTION 3

SIMULATION OF THE SILANE COMBUSTION PROCESS

Using the Jachimowski model described in section 2 and the chemical kinetics program (2), computer simulations have been carried out for conditions corresponding to experiments using the hypersonic nozzle. Experimental fuel off duct pressures varied between 13-22 kPa over the enthalpy range considered but simulations were consistently run with an initial pressure of 20 kPa. Effects of freestream free radical oxygen concentration, concentration of silane in hydrogen, and equivalence ratio are discussed and results compared with experiment. A sensitivity analysis of reaction rates is carried out at a condition where results of experiment correspond well with experimental results. An examination of net conversion rates at this same condition indicates important reactions at various stages of the ignition process.

3.1 Effect of Freestream Free Radical Oxygen Concentration

All work presented in this section concerns combustion of a 20% silane/hydrogen mixture at an equivalence ratio of one. Fig. 3.1 shows that at 1500 K or a freestream stagnation enthalpy of 8.7 MJ/kg, increasing the initial concentration of freestream free radical oxygen has little or no effect on the ignition distances. Results from this simulation compare favourably with the experimental results for a 20% mixture as shown in Fig. 3.2. Note that for computer simulations the point X=0 refers to the point of injection, rather than the position of the leading edge. The experimental points appear scattered, but at these high initial temperatures, pressure rises due to combustion are relatively low, so any disturbances within the model would look significant against the the combustion profile. It can be seen, however, that there is indeed rapid combustion that comes up to roughly the level predicted by the computer simulation. It is suggested therefore that at this high enthalpy, the high dissociation expected in the shock tunnel (α = 10%) has no noticeable effect on the ignition delay time.

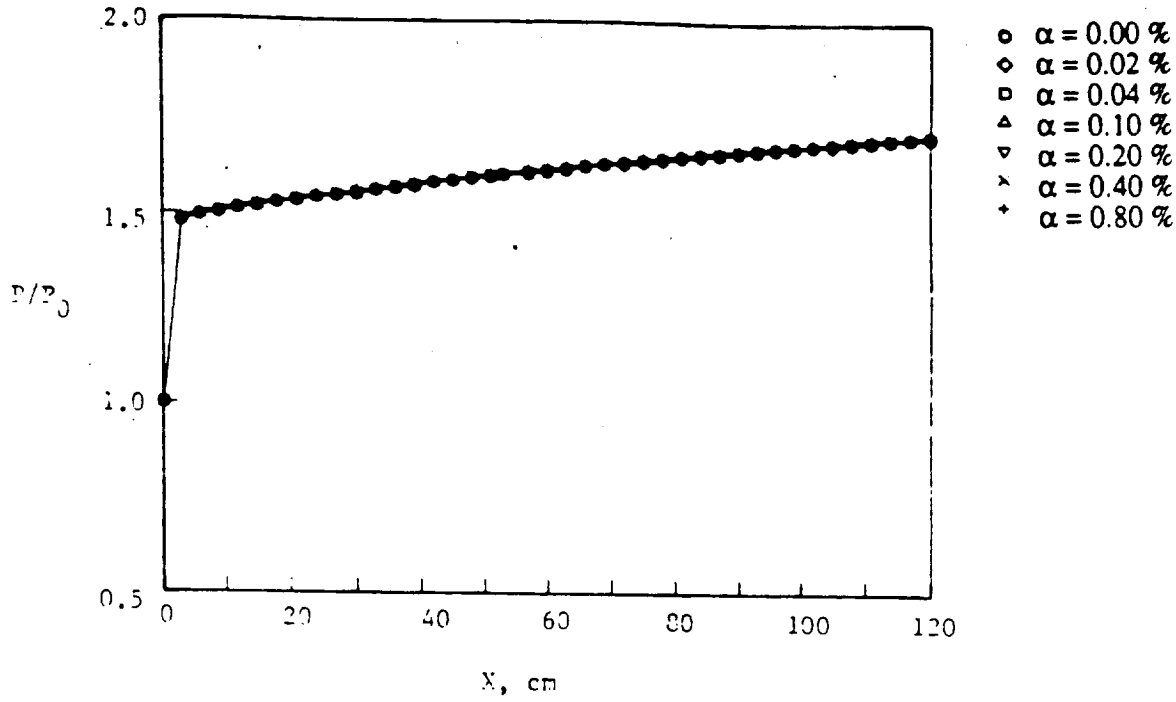

Fig. 3.1 20% Silane/Hydrogen Combustion Simulation.
Effect of Concentration of Free Radical Oxygen. Mach 5 nominal.
H_S = 8.7 MJ/kg, P_I = 20 kPa, T_I = 1500 K, ϕ =1.0

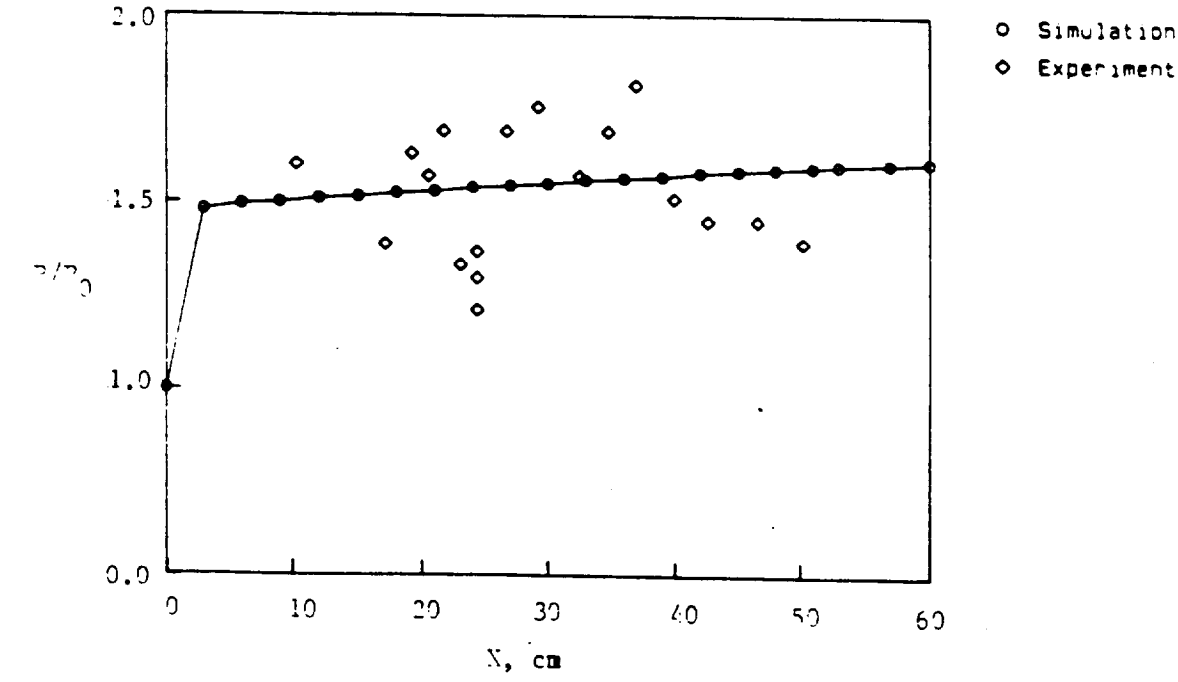

Fig. 3.2 20% Silane/Hydrogen Combustion.
Comparison of Simulation with Experiment. Mach 5 nominal.
H_S = 8.7 MJ/kg, P_I = 20 kPa, T_I = 1500 K, ϕ =1.0, α = 10%

At an initial temperature of 1000 K or a freestream stagnation enthalpy of 6.1 MJ/kg, simulations show the ignition distance decreases from just over 20 cm to 5 cm as the initial α is increased from 0.0% to 0.8% (Fig. 3.3). At this condition, the shock tunnel produces flows with $\alpha = 1.5\%$. According to the simulation, this would bring the rapid pressure rise to around 20 cm closer to the point of injection than when compared to a flow with no oxygen dissociation. Fig. 3.4 shows that in the experiment, results agree favourably with the simulation run with with an initial free radical oxygen concentration of 1.5%. It is interesting to note that in experiment, the pressure falls off with distance down the duct.

Fig. 3.5 shows that at an initial temperature of 650 K ($H_S = 4.2$ MJ/kg), even small amounts of free radical oxygen have a very significant effect on the ignition distances predicted by the computer simulation. At this enthalpy $\alpha = 0.18\%$ is expected in the shock tunnel. It can be seen by comparing the results for a 20% silane mixture shown in Fig. 3.6 with the simulation for $\alpha = 0.18\%$ that ignition distance is about the same. At this temperature as at the higher temperature of 1000 K, a pressure drop is observed as the gas progresses down the duct. This trend appears to be repeated for most cases with silane injection, particularly at the higher concentrations. A possible cause of this may be that after ignition and burning of the silane/hydrogen mixture is complete, heat transfer to the walls of the model may cause condensation of SiO_2. This conversion from gas to solid would tend to lower pressure with distance more drastically than the effect due to a drop in temperature alone, as found in say, pure hydrogen combustion. Results for a 20% silane/hydrogen mixture at nominal Mach numbers of Mach 3.5 and 4.5 show a similar trend as shown in (1,9). It should be noted that for hydrogen combustion, where water remains as a vapour at relatively low temperatures, that there is little pressure fall off as found in (1).

At a lower initial temperature of 540 K ($H_S = 3.43$ MJ/kg), ignition distances are dramatically increased for the lower radical concentrations, as predicted by the computer simulation (Fig. 3.7). However, Fig. 3.8 shows that in experiments with $\alpha = 0.13\%$, the 20% silane mixture ignites about 15 cm from the point of injection. This compares with about 65 cm for the

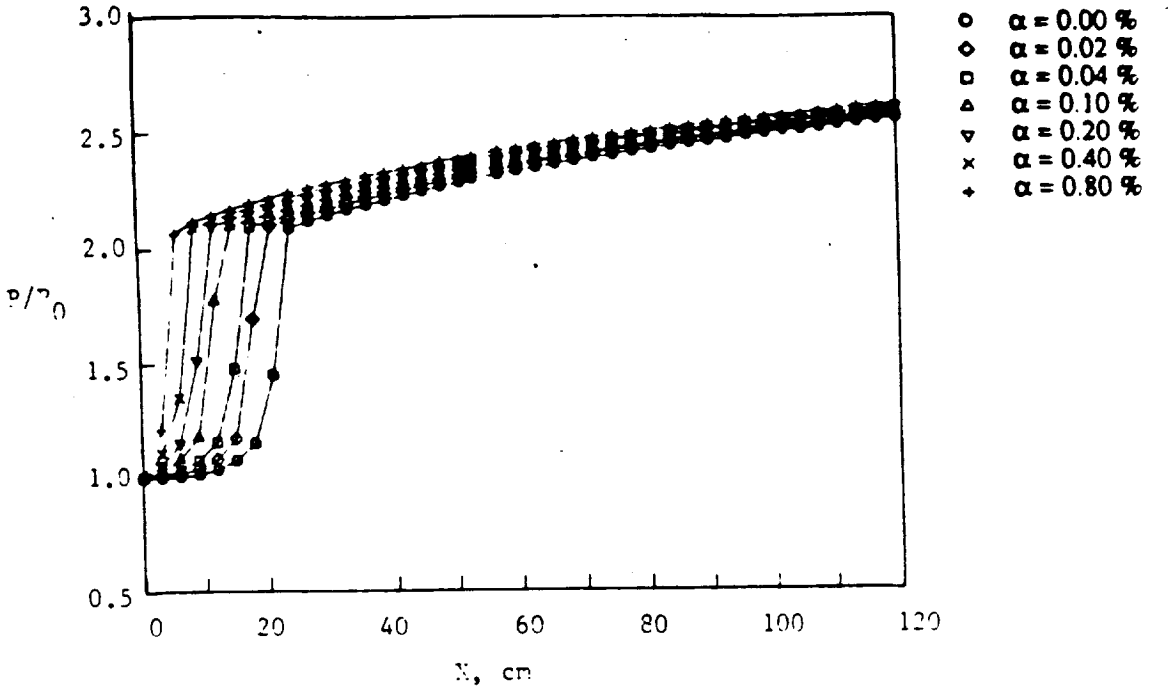

Fig. 3.3 20% Silane/Hydrogen Combustion Simulation.
Effect of Concentration of Free Radical Oxygen. Mach 5 nominal.
H_S = 6.1 MJ/kg, P_I = 20 kPa, T_I = 1000 K, ϕ =1.0

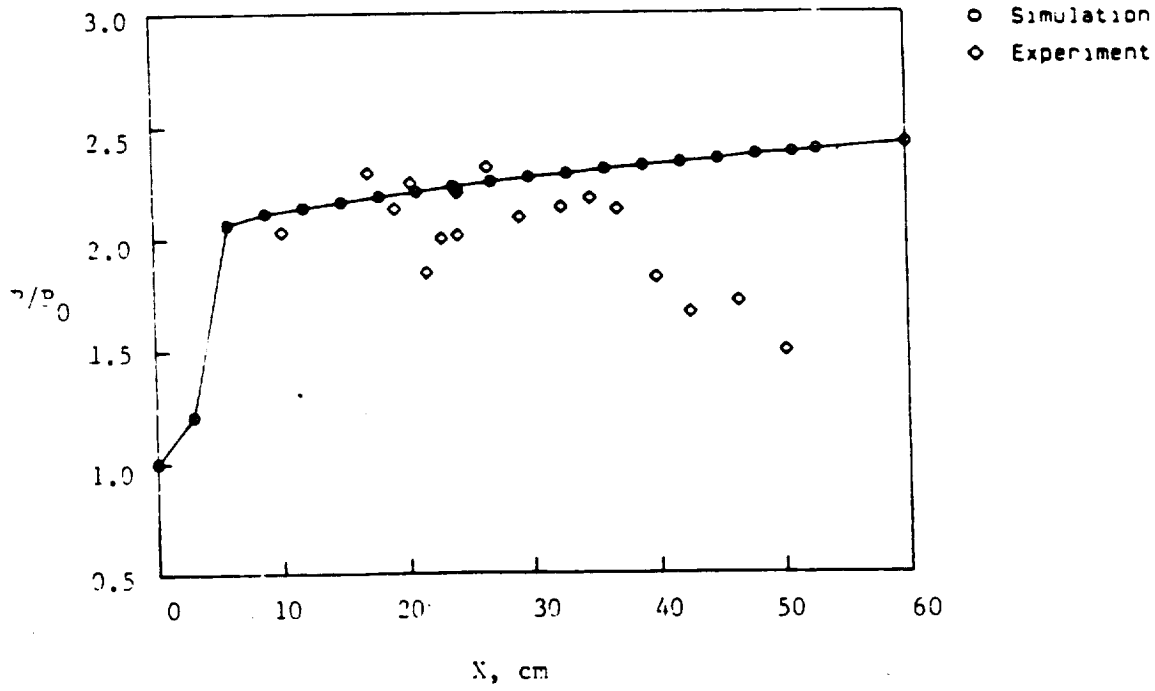

Fig. 3.4 20% Silane/Hydrogen Combustion.
Comparison of Simulation with Experiment. Mach 5 nominal.
H_S = 6.1 MJ/kg, P_I = 20 kPa, T_I = 1000 K, ϕ =1.0, α = 1.5%

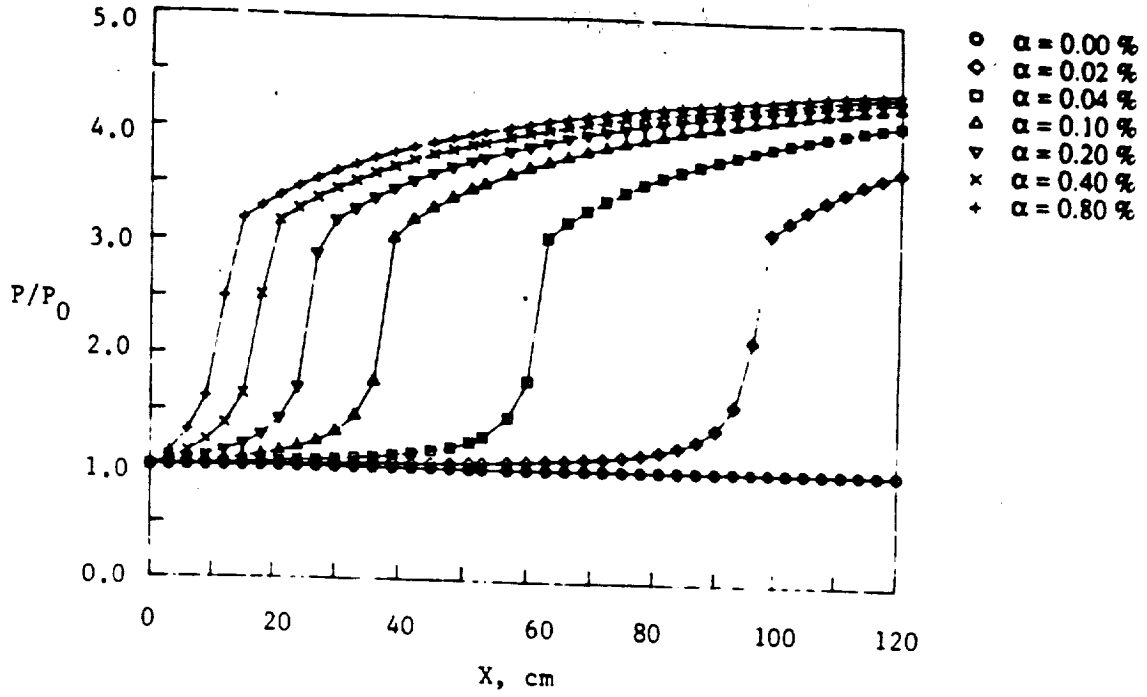

Fig. 3.5 20% Silane/Hydrogen Combustion Simulation.
Effect of Concentration of Free Radical Oxygen. Mach 5 nominal.
H_S = 4.2 MJ/kg, P_1 = 20 kPa, T_1 = 650 K, ϕ =1.0

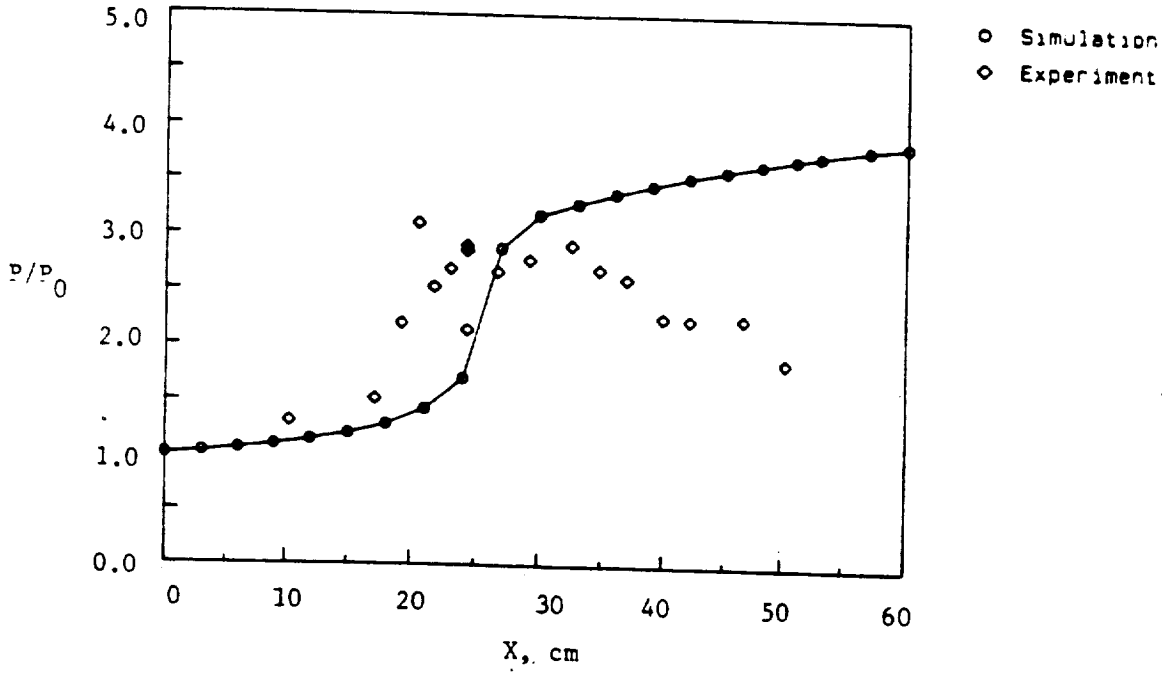

Fig. 3.6 20% Silane/Hydrogen Combustion.
Comparison of Simulation with Experiment. Mach 5 nominal.
H_S = 4.2 MJ/kg, P_1 = 20 kPa, T_1 = 650 K, ϕ =1.0, α = 0.18%

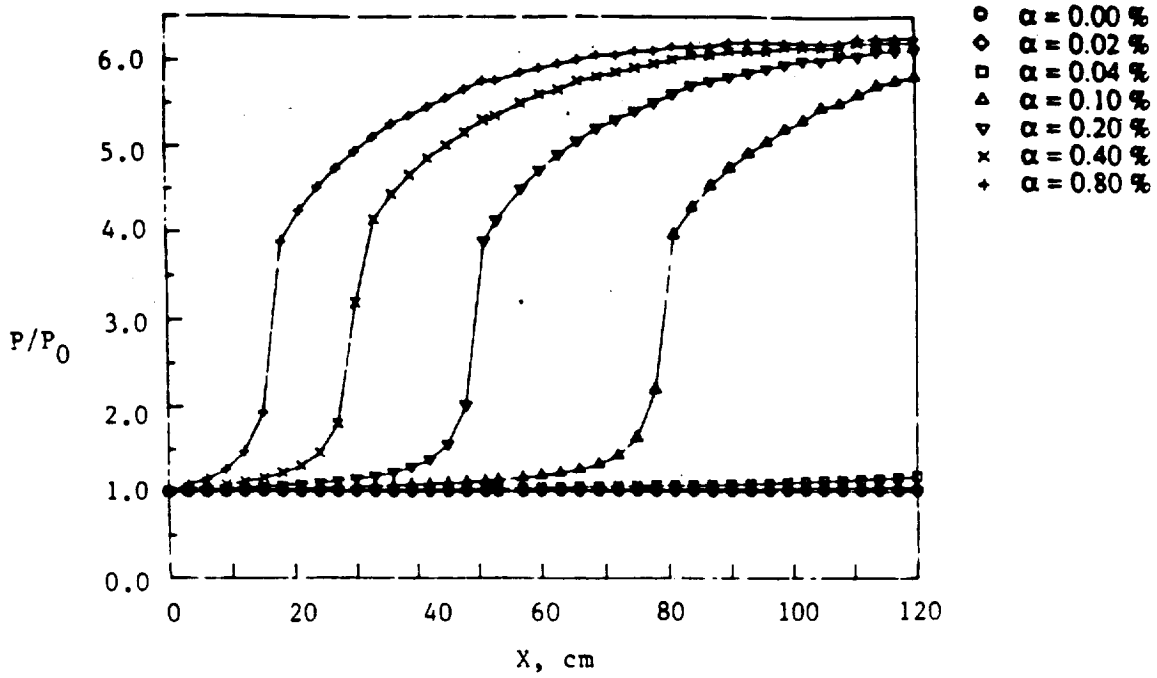

Fig. 3.7 20% Silane/Hydrogen Combustion Simulation.
Effect of Concentration of Free Radical Oxygen. Mach 5 nominal.
H_S = 3.43 MJ/kg, P_I = 20 kPa, T_I = 540 K, ϕ =1.0

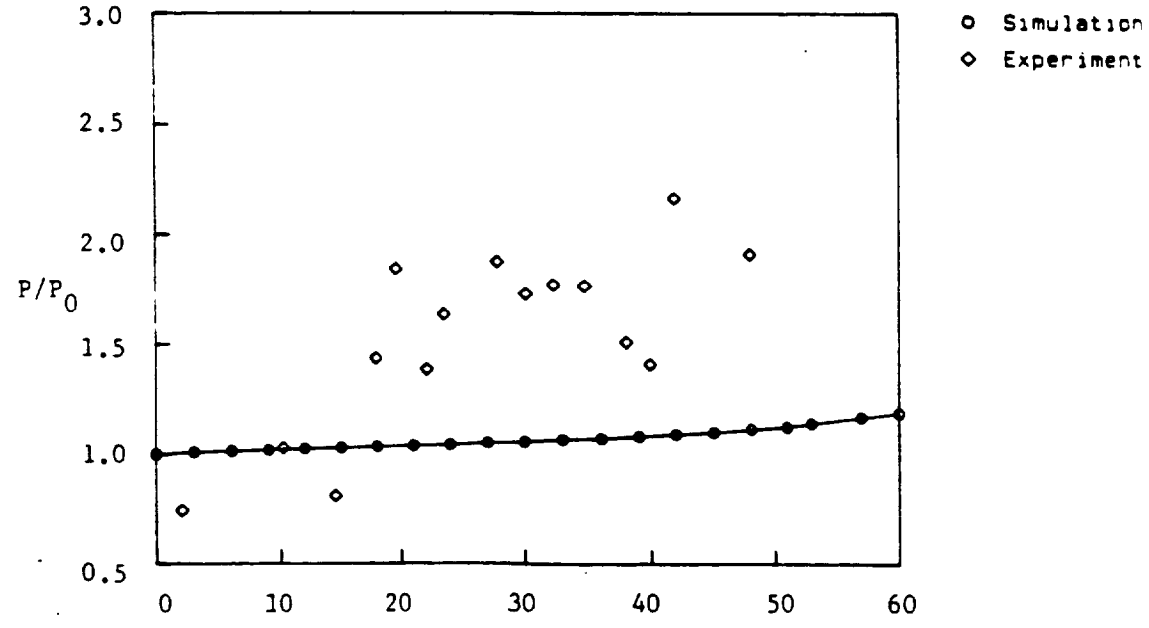

Fig. 3.8 20% Silane/Hydrogen Combustion.
Comparison of Simulation with Experiment. Mach 5 nominal.
H_S = 3.43 MJ/kg, P_I = 20 kPa, T_I = 540 K, ϕ =1.0, α = 10%

premixed gases as predicted by the 1-D program. The pressure rise observed in the experiment is, however, only of the order of 20 kPa or 0.2 atm compared with 100 kPa or 1.0 atm predicted for "full" burning of the silane/hydrogen mixture as shown in Fig. 3.7. This suggests that there is partial burning of the fuel jet and that ignition is caused prematurely by some other effect because the freestream temperature is too low. The ignition at 540 K may be due to high temperatures produced in the boundary layer on the injection strut. Assuming a laminar compressible boundary layer, it was calculated that the maximum temperature found in the boundary layer would be 1060 K at this condition. This temperature together with a free radical oxygen concentration of 0.13 % found in the freestream would be consistent with the ignition distance of around 10 cm predicted in Fig. 3.2. The partial burning of the fuel jet could be caused by the quenching of the complete combustion process by the cooler freestream.

It should be noted that it was at this inlet temperature, pressure, and Mach number that higher steady pressures were achieved experimentally with lower silane concentrations. It appears therefore, burning was incomplete but involved both components of the fuel mixture. This effect is not understood and is not modelled by the chemical kinetics program in this case.

A simulation was run (including α = 0.06% calculated for conditions found at the exit of the nozzle) for a lower intake temperature of 410 K (H_S = 2.65 MJ/kg) and indicated no combustion over 120 cm. Experiments, however, showed ignition at about 15 cm from the injection point (9) but final pressure levels did not reflect complete combustion. It was hypothesised that preferential burning of the silane component of the fuel mixture occurs at these low temperatures and this is supported by experiments at Mach 4.5 and Mach 5. The chemical kinetics program, however, does not appear to model this behaviour.

Experiments suggest therefore that if the reaction scheme is valid, then freestream radical production at high enthalpies has no appreciable effect on the ignition of 20% silane/hydrogen mixtures.

At the intermediate freestream temperature of 650 K, oxygen radical concentrations play an important part in the combustion process therefore shock tunnel simulations may not be representative of real flight situations.

At the lower intake temperatures of 540 K and 410 K, experiments show short ignition delay times despite the very low free radical oxygen concentrations produced by the shock tunnel. This suggests that combustion is occurring because of another effect. It may be the high temperature produced by the boundary layer on the injection strut. Pressure rises due to burning however, are lower than those expected for complete combustion of the silane/hydrogen mixture as predicted by the computer program. This suggested that there is partial burning due to the low freestream temperature or preferential burning of the silane component of the fuel mixture.

3.2 Effect of Silane Concentration

Conditions which had previously shown good agreement with experiment were chosen for investigating the effect of varying the concentration of silane in hydrogen. It has been shown that at a freestream stagnation enthalpy of 4.2 MJ/kg, the simulation compares favourably with experiment for a 20% mixture when free radical oxygen produced in the shock tunnel is included in the analysis.

Fig. 3.9 shows that at this condition, pressure profiles indicate a change in ignition trends as concentration is increased. At 1%, there is minimal ignition over 80 cm. As the concentration is increased from 2.5% to 20%, ignition distances are decreased and the ignition process is indicated by more rapid pressure rises. This compares favourably with experiment as shown in (9) where similar trends are observed, although ignition distances tend to be smaller.

3.3 Effect of Equivalence Ratio

Equivalence ratio was varied for the same condition. Fig. 3.10 shows that ignition delay times do not vary much up to an equivalence ratio of about 2.0. However, at an equivalence ratio of 5.0, ignition delay is increased significantly. This could be due to the heat capacity of the excess fuel robbing the ignition process of the necessary heat. Final pressure levels are about the same for ratios between 1.0 and 2.0. Below equivalence ratios of 1.0, final pressure levels are sensitive to small changes in ϕ. This trend was observed in experiments nominally at Mach 4.5, where equivalence ratios were nominally 0.6.

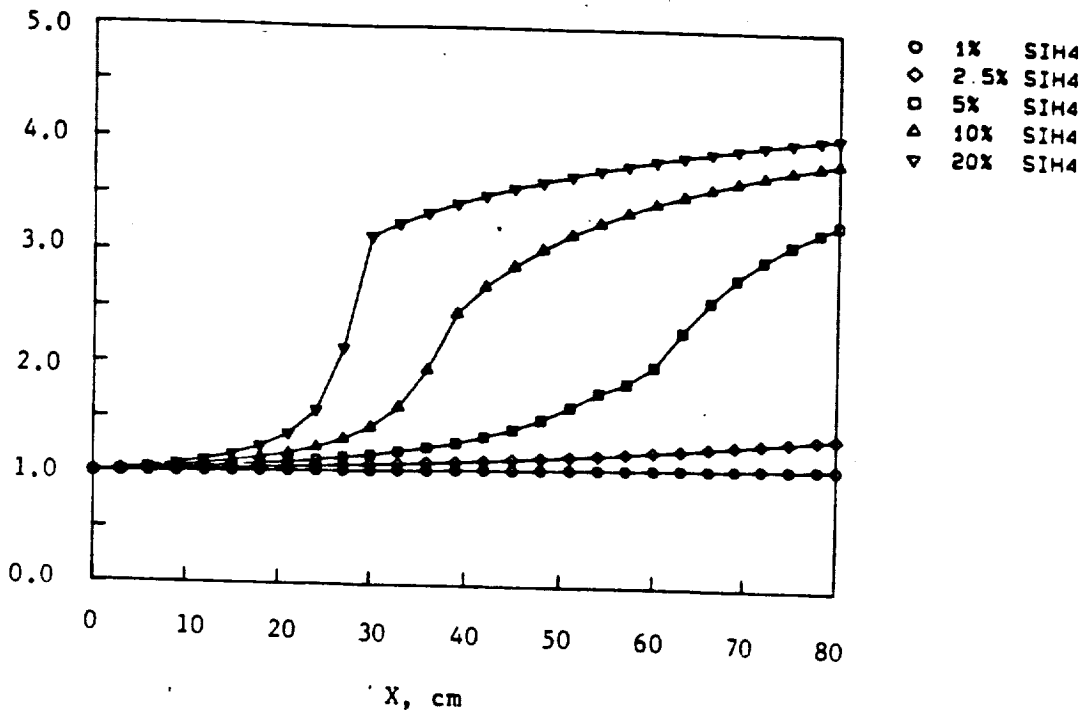

Fig. 3.9 Silane/Hydrogen Combustion Simulation.
Effect of Concentration of Silane. Mach 5 nominal.
H_S = 4.2 MJ/kg, P_I = 20 kPa, T_I = 650 K, ϕ =1.0, α = 0.18%

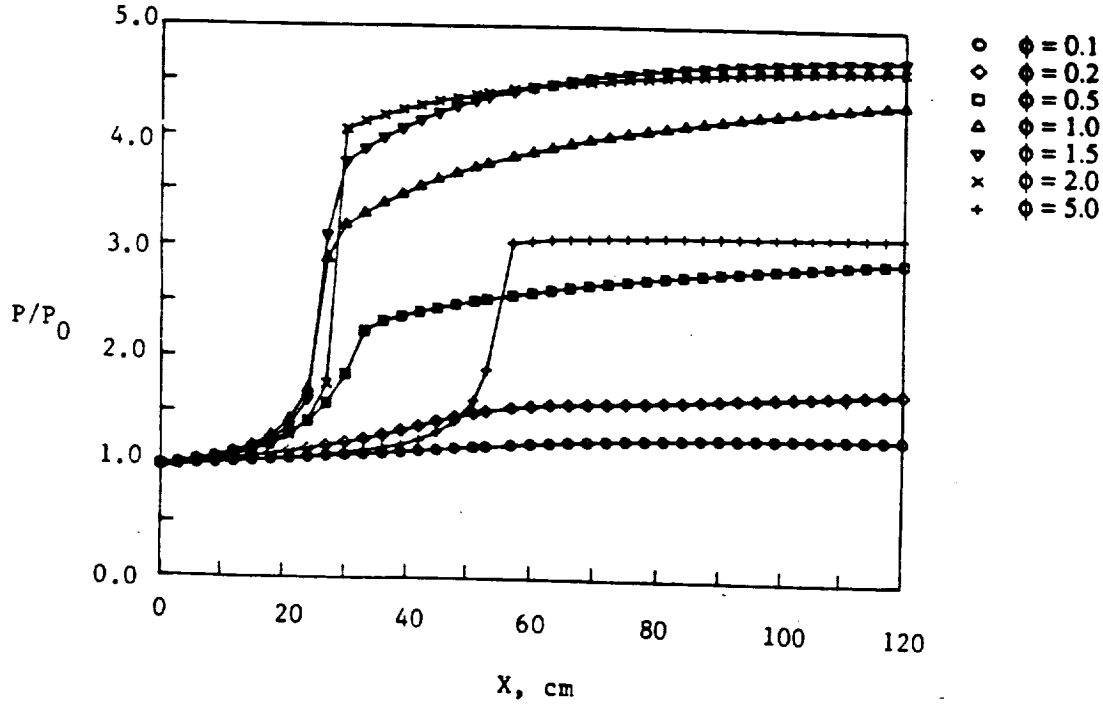

Fig. 3.10 20% Silane/Hydrogen Combustion Simulation.
Effect of Equivalence Ratio. Mach 5 nominal.
H_S = 4.2 MJ/kg, P_I = 20 kPa, T_I = 650 K, ϕ =1.0, α = 0.18%

3.4 A Sensitivity Analysis of Reaction Rates

The ignition mechanism tends to be made up of four processes. These are:

1. Breakdown of the silane to produce free radicals.
2. Production of intermediate species.
3. Ignition of silane to produce heat.
4. Subsequent ignition of remaining hydrogen.

A sensitivity analysis of reaction rates for reactions involving silicon containing species is presented in this section. To reduce complexity, results are presented with reference only to the 23 reactions concerning silane oxidation. This is a reasonable approach because with the relatively high concentration of 20% silane in hydrogen considered for this case, the reactions involving silane are more or less complete before the hydrogen oxidation begins (section 2.4). The reactions involving silicon therefore tend to be inter-related with one another to a greater extent than with the 17 reactions which describe the hydrogen oxidation.

Rate coefficients of the silane reaction scheme shown in Fig. 2.1 were successively varied by factors of 2 and 0.5 for the simulation that gave best agreement with the experimental results. This was at the condition discussed in section 3.2 with $H_S = 4.2$ MJ/kg, $T_I = 650$ K and $P_I = 20$kPa with the free radical oxygen included in the analysis. The sensitivity analysis was based on atomic oxygen mass fractions computed for the experimental conditions at distances along the duct. Atomic oxygen was chosen as the parameter for observation because of its apparent importance in the ignition process at this condition. Plots of mass fraction against length corresponding to distance from injection are shown in Figs. 3.11 (a) to (i), with rate coefficients k1 to k23 corresponding to the reactions R1 to R23 shown in the accompanying table. The result for this condition using original rate coefficients is shown by a continuous line. The importance of each reaction is signified by the deviation from the original mass fraction profile when the rate coefficient corresponding to that reaction is halved or doubled. Points corresponding to the most significant reactions have been connected with broken lines.

From pressure-distance profiles which are not presented here, it was found that ignition (as signified by a rapid rise in pressure) consistently took place when the pool of free radical

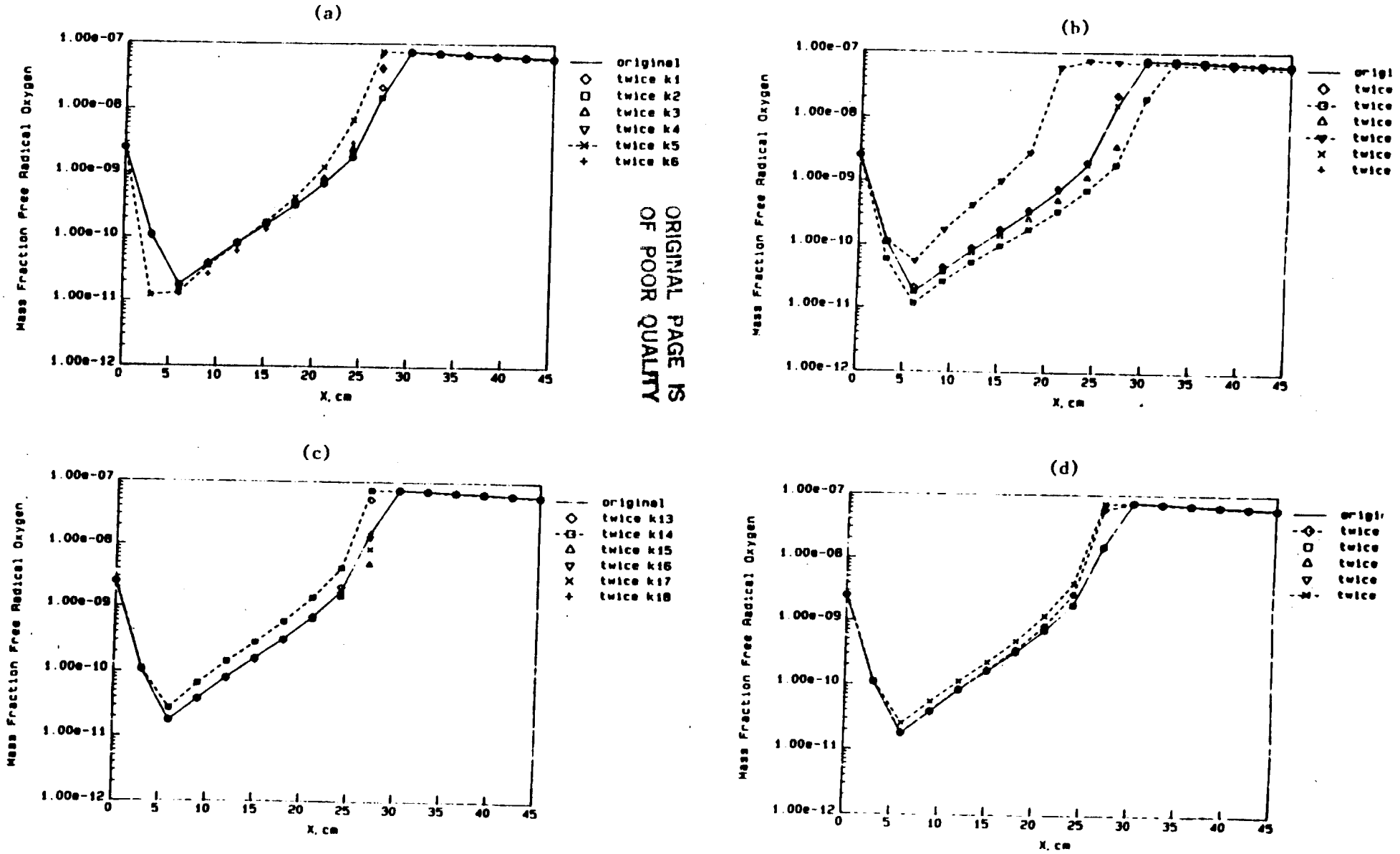

ORIGINAL PAGE IS
OF POOR QUALITY

Fig. 3.11 20% Silane/Hydrogen Combustion Simulation.
Sensitivity Analysis of Reaction Rates. Mach 5 nominal.
H_S = 4.2 MJ/kg, P_I = 20 kPa, T_I = 650 K, ϕ =1.0, α = 0.18%

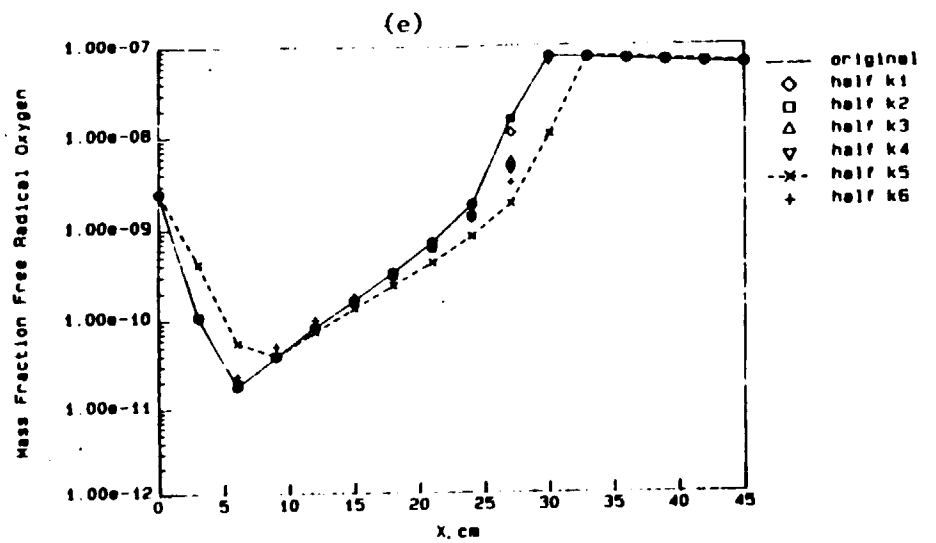

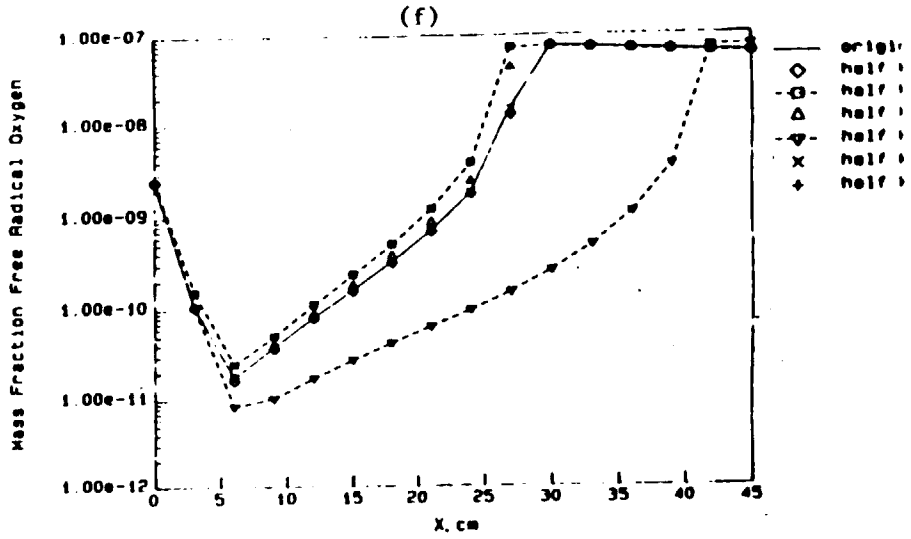

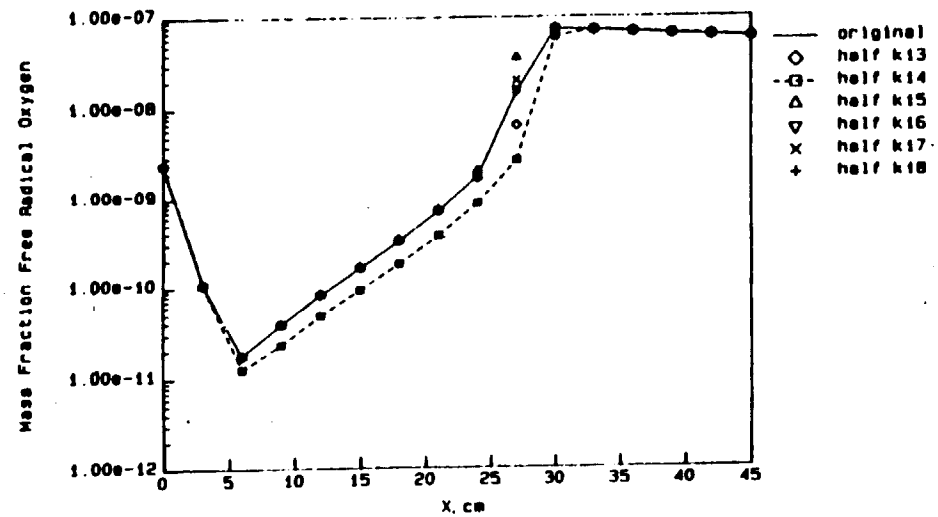

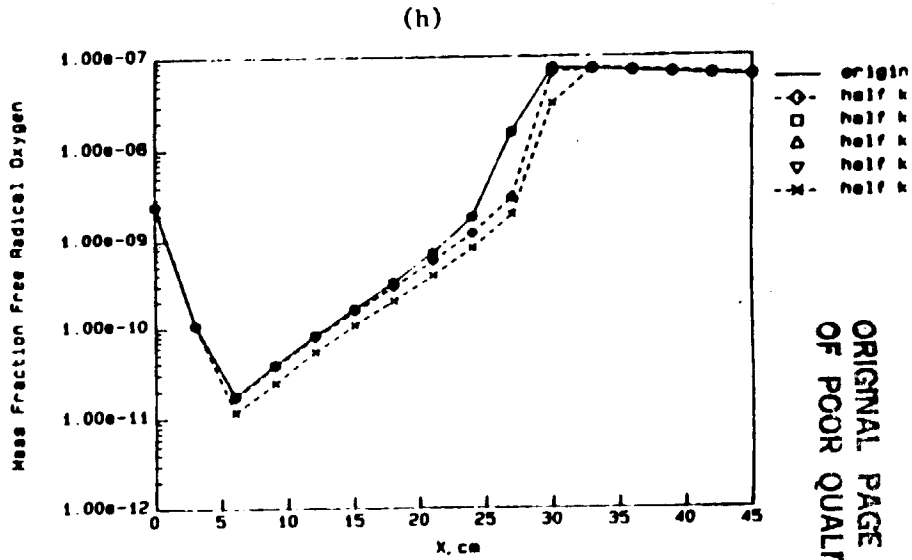

Fig. 3.11 20% Silane/Hydrogen Combustion Simulation.
Sensitivity Analysis of Reaction Rates. Mach 5 nominal.
H_S = 4.2 MJ/kg, P_I = 20 kPa, T_I = 650 K, ϕ =1.0, α = 0.18%

	Reaction	Rate coefficient
R1	$SiH_4 \rightarrow SiH_2 + H_2$	6.0×10^{13} exp(-54960/RT)
R2	$SiH_4 + O_2 \rightarrow SiH_3 + HO_2$	2.0×10^{11} exp(-44000/RT)
R3	$SiH_4 + HO_2 \rightarrow SiH_3 + H_2O_2$	3.0×10^{12} exp(-5600/RT)
R4	$H + SiH_4 \rightarrow H_2 + SiH_3$	1.5×10^{13} exp(-2500/RT)
R5	$O + SiH_4 \rightarrow OH + SiH_3$	4.2×10^{12} exp(-1600/RT)
R6	$OH + SiH_4 \rightarrow H_2O + SiH_3$	8.4×10^{12} exp(-100/RT)
R7	$H + SiH_3 \rightarrow SiH_2 + H_2$	1.5×10^{13} exp(-2500/RT)
R8	$O + SiH_3 \rightarrow SiH_2O + H$	1.3×10^{14} exp(-2000/RT)
R9	$OH + SiH_3 \rightarrow SiH_2O + H_2$	5.0×10^{12}
R10	$SiH_3 + O_2 \rightarrow SiH_2O + OH$	8.6×10^{14} exp(-11400/RT)
R11	$SiH_2 + O_2 \rightarrow HSiO + OH$	1.0×10^{14} exp(-3700/RT)
R12	$H + SiH_2O \rightarrow H_2 + HSiO$	3.3×10^{14} exp(-10500/RT)
R13	$O + SiH_2O \rightarrow OH + HSiO$	1.8×10^{13} exp(-3080/RT)
R14	$OH + SiH_2O \rightarrow H_2O + HSiO$	7.5×10^{12} exp(-170/RT)
R15	$H + HSiO \rightarrow H_2 + SiO$	2.0×10^{14}
R16	$O + HSiO \rightarrow OH + SiO$	1.0×10^{14}
R17	$OH + HSiO \rightarrow H_2O + SiO$	1.0×10^{14}
R18	$HSiO + M \rightarrow H + SiO + M$	5.0×10^{14} exp(-29000/RT)
R19	$HSiO + O_2 \rightarrow SiO + HO_2$	3.0×10^{12}
R20	$SiH_2O + HO_2 \rightarrow HSiO + H_2O_2$	1.0×10^{12} exp(-8000/RT)
R21	$SiO + O + M \rightarrow SiO_2 + M$	2.5×10^{15} exp(-4370/RT)
R22	$SiO + OH \rightarrow SiO_2 + H$	4.0×10^{12} exp(-5700/RT)
R23	$SiO + O_2 \rightarrow SiO_2 + O$	1.0×10^{13} exp(-6500/RT)

(1)

oxygen reached a "critical" mass fraction of roughly 3×10^{-9}. Ignition distances can be approximated by considering the point where the atomic oxygen mass fraction reaches this value. This means generally that if changing a reaction rate increased radical oxygen mass fractions above that of the original scheme to the "critical" value then the ignition distance was shorter than for the original scheme. Alternatively, if the original scheme reached this value before the modified scheme, then the ignition distance for the modified reaction was shorter than for the original scheme.

From the results, it can be seen that there are six reactions which have the largest influence when rate coefficients are varied. In order of importance from highest to lowest, these are

$$\text{R10...}SiH_3 + O_2 \rightarrow SiH_2O + OH$$
$$\text{R5...}O + SiH_4 \rightarrow OH + SiH_3$$
$$\text{R8...}O + SiH_3 \rightarrow SiH_2O + H$$
$$\text{R14...}OH + SiH_2O \rightarrow H_2O + HSiO$$
$$\text{R23...}SiO + O_2 \rightarrow SiO_2 + O$$
$$\text{R19...}HSiO + O_2 \rightarrow SiO + HO_2$$

It can be seen from Figs. 3.11(b) and 3.11(f) that varying the reaction rate of R10 has the greatest effect on the mass fraction profile. This is in agreement with the observation of Jachimowski of greatest sensitivity for this reaction as discussed in section 2.3. It should be remembered that it was this reaction's rate coefficient that Jachimowski adjusted so that numerical simulations corresponded with experimental shock tube results. The other two reactions which Jachimowski found to be most sensitive to changes in reaction rate were:

$$\text{R1...}SiH_4 \rightarrow SiH_2 + H_2$$
$$\text{R22...}SiO + OH \rightarrow SiO_2 + H$$

These reactions were not observed to be important in this sensitivity analysis. This is understandable because a small concentration of free radical oxygen was included in this particular analysis. Reactions involving atomic oxygen would therefore tend to become dominant reactions, as is indeed observed in this case with R5 and R8 being most sensitive after R10.

It should be noted that R8 retarded the ignition process when its rate coefficient was doubled and accelerated the process when its rate coefficient was halved. This is thought to be because R8 competes with other reactions for the radicals SiH_3 and O to produce the intermediate SiH_2O and atomic hydrogen. During the ignition process, SiH_3 and O appear to be very important in attacking oxygen and silane respectively in reactions R10 and R5, and so consumption of these radicals through other reactions would tend to reduce the rate of combustion.

The remaining reactions R14, R23 and R19 appear to be important reactions but to a lesser degree than R10, R5 and R8. Except for the reaction :

$$R10...SiH_3 + O_2 \rightarrow SiH_2O + OH$$

those that were observed to be sensitive for this case differed from those that Jachimowski observed, as described in section 2.3. It would appear therefore that choice of initial conditions has a large bearing on the results of a sensitivity analysis. In this case, the most important parameter that affected the outcome of the analysis was the inclusion of an initial amount of free radical oxygen.

3.5 A Comparison of Net Reaction Conversion Rates

In this section, net forward reactions rates (X_j) are plotted against distance (in Figs. 3.12 (a) to 3.12 (d)) for the same example as discussed in sections 3.2, 3.3, and 3.4. The magnitude of X_j gives approximately the importance of any single reaction amongst all those occurring. It is defined for different types of reactions in (2).

From these plots, it can be seen which reactions are relatively important and at which stage in the ignition process they occur. The rapid pressure rise signifying complete combustion occurs between 25 and 27 cm downstream from the starting point for the analysis (Fig. 3.13). Given this, it can be seen that there are four distinct processes which make up the ignition process.

For the first stage of the ignition process, atomic oxygen is rapidly consumed by the reaction

$$R5...O + SiH_4 \rightarrow OH + SiH_3$$

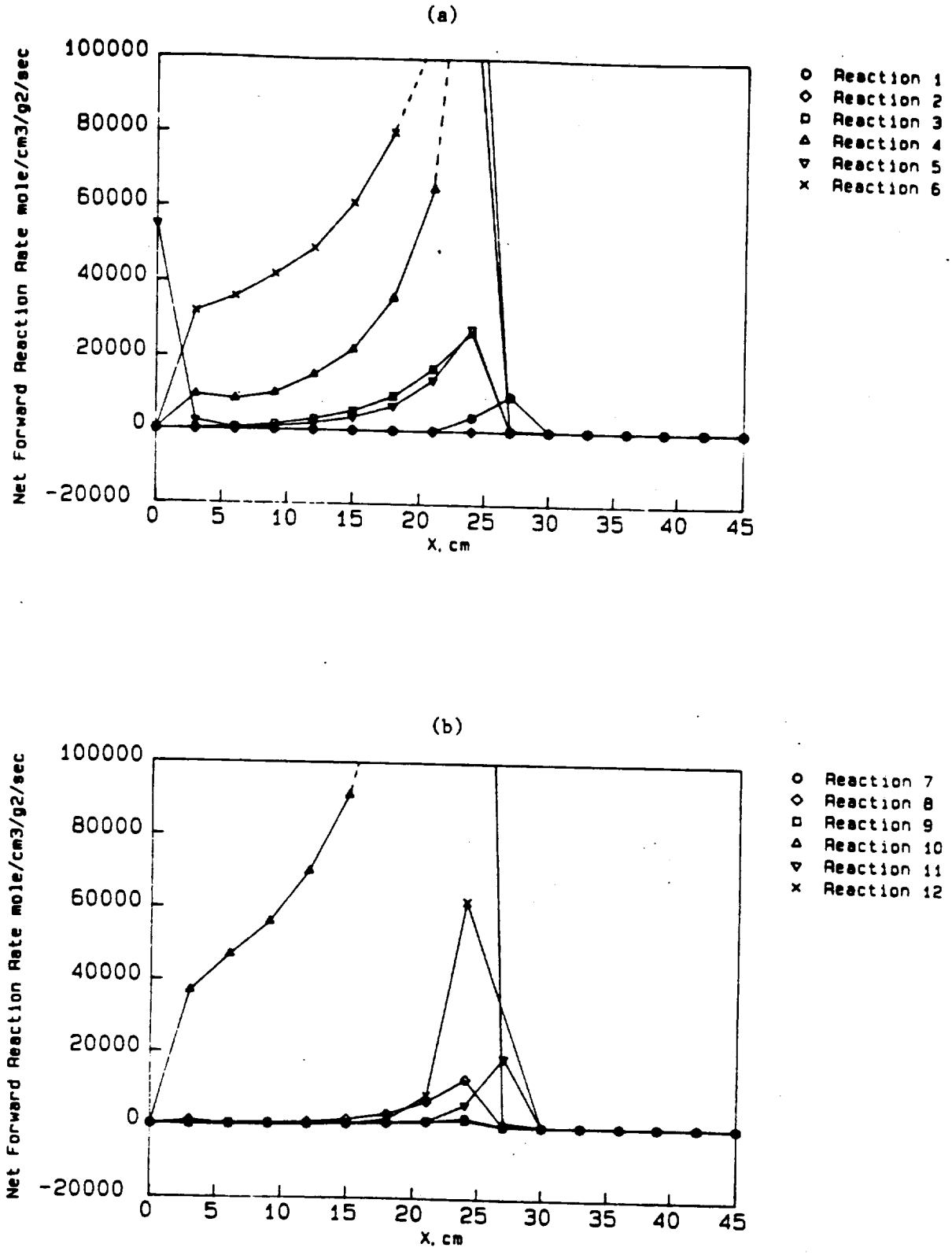

Fig. 3.12 20% Silane/Hydrogen Combustion Simulation.
Comparison of Net Forward Reaction Rates. Mach 5 nominal.
$H_S = 4.2$ MJ/kg, $P_1 = 20$ kPa, $T_1 = 650$ K, $\phi = 1.0$, $\alpha = 0.18\%$

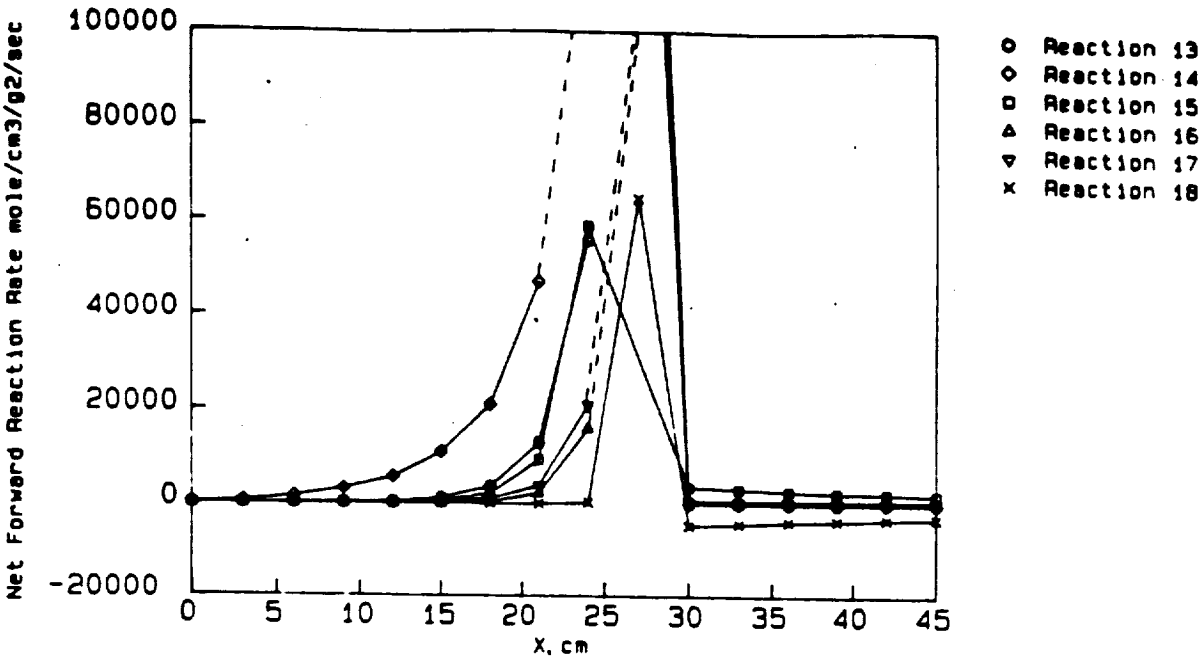

(d)

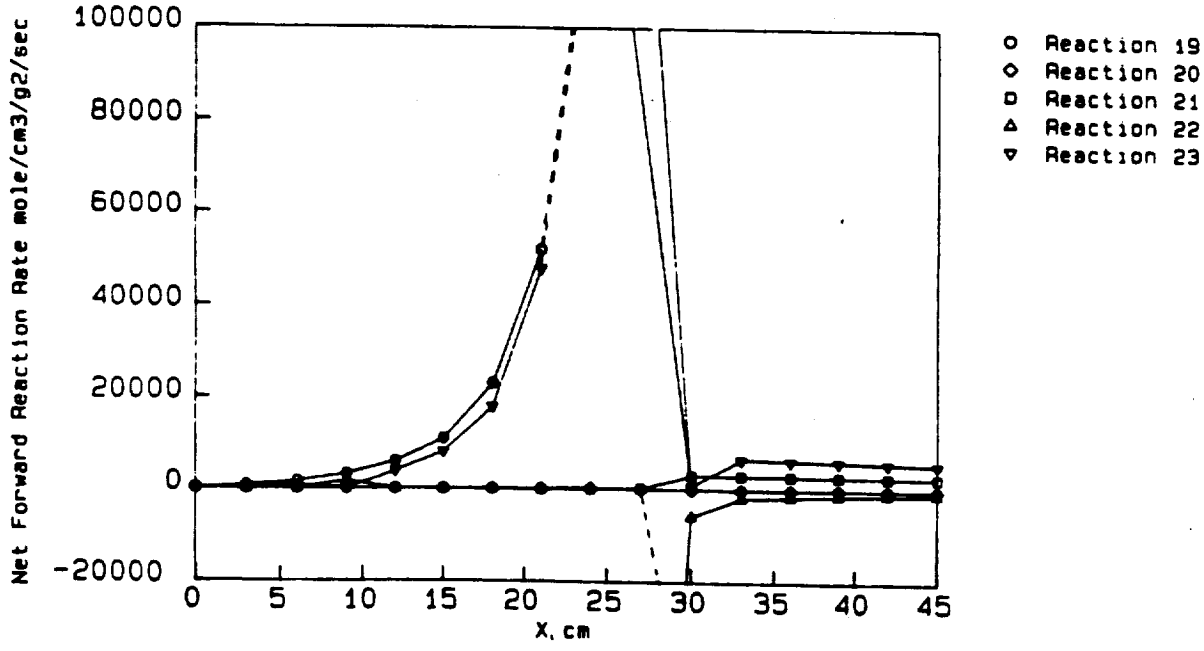

Fig. 3.12 20% Silane/Hydrogen Combustion Simulation.
Comparison of Net Forward Reaction Rates. Mach 5 nominal.
H_S = 4.2 MJ/kg, P_1 = 20 kPa, T_1 = 650 K, ϕ =1.0, α = 0.18%

and the conversion rate for this reaction drops to about zero at about 6cm. This corresponds with the point of minimum free radical concentration observed for this case as illustrated by the atomic oxygen mass fraction profiles in section 3.4 for the unadjusted reaction scheme. After this initial attack by the free radical oxygen on the silane, a pool of hydroxyl andSiH_3 radicals is established to feed the two reactions

$$R6...OH + SiH_4 \rightarrow H_2O + SiH_3$$
$$R10...SiH_3 + O_2 \rightarrow SiH_2O + OH$$

This is the second stage of the ignition process where it can be seen that one reaction sustains the other by producing the radicals the other needs. R6 provides R10 with the SiH_3 to attack the oxygen while R10 provides R6 with the OH to attack the silane. These two reactions become the dominant reactions for the early part of the ignition process up until about 15 cm.

Another important reaction (but to a lesser extent) during these early stages is

$$R4...H + SiH_4 \rightarrow H_2 + SiH_3$$

The atomic hydrogen which attacks the silane is produced from the reaction

$$O + H_2 \rightarrow OH + H$$

This is an example of the interelation of the silane oxidation process with a reaction involving the hydrogen component of the fuel mixture. The overall process at this stage, however, is dominated by the reactions R6 and R10 which involve the silane component of the fuel mixture.

Hydrogen abstractions from the parent fuel molecule by OH and H radicals tend to be the dominant reactions throughout the ignition process. Abstraction by O radicals produced by the shock tunnel accelerates the process significantly as observed in the first stage of the ignition process, but very little atomic oxygen takes part in hydrogen abstraction reaction R5 thereafter. This trend supports previous experience in hydrocarbon modelling work with stoichiometric fuel mixtures, as discussed in section 2.4.

During the second stage of ignition process, free radicals O, OH, H and SiH_3 are generated together with a quantity of the intermediate specie SiH_2O through the reaction R10.

After 15 cm, the third stage of the reaction process becomes apparent. Three interelated reactions start to become important and net conversion rates for these three reactions rise at about the same rate. The three reactions are

$$R14...OH + SiH_2O \rightarrow OH + HSiO$$
$$R19...HSiO + O_2 \rightarrow SiO + HO_2$$
$$R23...SiO + O_2 \rightarrow SiO_2 + O$$

It can be seen that these three reactions complete a reaction sequence that converts silane into silicon dioxide. The net release of heat from this process would then be responsible for the increased activity of almost all of the other reactions at about 20 cm. Net conversion rates then rise to a maximum for most reactions at about 25 cm. This distance corresponds with the "hydrogen ignition" point and the fourth stage of the process where the temperature is sufficient to cause the hydrogen to burn. This is evidenced by the rapid pressure rise between 25 and 27 cm as illustrated in Fig. 3.6.

Nomenclature

H_S	Stagnation Enthalpy, MJ/kg
M_I	Intake Mach Number
P_I	Intake Pressure, kPa
P_0	Average Fuel-off Duct Pressure, kPa
P_S	Stagnation Pressure, kPa
P	Local Static Pressure, kPa
ϕ	Equivalence Ratio
T_I	Intake Static Temperature, K
X	Duct Wetted Length, mm or cm
X_j	Net Forward Reaction Rate, mole/cm^3/g^2/s
α	Percentage Dissociation of Molecular Oxygen

BIBLIOGRAPHY

1. Morgan R.G., Paull A., Morris N.A., Stalker R.J. "Scramjet Sidewall Burning - Preliminary Shock Tunnel Results", Research Report 12/85, Dept. of Mech. Eng., University of Queensland, 1985. (NASA Contract NAGw-674)

2. Mc Lain A.G., Rao C.S.R., "A Hybrid Computer Program for Rapidly Solving Flowing or Static Chemical Kinetic Problems Involving Many Chemical Species.", NASA TM X-3403, July, 1976.

3. Morgan R.G., Department of Mech. Eng., University of Queensland, Private Communication.

4. Carson G.T. Jr., " Analytical Chemical kinetic Investigation of the Effects of Oxygen, Hydrogen, and Hydroxyl Radicals on Hydrogen-Air Combustion", NASA TN D-7769, November, 1974.

5. Lordi J.A., "Computer Program for the Numerical Solution of Non-Equilibrium Expansions of Reacting Gas Mixtures", NASA TP CR-472, 1966.

6. Beach H.L. Jr., Mackley E.A., Rogers R.C., and Chinitz. W, w. 1980 "Use of Silane in Scramjet Research", 17th Jannaf Combustion Meeting, Volume 1, (Debra Sue Eggleston Ed.), CPIA Publ. 329 (Contract N00024-78-C-5384), Appl. Phys. Lab. , Johns Hopkins Univ. pp639-659.

7. Jachimowski C.J., McLain A.G., "A Chemical Kinetic Mechanism for the Ignition of Silane/Hydrogen Mixtures", NASA TP 2129, February, 1983.

8. McBride B.J., Heimel S., Ehlers J., Gordon S., "Thermodynamic Properties to 6000K for 210 Substances Involving the First 18 Elements", NASA SP-3001, 1963.

9. Morgan R.G., Paull A., Morris N.A., Stalker R.J. "Further Shock Tunnel Studies of Scramjet Phenomena", Research Report 10/86, Dept. of Mech. Eng., University of Queensland, 1986. (NASA Contract NAGw-674).

10. Westbrook C.K., Dryer F.L., " Chemical Kinetics and Modeling of Combustion Processes ", Eighteenth International Symposium on Combustion, The Combustion Institute, Pittsburgh, PA, 1981, pp749-767.

11. Westbrook C.K., " Chemical Kinetic Modeling of Higher Hydrocarbon Fuels", AIAA Journal, Vol 24, Number 13, December 1986, pp2002-2009.

12.. Reid R.C., " The Properties of Gases and Liquids", McGraw Hill Publ., New York, 1966.

PRESSURE SCALING EFFECTS IN A SCRAMJET COMBUSTION CHAMBER

R.G. Morgan & R.J. Stalker

8 th International Symposium on air Breathing Engines.
Cincinnati, Ohio, June 15-19, 1987.

Pressure Scaling Effects in a Scramjet Combustion Chamber.

R.G.Morgan*, R.J.Stalker■
Department of Mechanical Engineering,
University of Queensland.

ABSTRACT.

The results are presented of a series of tests on a model scramjet performed in the free piston shock tunnel 'T3' in the Australian National University. The experiments were planned to give performance data over a range of pressure levels corresponding to flight at different altitudes. For each pressure level tests were carried out for enthalpies ranging from the ignition limits at the low temperature end, up to temperatures where the dissociation of combustion products severely limited heat release. The minimum temperature at which combustion was possible was found to be highly pressure sensitive for the experimental conditions used. At lower pressures higher temperatures were needed to initiate combustion within the transit time of the combustion chamber. Close to, but above, the ignition limit the amount of heat release increased markedly with pressure and also with combustion chamber length. At higher enthalpies combustion was not so sensitive to pressure rise. A finite element computer code was used to model the mixing and combustion processes. Away from ignition delay effects the program gives reasonable agreement with the measured heat release. At conditions where combustion is marginal, near the ignition limits, good agreement with experiment can only be obtained by adjusting the freestream oxygen dissociation fraction to unreasonable levels.

INTRODUCTION.

For combustion of fuel in a scramjet three processes are necessary, namely mixing of the fuel and air, heating of the fuel above its ignition temperature, and the allowance of sufficient time for reactions to take place. All of these processes are to a certain extent pressure dependent. An accelerating scramjet will experience a wide range of operating conditions. These include pressure, Mach number, and static temperature variations at the combustion chamber intake. An understanding of the behaviour of scramjets over the full range of flight conditions is therefore important.

Previous shock tunnel studies of scramjets have concentrated on basic thrust producing and heat transfer mechanisms, Refs 1 and 2. This paper reports the results of experiments to study pressure effects in a shock tunnel, and presents comparisons with a currently available chemical kinetics and mixing program, Ref 3.

The experiments were devised to give specific impulse against temperature data for a range of intake static pressures. From this data it was possible to identify three broad combustion categories in a pressure / temperature plane, Fig 9. In region 1, combustion is not possible within the confines of the chosen model. In region 2 combustion is possible, but the heat release is strongly pressure and temperature dependent. In region 3, combustion is only slightly sensitive to pressure and temperature, over the pressure range considered.

Some tests were performed with an extension block fitted to the combustion chamber, which allowed more time for mixing and combustion before expanding the flow in the thrust nozzle. This was seen to be effective in the combustion category 2, above, but had no measurable effect at the higher temperatures associated with category 3. It was also seen to shift the border of regions 1 and 2 to lower temperatures, indicating that the extra mixing length permitted combustion under conditions with a longer ignition delay time.

EXPERIMENTAL APPARATUS.

A schematic diagram of the experimental apparatus is shown in Fig 1. The free piston shock tunnel, T3 Ref 2, at the Australian National University was used to create the flow conditions corresponding to the intake of a scramjet combustion chamber.

The model consisted of a two dimensional duct of intake section 25 mm by 50 mm. Hydrogen fuel was injected on the centreline from an injector strut which spanned the whole width of the duct. The leading edge of the injector was extended clear of the intake so that disturbances from the leading edge would not enter the duct.

* Senior Lecturer, Mechanical Engineering, Member AIAA.
■ Professor, Mechanical Engineering, Member AIAA

After injection a constant area section of adjustable length served as a combustion chamber. The flow was expanded by a single 15 degree Prandtl Meyer expansion fan propagating from the lower wall, and thrust was developed on a straight thrust surface. The intake, combustion chamber and thrust surface were instrumented with pietzotronic pressure transducers. Thrust was calculated from the static pressure measurements, and specific impulse was determined from the difference between fuel on and fuel off thrust levels.

A steady flow of hydrogen was established prior to starting the shock tunnel by means of a pulsed valve, Ref 3, which was triggered off the recoil of the tunnel. A static pressure transducer in the injector plenum chamber was used to give a measure of the hydrogen mass flow rate.

A contoured nozzle of nominal Mach number 3.5 was used to create the required test conditions. The model intake static pressure was controlled by selection of a suitable shock tube driver rupture pressure. Further control on the intake pressure and Mach number was given by the use of adjustable wedges on the model inlet. These wedges created oblique shocks which reflected from the centreline and did not enter the model, thereby maintaining uniform intake flow. It should be noted that the use of the wedges was purely to give flexibility to the conditions achievable with a single contoured nozzle. They do not represent an attempt to model a scramjet intake, because, due to Reynolds number limitations, it was only possible to model the combustion chamber and a short thrust nozzle.

CALCULATION OF TEST CONDITIONS.

The flow conditions at the nozzle exit are estimated assuming equilibrium in the shock tube stagnation region behind the reflected shock, followed by a non-equilibrium expansion through the contoured nozzle. The non equilibrium expansion is computed using the computer code of Ref 6.

Frozen flow is assumed through the oblique shocks formed by the compression wedges, when used.

A total of 44 different shock tunnel operating conditions were used, all of which could be configured with 3 different wedge compression angles. It was impractical to perform a complete analysis of all the intake data, so interpolation was used for some cases. In Fig 2 a range of computed nozzle exit velocities against stagnation enthalpy is plotted, and in Fig 3 the curve fit used for the full range of conditions is shown. Fig 4 shows the dependence of Mach number with stagnation enthalpy. The Mach number is reduced at higher enthalpies due to the a reduction in the specific heat ratio.

The test conditions are tabulated in table 1. Equivalence ratios were nominally set to 1. with minor fluctuations between runs.

EXPERIMENTAL RESULTS.

The shock tunnel was operated in the undertailored mode, which was found to maximise the uncontaminated test time, which is especially important in combustion applications. This condition produces a small drop in the stagnation pressure during the run. In order to confirm that the expansion through the nozzle produced a steady Mach number, the static pressures in the model were normalised with respect to the shock tunnel stagnation pressure. Readings were taken only when all the normalised static pressures were steady. All computations performed on the data assumed steady flow conditions.

Specific impulse was calculated by taking the difference between fuel on and fuel off thrust levels, normalised by stagnation pressure to account for minor fluctuations between nominally identical runs.

In Fig 5 the effects of pressure at a Mach number of 3.25 are shown for a short combustion chamber. A 5 degree angle was used on the compression wedges to create this condition.

A striking feature of this figure is the dependence of ignition temperature on static pressure. It can be seen that combustion is possible down to temperatures of about 700 K at a pressure of 250 kPa. As the pressure drops the minimum temperature required to support combustion increases. At 50 kPa combustion is not possible at temperatures below 1200 K.

It is also noticeable that when conditions are such that combustion can occur at temperatures below 1000 K, very high values of specific impulse are

achieved. This is thought to be due to the low combustion temperature which suppresses dissociation of the combustion products.

Combustion could be induced at temperatures below 1000 K either by means of high pressures or by the use of a long combustion chamber, and in both cases high values of specific impulse were achieved. Fig 6 shows previously published data from Ref 7. for an intake pressure of 150 kPa at Mach 3.5. It is seen that the longer duct produced similar results to the short duct at a higher pressure.

In Fig 5 it can be seen that in the region between 700 K and 1000 K the amount of combustion , as indicated by specific impulse, is very pressure sensitive. This is possibly because combustion is marginal near the ignition limits, and a small rise in pressure can markedly reduce the ignition delay times and permit more heat release within the duct. However, if the conditions are such that substantial combustion occurs, that is for long ducts or high pressures, then the strong pressure dependency disappears. This may be seen by comparing the peak values of specific impulse in Figs 5, 6 and 7.

In Fig 8 the effect of extra combustion chamber length is shown for the high pressures produced by the 5 degree scoop. It is seen that the only difference is a slight lowering of the ignition temperature, and very high levels of specific impulse at the temperatures just above quenching. The data may be seen to be all following the same pattern, with the pressure and combustion chamber length determining the point of departure from the common curve. The shape of the curve is similar to the idealised condition of equilibrium combustion also shown in Fig 6.

At higher enthalpies, corresponding to intake temperatures above 1500 K, the performance appears to be fairly independent of pressure. An exception to this is given by the 50 Kpa intake pressure condition shown in Fig 5, which shows signs of reduced output at temperatures up to 1800 K.

In Fig 9 three combustion zones are loosely defined in the pressure temperature plane, using the specific impulse results. In region 1 no combustion is possible for the configuration chosen. In region 2 combustion occurs, but with a strong pressure dependence due to ignition delay effects. Region 3 includes those cases where combustion is pressure independent. The exact boundary between regions 2 and 3 at higher temperatures is unclear, but it appears to lie between 50 and 75 Kpa. Figure 9 refers only to the short combustion chamber. There is not enough data to fully define a similar curve for the longer combustion chamber, but the available data suggests a shift of all the boundaries to lower temperatures occurs.

It should be stressed that Fig 9 only applies to the specific experimental configuration used. Its main value lies in providing data to test theoretical models, rather than being representative of a flight situation. It does indicate however, that scramjets designed to optimise specific impulse are likely to be operating in pressure sensitive regions. It also suggests that the low pressures associated with very high altitude flight might experience ignition problems, even at high temperatures.

NUMERICAL SIMULATION.

An attempt was made to model the mixing and combustion processes in the scramjet using a two dimensional parabolic computer code. The program is based on ref 3, but incorporates finite rate chemistry. It is two dimensional in that it considers transverse gradients of temperature, chemical species , turbulence and velocity. However, it cannot model transverse pressure gradients, which have been shown in Ref 1 to be significant in the thrust producing processes of two dimensional scramjets.

In Fig 10 a schematic is shown of the way in which the combustion zone is expanded in order to develop thrust. Most of the combustion occurs in a limited mixing region around the centreline, upstream of the expansion propagating from the start of the diverging section. In this narrow ducted region it may seem not unreasonable to assume that the effects of combustion are felt uniformly across the section of the duct, and that a one dimensional pressure treatment may give sufficient accuracy.

The authors, in as yet unpublished work, have developed a procedure for matching the output from the quasi two dimensional mixing program with linearised small perturbation wave theory in the expanding region. This has produced good

correlations both with the experimentally recorded pressure profiles, and with the calculated values of specific impulse.

A different approach was adopted for this paper, due to the large amount of data to be processed. By inspection of Fig 10 it can be seen that the exhaust nozzle flow will be expanded by multiple reflections of the 15 degree corner expansion between the cowl and the thrust surface. However, it was shown in Ref 1 that valid comparisons with a one dimensional code can only be made after the elimination of all transverse disturbances, that is, in the presence of parallel exhaust field. For the present configuration this means allowing the full reflection of the corner expansion from the cowl to propagate through the jet.

Therefore the mixing program was run with an expanding section such that the area ratio experienced by the duct is the same as that produced by the double pass of a 15 degree expansion fan traversing the jet. This gives an area ratio of 10.3 for the nominal nozzle exit mach number of 3.5. Corrections to this value have not been made to account for Mach number variations between conditions.

To give a direct comparison with the computations, the experimental results have to be modified as outlined in Ref 1 to compute the thrust that would have been realised if all the disturbances were eliminated by contouring of the thrust surface. This has not been done in this instance, because the technique of Ref 1 does not apply to long combustion chambers with a significant pressure rise upstream of the corner. The data is therefore presented not for direct quantitative comparison with experiment, but rather to indicate trends, and to predict theoretical maxima for a perfect expansion without wave drag.

In Fig 11 the results of the computations are summarised.

Quantitative trends which are evident in the experimental data also appear in the computations. Thus, at a given static pressure, the long duct yields higher specific impulse than the short duct at temperatures just above ignition, but at higher temperatures the length of the duct does not make much difference. Also, with a given duct length, the specific impulse falls as the pressure falls.

The program does predict the sharp drop in specific impulse which occurs near the ignition point, and the high levels of specific impulse observed for the long duct at lower temperatures. However, a consistently high ignition temperature is given, except for the 50 kpa case. The high values of specific impulse observed just above the ignition temperature for the short duct in the 200 to 500 kpa range, Fig 7, were not predicted.

The results presented in Fig 11 were obtained with oxygen dissociation levels as obtained from the non equilibrium nozzle expansion program, Ref 6. Free stream turbulence was input as a constant fraction of the second power of velocity.

Agreement with individual data points can always be obtained by adjustment of various parameters in the program, such as free stream turbulence and oxygen dissociation levels. The effect of the boundary layer which forms on the outside walls of the injector strut is also unknown, but viscous heating may be important in determining the free stream ignition temperature.

The instrumented portion of the model only covers that section of the jet which is expanded by the first pass of the expansion fan, however as explained above the computations had to be performed on a double pass in order to produce a parallel, axial outlet. The computations would therefore be expected to overpredict the thrust, because of the jet expansion which occurred in uninstrumented regions of the model ,which did not contribute to the measured thrust production.

Not withstanding the prediction of qualitative trends, it is clear that the computational model fails in that it underpredicts specific impulse, and does not give a correct ignition temperature. There are two possible reasons for this.

The first is that the mixing and chemistry models used in the program may not be adequate, and as far as the ignition point is concerned this is the most likely cause.

The second is that while the one dimensional approximation may give reasonable results in the constant area duct section, and the unpublished results mentioned above suggest that this is so, a one dimensional treatment may not be correctly used to model the expansion of the jet. As the expansion traverses the

jet. different points at the same axial location will see different pressures. and this might have a significant effect on thrust production.

CONCLUSIONS.

Scramjet performance shows a strong pressure dependency in regions near to the ignition limits. In regions of maximum thrust, which are desirable target operating conditions, pressure effects are also evident at the lower temperatures. At higher enthalpies, ie at intake temperatures above 1500 K, combustion is insensitive to pressure above intake pressures of 50 Kpa.

Numerical modeling procedures are not yet adequate for quantitative thrust predictions, but can give a useful indication of general trends.

ACKNOWLEDGMENTS.

This work was performed under a grant from the NASA Langley Research Center, Hypersonics Propulsion Branch.

The experimental work was performed in the shock tunnel of the Physics department of the Australian National University, and the assistance of many members of the staff for all the back up support required for the operation of a major test facility is greatly appreciated.

References.

1. R.J.Stalker,R.G.Morgan.
"Supersonic Combustion with a Short Thrust Nozzle".
Journal of Combustion and Flame,Vol. 57, No. 1,
July 1984, pp 55-70.

2. R.G.Morgan,R.J.Stalker.
"Shock Tunnel Measurements of Heat Transfer in a Model Scramjet".
AIAA Journal of Spacecraft and Rockets.
Vol 23, No 5. Sept-Oct 1986. pp 470-475.

3. J.S.Evans, C.J.Schexnayder Jr., H.L.Beach Jr.,
"Application of a two - dimensional parabolic computer program to prediction of turbulent reacting flows."
NASA Tech. Paper 1169, March 1978.

4. R.J.Stalker.
"Development of a hypervelocity wind tunnel".
The Aeronautical Journal of the Royal Aeronautical Society. 76, 1972, pp 374-384.

5. R.G.Morgan,R.J.Stalker.
"Fast Acting Hydrogen Valve".
Journal of Physics E.
Sci. Instrum. Vol. 16. 1983. pp 205-207.

6. J.A.Lordi, R.E.Mates, J.R.Moselle.
"Computer program for the numerical solution of non-equilibrium expansion of reacting gas mixtures".
NASA rep. NASA CR-472. 1966.

7. R.G.Morgan,R.J.Stalker.
"Hypersonic Air Breathing Propulsion".
I.E. Aust Multidisciplinary Proceedings, Vol. GE9,No. 1,July 1985.

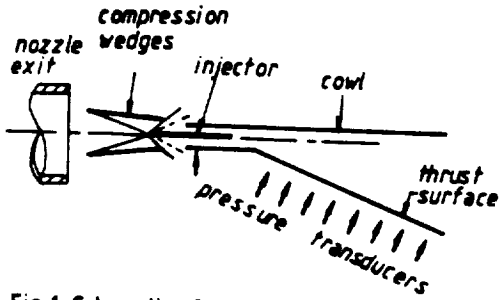

Fig 1. Schematic of experimental apparatus

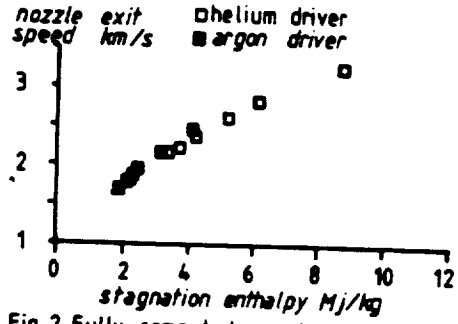

Fig 2. Fully computed nozzle exit speeds, rupture pressure 46 Mpa

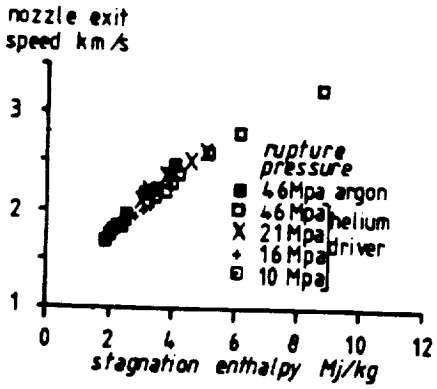

Fig 3 Curve fitted nozzle exit speeds

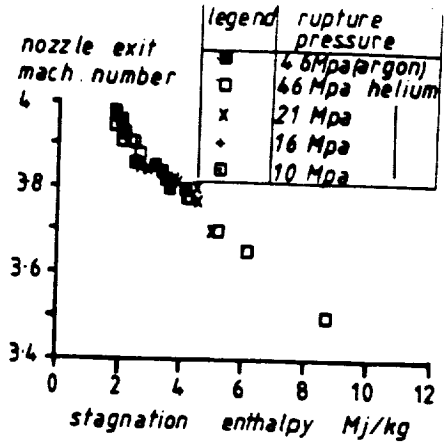

Fig 4. Curve fitted mach number

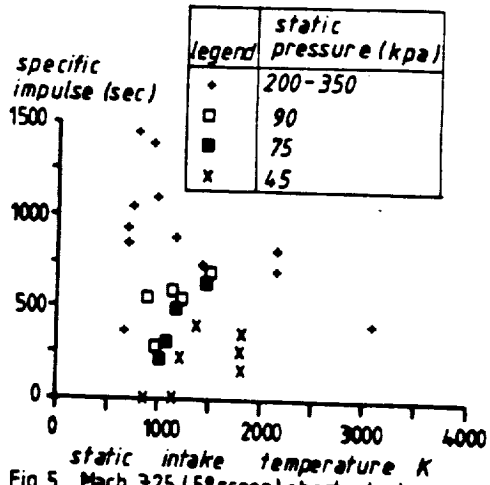

Fig 5. Mach 3·25 (5° scoop) short duct

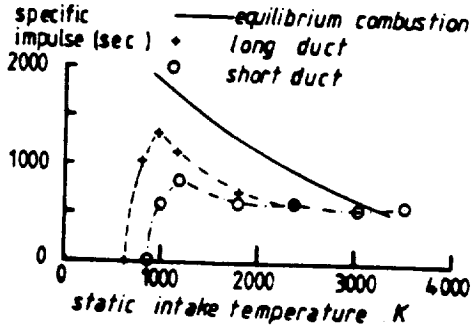

Fig 6. Mach 3·5, intake static pressure 150 kpa

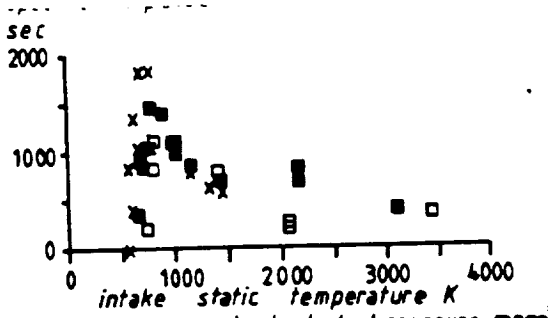

Fig 7. Effects of combustion chamber length and pressure.

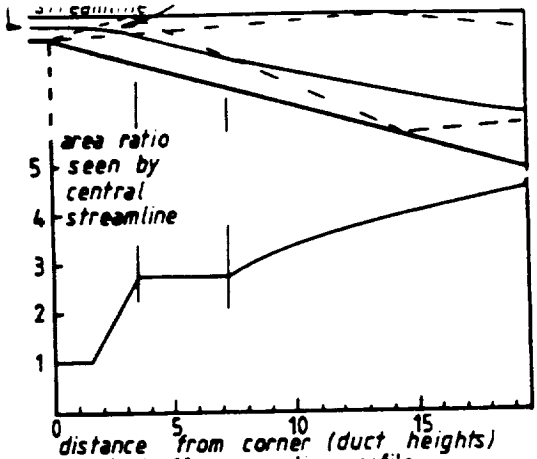

Fig 10 fuel off area ratio profile

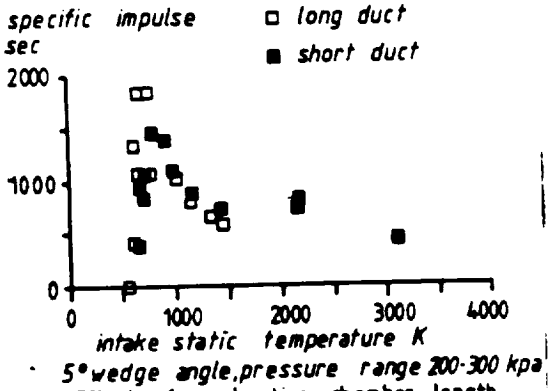

Fig 8. Effect of combustion chamber length.

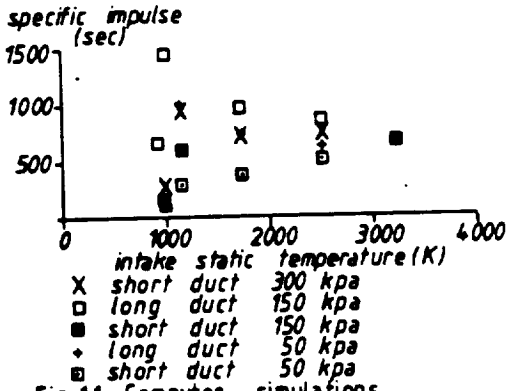

Fig 11. Computer simulations.

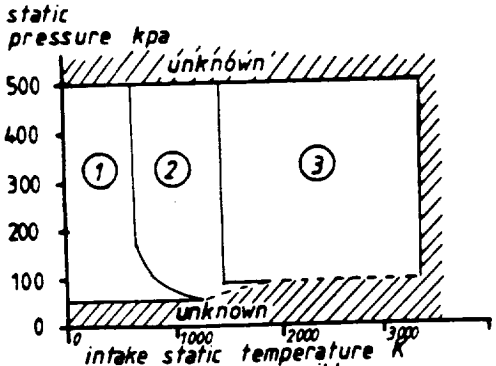

Fig 9. Approximate combustion zones. Short duct.

Table 1

Rupture Pressure kpa	Compression wedge setting	Enthalpy Range MJ/kg	Intake pressure kpa	Intake temperature K
46	no scoop	8.72-1.87	160-60	2520-445
	2.57° scoop	8.72-1.87	245-92	2815-504
	5° scoop	8.72-1.87	356-139	3110-564
	7.5° scoop	8.72-1.87	500-207	630-3440
21	no scoop	4.35-2.96	38-35	1200-781
	2.57° scoop	4.35-2.96	60-56	1350-881
	5° scoop	4.35-2.96	90-83	1510-982
	7.5° scoop	4.35-2.96	131-122	1680-1100
16	no scoop	4.27-3.08	32-31	1180-817
	2.57° scoop	4.27-3.08	51-49	1330-921
	5° scoop	4.27-3.08	77-74	1480-1030
	7.5° scoop	4.27-3.08	112-108	1650-1150
10	no scoop	5.12-2.66	21-19	1450-690
	2.57° scoop	5.12-2.66	33-30	1630-779
	5° scoop	5.12-2.66	49-45	1810-869
	7.5° scoop	5.12-2.66	70-67	2010-970

PRESSURE SCALING IN THE SCRAMJET MODEL

P. Jacobs

Pressure Scaling in the Scramjet Model

1. Introduction

Previous experimental data [1] obtained in the shock tunnel shows a range of intake temperatures where the integrated pressure profile (specific impulse = I_p) is very pressure sensitive. For higher temperatures, I_p was insensitive to pressure, while for lower temperatures, the ignition limits were pressure sensitive. These results may be interpreted in terms of the reaction and ignition time correlations with pressure and temperature reported in [2] and [3]. The correlations given in [3] are

$$\tau_i = \frac{\ell_i}{v} = \frac{8\times10^{-9}\ \exp(9600/T)}{p} \qquad (1)$$

$$\tau_R = \frac{\ell_R}{v} = \frac{0.000105\ \exp(-1.12T/1000)}{p^{1.7}} \qquad (2)$$

where τ_i = ignition time (sec) $\quad \ell_i$ = ignition length (m)
τ_R = reaction time (sec) $\quad \ell_R$ = reaction length (m)
v = flow velocity (m/s)
T = inlet temperature (K)
p = static pressure (atm)

Hence, near the ignition limits, where ℓ_i is close to the length of the model ℓ_m, a decrease in p will increase ℓ_i and result in no combustion within the model. Also, a decrease in T will lead to an (exponential) increase in ℓ_i and a very sharp drop in I_p.

In the range of conditions where the fuel always ignites within the model length, I_p will be most sensitive to pressure when ℓ_R is greater than ℓ_m. Hence, above a certain temperature (found to be approximately 1400K in [1]), I_p will be relatively insensitive to changes in p.

The aim of this experiment (to be performed in August 1988)

is to experimentally determine these pressure-length correlations (1), (2) in the T4 shock tunnel. With the relatively high static pressures generated by the shock tunnel, we hope to vary the duct pressure in the combustor model by a factor of 10 and be able to observe a pressure rise due to combustion.

2. The Experiment

The experiment will involve the measurement of pressure distributions in three constant-area combustion chamber models with different intake pressures but otherwise equivalent flow conditions (i.e. same mach number M, temperature T and species concentrations). Each model will be scaled geometrically to give $p\ell_m$ = constant where ℓ_m=1.0 for the largest model (also the lowest pressure).

There are, however, problems involved in getting the shock tunnel to provide equivalent flows with a range of pressures, and there are also problems in manufacturing three geometrically similar models with an order- of- magnitude difference in size. At one end, the largest model has to fit into the available test facility and be short enough to establish steady flow within the available test time. At the small end, we cannot manufacture injector struts smaller than 3-4 mm thick and have them operate successfully at the high fuel injection pressures required. Fortunately, (in the light of comments made on source flow nozzles [4]) we expect that the experiment will be insensitive to small differences in injector scale.

The more difficult problem concerns the generation of different pressure flows. Inlet flow for the small model (high p)

will be provided by expanding the test gas from the shock tube reservoir through a mach 4 nozzle. It will then directly enter the model intake as shown in figure 1. The larger models require the same parallel flow but a lower pressures. We considered three proposals for generating these low pressure flows...

1. Run the shock tube at different reservoir conditions and expand the flow through the same mach 4 nozzle. Unfortunately, changing the pressure in the shock tube reservoir while keeping the temperature constant leads to a change in entropy (see e.g. the Mollier diagram for air in chemical equilibrium [5]). Harris & Warren [6] have shown that the gas composition is strongly correlated with the entropy in the reservoir and, for a factor of 10 change in pressure, we feel that the corresponding change in free radical concentrations is too great for this experiment.

2. Run the shock tube at the same nominal conditions (as for the high pressure case), expand the gas through a first nozzle, collect it in a second stagnation region (so that there is a drop in total pressure through the normal shock preceding this region) and then expand the gas through a second contoured nozzle to the final flow conditions. This proposal suffers a similar problem to proposal 1 as the gas (with increased entropy) will reach chemical equilibrium in this second region.

3. Run the shock tube at the same nominal conditions, expand the gas to a higher mach number (say 8 - 10) and pass the chemically frozen gas through a set of compression wedges to give M=4 at the model intake. The shocks from the compression wedges provide a drop in total pressure (and increase in entropy) and hence a drop

in static pressure relative to the small model without a change in the gas composition (as there are relatively low temperatures behind the oblique skocks). The disadvantage here is that, to provide adequate total pressure drop across the compression shocks, we initially need to expand the gas to high mach numbers (approx. 10) or, for moderate.values of M (approx. 8) we need to "shock down" to low mach numbers at the model inlet. The former option requires an extremely large nozzle and correspondingly large set of compression wedges (which are too large for the available facility) to provide an adequate flow for the large model intake.

The final configuration for the large model (low pressure) is shown in figure 2. We run the shock tube at the same nominal conditions as for the high pressure model, expand the test gas to M=8, compress it to M=3 before the model intake, and then expand it to M=4 within the model (but before the point of fuel injection). This provides us with a design that will (just) fit within the current facility.

The operating condition for the small model will have (approximately) T=1600K, v=3286m/s, M=4, p=1.17atm and a dissociation fraction for oxygen α_o=1.68%. These values were computed using a one-dimensional code [7]. Table 1 provides a more complete list of the test conditions. At this temperature and dissociation level, we expect ignition to occur at (or very close to) the injector. Although the flow will be three-dimensional and involve turbulent mixing of the fuel jet, we expect that (if the mixing effects scale with the Reynolds number) we will be able to decouple the mixing effects from the chemical

kinetic effects by having the same Reynolds number in each model.

The ignition and reaction lengths (as measured by temperature rise) were computed for a premixed flow using a one-dimensional chemical kinetic code [8]. For a fuel equivalence ratio ϕ=1.0 and the flow conditions mentioned above, the numerical code gives $\ell_R(p=1.17)$=0.095m and $\ell_R(p=0.2)$=1.9m. These values may be compared with $\ell_R(p=1.17)$=0.044m and $\ell_R(p=0.2)$=0.887m computed from the correlation (2). Although the lengths are different by a factor of 2, the equivalent exponent of pressure is only 1% different. The numerical simulations also confirmed that the reaction length was insensitive to α_o (see also [1]).

Measurements of the reaction length in the models will be obtained indirectly by measuring the static pressure at the wall at several downstream locations. To obtain sufficient spatial resolution we may have to construct a single pressure profile from several shots with the pressure transducers at slightly different locations for each shot. However, we will not be able to avoid the confusing pressure disturbances introduced at the trailing edge of the injector and caused by the mismatch in pressure of the fuel jet and the free stream. If it can be arranged, we might also try to measure ignition lengths from optical emissions.

3. Results

... should be interesting when we get them.

4. References

1. R.G. Morgan & R.J. Stalker 1987 : "Pressure scaling effects in a scramjet combustion chamber". 8th Int. Symp. on Air Breathing Engines, Cincinnati Ohio, June 15-19.

2. G.T. Carson 1974 : "Analytical chemical- kinetic investigation of the effects of oxygen, hydrogen and hydroxyl radicals on hydrogen-air combustion". NASA TN D-7769.

3. P.W. Huber, C.J. Schexnayder & C.R. McClinton 1979 : "Criteria for self- ignition of supersonic hydrogen-air mixtures". NASA Technical Paper 1457

4. R.G. Morgan, A. Paull, N.A. Morris & R.J. Stalker 1986 : "Further shock tunnel studies of scramjet phenomena -- NASA contract NAGW-674" Research report 10/86, Department of Mechanical Engineering, University of Queensland.

5. W.J. Little 1963 : "Mollier diagram for air". Technical documentary report AEDC-TDR-63-190, Arnold Engineering Development Centre.

6. C.J. Harris & W.R. Warren 1964 : "Correlation of nonequilibrium properties of expanding air flows". R64SD92 Space Sciences Laboratory, General Electric.

7. J.A. Lordi, R.E. Mates & J.R. Moselle 1966 : "Computer program for the numerical solution of nonequilibrium expansion of reacting gas mixtures". NASA CR-472

8. D.A. Bittkeer & V.J. Scullin : "General chemical kinetics computer program for static and flow reactions, with application to combustion and shock-tube kinetics". NASA Technical Note D-6586.

Table 1 : Hypothetical Test Conditions

Parameter	Units	Model					
		Small		Medium		Large	
		nozzle exit	before injection	nozzle exit	before injection	nozzle exit	before injection
M	--	4.23	4.17	5.64	4.17	8.16	4.17
p,static	atm	1.17	1.17	0.174	0.4722	0.0138	0.114
T	K	1599	1630	1001	1620(0.6)	501	1683(3)
ρ x10^4	g/cc	2.56	2.51	0.612	1.026	0.0965	0.251
v	m/s	3286	3274	3500	3295(0.6)	3649	3326(2)
α_o	%	1.68		2.02		2.67	
γ	--	1.31		1.34		1.39	
ℓ_m	m	0.1		0.4		1.0	
θ_w	deg	---		12.0		15.0	
θ_i	deg	10.0		10.0		10.0	

Quantities in parentheses are percentage differences between the current model and the small model.
Shock tube stagnation conditions are H_o = 7.5 MJ/kg, P_o = 450 atm, and T_o = 5000 K.

ORIGINAL PAGE IS
OF POOR QUALITY

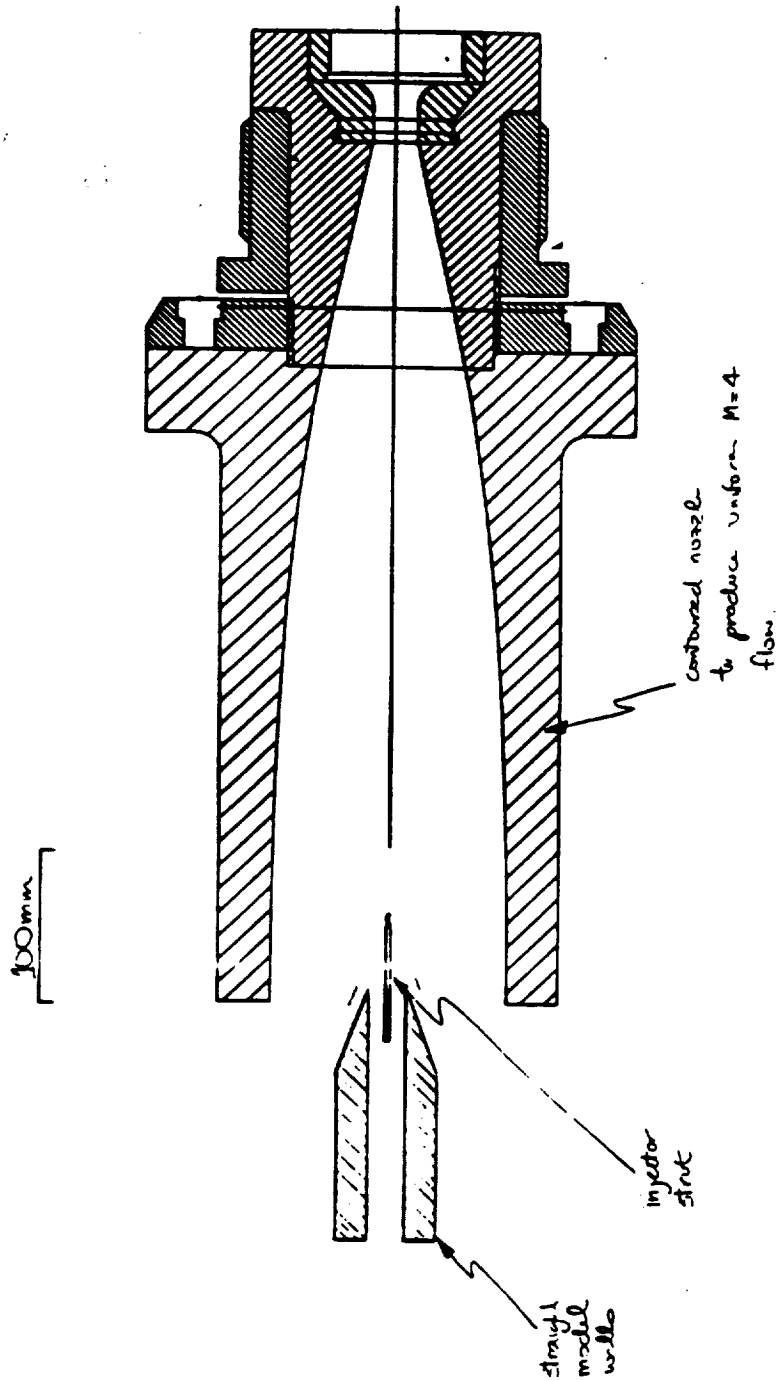

figure 1 : Small model configuration (high pressure)

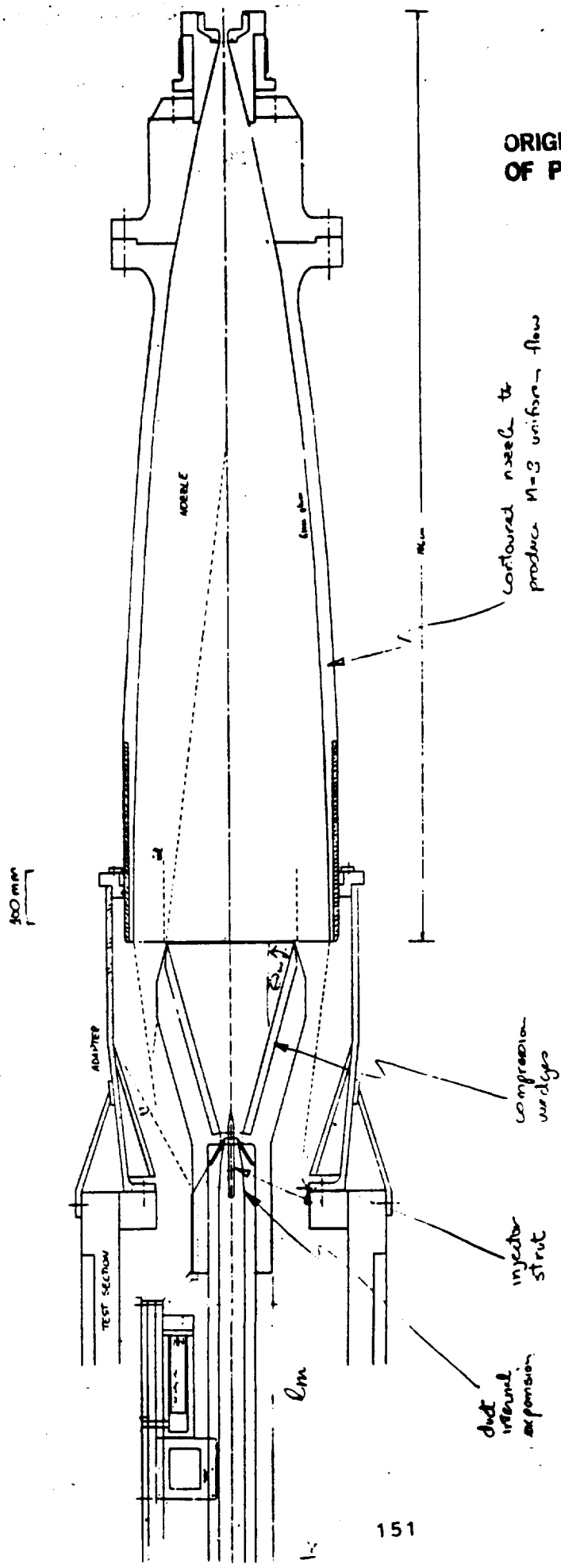

figure 2. Long model configuration (low pressure)

EXPERIMENTS ON AN EXPANSION TUBE WITH A FREE PISTON DRIVER

A. Paull, R. Stalker & I. Stringer

EXPERIMENTS ON AN EXPANSION TUBE WITH A FREE PISTON DRIVER

A. Paull[+], R. Stalker[*], and I. Stringer[#]
Mechanical Engineering Department,
The University of Queensland, Australia.

Abstract

This paper presents the preliminary test flow results from the University of Queensland's free piston expansion tube. It has been shown that pitot pressure measurements are qualitatively similar to those from the Langley facility. Furthermore, additional test conditions which have acceptably steady flows of air are demonstrated to exist using pitot pressure measurements. Shortened test times are explained partially by contamination from low density driver gas bubbles and reflection of expansion waves from the driver-test gas interface.

Introduction

A renewed interest in hypersonic flight has naturally created a renewed interest in test facilities which are capable of producing high enthalpy flows. The expansion tube is an impulse facility which in theory is capable of simulating a wide range of hypersonic conditions. However, an extensive investigation made by Miller (1977) on an ~~and~~ driven expansion tube found only a narrow band of conditions for each test gas in which the test flows were acceptably steady. At the University of Queensland an expansion tube was built with a free piston driver in order to determine if the versatility of the free piston driver would allow the 'window of test conditions' to be widened.

This paper reports on experiments performed with the University of Queensland expansion tube. In these experiments the objectives were

(i) to obtain a comparsion of the centre-line pitot pressure measurements of the University of Queensland and the Langley tube for similar running conditions,

(ii) to show that different test conditions could be obtained using different driver gases,

(iii) to show test conditions of the same stagnation enthalpy could be obtained with different test gas pressures.

Description of Facilities

Langley's Six Inch Expansion Tube

A full description of the Langley six inch expansion tube is given by Moore (1975). Briefly the driver is 2.44 m in length with an internal diameter of 0.356 m. The shock tube or driven section is 4.64 m long with an inside diameter of 0.152 m. The acceleration tube is 17 m long with the same inside diameter. Both the shock tube and acceleration tube could be varied in length. The dump tank has an approximate volume of 12.8 m^3 and is 10.7 m long with an internal diameter of 1.22 m.

+ Research Associate.
* Prof. Space Engineering.
# Research Fellow.

University of Queensland's Expansion Tube

The University of Queensland expansion tube (see figure 1) has a free piston driver which is 2.3 m long, 0.1 m internal diameter and uses a 3.4 kg piston. The shock tube and acceleration tube are 2.08 m and 3.18 m long respectively and both have an internal diameter of 0.0386 m. The acceleration tube empties into a dump tank-test section with a volume of approximately 0.15 m^3. Initially the driver and shock tube are separated by the primary diaphram and the shock tube and acceleration tube are separated by the less substantial secondary diaphram. The primary diaphram was either 0.1 mm thick cold roled mild steel or 1.57 mm thick aluminium. The secondary diaphram was 0.023 mm thick cellophane. The acceleration tube and dump tank are reduced to the same initial pressure.

The shock speeds in both the shock tube and acceleration tube were measured using ionization gauges. Three gauges were used in the shock tube and four were used in the acceleration tube. From these gauges both the speed and attenuation of the shock can be measured.

Two pressure traces were recorded every run. The wall pressure in the shock tube immediately upstream of the secondary diaphram was observed in addition to the pitot pressure at the exit of the acceleration tube. Each record consisted of 2048 data points and was sampled at a rate of one megahertz.

General Theory

Figure 2 displays the wave diagram for operation of an expansion tube. Viscous effects have been neglected. It shows that a shock produced by bursting the primary diaphram propagates at a constant velocity through the shock tube until striking the secondary diaphram. This diaphram then bursts and the shock is instantaneously accelerated and subsequently moves at a constant velocity down the acceleration tube. It is followed by the test-acceleration gas interface and the unsteady expansion produced from the bursting of the secondary diaphram. Miller (1977) notes that the maximum theoretical test time is that time between the arrival of the test gas and the unsteady expansion. However, this can be decreased.

The test time can be shortened by the existence of "bubbles" or regions which are lower in density than the test gas (Gourlay (1988)). Their presence results in large oscillations of the pitot pressure and their arrival makes the test flow useless. It is believed that these bubbles result from mixing at the driver-test gas interface and are regions in which the driver and test gases continually mix. When these low density bubbles encounter the unsteady expansion they accelerate through its pressure gradient and emerge into the test gas with a higher velocity than both the velocities of the unsteady expansion and the test gas. Hence, if the

expansion has not already reached the pitot probe then these bubbles will arrive earlier and it is their initial arrival time which determines the test time.

Obviously, due to the instability of the driver-test gas interface, bubbles of driver-test gas mixture will exist in the test gas if the density of the driver gas is less than that of the test gas. However, less obviously, bubbles lower in density than the test gas can also exist in the test gas even if the density of the driver gas is greater than that of the test gas. This can occur provided the temperature and molecular weight of the moving test gas are greater than those of the driver gas. Under such conditions and assuming the pressure and temperature of the test gas remain constant (that is, the bubbles are small) a bubble of pure driver gas mixes with the test gas and in the "bubble" there is an exchange of heat between the two gases. The driver gas would be heated by the test gas and thus its density would decrease. Furthermore if the molecular weight of the test gas is greater than that of the driver gas then the density of the driver gas would decrease below that of the test gas and thus a region of low density gas (or "bubble") would form. Obviously the test gas in the "bubble" would be cooled and thus its density increased. However as the bubble is a region which is continually mixing with the test gas this would be insignificant for an initially small bubble of driver gas.

A second phenomenon which can shorten Miller's test time is the reflection off the driver-test gas interface of the unsteady expansion centred at the secondary diaphram. From figure 2 it can be seen that as this expansion reflects off the driver-test gas interface it propagates back through itself and enters the constant pressure region of test gas. If the acceleration tube is of sufficient length then this reflection would arrive at the pitot probe before the expansion itself and thus change the static pressure of the test gas. If the reflection produces an unacceptable pressure change then the test flow is subsequently useless.

In addition steady test flows can also be disturbed by reflections of the unsteady expansion off the bubbles as they accelerate through the expansion. This phenomenon would be of second order to that produced by the reflection of the expansion off the driver-test gas interface as the density difference across this interface is greater than that across a bubble's surface.

A third phenomenon which may produce fluctuations in the pitot pressure measurements is the existence of lateral pressure waves which oscillate across the tube and are transported downstream by the movement of the gas. It is postulated these waves are produced by the breaking of the secondary diaphram. However, this mechanism is not yet fully understood.

Results

I Comparison of Pitot Pressures

One of the first experiments performed was to show that the centre line pitot pressure measurements for an air test gas in the Langley tube could be qualitatively reproduced in the University of Queensland's facility. This is important, for if established it would then be reasonable to assume that any advance made with the University of Queensland's tube would also be applicable to the much larger Langley facility. Obviously a quantitative comparison of the two facilities can not be made due to their different physical dimensions. However, it might be expected that qualitatively similar flows would occur if

(i) the Reynolds numbers based on tube diameters are the same, and
(ii) the shock speeds in the shock tubes are similar.

If the Reynolds numbers are to be the same then, as the diameter of the Langley tube is four times that of the University of Queensland tube, the density and thus the initial filling pressures of both the shock and acceleration tubes of the University of Queensland facility should be four times that of the Langley tubes.

Verification of the above expectations is obtained from a comparison of the pitot pressure profiles for a series of experiments in which only the acceleration tube filling pressure was varied. The Langley results (Miller (1977)) are reproduced in figures 3a-3f and the University of Queensland measurements can be seen in figures 4a-4f. The Langley shock tube filling pressure was 3.5 kPa and the acceleration tube filling pressure was varied between 2.0 Pa and 24 Pa. The University of Queensland shock tube filling pressure was 13.7 kPa and the acceleration tube filling pressure was varied between 6.6 Pa and 265 Pa. A helium driver was used in the Langley tube and the shock speed in the shock tube was 2.4 km/s. The shock speed in the University of Queensland tube was 2.00±0.05 km/s and the driver gas was argon.

From figure 3a it can be seen at the lower acceleration tube filling pressures that both the Langley and the University of Queensland pitot pressures oscillate about a monotonically increasing pressure. This is believed to be produced by lateral pressure waves. However, this is not fully understood. If the acceleration tube is filled to 32 Pa it can be seen that the University of Queensland facility has an acceptable flow between 30 μs and 80 μs after the initial shock (total enthalpy = 9 MJ/kg.) In comparison the Langley tube has its best recorded flow for an acceleration tube filling pressure of 6 Pa (total enthalpy = 15 MJ/kg) which is nominally the equivalent condition under the above assumptions. As the acceleration tube filling pressure is increased the lower frequency oscillations give way to higher frequency oscillations and the step due to the acceleration gas becomes more obvious in both sets of results. The only major qualitative difference between the two sets of data is that at the higher filling pressures the Langley pitot pressure measurements dip strongly after the initial rise, where as the University of Queensland's results do not.

II New Test Flows At Different Enthalpies

Experiments performed on the Langley facility (Miller (1977)) lead to the disappointing result that for each test gas only a narrow band of conditions were found in which the pitot pressure was acceptably steady for a reasonable peroid. In contrast, at the University of Queensland, helium, air and argon have been used as drivers to produce three test conditions ((i)-(iii) below) which have an acceptably steady flow of air over a range of test times.

For each of these test conditions the primary diaphram was 0.1 mm cold rolled mild steel with a burst pressure of approximately 35 MPa and the secondary diaphram was cellophane. The acceleration tube was filled with air.

(i) Figure 5 displays the pitot pressure when the shock tube was filled to 3.5 kPa and the acceleration tube was filled to 17 Pa. A helium driver was used. From the shock speed in the acceleration tube it can be shown that total enthalpy of this test flow is 42 MJ/kg. It can be seen that a very steady flow with a total pressure of 800 kPa exists for 70 μs, after which bubbles of driver gas and the effects of the expansion appear.

(ii) An air driver gas was used to produce the pitot pressure trace given in figure 6. The shock tube filling pressure was 1.7 kPa and the acceleration tube was filled to 7.3 Pa. The total enthalpy was 11 MJ/kg. It can be seen that a reasonably steady flow exists for approximately 200 μs for a total pressure of 128 kPa.

(iii) Figure 7 displays the best pitot pressure measurement produced with an argon driver. The shock tube filling pressure was 3.5 kPa and the acceleration tube was filled to 33 Pa. Although this result is not as clean as that for the helium driver it can be seen that after the initial rise due to the acceleration gas there is approximately 100 μs of test time in which the pitot pressure would vary no more than ±5 % from 535 kPa. The total enthalpy for this test condition is 8.6 MJ/kg.

These conditions were repeatable approximately three out of every four times.

III New Test Flows At Different Pressures

If the test time is indeed limited by the mechanism outlined above, then the characteristics in figure 2 would be the same provided the ratios of

(i) the primary diaphram burst pressure to the shock tube filling pressure, and

(ii) the shock tube filling pressure to the acceleration tube filling pressure

are preserved. Thus, in theory, similar qualitative pitot pressure traces should be seen if these ratios remain static. Only the pressure level should change. The shock speeds and thus the total enthalpy should remain the same.

This conclusion was tested by performing experiments at reduced operating pressure levels. Figures 8a-8f are the pitot pressure traces when the acceleration tube filling pressure was varied from 2.7 Pa to 133 Pa and the shock tube filling pressure was 1.7 kPa. The primary diaphram bursting pressure was approximately 18.5 MPa and the driver gas was argon. In figures 9a-9f the shock tube filling pressure was 3.4 kPa and the acceleration tube filling pressure was varied between 5.3 kPa and 266 kPa. The primary diaphram bursting pressure was 35 MPa and the driver gas was again argon. The above ratios ((i) and (ii)) have been basically preserved but the overall pressures have doubled.

It can be seen from these preliminary results that the inviscid theory would appear to be correct. At the lowest acceleration tube filling pressure there is a gradual rise in pressure followed by a relatively noisy flow that is believed to result from the lateral pressure oscillations produced by bursting of the secondary diaphram. As the acceleration tube filling pressure is increased the reflection of the expansion arrives earlier and the step due to the acceleration gas becomes more pronounced. Furthermore the acceptable test time increases from figures 8a and 9a to 8c and 9c and then decreases as the effect of the bubbles and reflected expansion become more and more dominant. The pressures of the plateaus of figures 8c and 9c are 140 kPa and 280 kPa respectively. The enthalpies of these flows are 8.6 MJ/kg and 8.2 MJ/kg respectively.

Conclusions

(i) The Langley facility and the University of Queensland facility are qualitatively comparable for similar Reynolds numbers and shock tube shock speeds.

(ii) Different driver gases can be used to obtain steady flows for different stagnation enthalpies.

(iii) Preliminary results indicate that different operating pressure levels can be used for similar stagnation enthalpies provided the ratios of the diaphram burst pressure to the shock tube filling pressure and the shock tube filling pressure to the acceleration tube filling pressure are maintained constant.

References

Gourlay, C.M. Personal communication. (1988)

Miller, C.G. Operational Experience in the Langley Expansion Tube with Various Test Gases. NASA TM 78637. (1977).

Moore J.A. Description and Initial Operating Performance of the Langley 6-Inch Expansion Tube Using Heated Helium Driver Gas. NASA TM X-3240. (1975).

Notation

P_A Acceleration tube filling pressure

P_s Shock tube filling pressure

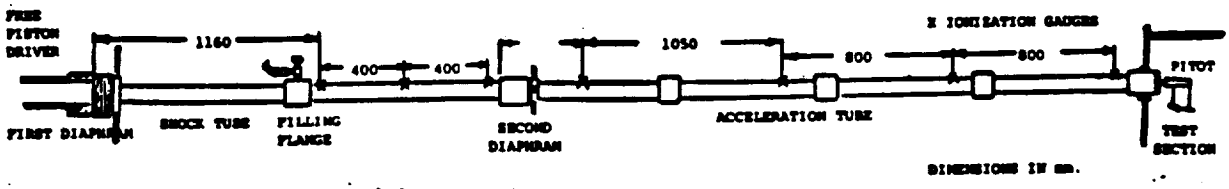

FIGURE 1. EXPANSION TUBE: General Arrangement.

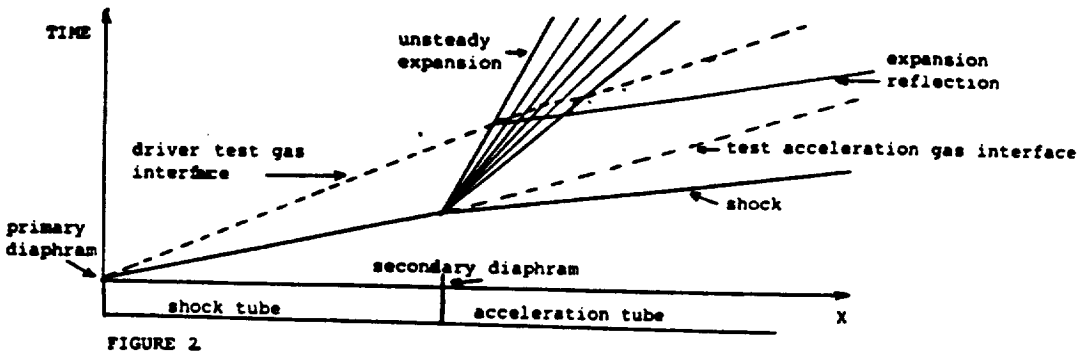

FIGURE 2

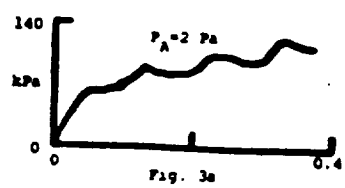

Fig. 3a

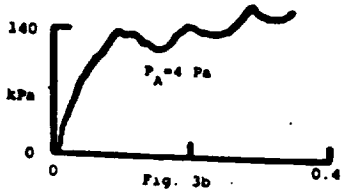

Fig. 3b

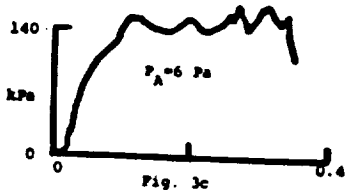

Fig. 3c

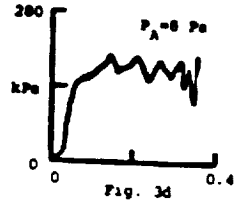

Fig. 3d

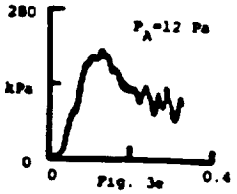

Fig. 3e

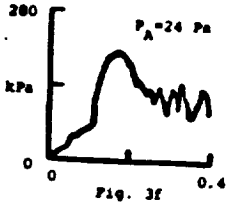

Fig. 3f

Langley Expansion Tube

P_S = 3.4 kPa. He Driver

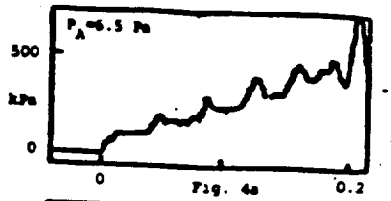

Fig. 4a

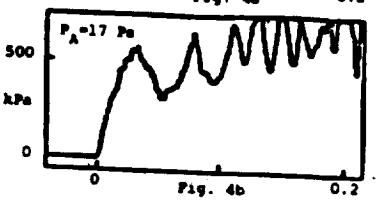

Fig. 4b

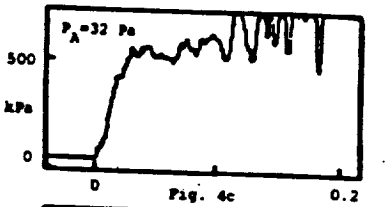

Fig. 4c

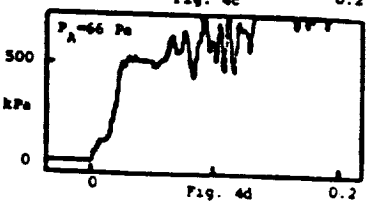

Fig. 4d

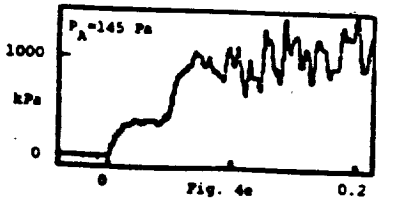

Fig. 4e

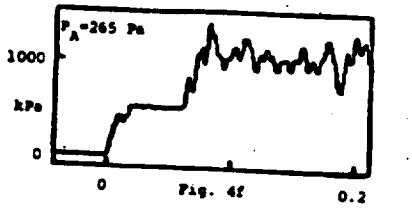

Fig. 4f

University of Queensland Free Piston Expansion Tube

P_S = 13.7 kPa. A Driver

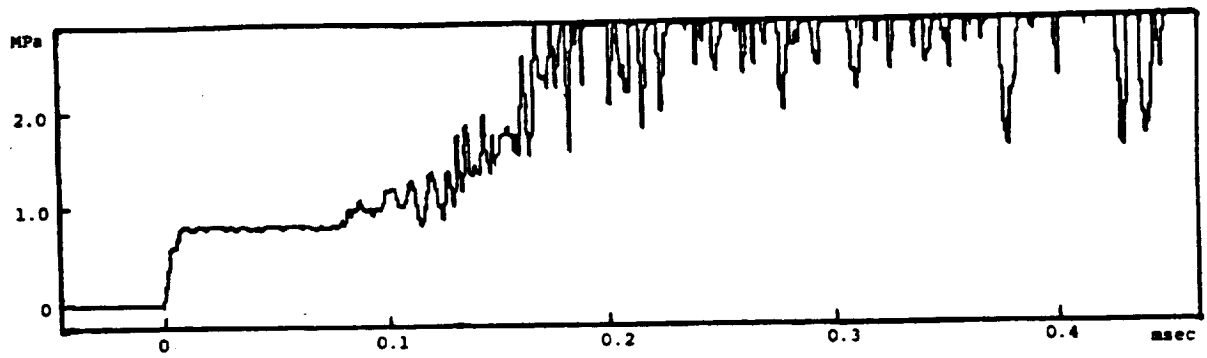

FIGURE 5. Pitot Pressure Trace for a He Driver with P_S = 3.5 kPa and P_A = 17 Pa.

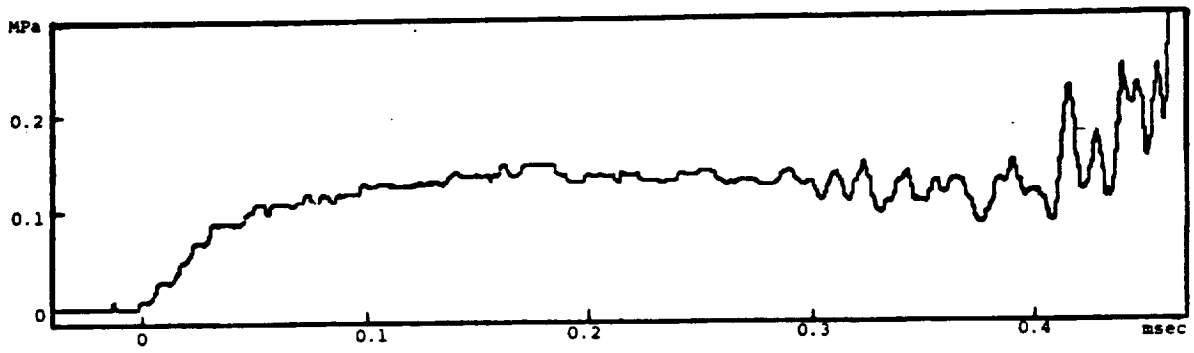

FIGURE 6. Pitot Pressure Trace for an Air Driver with P_S = 1.7 kPa and P_A = 7.3 Pa.

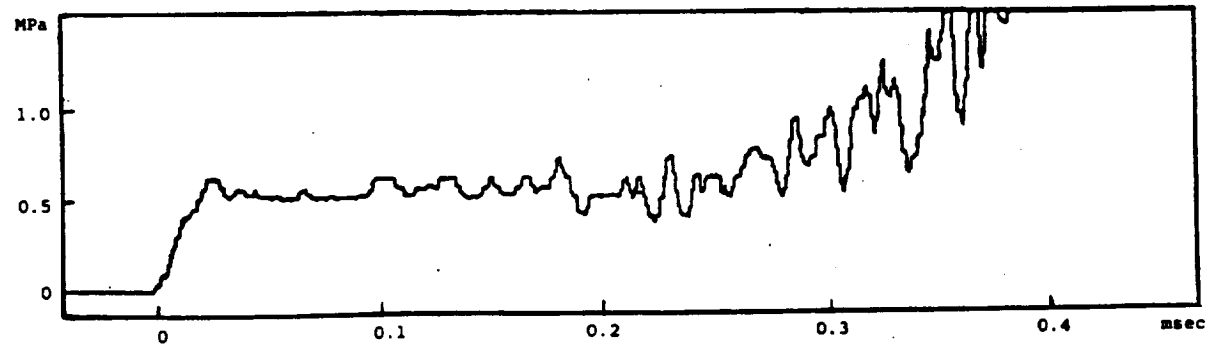

FIGURE 7. Pitot Pressure Trace for an Argon Driver with P_S = 3.5 kPa and P_A = 33 Pa.

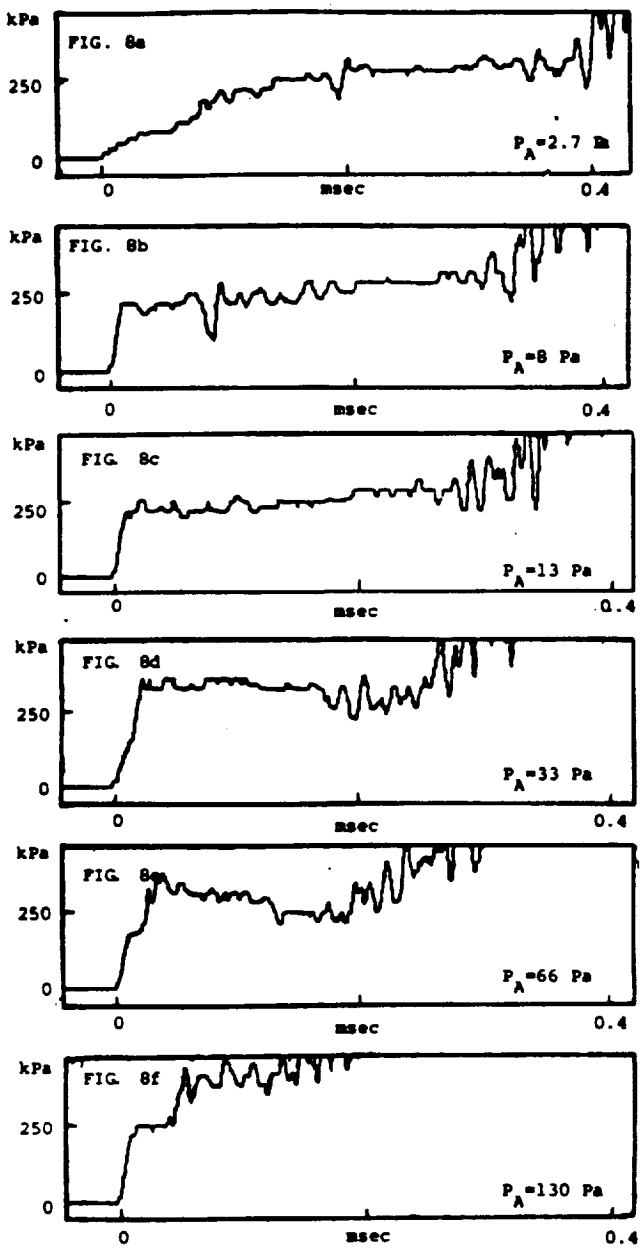

FIGURE 8. Pitot Pressure Traces. Ar Driver
P_s = 1.7 kPa

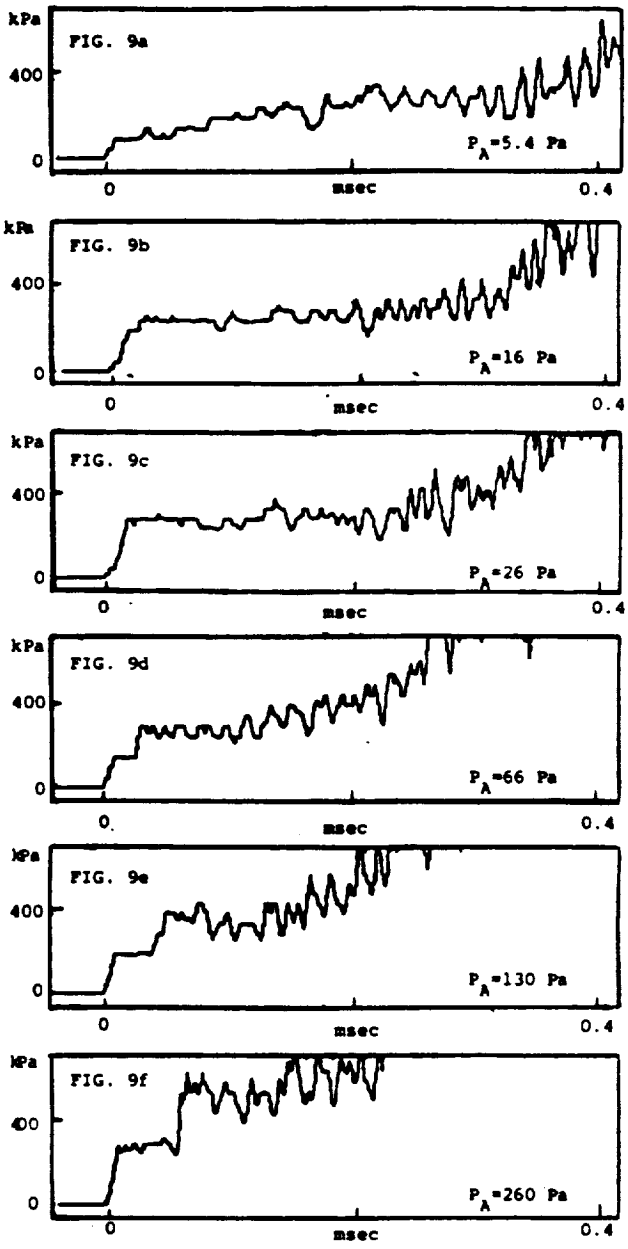

FIGURE 9. Pitot Pressure Traces. Ar Driver
P_s = 3.4 kPa

ADDENDUM

Recent Scramjet Group Publications

1. Stalker, R. J. and Morgan, R. G.: Parallel Hydrogen Injection Into a Constant Area, High Enthalpy Airflow. AIAA Journal, Vol. 20, No. 10, 1982.

2. Morgan, R. G. and Stalker, R. J.: Fast Acting Hydrogen Valve. Journal of Physics E. Sci. Instrum., Vol. 16, pp. 205-207, 1983.

3. Morgan, R. G. and Stalker, R. J.: Experiments on a Simple Scramjet Model. Proc. Eighth Australian Fluid Mechanics Conference, University of Newcastle, pp. 10 C1-10 C4, 1983.

4. Stalker, R. J. and Morgan, R. G.: Supersonic Combustion with a Short Thrust Nozzle. Journal of Combustion and Flame, Vol. 57, No. 1, pp. 55-70, 1984.

5. Netterfield, M. P.; Stalker, R. J.; and Morgan, R. G.: The Reflection of an Expansion Fan from a Mach Number Gradient in a Scramjet Exhaust. University of Queensland, Department of Mechanical Engineering Research Report 7/84, 1984.

6. Morgan, R. G. and Stalker, R. J.: Hypersonic Air Breathing Propulsion. Paper presented to the first I.E.Aust. Symposium on Space Technology, Australian National University, Canberra, 1984.

7. Morgan, R. G. and Schultz, D. L.: Infrared Scanning in Transient Wind Tunnels. Paper 10A, 3rd Australian Conference on Heat and Mass Transfer, University of Melbourne, 1985.

8. Morgan, R. G. and Stalker, R. J.: Heat Transfer in a hydrogen Scramjet Model. Paper 17D, 3rd Australian Conference on Heat and Mass Transfer, University of Melbourne, 1985.

9. Morgan, R. G. and Stalker, R. J.: Shock Tunnel Measurements of Heat Transfer in a Model Scramjet. Paper 85-0908, AIAA 20th Thermophysics Conference, 1985.

10. Paull, A.; Morris, N. A.; Morgan, R. G.; Stalker, R. J.: Scramjet Sidewall Burning - Preliminary Shock Tunnel Results. University of Queensland, Department Mechanical Engineering Research Report 12/85, 1985.

11. Morgan, R. G.; Paull, A.; Morris, N.A.; Stalker, R. J.: Hydrogen Scramjet With Sidewall Injection. Paper presented to the 2nd I.E.Aust. National Symposium on Space Engineering, Sydney, 1986.

12. Paull, A.; Morris, N. A.; Morgan, R. G.; and Stalker, R. J.: High Reynolds Number Heat Transfer to the Cold Walls of a Model Scramjet. Presented at the 9th Australian Fluid Mechanics Conference, Auckland, 1986.

13. Paull, A.; Morris, N. A.; Morgan, R. G.; Stalker, R. J.: Further Shock Tunnel Studies of Scramjet Phenomena. University of Queensland, Department of Mechanical Engineering Research Report 10/86, 1986.

Report Documentation Page

NASA National Aeronautics and Space Administration

1. Report No.	2. Government Accession No.	3. Recipient's Catalog No.
NASA CR-181721		

4. Title and Subtitle	5. Report Date
Shock Tunnel Studies of Scramjet Phenomena	September 1988
	6. Performing Organization Code

7. Author(s)	8. Performing Organization Report No.
R. G. Morgan, A. Paull, R. J. Stalker, P. Jacobs, N. Morris, I. Stringer, and C. Brescianini	
	10. Work Unit No. 505-62-81-61

9. Performing Organization Name and Address	11. Contract or Grant No.
University of Queensland Department of M.E. St. Lucia, Queensland 4067 AUSTRALIA	NAGW-674
	13. Type of Report and Period Covered
12. Sponsoring Agency Name and Address National Aeronautics and Space Administration Langley Research Center Hampton, VA 23665-5225	Contractor Report
	14. Sponsoring Agency Code

15. Supplementary Notes

Langley Technical Monitor: Griffin Y. Anderson
Final Report - Supplement 3, NAGW-674

16. Abstract

Commissioning of the new shock tunnel T4 at the University of Queensland implied that it was no longer necessary to focus the work of the research group about an annual test series conducted in the T3 shock tunnel in Canberra. Reflecting this, it has been possible to organize the group for work to proceed along lines such that particular personnel are associated with particular project areas.
Thus the format of this report consists of a series of reports on specific project areas, with a brief general introduction commenting on each report. The introduction is structured by project areas, with the title of the relevant report stated under the project area heading. The reports themselves follow in the order of the project area headings.

17. Key Words (Suggested by Author(s))	18. Distribution Statement
scramjet, combustion, hypervelocity mixing, facility	Unclassified - Unlimited Subject Category 07

19. Security Classif. (of this report)	20. Security Classif. (of this page)	21. No. of pages	22. Price
Unclassified	Unclassified	160	A08

NASA
FORMAL
REPORT